Universidade de Lisboa

Faculdade de Farmácia

Departamento de Farmácia Galénica e Tecnologia Farmacêutica

U

LISBOA

UNIVERSIDADE
DE LISBOA

**The link between altered glucosylceramide composition and membrane properties:
From membrane biophysics to Gaucher Disease**

Ana Raquel Pinto Varela

Orientadores: Doutora Liana C. Silva

Professor Doutor Manuel Prieto

Professor Doutor Anthony H. Futerman

Tese especialmente elaborada para a obtenção do grau de Doutor no ramo de Farmácia, especialidade de Tecnologia Farmacêutica.

2015

Universidade de Lisboa

Faculdade de Farmácia

Departamento de Farmácia Galénica e Tecnologia Farmacêutica

U

LISBOA

UNIVERSIDADE
DE LISBOA

The link between altered glucosylceramide composition and membrane properties:
From membrane biophysics to Gaucher Disease

Ana Raquel Pinto Varela

Orientadores: Doutora Liana C. Silva

Professor Doutor Manuel Prieto

Professor Doutor Anthony H. Futerman

Tese especialmente elaborada para a obtenção do grau de Doutor no ramo de Farmácia, especialidade de Tecnologia Farmacêutica.

Júri:

Presidente: Doutora Matilde Castro

Vogais:

— Doctor Giovanni D' Angelo,

— Doutor Vitor Manuel Vieira da Costa.

— Doutor Nuno Fernando Duarte Cordeiro Correia dos Santos,

— Doutor Manuel José Estevez Prieto.

— Doutor Fñbio Monteiro Femandes.

— Doutora Helena Isabel Fialho Florindo Roque Ferreira

— Doutora Liana Casquinha Silva

The link between altered glucosylceramide composition and membrane properties:
From membrane biophysics to Gaucher Disease

Dissertação apresentada à Faculdade de Farmácia da Universidade de Lisboa para prestação de provas de Doutoramento em Farmácia, Especialidade em Tecnologia Farmacêutica.

To my Mother, Father, "baby" Brother and André.

"If you can find a path with no obstacles, it
probably don´t lead anywhere."

Frank A. Clark (1911-   )

Acknowledgments

In the end of this amazing marathon, which was the development and execution of my PhD project, I was able to enter in the world of biophysics and fluorescence. Since, this was quite a new and complex world, I needed the help of many persons and entities to be able to execute and overtake all the tasks and difficulties that I have encountered Therefore, I want to express my gratitude to all the people that I have met during my PhD and that helped me in the process, especially to the ones bellow.

First of all, I would like to express my appreciation to my advisors.

To Dr. Liana C. Silva, which was fundamental in my PhD. Thanks for giving me the opportunity to be a part of your research team, in the Intracellular Trafficking Modulation for Advanced Drug Delivery Research, for the support and guidance throughout this journey. And for pushing my limits, which made me grow as an individual and as a researcher.

I want to express my gratitude to Prof. Dr. Manuel Prieto for receiving me in the Molecular Biophysics Group of *Instituto Superior Técnico* (IST), for allowing me to perform the biophysical studies at the *Centro de Quimica-Física Molecular* (CQFM) of IST, for the good discussions, and for always keeping his good mood.

I also want to thank Prof. Dr. Anthony Futerman for receiving me in the Department of Biological Chemistry of Weizmann Institute of Science , where I was able to perform the cellular studies. Moreover, I also want to thank Professor Tony for his kindness and for all the good discussions.

An acknowledgment is also owed to *Faculdade de Farmácia da Universidade de Lisboa*, *Instituto Superior Técnico* and Weizmann Institute of Science. For opening their facilities to me, enabling the development of this thesis work.

I also want to acknowledge the Federation of European Biochemical Societies, which had awarded me with conference grants, which allowed my participation in more conferences, giving me the opportunity to share my work and debate it with scientists from all over the world.

A big thank you for the friendship off all the present and former people in the Nanomedicine and Drug Delivery Systems, which today is integrated in the Drug Development group of the iMed.ULisboa, especially to Carina, Joana Silva, Ana Saraiva, Natércia, Eva Zupančič, Ana Matos, Nuno Martinho, João Conniot, Liane Moura, Joana Marto and Helena Florindo. Thank you all for supporting me and for making me laugh in the hard times.

To my friends, colleagues, and Professors in the Centro Química-Física Molecular, in the Instituto Superior Técnico, namely to Mª João Sarmento, Joana Ricardo, Tânia Sousa, Sandra Pinto, Ana Melo, Marina Monteiro, Bruno Castro, Samuel Jacob, Paulo Caldas, Lourdes Renart, Rocio Esquembre , Fábio Fernandes and Prof. Dr. Ana Coutinho.

To Professor Hermínio Diogo, for letting me use his facilities.

To Professor Amélia M.P.S. Gonçalves da Silva, for letting me use her lab to develop part of my experiments, and for all the help in the interpretation of the results regarding the Langmuir monolayers.

To Prof. Dr. Erich Gulbins, for welcoming me in his group in the *Institut für Molekularbiologie* in the *Medizinische Fakultät Universitätsklinikum* in Essen, were I was able to evaluate specific interactions between sphingolipids and bacteria.

To all my dearest friends, for always keeping me up, namely Iris Santos, Pedro Pelado, Inês Ferreira, Natália Ferreira, Duarte Ferreira, João Romano, Joana Silva, Carina Peres, Ana Saraiva e Natércia.

Last, but not least I want to thank my family specialy to my Mum, Dad and baby brother, without you I would not be here, and André Carvalho, for all the support, love, and many many patiente, thank you !!!!!!

This thesis was supervised by

- Dr. Liana C. Silva (supervisor)

Assistant Researcher

Research Institute for Medicines (iMed.ULisboa), Faculdade de Farmácia, Universidade de Lisboa, Portugal

- Prof. Dr. Manuel Prieto

Full Professor (co-supervisor)

Centro de Química-Física Molecular & IN - Institute of Nanoscience and Nanotechnology, Instituto Superior Técnico, Universidade de Lisboa, Lisboa, Portugal

- Prof. Dr. Anthony H. Futerman

Full professor (co-supervisor)

Department of Biological Chemistry, Weizmann Institute of Science, Rehovot, Israel

This work was developed at

Abstract

Lipids are one of the most abundant molecules in a cell and are involved in the regulation of cell events. One of the mechanisms by which lipids control cell signaling is by altering membrane biophysical properties. Therefore, the biophysical properties of several lipids have been thoroughly characterized. However, some bioactive lipids like glucosylceramide (GlcCer) still have their properties poorly studied. GlcCer is a lipid involved in several cell processes. A deregulation in its metabolism triggers damaging signaling pathways ultimately leading to the development of a pathologic state, such as Gaucher Disease (GD). This disease results from the abnormal accumulation of GlcCer in cells, mainly in the lysosomes. Even though the biochemistry and biology context of GD is a subject of intensive research, the molecular mechanisms that underlie this disease remain elusive, likely due to the inherent complexity and heterogeneity of the disease. An underexplored branch of research, related to the understanding of the biophysical impact of increased levels of GlcCer in biological membranes, might provide additional insight into the mechanisms underlying this complex disease. Therefore, research that aims to characterize the biophysical features of GlcCer and its interaction with other membrane lipids is required. Using complementary techniques, including fluorescence microscopy and spectroscopy, a thorough biophysical characterization of GlcCer was performed. This comprised the study of the effect of increasing molar fractions of GlcCer in the biophysical properties and morphology in a variety of model membranes containing different lipid composition, as well as in wild type and Gaucher Disease-derived fibroblasts. Since GlcCer is present at higher abundance in the plasma membrane (PM) and in the lysosome, the studies were performed in conditions mimicking the pH environment of those cellular sites.

This detailed study revealed that: I) GlcCer increases the order of fluid membranes, II) GlcCer promotes membrane morphological alterations, such as tubules, III) GlcCer effect in membrane properties is pH sensitive, promoting an higher packing at neutral pH, IV) GlcCer impact in the membrane is modulated by cholesterol (Chol) in a concentration dependent manner, V) fibroblasts from GD patients, which are enriched in GlcCer, have a higher global membrane order in comparison to wild type fibroblasts, coherent with the observations in model membranes.

These conclusions indicate that GlcCer accumulation in cells alter the biophysical properties of its membranes, possibly affecting protein activity and trafficking. These alterations could underlie some of the effects triggered by GlcCer that might contribute to the development of Gaucher Disease.

Resumo

As membranas celulares têm diversas funções, entre as quais podem identificar-se a função de interface na interação com moléculas extracelulares e a participação ativa na regulação da sinalização celular. As várias funções das membranas celulares sugerem que se trata de um organelo de estrutura complexa, no entanto, nem sempre esta foi a ideia vigente. A definição de membrana evoluiu significativamente desde que um dos mais importantes modelos de membrana, o modelo de Mosaico Fluido (FMM) de Singer e Nicholson foi proposto em 1972. Neste modelo, proteínas integrais ou periféricas estariam totalmente envolvidas ou apenas suportadas, respetivamente, por uma bicamada lipídica fluida, onde as proteínas poderiam difundir livremente. Neste modelo, os lípidos eram tidos como meras entidades estruturais sem qualquer função ativa nos processos celulares. No entanto, os desenvolvimentos tecnológicos forneceram novos dados em relação às membranas celulares que não eram compatíveis com o modelo de FMM, nomeadamente a formação de domínios lipídicos, tais como os domínios *raft*. Estes domínios selecionariam diferentes proteínas para diferentes zonas da membrana e, devido ao seu elevado empacotamento, poderiam também alterar a conformação proteica afetando a sua atividade. A capacidade dos lípidos membranares para segregarem e organizarem-se em domínios, afetando a difusão e a atividade proteica, conferiu aos mesmos um papel ativo na modulação de diferentes processos e sinalização celular. De acordo com a definição inicialmente proposta, os domínios *raft* são regiões da membrana enriquecidas em colesterol (Chol) e esfingolípidos (SLs), de entre os quais se podem nomear os glicoesfingolípidos (GSLs) (ex.glucosilceramida, GlcCer). Os SLs são uma classe lipídica com atividade biológica, sendo a sua estrutura base uma ceramida, por sua vez, formada por uma base esfingóide ligada a uma cadeia acilo de tamanho variável. Ao carbono C1 da ceramida podem ser adicionadas diferentes moléculas, como a glucose, formando-se assim a GlcCer.

A GlcCer tem diferentes funções celulares sendo, por exemplo, essencial para o desenvolvimento embrionário. O papel vital da GlcCer foi demonstrado pela inviabilidade de fetos de ratinho, que têm inibida a capacidade de sintetizarem GlcCer e consequentemente a maioria dos GSL complexos. O elevado impacto biológico da GlcCer pode em parte ser explicado, dado que a síntese de GSLs complexos, envolvidos em

diferentes processos vitais para o organismo, é dependente da GlcCer. Mais ainda, dado que a GlcCer está envolvida na formação de domínios lipídicos, como os *raft*, esta revela-se como um lípido que potencialmente controla diversos processos celulares, reafirmando o seu importante papel na célula. Exemplos documentados são: o papel da GlcCer no controlo das vias endocíticas, na interação célula-célula, na adesão celular e na influência da patogenicidade de vários microrganismos como o *Criptococus neoformans*. Contudo, este lípido apenas constitui uma pequena fração dos lípidos totais que existem na membrana, o que significa que para manter os níveis fisiológicos de GlcCer a sua síntese e degradação é altamente controlada. Consequentemente, um desequilíbrio numa via metabólica da GlcCer repercutir-se-á em efeitos negativos no funcionamento celular, o que poderá promover o desenvolvimento de patologias. De facto, o mau funcionamento de qualquer uma das moléculas envolvidas na degradação da GlcCer promove uma acumulação anormal deste lípido na célula, o que pode culminar no desenvolvimento de uma patologia designada de Doença de Gaucher (GD).

A etiologia mais frequente desta patologia deve-se a mutações no gene que codifica a enzima que degrada a GlcCer - a glucosilcerebrosidase (GCase). Na GD verifica-se uma significativa acumulação lisossomal de GlcCer, especialmente nos macrófagos. Isto deve-se à fagocitose intensa (de bactérias, fungos, diversos tipos de células, etc) que se verifica nos macrófagos, aumentando muito significativamente o aporte de GlcCer nos mesmos. Esta doença manifesta-se frequentemente por uma hiperplasia do fígado e do baço, no entanto, o sistema nervoso central, os ossos e outros tecidos poderão também ser afetados. A possibilidade de envolvimento de diferentes sistemas promove uma impressionante heterogeneidade de quadros clínicos nestes doentes. Também se verifica em muitas situações que a severidade ou o fenótipo dos pacientes com GD não é passível de ser relacionado com o seu genótipo, o que muitas vezes dificulta o prognóstico desta doença por parte dos clínicos.

Apesar do contexto biológico e bioquímico da GD já ter sido exaustivamente estudado, a biofísica inerente a esta doença tem merecido pouca atenção por parte dos investigadores. Assim sendo é premente realizar estudos biofísicos que abordem o impacto da GlcCer nas propriedades de membranas modelo e naturais, tal como estudar a interação da GlcCer com outros lípidos de membrana, nomeadamente com os que tipicamente se encontram nos domínios *raft*.

Estas questões poderão ser subdivididas em diferentes pontos, os quais irão ser desenvolvidos e esclarecidos nos capítulos II a V desta dissertação.

I) Quais são os efeitos da GlcCer, em membranas fluidas?; II) Será a GlcCer e outros esfingolípidos neutros sensíveis a alterações de pH?; III) Como é que a GlcCer interage com outros lípidos que tipicamente se encontram em domínios lipídicos, como o Chol?; IV) Como é que a GlcCer afeta as propriedades de modelos de membrana com uma composição típica de domínios *raft*? ; V) Haverá diferenças nas propriedades biofísicas globais das membranas de células saudáveis e de células enriquecidas em GlcCer?

Para responder as estas perguntas desenhou-se um extenso estudo biofísico que explora as propriedades biofísicas da GlcCer no contexto de membranas modelo com crescente complexidade e também em membranas celulares. Neste estudo, usou-se maioritariamente modelos de membrana, tais como as vesiculas multilamelares e vesiculas unilamelares gigantes (estas com curvatura e tamanho muito semelhante a uma membrana natural). O uso destes modelos permite controlar a composição das membranas em estudo, tal como estudar os efeitos específicos de certos lípidos. Diferentes tampões, com pH distintos, foram usados para a formação das membranas modelo, permitindo analisar o efeito do fator pH nas propriedades biofísicas dos lípidos.

A caracterização das membranas foi realizada através de diferentes técnicas complementares, nomeadamente: microscopia de fluorescência (confocal), espectroscopia de fluorescência, estudos em tina de Langmuir (onde se observou o comportamento das misturas em monocamadas) e de técnicas de dispersão dinâmica da luz e dispersão dinâmica electroforética.

Este detalhado estudo biofísico centrado no impacto da GlcCer em membranas com diferentes composições e a diferentes pH (7.4 e 5.5), revelou que: I) a GlcCer aumenta o empacotamento das membranas fluidas (compostas por fosfolípidos insaturados); II) promove alterações morfológicas nas membranas, como por exemplo, a formação de túbulos; III) o efeito organizador da GlcCer nas membranas é sensível ao pH, já que a pH neutro (7.4) a ordem das membranas que contêm GlcCer é maior que a pH ácido (5.5); IV) o impacto da GlcCer no empacotamento das membranas modelo depende da concentração de Chol na mesma, ou seja, o efeito da GlcCer nas propriedades biofísicas das membranas é regulado pelo Chol; VI) a ordem global das membranas de fibroblastos derivados de doentes com GD (células enriquecidas em GlcCer) é significativamente mais

elevada que a ordem global das membranas de fibroblastos controlo. Estes últimos dados são consistentes com os obtidos nos modelos de membrana, confirmando que as membranas artificiais são modelos adequados para prever o que ocorrerá a nível das membranas celulares.

Resumindo, neste trabalho verificou-se que a GlcCer promove um aumento da rigidez da membrana, no entanto, o seu efeito será condicionado pelos níveis de colesterol na membrana e pelo pH do meio celular. Em situações de aumento anormal dos níveis de GlcCer, como na doença de Gaucher, o elevado empacotamento e rigidez da membrana poderá afetar o transporte intracelular e a conformação de diferentes proteínas, promovendo alterações no comportamento ou até mesmo a morte celular. Os resultados obtidos nesta tese fornecem um apoio biofísico aos efeitos biológicos e patológicos promovidos pela GlcCer.

Palavras-chave: Glucosilceramida, membranas modelo, domínios, pH, espectroscopia de fluorescência, microscopia de fluorescência, propriedades biofísicas das membranas

Content Index

Chapter V - Glucosylceramide-Induced Biophysical Changes In Artificial And Cell Membranes

183

Figure Index

CHAPTER III- INFLUENCE OF INTRACELLULAR MEMBRANE PH ON SPHINGOLIPID ORGANIZATION AND MEMBRANE BIOPHYSICAL PROPERTIES

CHAPTER IV- GLUCOSYLCERAMIDE REORGANIZES CHOLESTEROL-CONTAINING DOMAINS IN A FLUID PHOSPHOLIPID MEMBRANE

CHAPTER V- GLUCOSYLCERAMIDE-INDUCED BIOPHYSICAL CHANGES IN ARTIFICIAL AND CELL MEMBRANES

Table Index

List of abbreviations

\<r>	Fluorescence anisotropy
ΔH	Transition Enthalpy
π	Pressure
π-A	Pressure-area
τ	Fluorescence lifetime
λ_{em}	Emission wavelength
λ_{ex}	Excitation wavelength
AFM	Atomic Force Microscopy
C16-Cer	N-palmitoyl-D-erythro-sphingosine
C16:0-Cer*	N-palmitoyl-D-erythro-sphingosine
C18:1-Cer	N-oleoyl-D-erythro-sphingosine
C24-Cer	N-lignoceroyl-D-erythro-sphingosine
C24:0-Cer	N-lignoceroyl-D-erythro-sphingosine
C24:1-Cer	N-nervonoyl-D-erythro-sphingosine
C18-GlcCer	D-glucosyl-ß-1,1'-N-stearoyl-D-erythro-sphingosine
C16-GlcCer	D-glucosyl-ß-1,1' N-palmitoyl-D-erythro-sphingosine
C16:0-GlcCer*	D-glucosyl-ß-1,1' N-palmitoyl-D-erythro-sphingosine
C16-SM	N-palmitoyl-D-erythro-sphingosylphosphorylcholine
C_p	Heat capacity
C_s^{-1}	Compressibility modulus
Cer	Ceramide
CerS	Ceramide synthase
CERT	Ceramide transfer protein
Chol	Cholesterol
CLSM	Confocal Laser Scanning Microscope
CNS	Central Nervous System
DLS	Dynamic Light Scattering
DOPE-Biotin	1,2-dioleoyl-sn-glycero-3-phosphoethanolamine-N-(biotinyl)
DPH	1,6-diphenyl-1,3,5-hexatriene

DSC	Differential Scanning Calorimetry
ER	Endoplasmic Reticulum
FAPP2	4-phosphate adaptor protein 2
FCS	Fluorescence Correlation Spectroscopy
FMM	Fluid Mosaic Membrane
FRET	Förster Resonance Energy Transfer
GalCer	Galactosylceramide
Gb3	Globotriaosyl ceramide
GBA2	Non-lysosomal β-glucosidade 2
GBA3	Neutral β-Glucosidase 3
GCase	β-Glucosidase
GCS	Glucosylceramide Synthase
GD	Gaucher Disease
GlcCer	Glucosylceramide
GLTP	Glycolipid Transfer Protein
GM1	Monosialotetrahexosylganglioside
GM3	Monosialodihexosylganglioside
GP	Generalized Polarization
GSL	Glycosphingolpid
GUV	Giant Unilamellar Vesicles
H_I	Micellar Hexagonal
H_{II}	Inverted Hexagonal
OH	Hydroxyl group
LacCer	Lactosylceramide
Laurdan	6-dodecanoyl-2-dimethylaminonaphthalene
L_α	Lamellar liquid crystalline
L_β	Lamellar gel
$L_{\beta'}$	Tilted gel
L_c	Lamellar crystalline
l_d	Liquid disordered
l_o	Liquid ordered
LM	Lysosomal Membrane

LUV	Large Unilamellar Vesicles
MLV	Multilamellar Vesicles
MMA	Mean Molecular Area
NBD-DPPE	1,2-dipalmitoyl-*sn*-glycero-3-phosphoethanolamine-N-(7-nitro-2-1,3-benzoxadiazol-4-yl)
P	Packing parameter
PALM	Photo-Activated Localization Microscopy
PC	Phosphatidylcholine
PdI	Polydispersity index
PE	Phosphatidyletanolamine
PI	Phosphatidylinositol
PIP$_2$	Phosphatidylinositol 4, 5-bisphosphate
PL	Phospholipids
PM	Plasma Membrane
POPC	1-palmitoyl-2-oleoyl-*sn*-glycerol-3-phosphocholine
PS	Phosphatidylserine
P$_\beta$	Rippled gel
Rho	Rhodamine
Rho-DOPE	N-rhodamine-dipalmitoylphosphatidylethanolamine
SIM	Structure Ilumination Microscopy
s$_o$	Solid ordered
SOPC	1-stearoyl-2-oleoyl-*sn*-glycero-3-phosphocholine
SL	Sphingolipids
SM	Sphingomyelin
SNARE	Soluble N-ethylmaleimide-sensitive-factor attachment protein receptor
Sph	Sphingosine
STED	Stimulated Emission Depletion
SUV	Small Unilamellar Vesicles
T$_m$	Main Transition Temperature
TMA-DPH	Trimethylammonium-diphenyhexatriene
t-PnA	*trans*-Parinaric Acid (octadeca-9,11,13,15-tetraenoic acid)

| UDP | Uracil-Diphosphate |
| **V-ATPase** | Proton pumping vacuolar-type ATPase |

(*****) Additional abbreviations according to the format of the published paper (Chapter II)

Outline

The work herein described is focused on the characterization of the impact of GlcCer in the biophysical properties of model and cell membranes, and also in the investigation of GlcCer interaction with other important membrane lipids. The final goal of this study is to reveal some of the biophysical properties that might be underneath the biologic effects of GlcCer, namely in the development of Gaucher Disease.

 Therefore the aims of this work included the characterization of:

I.   Binary lipid mixtures containing GlcCer and a common unsaturated phospholipid - Developed in Chapter II

II. Binary lipid mixtures formed by GlcCer or other uncharged sphingolipids and a fluid phospholipid in an environment mimicking the plasma and lysosomal membrane (pH 7.4 and 5.5, respectively) – Developed in Chapter III

III. Ternary mixtures containing GlcCer and Chol, at neutral and acidic pH – Developed in Chapter IV

IV. Quaternary mixtures with a composition typical of a raft membrane (fluid phospholipid, Chol and sphingomyelin (SM)) and GlcCer – Developed in Chapter V

V.   Global membrane properties of cells enriched in GlcCer (derived from Gaucher Disease patients) – Developed in Chapter V

This was achieved by analyzing the membranes with different and complementary techniques, such as fluorescence microscopy and spectroscopy, studies in Langmuir trough and with electrophoretic and dynamic light scattering. The detailed characterization of GlcCer biophysical properties performed in the framework of this thesis, allows to predict the biophysical impact of this lipid in biological membranes and might shed light into some of the mechanisms that underlie the biological effects of GlcCer, namely in the development of pathologies, such as Gaucher Disease.

This dissertation is divided into 6 chapters:

Chapter I contains a short review of the topics relevant for a better understating of the work described in this thesis. It includes references to the historical perspective, the concept and definition of biomembranes. The lipids biology and known biophysics are

described, namely those regarding GlcCer. Moreover, an extensive description concerning membrane lateral heterogeneity and the existence of specialized domains, such as rafts of which GlcCer is a part of, is presented. The last part of the introduction lists the membrane models used in biophysical studies and the techniques employed in the experimental work developed in the framework of this dissertation.

Chapter II describes the biophysical properties of 1-palmitoyl-2-oleoyl-*sn*-glycerol-3-phosphocholine (POPC)/ D-glucosyl-ß-1,1' N-palmitoyl-D-erythro-sphingosine (C16-GlcCer) systems with increasing molar fractions of the GSL. The model membranes were characterized by confocal microscopy, fluorescence spectroscopy and monolayer studies in Langmuir through. Through this study it was concluded that GlcCer increases the membrane order of fluid membranes and also alters the morphology of the membranes triggering the formation of tubules that could have a role in GlcCer biological function, like in cell to cell communication.

Chapter III addresses the issue of pH effect on the biophysical properties of neutral or zwitterionic sphingolipids like C16-GlcCer, N-palmitoyl-D-erythro-sphingosylphosphorylcholine (C16-SM), N-palmitoyl-D-erythro-sphingosine (C16-Cer) and N-nervonoyl-D-erythro-sphingosine (C24:1-Cer). It was possible to conclude that, in opposition to C16-Cer, GlcCer is sensitive to pH alterations inducing a higher packing of the membrane at pH 7.4. C16-SM and C24:1-Cer only evidence alterations induced by pH acidification, when present in high concentrations which are not biologically relevant.

In Chapter IV, a characterization of GlcCer interaction with Chol is carried out, at neutral and acidic environments. Through the use of confocal microscopy, fluorescence spectroscopy, electrophoretic and light scattering measurements, it was possible to understand that GlcCer impact on the biophysical properties of membranes is conditioned by Chol levels, emphasizing the importance that Chol presents in the modulation of membranes physico-chemical properties and also the relevance of GlcCer in the formation of putative *raft* domains. Moreover, in these lipid systems the packing order was higher at neutral environments in comparison to acidic ones.

Chapter V is a study focused in the impact of GlcCer on the biophysical properties of membranes containing lipids that are typically present in a raft domain (POPC, Chol and SM) at different pH. It was concluded that GlcCer increases the order of such membranes, more evidently at pH 7.4, and that the GlcCer-induced packing is reduced when the levels

of Chol in the quaternary mixtures increases. In addition, the global membrane packing was characterized in wild-type fibroblasts and in fibroblasts from patients with GD type I. It was observed that the global membrane order is higher in the fibroblasts with the GBA mutation, showing that an increase in the levels of GlcCer leads to a decrease in membrane fluidity, in agreement with data obtained in studies performed in model membranes. Altogether this supports the validity of model membranes as good predictors of cell membrane properties

Chapter I

Introduction

Chapter I

Chapter I - Introduction

1.1 Biological relevance of cell membranes

Since the discovery of the cell by Antonie van Leeuwenhoek and Robert Hooke in the 17th century, scientists try to characterize in detail this complex building block of all biologic systems.

Animal cells are constituted by an external plasma membrane (PM), the cytoskeleton and several subcellular compartments limited by membranes, such as the endoplasmic reticulum, mitochondria, lysosomes, Golgi apparatus and the nucleus[1]. It is evident that membranes have a central role in cell structure and functions. Cell membranes allow cell compartmentalization, individualization, and allow cell movement[1,2]. In addition membranes are involved in the majority of cell biochemical functions, since several enzymes and other proteins are located in these structures[3]. Nonetheless, membranes also determine the nature of all interactions between the cell and extracellular elements, e.g. cell to cell interactions[2]. This control may occur through the selective entrance/exit of ions and molecules of the cell or due to conformational changes induced in the membrane components[3]. Although the structural principles for all membranes are basically the same, they exhibit a remarkable diversity. Different protein and lipid composition enable membranes to have different properties and morphologies. Moreover, specific cellular membranes are altered in order to execute specific roles, such as the microvilli of the intestinal epithelium where invaginations of the membrane allow an optimized absorbance of different molecules[3, 4]. Besides that, cellular membranes can also present specific sites with specialized functions, characterized by significantly different properties comparing with the membrane bulk (e.g. tight junctions and desmosomes).[3]
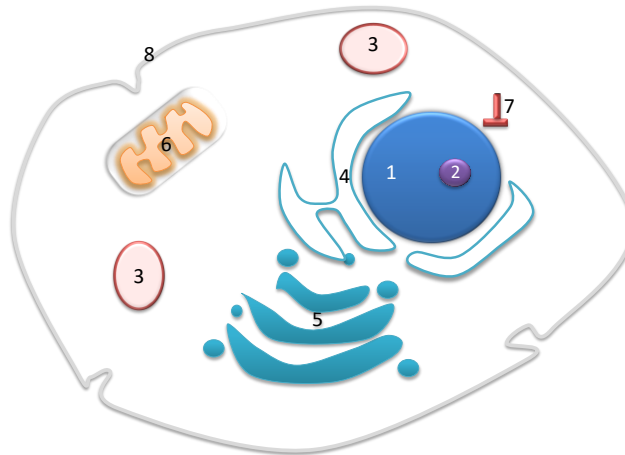
Figure 1 - Eukaryotic animal cell structure. Schematic representation of the main organelles of an animal cell.
1-Nucleus; 2- Nucleolus; 3- Lysosomes; 4-Endoplasmic Reticulum; 5- Golgi Apparatus; 6- Mitochondria; 7-Centriols; 8-Plasmatic Membrane, adapted from[1]

1.2. Membrane Models - Historical perspective

In the 20th century the work of several scientists shed light over the structure of cellular membranes. Overton was the first to hypothesize about the lipid nature of membranes [5]. Later in 1925, Gorter and Grendel described that the plasma membrane was composed of two lipid layers[6]. One decade later, in 1935, Davson and Danielli proposed a membrane model where the surface of each side of the lipid bilayer was covered by globular proteins (Tri-Layer Model, Fig. 2A)[7]. Due to the development of electron microscopy, Robertson was able to extend the concept of lipid bilayer to the sub-cellular compartments of the cell and propose an alternative version of the tri-layer model designated as Unit Membrane Model (Fig. 2B)[8]. In this model the proteins covering the membrane are unfolded in opposition to a globular conformation[8]. The theory of the Unit Membrane Model prevailed as the most accepted model until the 1970s, however, trans-membrane proteins were posteriorly included in the model as a consequence of new observations by Pinto da Silva and Branton[9]. In the 1970s, taking into account the already known facts about membranes and new data from several authors like Cone, Poo and Frye[10,11], Singer and Nicolson proposed the Fluid-Mosaic Membrane (FMM) model (Fig. 2C). In this model, peripheral and integral proteins diffuse freely in an asymmetrical lipid matrix[12]. Nevertheless, new techniques and extensive research developed in the area introduced new data that was not satisfied by the FMM original model[13]. Examples are the restriction in the lateral movement of lipids and proteins – the picket fence model - described by

Kusumi and colleagues[14, 15, 16, 17], and the evidence of lipid aggregates forming specialized domains, such as the raft domains reported by Simmons and Ikonen[18]. The use of the single particle tracking and single fluorescence molecule video enabled Kusumi and other authors to observe that protein membrane movement is not free due to structural membrane constraints [15, 17, 19]. The movement restriction occurs through the anchoring of transmembrane proteins to the cell cytoskeleton, forming fences that corral membrane proteins— 'fence model'[19, 20]. Moreover, lipids have also their movement limited by the compartments formed through the association between protein intracellular domains and the membrane skeleton network- 'anchored protein picket model', as evidenced by the works of Speroto and Mouritsen, and Fujiwara et al. [21, 22]. In addition, the formation of membrane domains can also be influenced by the cytoskeleton meshwork[20], suggesting that this membrane compartmentalization could modulate cell signaling by restricting a signaling complex or specific molecules to a defined membrane compartment[17].

The actual FMM model was altered in order to take into account the new data. Nowadays it includes in the membrane structure: aggregates of lipids forming domains (see section 7 for further details about membrane domains)[18], protein/glycoprotein complexes[23], membrane associated cytoskeletal fences[19, 24, 25] and extracellular matrix structures (e.g. collagen) (Fig. 2D). The new structures actively influence the macrostructure, dynamics and function of the biomembranes, also restricting the lateral diffusion and range of movement of membrane components[13, 26]. Nonetheless, there are still situations where the FMM model does not fit properly, as in the higher levels of organization where membrane crowding and specialized domains formation are rather important structural factors. However these were not taken into account by most membrane models[13].
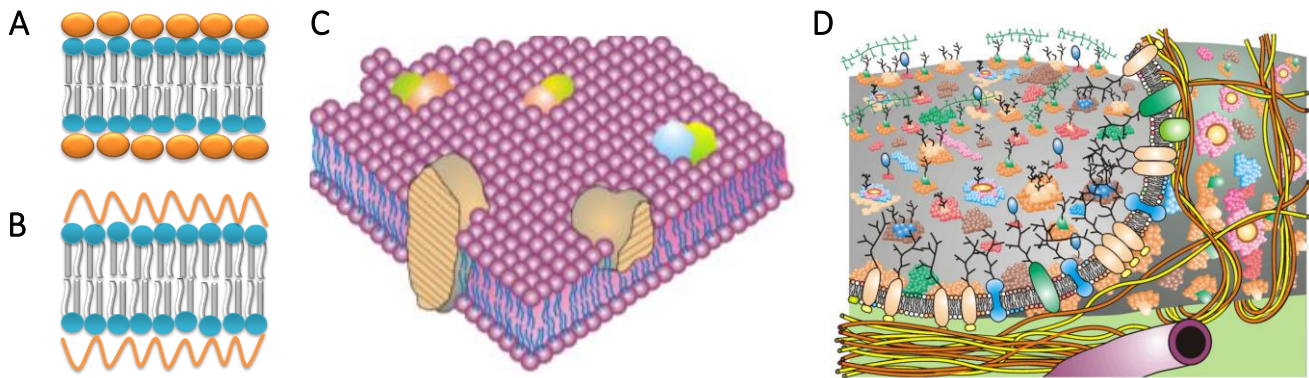
Figure 2 - Evolution of membrane models.
A Schematic representation of the Tri-layer model. B Representation of the Unit Membrane Model. C and D Original and actual representation of the Fluid Mosaic Membrane model, adapted from [13]

1.3 Chemical composition of membranes

As mentioned, cellular membranes are complex structures formed by different proteins and lipids that can be conjugated with different carbohydrates.

1.3.1 Carbohydrates

These are the most abundant molecules on Earth. Chemically these compounds are polyhydroxy aldehydes, ketones, or substances that upon hydrolysis yield such compounds. There are three main classes of carbohydrates: monosaccharides (a single aldehyde or ketone unit), oligosaccharides (2 to 19 units of monosaccharides) and polysaccharides (with 20 or more units of monosaccharides). In the membranes, three types of carbohydrates are found as glycoconjugates, i.e., linked to a protein or lipid. In the plasma membrane, the carbohydrates are normally, if not exclusively, facing the external side of the membrane[27].

1.3.2 Proteins

Membrane proteins are distributed either in the surface (peripheral) or immersed (integral) in the membrane matrix[2].

Integral proteins are embedded in the membrane bilayer. The portion of the protein that is inside the membrane is enriched in hydrophobic amino acids (e.g. leucine, valine, etc.).

These proteins can have different number of loops, orientations (dependent on the primary structure), and size of the globular domain in contact with the aqueous environment (which can contact with one or both sides of the membrane). These proteins have distinct functions. One example is the formation of channels that are involved in the control of ions or molecules exchange with the exterior (ex. aquaporins)[2]. It is important to enhance that these proteins are not rigid structures, their position and conformation are modulated by other proteins and/or lipids. In fact, lipids can directly influence the activity of a protein either by changing membrane fluidity[28,29] or acting as co-factors[30].

In contrast, peripheric proteins are attached to the surface of the cell membrane. Their removal does not disrupt the structure of the lipid bilayer. The membrane-protein interaction can be established directly with the membrane mediated by a covalent link with lipid anchors (such as Phosphatidylinositol 4,5-bisphosphate, PIP2) or with integral proteins[2].

1.3.3. Lipids

Hundreds of different lipid molecules were identified in cell membranes. According to their structure lipids can be categorized into 3 main classes namely, glycerolipids, sphingolipids and sterols.

Glycerolipids are characterized by a glycerol molecule with a phosphate esterified at the α-carbon and two long-chain fatty acids esterified to the remaining carbon atoms (Fig. 3)[2]; examples are phosphatidylcholine (PC) (commonly representing 50% of cell lipids) [31], phosphatidyletanolamine (PE) (constitutes 20% of most membranes), phosphatidylserine (PS) and phosphatidylinositol (PI)[31].

Sphingolipids (SLs), which compose 10 % of membrane lipids [32], are characterized by a sphingoid base (in mammals mainly sphingosine and dihydrosphingosine) connected by an amide linkage to a saturated or unsaturated long chain fatty acid (Fig. 3). Various substituents of the hydroxyl group (OH) of C1 of the sphingoid base are known, like phosphocholine[2, 31]. Ceramide is the simplest SL and constitutes the hydrophobic backbone of all SLs and their glycosylated derivatives, the glycosphingolipids [33]. These are SLs with a sugar moiety linked by a β-glycosidic bound to C1 of the OH group of ceramide, they do not have phosphate and are characterized by presenting mostly saturated acyl

chains [2, 34]. GSLs can be categorized in sub-groups according to the number, type of sugar residues, and the presence of sialic acid or of sulfur (see Fig. 4). Cerebrosides, such as glucosyl- and galactosylceramide (GalCer), are the simplest GSLs composed solely by uncharged ceramide monohexosides. In opposition, the sulfatides may present different number of sugar residues and derive from either GalCer or GlcCer. However, the common feature within this group of GSLs is the presence of sulfur (Fig. 4). Another important group of GSLs is the globosides that may be further sub-divided into Globo-, iso-Globo-, Lacto/neoLacto- and Ganglio-series. The globosides are the product of the sequential addition of other sugars to lactosylceramide (LacCer), which in turn is formed by the addition of a β-galactose to the glucose of GlcCer. The fourth group is the gangliosides. These are the most complex GSLs in which the hydroxyl group of C1 of ceramide is substituted by an oligosaccharide chain containing hexose and sialic acid or neuraminic acid. Depending on the pH, the gangliosides are either neutral or negatively charged, i.e. amphipathic. A representative member of this group is the monosialotetrahexosylganglioside (GM1) [2, 35].

Sterols are derivatives of cyclopentanoperhydrophenanthrene and are characterized by planar and rigid nucleus (constituted by four fused cycles) with substituents above and below the plane. The most representative member of this category in mammals is Chol (Fig. 3)[2] Being the most abundant lipid in the eukaryotic membranes, ranging from 25 to 50 mol % of the total lipid fraction, it plays a crucial role in the physico-chemical properties of cellular membranes[36, 37].
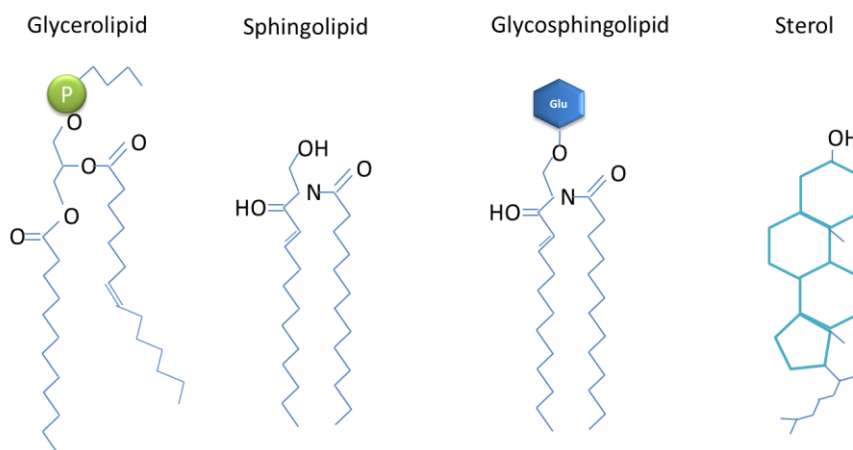
Figure 3 Lipid Classes and Structure.
In mammalian membranes the most abundant lipids are the glycerolipids, particularly PC lipids, which are responsible for the fluidity of the bulk membrane. Sterols constitute ≥25 % of total lipids, whereas

sphingolipids represent 10 % of the total lipids. Both SL and Chol are involved in several cellular processes [32].

2 Membrane lipids and their biological role

It is not possible to separate the evolution of the membrane model concept from the evolution of the role of lipids in the cell.

If at first lipids were thought to be structural components of the membrane, nowadays it is known that lipids have many functions in the cell. Besides from forming the crucial lipid barrier and the matrix of cellular membranes as well as providing the cell the potential for budding, fusion, and fission[31], they are also anhydrous reservoirs for efficient storage of caloric reserves and essential for membrane synthesis, where fatty acid and sterols are needed as components [33]. Additionally, some lipids also have bioactive properties acting as first and second messengers in signal transduction and molecular recognition processes[33, 38]. Lipids can regulate cellular processes through the modulation of membrane biophysical properties, which affects protein sorting and conformation[31, 33, 38]. The properties and functions of SLs and GSLs will be further described in the following sections.

2.1 Sphingolipids

In the past century an emphasis was made in the study of SLs, since several major signaling lipids were identified in this lipid class, such as ceramides, SM and their glycosylated derivatives. All SLs derive from the same molecule, i.e. ceramide. This lipid is formed by linking a sphingoid backbone via *N*-acylation to the C-2 of a fatty acid chain of variable length and unsaturation degree. Ceramide is the hydrophobic backbone of all SLs, which places this lipid in the center of SL metabolism. All other SLs are formed by the attachment of different molecules to the terminal hydroxyl of ceramide (see Fig.4). An example is the attachment of a phosphocholine headgroup, yielding SM; whereas addition of a glucose or galactose moiety is the first step in the formation of GSLs. The reason for the existence of almost countless SLs is yet to be clarified, but it is hypothesized that it might be related to a specific role of each of these lipids, or to the necessity of specific combinatorial patterns that will trigger a specific signaling pathway [39].

2.1.2 Ceramides

Ceramides are central molecules in SL metabolism, in fact, ceramides are a family of different molecules with different acyl chains characterized by different lengths and saturation degree[40]. Its metabolism is complex, involving more than 28 enzymes where are included: 6 different ceramide synthases (CerS), five ceramidases and at least 5 sphingomyelinases. One of the reasons for such redundancy, namely in the CerS, is the specificity that each enzyme has for different acyl chain lengths[40]. Commonly, mammal ceramides present acyl moieties with long chains (16 to 24 carbons) and often saturated. However, specific types of cells also express ceramides with very long and unsaturated acyl chains, such as C28 to C32 with 5 to 6 double bonds in adluminal germ cells and spermatozoa [41]. Besides being the "hub" of SL metabolism, ceramide has other roles in the cell, namely as a key lipid in the modulation of several signaling pathways. Ceramide may regulate cell events by changing membrane properties forming specialized domains which affect protein sorting, diffusion, conformation, etc.[42]; or acting as a second messenger in signaling cascades[43] such as in stress stimuli response [44, 45] or in the tuning of cell processes, i.e. autophagy and apoptosis[46, 47].

2.2 Glycosphingolipids

GSLs are the most structurally diverse class of complex SLs. More than 500 different GSLs have been described, the main sugars being glucose, galactose, fucose, N-acetylglucosamine, N-acetylgalactosamine and sialic acid (acidic GSLs) [39]. GSL are commonly composed by a sphingoid base (mainly with 18 to 20 carbons) and a long, mostly saturated amide-linked acyl chain; the structure of the polar headgroup may vary significantly, ranging from one neutral monosaccharide moiety to big assemblies of carbohydrates and sialic acid, which gives the gangliosides their charged nature[34]. GSLs are normally classified as acidic or neutral[48]. Due to the presence of the sugar moiety, GSLs are mainly present in the extracellular leaflet of the plasma membrane[3]. Although these lipids are minor constituents of the plasma membrane, contributing less than 5% to the total cellular lipid pool[49], they have vital roles in the cell acting both as first and second messengers in several signaling and regulatory pathways[50, 51]. In addition, GSLs are important for membrane stability, permeability[52] and are active participants in crucial cell processes including cell-to-cell adhesion[50], interaction with microbial toxins[39],

modulating immunity response[53], acting as growth factors[54], cell differentiation[55], etc. Lipid glycosylation is also associated with the development of pathologies, namely cancer [54]. The vital nature of GSLs was first identified when null mice for glucosylceramide synthase (GCS), the first enzyme in GSL biosynthesis, died in the embryonic stage [56]. Other characteristic of GSLs is that their profile changes with the age of the cell and/or organism and also with the presence of a pathological state[57, 58, 59, 60].

The *de novo* synthesis of GSLs begins with the formation of GlcCer or GalCer, by the addition of a glucose or galactose moiety, respectively, to the ceramide backbone. Complex GSLs are further synthesized by the consecutive addition of sugar moieties, in the luminal side of the Golgi membrane, by glucosyltranferases, syalitransferases, GalNac transferases and GalCer sulfotransferases (Fig. 4). GalCer is the major precursor of sulfatides, whereas GlcCer is the major precursor of complex GSLs. After their synthesis the majority of GSLs are carried by vesicular transport to the plasma membrane, where they reside and accomplish their functions[49, 61]. The GSLs are afterwards recycled, passing from the PM to the early endosomes and then to the late endosomes/lysosomes, where these molecules are degraded[51].

Since this Thesis is centered in the biophysical properties of GlcCer, the next section will focus on the description of GlcCer synthesis, trafficking, topology and metabolism.
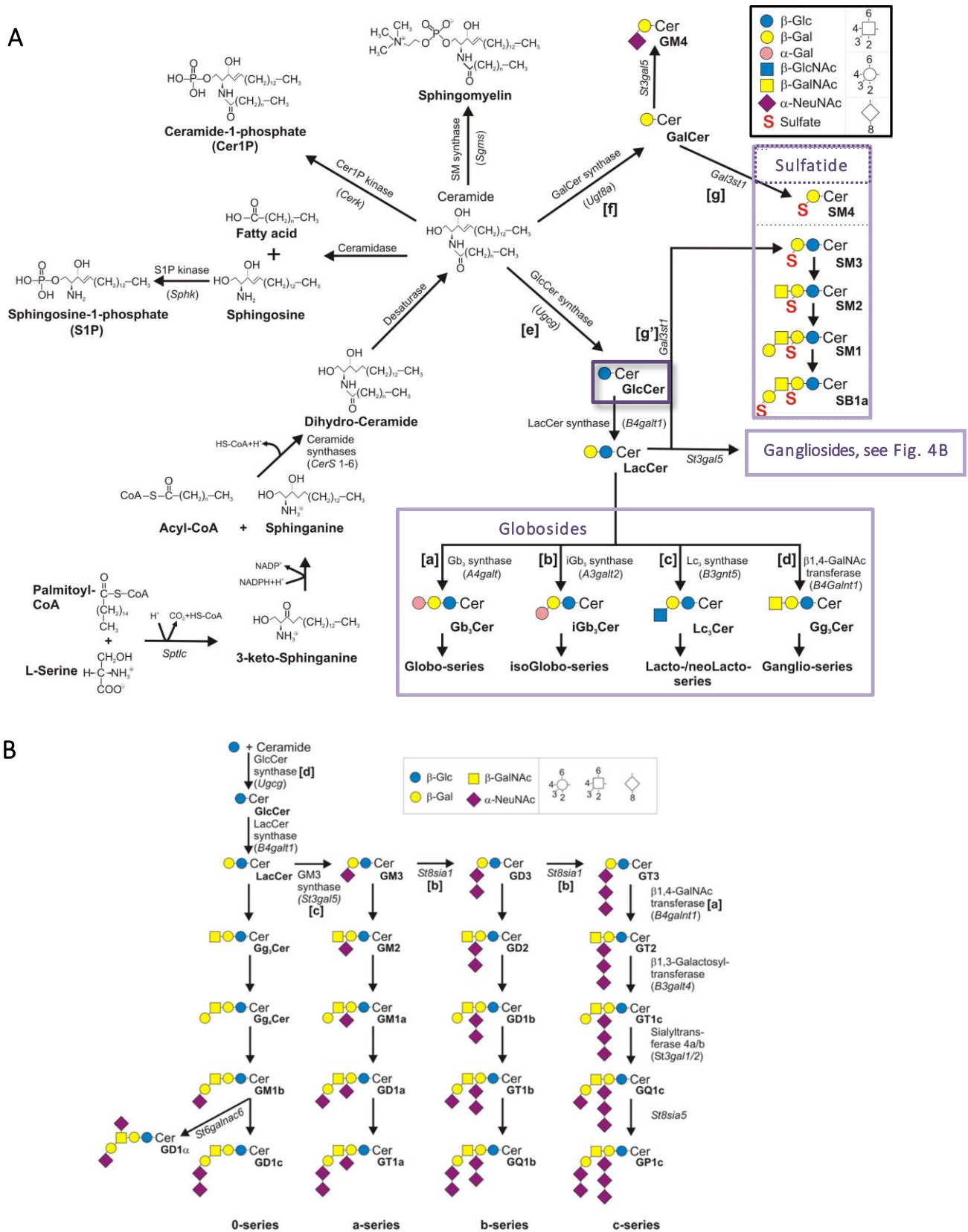
Figure 4 - Complexity of GSL metabolism
Glycosphingolipids is a lipid class with more than 500 molecules. (A) The glycosylation of ceramide forms GalCer or GlcCer (different only by the position of one hydroxyl group in the sugar headgroup). The addition of more carbohydrates forms the complex GSLs such as gangliosides. (B) Descriptive metabolism of gangliosides. Adapted from[62]

2.3 Glucosylceramide

2.3.1 Structure, metabolism and topology.

GlcCer or β-ᴅ-glucosyl-ceramide is the most abundant basic structure in GSLs and it is ubiquitous in mammalian tissues. GlcCer is formed in the cytosolic leaflet of Golgi apparatus by the glycosylation of ceramide via GCS, also known as uracil-diphosphate (UDP)-Glucose ceramide glucosyltransferase. GCS is a 45KDa type III membrane bound protein located in the cytosolic leaflet of *cis*-Golgi[63,64]. In mammals, the ceramide backbone of GlcCer has commonly an acyl chain length between 16 and 26 carbon atoms, however ultralong-chain hydroxyl fatty acids with up to 36 carbon atoms are present in the epidermis[62].

It is worthy to mention that GlcCer is the only GSL that is synthesized in the cytosolic leaflet of the Golgi apparatus, having its carbohydrate moiety extended into the cytosol [65, 66]. After its synthesis, GlcCer is transported to the luminal side of the Golgi, where it is converted into more complex GSLs by two proposed pathways. According to one model, GlcCer is transported from the Golgi to the ER by 4-phosphate adaptor protein-2 (FAPP2) and is flipped to the luminal side by low-specificity phospholipid flippases. From the ER GlcCer returns to the Golgi by vesicular transport. The second model also involves FAPP2, however, in this hypothesis FAPP2 transports GlcCer from the *cis*-Golgi to the *trans*-Golgi network (TGN), to be flipped by an unidentified protein into the luminal side of the Golgi[67]. In addition, GlcCer can be carried to the cytoplasmic leaflet of the PM via a nonvesicular-transport that involves a glycolipid transfer protein (GLTP) and FAPP2[65, 67]. In fact, 45% of all synthesized GlcCer is located in the PM[61]. In this organelle, half of GlcCer remains in the cytoplasmic leaflet and the rest is translocated to the extracellular leaflet for surface expression[68].
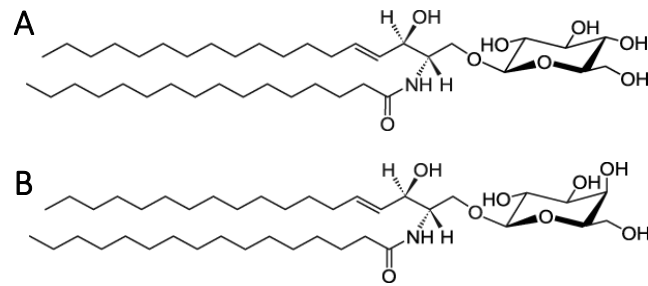
Figure 5 - Structure of cerebrosides.
Structural representation of (a) C16-GlcCer and (b) C16-GalCer. The polar head is composed, respectively, by a glucose or galactose residue attached to the hydrophobic backbone formed by ceramide (adapted from [69]).

Today is accepted that GlcCer should be found in the PM and in the Golgi apparatus (in the cytosolic face). However, evidence shows that GlcCer is present in other organelles, like ER where, potentially, it can be flipped to the luminal side or degraded[67]. In addition, studies made with GlcCer analogues support that this GSL can be internalized from the PM by either endocytic and non-endocytic (transbilayer movement - "flip-flop") pathways and transported to intracellular membranes, such as the nuclear membrane, or transported to the PM of other cells [70]. Furthermore, GlcCer is also internalized from the PM and transported to the lysosome lumen, via endosomal pathway for degradation.

GlcCer is mainly catabolized by the complementary action of an acid β-glucosidase (GCase), a modulator protein (Saposin C) and anionic lipids [71]. GCase is recruited to the lysosome by LIMP-2 (lysosome mempbrane protein-2) [72], and in the late endosome/lysosome, due to the drop in the pH GCase, dissociates from LIMP-2 to associate instead with Saposin C (SAP-C)[72]. SAP-C destabilizes the lipid membrane exposing GlcCer and also directly activates GCase in an allosteric manner, enhancing GCase activity and promoting GlcCer degradation[71]. Furthermore, the presence of anionic lipids, such as phosphatidylserine and phosphatidylglicerol, in the membrane site where the complex of SAP-C and GCase are anchored substantially increases GlcCer cleavage by GCase[71]. Although, the lysosomal route is the mainly studied, GlcCer can also be hydrolyzed in extralysosomal locations through the activity of β-glucosidase 2 (GBA2)[65,67] or of a neutral β-glycosidase (GBA3)[73]. GBA2 is a peripheral protein that catalyzes GlcCer degradation in the ER, in the Golgi [67] and in the PM[74]. The highest expression of this glucosidase is observed in the brain and testis and, in resemblance to GCase, it requires a co-factor and/or to be associated with the membrane to have its activity optimized.

Moreover, the activity of GBA2 seems to be regulated by GBA1[67]. GBA3 is located in the cytosol and it is actually a glycosidase, since it can cleave the link between Cer and different sugars[75]. These three enzymes differ in the optimum pH, cell location, inhibitors and the required co-factors.

From the hydrolysis of GlcCer, β-glucose and ceramide are formed[11, 65] (Fig. 6).
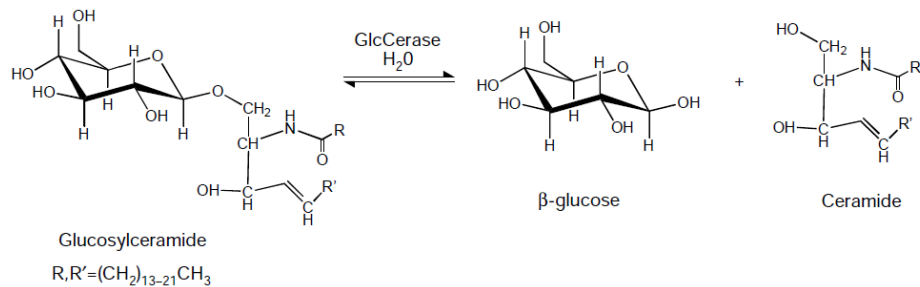
Figure 6 - Cleavage of the β-glucosidic bound of GlcCer by GCase
The hydrolysis of the β-glucosidic link of GlcCer yields ceramide and glucose. Image from [76]

2.3.2 Physiological roles

GlcCer is vital for the cell. This GSL plays a key role in cell maintenance and regulation through different mechanisms: i) modulating the physical properties and physiological functions of membranes[77], ii) being the precursor for more than 300 different species of mammal GSLs, iii) regulating the levels of ceramide, which in turn is also a second messenger implicated in several cell events[78], and iv) acting as an intracellular messenger[48].

Specific examples of some of these mechanism include the increase of membrane order through the formation of strong hydrogen and van der Walls interactions with the neighbor lipids[79]. Additionally, the segregation of GlcCer into specialized domains [79] influences the sorting and conformation of proteins, triggering or modulating cell signaling[77]. The latter mechanism is observed in melanocytes, where GlcCer is involved in melanosome biogenesis [77] and in the modulation of cell trafficking to this organelle. By stimulating the V-type ATPase proton pump and by sorting specific proteins, GlcCer induces the formation of a protein coat that enables vesicle binding to the Golgi and further transport towards the melanosomes[56], allowing the formation of melanine. GlcCer has also an active role in the neurons development, stimulating calcium release from neurons via the ryanodine receptor[80].

GlcCer is further involved in several other biological events such as: regulation of membrane trafficking along the endocytic pathway, which is crucial for the maintenance of membrane functions[81], promotion of cancer cells survival decreasing the Cer pool in the cell [82], spermatozoa development[65], regulation of certain immune responses[48], pathogenicity of microorganism[83], regulation of cholesterol levels and/or cellular distribution[81], regulation of phospholipid synthesis[84], inhibition of the coagulation process[48], etc.

In addition, GlcCer is the major cerebroside outside the central nervous system. In certain conditions, GlcCer can partially replace the functions of GalCer - a lipid with an identical structure, differing only in the spatial position of one hydroxyl group in the sugar head (Fig. 5) - maintaining the tight and compact structure of the myelin sheath [63, 85]. It is worthy to notice that the effect of GlcCer depends both on the cell type[82, 86] and the acyl chain length of this GSL [62, 87].

3 (Glyco)Sphingolipids role in pathological situations

In the last decades, SLs and GSLs have been linked to the development of several diseases, namely immune[88], infectious[89], respiratory, metabolic[51] and neurological diseases (as Parkinson´s disease, PD[90]).

Regarding GSLs, the major attention has been driven towards the complex GSLs, since they were the first to be identified as precursors in the development of different pathologies, such as cancer where increased levels of gangliosides are linked to the severity of the pathology[39]. They are also implicated in infectious diseases, such as influenza[91] and HIV[92] where globosides (e.g. globotriaosyl ceramide, Gb3) and gangliosides (e.g. monosialodihexosylganglioside, GM3) are involved in the viruses internalization. However, in the past decades several studies have reported that the simple GSLs, like GlcCer, also present a major role in the development of human pathologies. This is more evident taking into account that GlcCer regulates several cell processes. Accordingly, if the cell pool of GlcCer is unbalanced, the cell events regulated by this lipid will be affected (see sub-title 2.3.2). Additionally, GlcCer is involved in the pathogenicity of microorganisms that infect humans, enabling the infection and dissemination of *Cryptococcus neoformans*[93]; and the binding of influenza virus with cell

membranes, since it interacts with GM3 to an efficient binding of the virus[94]. GlcCer is also involved in the development of cancer, by promoting drug resistance through the synthesis of complex GSLs[95], diabetes[96], batten disease[97], etc. In addition, the accumulation of abnormal amounts of GlcCer drives significant damages in cells, leading to the development of a metabolic disease - **Gaucher Disease**

3.1 Gaucher Disease

Gaucher Disease (GD) is the most common lysosomal storage disease (affecting 1/40,000 to 1/100,000 individuals) having its higher prevalence in the Jewish population, especially in Ashkenazi Jewish descendant (1/ 1000)[98]. This disease was discovered in 1882 by Dr. Philipe Gaucher, and in 1960's Brady and colleagues reported that it was a metabolic disease[98]. This pathology is caused by an impaired function of GCase (main reason), Sap-C (abnormal juvenile form[99]) or in any factor that interferes with GCase transport along its secretory pathway, leading to cellular accumulation of GlcCer [100]. Although, GlcCer accumulates in all cells, its storage is mainly observed in one cell lineage, i.e. the macrophages. Due to constant phagocytosis of dead cells, the quantity of GlcCer that these cells have to degrade is significantly higher compared to any other cell [101, 102].
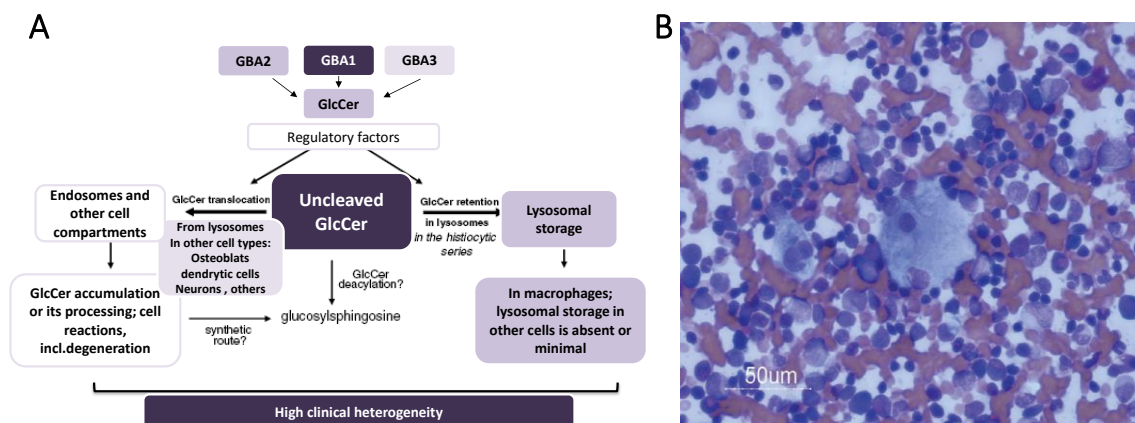
Figure 7 - Biological outcome of GlcCer abnormal accumulation in the cell
 (a) Two scenarios are proposed: either GlcCer is stored in the lysosomes and, in macrophages that will transform into Gaucher Cells as a result of GlcCer accumulation; or GlcCer will accumulate in other cell[103, 104] compartments (like endosomes[105]) where it might be stored or processed to alternative metabolites (other than ceramide and glucose[106]) (adapted from [106]). (b) Image of a Gaucher Cell from the bone marrow of a patient (adapted from [107]).

Accumulation of GlcCer in the lysosomes of macrophages, converts it to storage cells with well-known cytology known as the Gaucher Cells. In addition, GlcCer also accumulates in other cells like osteoblasts, thymic T cells[104] and neurons[103] (Fig. 7). As a consequence, pro-inflammatory responses and altered GSL distribution are observed, ultimately resulting in hepatosplenomegaly, abnormal bone turnover, pulmonary hypertension and, in some cases, central nervous system (CNS) impairment [11, 106, 108]. In non-macrophage cells, GlcCer lower accumulation inside the lysosomes is probably due to residual activity of GBA1, and/or due to an alternative route of processing the excessive GlcCer (Fig. 7). In the last hypothesis non-macrophage cells would be able to transfer GlcCer to extra-lysosomal compartments where it can be processed and/or stored. According to this hypothesis, the biological outcome would be dependent on the cell type, compartment of storage, genetics, and environmental factors, each of them leading to different phenotypes [106]. Such scenario would also explain why there is minor accumulation of GlcCer inside lysosomes besides from macrophages [106]. Other possible explanation for GD clinical phenotypes heterogeneity and the non-correlation between genotype and phenotype is the activity of non-lysosomal glucosidases, such as GBA2[67]. GBA2 influence in GD phenotype is supported by reports that patients with the same GCase mutations have different activities of GBA2[109]. Furthermore GCase crosstalk with GBA2 and other glycohydrolases such as β-galactosidase could be one more factor influencing GD phenotype [67, 109].

Regarding the clinical expression, GD has been divided into three major subtypes, namely type 1, 2 and 3. However, a recent trend considers GD as a continuum of disease states[102]. Type 1 is the most common form of GD and is essentially a macrophage disorder, lacking primary central nervous system involvement. Type 2 is the acute neuropathic form, characterized by neurological impairment in addition to the clinical manifestation observed in GD type 1. These patients usually die until the second or third year of age. Type 3 also presents neurological symptoms but they appear later in life compared to type 2. Patients normally live until their third or fourth decade [102]. In addition, due to the amazing heterogeneity in the GD clinical phenotypes other subtypes of GD were described such as the perinatal-lethal[110] and cardiovascular[111].

GD is a very complex disease, and in the last years several studies report that this disease can affect different systems besides the typical ones, namely the immune system[112] and

bone formation[104, 113]. Additionally GD (namely the GCase mutation) might be a risk factor for the development of other pathologies such as PD[90] .

Nowadays, different treatments like enzyme replacement therapy and inhibitors of GlcCer synthesis are available to all GD patients, however, many of them do not respond to therapy[114]. Since there is no clear justification for the correlation between GlcCer accumulation and the development of Gaucher Disease, and for the high complexity in the clinical phenotypes, different approaches to study this disease need to be developed. For instance a study focused in the biophysical alterations induced by GlcCer could provide new insights into the molecular alterations underneath the deleterious effects of GlcCer accumulation.

Glucosylceramide as a target and tool for the treatment of different diseases

Besides from being involved in the development of several human pathologies (such as cancer[115] and infectious diseases[116]), the control of GlcCer synthesis or degradation is also suggested as a pathway to manage and treat disease[117].

Orally administered GlcCer improves the profile of skin barrier, through the up-regulation of genes associated with either the cornified envelope and tight junctions formation [118]. Another medical application of short-chain GlcCer is in the formulation of nanovesicles, improving the delivery and efficacy of doxorubicin in solid tumors. This probably occurs due to an increase of tumor cell membrane permeability through the formation of channels or by the introduction of lipid packing defects by the short-chain GlcCer, which enhances the bioavailability of doxorubicin in the tumor [119]. Moreover since lower amounts of doxorubicin are needed, the toxic effects are significantly reduced[119]. In addition oral GlcCer inhibits inflammatory processes[120] and even controls the growth of specific types of cancer[121], foreseeing future medical applications for GlcCer .

4 Lipids biophysics − Correlation between biophysics and biology.

The lipid classes (see section 1.3.3) can be differentiated by their distinct chemical structure, which is also a major determinant of how lipids organize in the membrane[122]. The lipid-induced (biophysical) alterations in membrane properties are extremely important in several biological processes. This has been supported by increasing data[56,

[123, 124], which stimulated an extensive research regarding the direct effects of lipids in membranes properties. Stressing the previous idea, today it is a fact that both the biochemistry and the biophysics play major roles in the final biological outcome. Hence, in order to understand a cell response to a certain stimulus, it is necessary to comprehend the chemical and physical alterations behind that process[122].

The biophysical properties of a membrane are determined by its lipid and protein composition, and by the lipid-lipid, lipid-protein and protein-protein interactions. The lipid-lipid interactions are fundamental in governing the global membrane biophysical properties [34, 54, 125, 126]. Lipids are involved in the control of the thickness and packing, i.e. fluidity, of the membrane[127]. This is due to the different lipid headgroup and acyl chain structures, which will determine the interplay of the lipids with the neighbor molecules and thus the properties of the membrane. In addition, the electrostatic charge of the lipids also influences directly the membrane organization. Examples include the anionic lipids that mediate interactions with cationic regions of the membrane associated with proteins and also influence the spatial organization of protein ligands (ex: polyphosphoinositides)[127]. Moreover, lipids can phase separate from the bulk of the membrane, forming specialized membrane domains, which are key players in several cellular processes, for example, recruiting proteins from the cytosol, that subsequently organize secondary signaling or effector complexes[33]. The capacity of lipids to organize in different phases is one of their major characteristics and one of the features that make them unique structures.
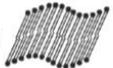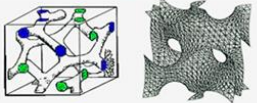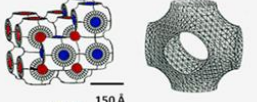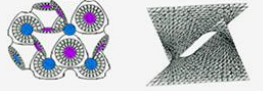
4.1 Lipid-Water systems – Lipid phases

Lipid and water mixtures are polymorphic. Lipids can organize into different lyotropic phase structures depending on the lipid composition, water content, temperature, pressure, ionic strength, pH, shape and dimensions of the lipid molecule[3] (Figure 8). The lipid shape and size are the most critical parameters. Taking the hydrocarbon volume (V), the area of the headgroup (a) and the critical length of the hydrocarbon volume (l) of the lipid, it is possible to define the membrane packing parameter ($P = (V/a*l)$). This parameter can be used to predict which type o phase will be favored for a particular lipid[3] (Figure 8). Practical examples are the lipids that have a cone- (*P>1),* inverted cone- (*P <1/2)* and

cylindrical- (1/2<P<1) shape, which promote inverted hexagonal phases, spherical micelles and lamellar bilayers, respectively[3].

In addition, thermodynamic restrictions also influence how the lipid acyl chain and headgroup will interact with other lipids and aqueous solvent, forming lamellar or non-lamellar phases. Examples of the major thermodynamic driving forces are: i) *van der Waals* forces, observed between adjacent acyl chains), ii) hydrogen bonding, which promote strong interactions between polar headgroups with electronegative atoms namely, nitrogen or oxygen, with an hydrogen and iii) hydrophobic forces, described as a driving force that minimizes the contact between the water and nonpolar portions of a molecule, in this case the lipids acyl chain[3].

The main lyotropic structures formed by lipids in an aqueous environment are divided into two main categories: non-lamellar and lamellar phases. Non-lamellar phases are typically constituted by phospholipids (PLs) with small weakly hydrated headgroups and by SLs, like ceramides. These phases can have different types of organizations, as the inverted hexagonal (H_{II}) where the lipids are packed into cylinders with the polar headgroups facing the inside of the cylinder where there is a column of water. In this hexagonal phase the center of the "tube" is an aqueous channel[3, 128, 129, 130]. Non-lamellar structures are transiently formed in specific organelles (e.g. mitochondria), and are involved in the formation of tight junctions, membrane fusion and possibly in other cell events[128]. Lamellar phases are biologically the most important phases, being responsible for the structure of the lipid bilayer. Within lamellar phases lipids might organize into lipid crystals (crystalline phase), gel (solid-ordered, s_o) and fluid phases[128].

Lattice type	Phase	Nomenclature	Structure
Lamellar	Crystalline	L_c	
	Gel(solid-ordered)	L_β	
	Tilted gel	$L_{\beta'}$	
	Ripple gel	$P_{\beta'}$	
	Fluid (liquid disordered)	L_α	
Hexagonal	Type I	H_I	
	Type II	H_{II}	
Cubic	G (gyroid)	$Ia3d\ (Q_{II}^G)$	
	P(primitive)	$Im3m\ (Q_{II}^P)$	
	D (diamond)	$Pn3m\ (Q_{II}^D)$	

Figure 8 - Nomenclature and schematic representation of some lyotropic phases.
The figure shows different lyotropic phases divided in three main classes depending on the volume occupied by the headgroup and by the acyl chains, which affects membrane organization and biophysical properties. The different classes are characterized by differences in the packing parameter (P), which takes into consideration the hydrocarbon volume (V), the area of the headgroup (A) and the critical length of the hydrocarbon volume of the lipid ($P = (V/a*l)$) [131]. The lyotropic phases are divided in i) Lamellar, represented by different phases including, L_c (lamellar crystalline), L_β, L_β' and, P_β (lamellar gel) and L_α (lamellar liquid crystalline, when $1/2 < P < 1^3$) (adapted from [128]); and in ii) non-lamellar phases such as: inverted hexagonal (H_{II}) when $P < 1$; micellar hexagonal when $P > 1/2$ (H_I) phases[3].; and iii) cubic phases that have high degree of complexity and large variety of forms, here is exemplified three bicontinuos lipids cubic phases with different space groups (adapted from [132]).

- Crystalline phase (l_c)

Several lipids form crystalline lamellar- l_c –phases. These three dimensional structures, and therefore with a real crystal nature, are formed at low temperatures and/or in anhydrous, or in very low water conditions (co-crystallization)[128]. In this phase the saturated acyl chains are in an all-*trans* configuration, thus promoting a very tight packing of the membrane[3]. The lipid headgroud normally lies flat in the plane of the bilayers, and

if possible establishing intermolecular hydrogen bonds[3]. Nonetheless, if the polar headgroup is bulky, packing problems may arise, and changes in the membrane organization may occur[3].

Some lipids, when incubated in water at low temperatures, adopt the so-called subgel phases, which are lamellar stacks of two-dimensional crystalline bilayers. In a few cases, namely in membranes with charged lipids like phosphatidylglycerol, the crystalline bilayers can be swollen apart in water by electrostatic repulsion[128].

- Gel or Solid phase (l_β)

This phase is usually formed at low temperatures and requires the presence of water. The minimum water content to consider fully hydration of the bilayer on the gel phase depends on the lipid headgroup size, polarity and charge, but is usually low. In this type of phase, the hydrocarbon chains are ordered in an all-trans conformation and slow rotation along the long-axis occurs. The headgroups are normally disordered and the rate of lateral diffusion is very slow (typically 10^{-3} μm^2 s^{-1})[33, 128]. In the gel phase, the hydrocarbon chains are, as mentioned, predominantly in an all-trans configuration where the cross-sectional area is minimal (each chain presents a cross-sectional area of ≈ 20 Å^2) and the bilayer thickness is maximal (corresponding to the length of a fully extended chain, e.g., ≈ 45Å nm for palmitoyl chains). The headgroups and the hydrocarbon chains are closely packed. In this phase, the acyl chains are perpendicular to the bilayer surface for lipids with small headgroups (e.g., PE, ≈ 39 Å^2) and tilted for lipids with larger headgroups (e.g., PC, ≈ 50 Å^2) in order to optimize the packing [3, 128,133]. In addition, at a certain range of temperature ripple phases may form. These metastable phases, characterized by deformed lamellae resembling ripples with a wave-like appearance in electron microscopy, can occur in the interval of the pre- and main transition temperature[3, 134] of lipid membrane. Therefore the lipid gel-phase comprises different "sub-types" of organizations; the L_β (gel), L_β' (tilted gel) and P_β (rippled gel)[128].

- Fluid phase (l_α including l_d and l_o)

Fluid phases are the most representative lipid organization in biological membranes. In a fluid phase the water content increases, the interfacial area per molecule expands, and

the bilayer thickness decreases relatively to the gel phase. There is a considerable disorder in the acyl chains and lateral diffusion is increased (typically $\approx 10^{-11}$ m^2 sec^{-1}) [3, 128]. Lipids are able to move with considerable freedom in the plane of the membrane parallel to the membrane surface, but in a direction perpendicular to the membrane surface lipids cannot translate extensively. The lipids are therefore not in a true liquid state in which their movement would be isotropic, but in a two-dimensional fluid. Within fluid phases the degree of conformational freedom defines two other phases: liquid-ordered, commonly formed in the presence of cholesterol (l_o,), and liquid-disordered (l_d) phases [135].

In the fluid phase (l_d), the rotation around each C-C bond (*trans-gauche*) is rapid and the number of gauche configurations increases. The introduction of a gauche bond induces a kink in the chain similar to those observed in unsaturated chains mainly with *cis* double bonds. These kinks lead to an increase in the cross-sectional area of the hydrocarbon chain (from a minimum of ≈ 19Å^2), a decrease in bilayer thickness, for e.g., from ≈ 45 Å in the gel to ≈ 35 Å in the fluid phase for palmitoyl chains, and provide structural discontinuities in the bilayer in which small molecules can reside [3]. The separation distance between the headgroups in the fluid phase is higher as compared to the gel phase, and water molecules are required to act as spacers or to bridge between adjacent headgroups, resulting in a higher hydration of this phase [3]. Due to this higher separation distance and the increase in the cross-sectional area of the chains, the fatty acyl chains of lipids are arranged parallel to the bilayer surface and even for lipids with larger headgroups the chains do not need to tilt[3].

The l_o phase is characterized by relatively high lateral diffusion in a very similar diffusion rate as it occurs in the l_d, however slower, and a tight lipid packing resembling the gel phase. Therefore it is an intermediate state between the l_d and the gel phases. These intermediary properties are commonly promoted by the presence of Chol[136, 137, 138]. The l_o has been indicated as the putative "raft" phase[138, 139]. Since raft domains, normally characterized as domains enriched in Chol and SLs[140], have been linked to several cell events further attention will be given regarding the structure and the biological role of these domains (see section 7.2).

4.2 Lipid phase transitions (phase diagrams)

The lipids phase transitions (e.g. from gel to l_d) may be induced by an alteration in several factors that have an impact in the lipid-lipid or in the lipid-water interaction, such as pressure, temperature, solvent ionic strength and pH. Although normally biological membranes do not evidence a bulk alteration of phase transition, it may occur transiently, due to the segregation of lipids into organized domains[141], the study of lipid phase transitions may provide further information about the behavior of particular lipids or lipid mixtures that are present in cell membranes. The most studied transitions are between the gel and fluid phases, and the most commonly researched transitions are the thermally induced. These type of transitions are normally studied using differential scanning calorimetry (DSC)[3].
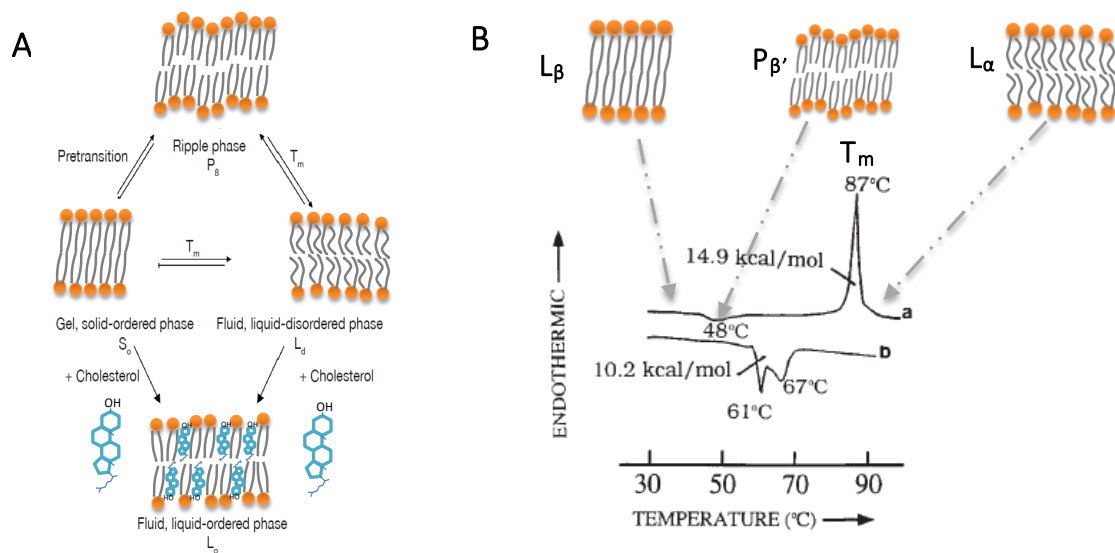
Figure 9 - Lamellar phase transitions
A-Scheme illustrating the different lamellar physical states adopted by a lipid bilayer in aqueous medium (adapted from[36]). B- DSC of hydrated C16-GlcCer (a) initial heating scan (b) cooling scan (adapted from[142]).

DSC enables to monitor the changes in the physical state undergone in a pure or lipid mixture due to temperature alterations. A DSC thermogram reports the transition enthalpy of the sample (ΔH), which represents the actual heat required for the entire transition, and also informs about the heat capacity (C_p), which corresponds to the amount of heat required to raise the temperature of the sample in 1 degree Celsius of the studied lipid or lipid mixtures[3]. Figure 9 depicts a DSC thermogram of pure C16-

GlcCer. In the figure, the specific heat, referred as *Endothermic*, is plotted as a function of temperature. A peak in the specific heat is an indication of a phase transition. In this case, two peaks are detected corresponding to the pre-transition and main transition, which correspond to a transition between two gel states and between gel and fluid phase, respectively. The main transition, T_m (temperature where 50% of the transition is complete), occurs in all lipids, whereas the pre-transition is usually found in lipids with bulky polar headgroups like GSLs. The pre-transition is characterized by a change in the tilt of the hydrocarbon chains and a melting of the headgroups, with a concomitant increase in the superficial area due to the formation of a ripple phase [3, 143]. Theoretically, the T_m should appear in the DSC thermogram as a spike at a determined temperature, however, due to the presence of impurities in the lipid sample, the phase transition is often spread over a width of few degrees. Moreover, the T_m of a lipid is the result of a balance between different factors, such as the conformation of the acyl chain (*gauche* or *trans*) or the presence of double bonds[3].

In the case of the study of a lipid mixture, due to structural differences between the lipid molecules, the transition from gel to fluid phase is not direct. Between the two opposite phases, there is a broad range of temperatures where two or more immiscible phases coexist, depending of the number of lipids [144]. The phases could be gel and fluid or two different gel phases[144, 145]. These complex transitions can be schematically represented by phase diagrams (Figure 10).

Besides DSC, other techniques sensitive to alterations in the lipid phase, can be applied to define the boundaries of a phase diagram, such as fluorescence spectroscopy[146] and H^2-NMR[147]. The thermal-induced phase transitions of different pure or lipid mixtures can provide further information about the behavior of such molecules in more complex systems.
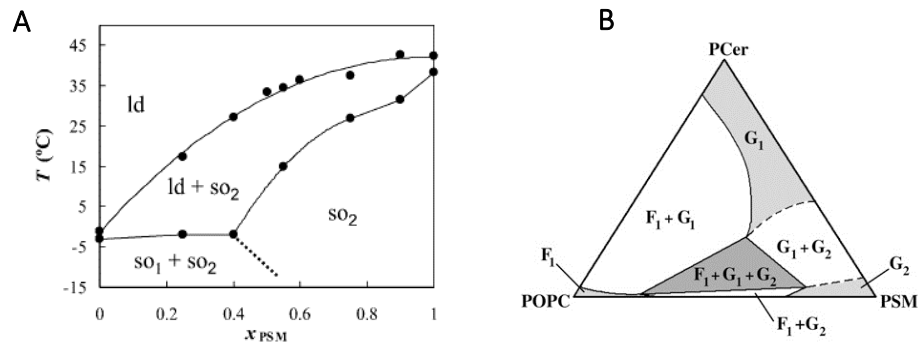
Figure 10 - Lipid phase diagrams

A-binary phase diagram of POPC/PSM (adapted from[148]) and B- ternary phase diagram of POPC/PSM/PCer ternary phase diagram at 24°C (adapted from[146])

4.3 Membrane dynamics– Fluidity concept

Cellular membranes are very dynamic systems with constant lipid and protein movement[36]. However, their diffusion is not free and different lipid phases present various diffusion coefficients, implying that, depending on the membrane order, lipids and proteins will have their diffusion more or less restricted. The concept that qualitatively defines the average movement resistance in the membrane is its "fluidity"[3]. The degree of freedom of the lipids and proteins movement is directly related to it: the lower the fluidity the higher the membrane restriction to lipid and protein diffusion. Lipids can undergo different types of movement in a cell membrane (Figure 11): the lateral diffusion that defines the ability of a lipid to exchange position with its neighbor (duration < 1 min); the rotational movement, the most frequent type of diffusion, which determines the angular rotation of the lipid around its axis perpendicular to the plane of the bilayer (duration in the range of nanoseconds); conformational changes (duration in the range of picoseconds), namely *trans-gauche* isomerization that in consequence could have an impact in the lipid order of the membrane; and transversal diffusion, commonly known as flip-flop, where the lipid moves from one membrane leaflet to the other, in a timeframe that ranges from seconds to days depending on the lipid structure. For instance Chol takes less than one second to undergo flip-flop, due to its small polar headgroup, restricted to one hydroxyl group[3, 36], while PC requires more than 12 hours to flip-flop between the two leaflets, due to its large headgroup [149, 150]. Additionally,

proteins can also laterally diffuse in the membrane, however, with a much slower velocity compared to lipids[36].

Furthermore, the evaluation of membrane fluidity is commonly done by the analysis of small molecules incorporated in the membrane - the spin or fluorescent probes (see section 9). Several parameters of these probes are quantified by spectroscopic techniques, namely the steady-state anisotropy (or polarization) of fluorescent probes. Nonetheless these studies have limitations that could introduce bias in the interpretation of the results, such as preferred sites of the probe to interact with membrane (e.g. domains, near proteins), and also the fact that the bilayers are not a 3D homogenous liquid, presenting variations in the order from the center (acyl chains) to the surface (polar headgroup)[3]. Therefore, fluidity as unique parameter is not enough to characterize the physical state of a membrane, however, is useful to follow alteration in the membrane state due internal or external factors (e.g. lipid content and temperature, respectively).

Since in membranes (especially in models), the fluidity is strongly related with the lipid packing, any factors that alter lipid interaction will affect the fluidity of the membrane[3]. In addition, taking into account that several cellular processes are dependent of membranes, the physical state of cell membranes is tightly regulated. For example, some microorganism when exposed to abrupt changes in temperature, modify the lipid content of their membrane to keep its basal fluidity[151].

Biological membranes are normally in a fluid phase (l_d or l_o). Until some years ago, one of the dogmas about membranes referred that the gel phase was incompatible with the proper function of proteins, due to the high packing and therefore was not found at least in eukaryotic cells[3]. This inference was challenged by the identification of gel domains in the membranes of *Saccharomyces cerevisiae*[152] and in HEK cells[153].
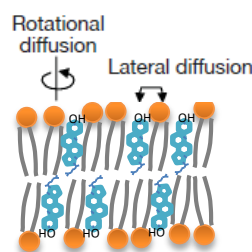
Figure 11 - Types of lipid diffusion in the membrane

The lipid diffusion (i.e. flip-flop), the activity of ATP-requiring enzymes and the packing forces are some of the factors determining the different curvatures of the inner and outer surfaces of the bilayer and concomitantly the heterogeneous distribution of lipids in the membranes. The flip-flop allows to transport lipids with large glycosylated head groups to the extracellular environment and keep the anionic lipids on cytosolic leaflet of the plasma membrane. Lipid asymmetry is not strictly conserved and varies between different cell types and activity states[154, 155].

Taking into consideration that in the previous sections the information regarding lipid phase organization and transition was given in a general manner, not making any extensive characterization to any lipid, in the following topics the specific biophysical properties of SLs and GSLs (especially GlcCer) will be described.

5 Biophysical properties of Sphingo- and Glycosphingolipids

5.1 Sphingolipids

Ceramide is the backbone of all SLs and therefore understanding of its biophysical properties is essential to comprehend of the biophysical features of more complex SLs. In the next section a description of some of ceramide characteristics will be described.

5.1.2 Ceramide

As referred in section 2, ceramide is a critical lipid in the maintenance of normal cell function. This is in part due to the complex and multifactorial membrane alterations induced by ceramide. Factors such as ceramide structure, membrane lipid composition and membrane properties strongly influence the effect of ceramide in membrane biophysical properties[156]. Ceramides with different acyl chains will promote distinct biophysical alterations in the membranes[157], which is probably related to their functions in the cell[40]. In fact different tissues have different CerS expressions and therefore are enriched in different types of ceramides [158].

One of the most evident biophysical properties of ceramide is the capacity to segregate into highly ordered gel phase in a variety of lipid mixtures[159, 160, 161]. This characteristic is mainly due to the strong hydrophobic nature of ceramide (very small polar headgroup

combined with the typically saturated long acyl chain) and also to its ability to form strong intermolecular interactions (ceramide acts as both an electron donor and acceptor for H-bonds)[161, 162]. The previous facts also explain ceramide very high T_m, e.g. 94.1°C for C16-Cer[163]. The extreme order of ceramide-induced domains is evidenced, for example, by the exclusion of probes that typically partition into the gel phase[146, 159, 160]. Moreover, not only ceramides segregate into high ordered domains but also increase the packing properties of the fluid phase, even when present in very small levels[157, 160].

Furthermore, membranes containing ceramides often display coexistence of multiple phases[147, 148] which reflects the complex polymorphic phase behavior and the tendency of this lipid to form metastable phases[161] that are illustrated as complex phase diagrams [162, 164, 156]. Moreover, due to its cone shape structure ceramide induces a tension in the membrane promoting a negative curvature. This bending destabilizes the bilayer and might increase transbilayer lipid movements and transition into nonlamellar inverted hexagonal phases[129, 165, 166]. This has high biological relevance, since the formation of nonlamellar phases could be underneath ceramide-induced membrane internalization (e.g. endocytosis), and intramembrane efflux[130, 167, 168]. Additionally, ceramide ability to regulate membrane packing [160, 169], influence membrane lateral organization, and promote the formation of domains [170, 171, 172] has remarkable biological implications[173]. One example is the modulation or triggering of cell events, which is based on the incorporation or exclusion of proteins and lipids from ceramide-containing domains[156].

Nonetheless, it needs to be stressed that the biophysical impact of ceramide is strongly dependent on ceramide acyl chain structure: unsaturated ceramides, such as C24:1-Cer or N-oleoyl-D-erythro-sphingosine (C18:1-Cer), induce a lower membrane packing compared to saturated ones[156, 157, 162]. In addition, asymmetric ceramides are involved in the formation of interdigitated gel phases[157, 162, 174], meaning that the presence of these ceramide species in one leaflet may interfere with the packing properties and organization of the other leaflet. This certainly affects cell events that occur in the opposing leaflet[156]. Interdigitated gel phases formed by ceramides might also underlie the ability of these ceramide species to form tubular structures [157, 162].

Furthermore, studies with model membranes have shown that the biophysical impact of ceramide is altered depending if it is generated in *situ* or if this SL was already mixed with the other membrane lipids. The differences are mainly in how ceramide distributes in the

membrane. In raft-like membrane models with premixed ceramide, it is observed the formation of uniform ceramide-enriched gel domains surrounded by l_o regions, whereas ceramide generated by sphingomyelinase induces the formation of heterogeneous ceramide-rich gel domains mainly located at the boundaries of the l_o regions[175, 176]. Moreover, taking into account the strong intermolecular forces that characterize ceramide, it is not surprising that the nature of the neighbor lipids will affect its biophysical behavior. Depending on the surrounding lipid structures, ceramide-induced ordering effect in the membrane can be enhanced (e.g. by SM) or in contrast perturbed (e.g. by Chol)[146, 177, 178, 179]. Evidencing this effects are studies performed in POPC/SM/Chol raft-mimicking membranes showing that ceramide affects the packing properties and lipid lateral organization of these mixtures, particularly when the l_o fraction, and thus, the Chol content is low [177, 178]. This can be related to specific interactions that occur between ceramide and SM that enhance the ability of the SLs to segregate into gel domains[177]. In opposition, ceramide becomes more miscible in the l_o phase when the fraction of this phase is increased [177]. Nonetheless, the effect of ceramide on the packing properties and lateral organization of these mixtures is more pronounced than of other SLs such as sphingosine (Sph), which is related both to the ability of ceramide to drive more tightly packed gel domains and to its high immiscibility in the fluid phase[,156, 160, 173, 177]. The countless factors that affect ceramide impact in membrane biophysical properties suggests that there is a fine balance between a physiological and pathological effect of ceramide.

5.2 Glycosphingolipids

In this section a general description of the biophysical properties of GSLs is presented. From the hundreds of different GSLs, biophysical studies in membrane models have only been made in a few representative species like, GM1, GM3, LacCer, GlcCer and GalCer [34]. All GSLs share a sugar headgroup as a common characteristic, which is also what differentiates them from other lipids. The carbohydrate nature of the headgroup carries with it all the complexity of the interactions among sugar groups [180]. An example is the hydration profile, which is characteristic and distinct for GSLs, SLs and PLs. The hydroxyl groups present in the sugar headgroup strongly interact with water molecules forming a

water shell around it. In addition, the average size[181] of the carbohydrate moiety and the packing properties of the membrane[182] are directly influenced by this water shell[156].

GSLs are molecules that act both as hydrogen bond donors and acceptors, undergoing side-by-side (*cis*) interaction based on the presence of the hydroxyl and acetamide group, this strong interactions promote a tight packing between GSLs and other lipids which segregate from the membrane bulk forming domains (namely "rafts" and glycosynapses) [54, 156, 183, 184].

Clustered GSLs may interact with various functional components on cell membrane, such as integrins, growth factor receptors, tetraspanins, and non-receptor cytoplasmic protein kinases (for e.g., Src family kinases, small G-proteins) to form glycosynaptic domains controlling GSL-dependent or -modulated cell adhesion, growth, and motility [54].

The high hydroxylation present in the GSLs sugar headgroup stabilizes the interactions between these and the neighbor lipids by intensifying the number of strong hydrogen bond interactions, leading to a higher T_m in comparison to PLs and other SLs [156, 182]. Moreover, smaller GSLs have higher T_m values due to tighter lateral packing density in membranes [34], whereas larger headgroup have the opposite effect [185]. Long chain GSLs present a complex mesomorphic behavior with high chain melting temperatures and irreversible transitions between different stable and metastable gel phases, probably due to chain interdigitation (mainly in asymmetrical species) and to alterations in the hydration profile of GSLs [34, 186, 187, 188]. In addition, it is worthy to stress that GSL-containing domains typically exhibit characteristics of a gel-phase[79] and are largely influenced by their high T_m[189]. The latter features are also the cause for GSLs phase separation from membranes enriched in PLs[156, 190, 191]. The GLs segregation can occur into domains containing only GSLs or other lipids such as SLs and Chol stabilizing them against temperature dissociation[79, 156]. The hydration profile has also a relevant impact in the T_m of GSLs domains, for example negatively charged GalCer sulfatides have lower T_m compared to the lipid from where they derived, GalCer, which is related to the higher hydration of sulfatides since the water molecules increase the size of the headgroup disturbing the membrane packing [34]. In addition, the hydration degree can define the stability of the domains formed by sulfatides[34]. Moreover, charged GSLs, namely sulfatides and gangliosides, can form stable ordered domains in the presence of counter ions like calcium, which reduce the repulsive forces or increase the attractive

intermolecular interactions between the GSLs molecules within the plane of the membrane[34, 192]. Another factor that disturbs the biophysical properties of the domains containing GSLs, mainly of the charged ones, is the environment´s pH [193, 194]. Furthermore, both the ceramide backbone and the sugar headgroup structure, which may be charged, will determine GSLs partition between different phases[195]. Additionally, in cellular membranes the GSL-protein interactions will also certainly influence the lateral segregation of these lipids [34].

Moreover, it is described that, in opposition to ceramides, GSLs stabilize the lamellar phases, blocking the conversion to nonlamellar structures (mainly inverted hexagonal phase, H_{II}), which results in the inhibition of membrane fusion[156]. The stabilizing effect of GSLs is based on the cylindrical or inversed conical shape depending on the size of the headgroup of these lipids, and it is potentiated by the negative charge of gangliosides and sulfatides[196] (Figure 12). These observations justify why GSLs are so important in the control of membrane stability.

Another important feature to take into account about GSLs is the sugar headgroup chirality. This property influences the size and shape of the GSL-containing domains. It potentiates the formation of non-flat membrane domains, caveolae, membrane budding and flasky bodies expanding from the membrane or digging into it[156, 197]. Moreover, GSLs asymmetrical species, in resemblance to Cer, promote alterations in membrane morphology, such as the formation of tubular structures[156, 198]. The tubular protruding could be consequence of transbilayer acyl chain interdigitation promoted by the very long asymmetric acyl chains.[199]. Furthermore, the tubules observed in GSL-containing mixtures may also arise from metastable tilted structures such as macro-ripple phases[198] and from molecular chirality, which increases the bending force [156, 200]. In addition, other factor that induces the formation of tubules in GSL-containing mixtures is the alteration of environment properties, namely by changing the solvent nature from an aqueous to a non-aqueous one[199, 201, 202]. This phenomenon occurs likely due to perturbations in the superficial tension of the membrane[156,190, 192, 193].

Summarizing, GSLs are complex molecules, with very particular characteristics that define how these lipids exert some of their roles in the cell. In the next topic it will be described the biophysical properties of cerebrosides.
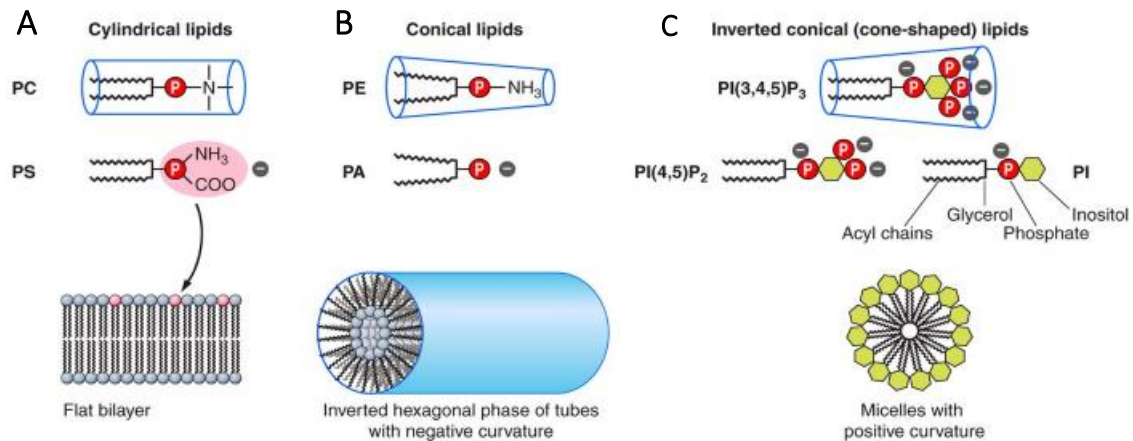
Figure 12 - Membrane induced-curvature by lipids
Schematic representation of the correlation between lipids shape and membrane organization. A - Lipids with a cylindrical shape (e.g. phosphocholine) promote a neutral membrane curvature of the membrane and thus promote an organization into lamellar phases. B- Lipids with a cone shape induce a negative membrane curvature (e.g. ceramide), driving the formation of nonlamellar phases such as H_{II}. C- The lipids with an inverted cone shape (e.g. GSLs and other lipids with larger headgroups) promote a positive membrane curvature inducing the formation of micelles (adapted from[203]).

6 Cerebrosides biophysical properties

Cerebrosides, which are the simpler GSLs, comprise two constituents GalCer and GlcCer. Although the last two molecules only differ in the spatial position of one hydroxyl group, their biophysical and biological profile is substantially different [79]. Notwithstanding, some of their properties are still similar. An example is their thermotropic behavior. Cerebrosides display a high T_m, 85°C to C16-GalCer and 87°C for C16-GlcCer, and a complex thermotropic phase behavior, which consist in multiple transitions between different stable and metastable phases[142]. In resemblance to ceramides, the thermic transitions are influenced by the acyl chain of the cerebrosides and by the type and number of sugar residues [142, 204] (see section 5.1). These features also influence the interaction of GSLs with other lipid components, and their effect on membrane biophysical properties.

Studies in artificial membranes have shown that GlcCer and GalCer, have different capacity to form and to be incorporated into bilayer ordered domains[79]. These properties are significantly affected by the nature of the interaction between cerebrosides and neighbor lipids[79, 180]. Furthermore, either GlcCer or GalCer can increase the order or phase separate from fluid membranes into cerebrosides-enriched highly-ordered gel

domains[79] . Nonetheless, domains enriched in GalCer are thought to be more stable, due to a high efficiency of the hydrogen bonding network with the surrounding water molecules, and between the hydroxyl groups from opposing GalCer molecules [182, 202]. In addition, Mannock et al. reported that glycerolipids containing galactose and glucose headgroups have different impact in domain stability [205]. The latter study is in agreement with previous observations regarding GalCer and GlcCer interactions, describing a larger extent of hydrogen bonding in galactoglycerolipids compared to the glucoglycerolipids [205].

Moreover, the differences in the interplay between GalCer and GlcCer with other membrane lipid components were noticed in studies conducted in more complex model membranes. For example, GSLs are capable to segregate into GSL-enriched domains in which Chol is miscible when the membranes also contain SM [34]. However, the miscibility of GSLs with cholesterol is dependent of the GSL structure. For instance while C16-GlcCer accommodates some sterol at low temperature, C16-GalCer presents a very low association with Chol-enriched domains[79]. In addition LacCer, which has an additional sugar residue than cerebrosides (Figure 4), interacts easily with Chol showing that the headgroup size does not compromises this association[79]. Nevertheless, the tight packing observed in domains enriched in saturated mono and di-glycosphingolipids hinders the incorporation of Chol into these domains [79]. The different miscibility of Chol into GSL-containing membranes might correlate with Chol role as a modulator of membrane fluidity [79, 206].

Summing up, cerebrosides, although structurally quite similar, have different biophysical properties that are in need of further research to provide a more detailed characterization of the biophysical behavior of these two molecules.

Some of the biological roles of GlcCer are linked to the involvement of this lipid in the formation of domains containing other lipids, like Chol or SM- raft like domains, and specific proteins[207, 208].

Thus, it is important to explore in more detail the possible factors that influence the size, shape and packing of such domains. Moreover, the role of such lateral separation (including domains containing GlcCer) will be further explored in the context of membrane regulation.

7 Lateral heterogeneity in membranes - Membrane domains and cell regulation

7.1 Domains Shape and size

The main factors that drive SLs and GSLs to phase separate into domains (with different properties from the membrane bulk) were previously described (section 5). However, the forces and factors that influence domains shape and size need to be clarified. The shapes and the sizes of SL-enriched domains are defined by a conjugation of different factors, including the balance between the domain line tension and dipole-dipole repulsion. If the dipole-dipole repulsion is stronger than the line tension, flower-shape domains are formed, if the opposite occurs round-shaped domains are predominant[209]. The balance between these factors is dependent on the type of phases forming the interface of the domains. Accordingly, flower-, polygonal- or linear-shape domains are typically observed when gel-fluid (*gel*/l_d) phases coexist[171, 210, 211], as in mixtures of phospholipids with Sph [212, 213], SM[214], different acyl chain ceramides[157], and cerebrosides[210] (Figure 13). Round-shape domains result from fluid-fluid (liquid disordered (l_d)/l_o) phase separation[171], such as observed in diverse mixtures containing Chol and SM (e.g. POPC/SM/Chol, DOPC/SM/Chol)[148, 215] and also in more complex mixtures containing Sph (POPC/SM/Chol/Sph)[212] or ceramide (POPC/SM/Chol/Cer)[159] (Figure 13).
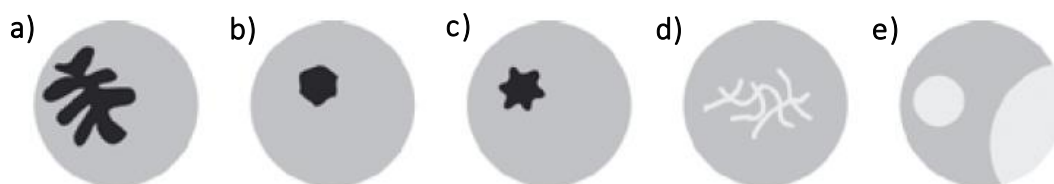
Figure 13 - Different shapes of membrane domains
Types of membrane domains that can be found in model membranes a) dendritic, b) and c) polygonal or star –like, d) linear and e) Circular or round. Adapted from [211]

Since membrane domains are maintained through strong hydrogen bonds among lipid headgroups, van der Waals interactions between the hydrocarbon acyl chains and electrostatic repulsions between the lipid dipoles[216], several external factors that perturb these interactions, namely alterations in the pH, might disturb the SL-containing domains

size and shape (Fig. 14). This is important, considering that these alterations occur under physiological settings. One example is the endocytic pathway, where the pH values range from ≈7 in the PM to ≈5 in the lysosome[217, 218] Fig. 14). The lipid domains that have their biophysical properties more susceptible to alterations in the pH are the ones containing charged or zwitterionic lipids, namely sulfatides[194] and SM[219], respectivelly.
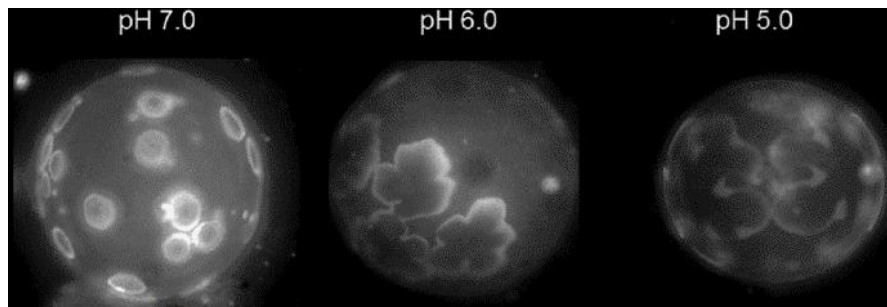
Figure 14 - pH modulation of domains shape and size.

The pH impact is shown in vesicles composed by saturated PLs and Chol, adapted from[216]. In this specific lipid mixture (DOPC/DSPS/Chol), the increase of the environment acidification contributes to a tighter lipid packing in the domains, that at pH 5.0 acquire a flower shape which is typical of the l_d/*gel* phase boundaries.

7.2 Biological relevance of lateral heterogeneity induced by SLs –Lipid Microdomains

It is a fact that lipid and proteins in mammalian cells can organize into morphological distinct domains, like the apical and basolateral domains in the plasma membrane of endothelial cells [138]. However, the existence of specialized membrane domains, known as rafts, is still generating a lot of controversy. The original raft hypothesis refers to domains that are enriched in Chol and SLs, and present an organization typical of a l_o phase (Fig. 15), meaning that these domains have a higher order than the bulk of the membrane. Extensive studies in model membranes, with different lipid compositions, support the existence of phase separation into l_d and l_o domains, further confirming one of the premises of the raft hypothesis, i.e. that lipids can drive the formation of membrane domains in the absence of proteins[220, 221]. The other premise gives proteins (some of them signaling molecules) different affinities for the different types of membrane phases, with some presenting a higher partition to the l_o (typical of rafts) and others to the l_d phase. Thus, rafts would be involved in cell sorting, trafficking and also in

the cell signaling[221]. The higher partition of some proteins to the raft domains also facilitates some protein-protein interactions, increasing signaling efficiency[220]. Therefore, the original definition of lipid rafts described it as a 'preferential packing of SLs and Chol [results] in moving platforms, or rafts, onto which specific proteins attach within the bilayer' [18]. However, the acceptance of cell rafts is still generating controversy. Its definition was firstly vague and rafts structure was based in the characterization of DRMs (detergent-resistant membranes domains)[221], which in turn had their composition influenced by the detergent selective extraction of lipids and proteins from the membrane, leading to misinterpretations[138, 221]. Another important problem was the impossibility to confirm the existence of raft domains in cell membranes with imaging techniques. This might be due to the very small size of raft domains, under the diffraction (resolution) limit of optical microscopy ≈200–300 nm[220]. The technological development, e.g. photo-activated localization microscopy (PALM), stimulated emission depletion (STED) and structure illumination microscopy (SIM), detected cell domains with very small sizes (10-200nm), but also introduced new concepts into the original rafts hypothesis. Namely, the influence of these domains in protein diffusion, the highly dynamic nature of rafts interacting with several cell elements such as the cytoskeleton, which is now also known to have an active part in the formation of rafts during signaling (Fig. 15) events[220]. Therefore, rafts are now defined as 'small heterogeneous, highly dynamic, sterol- and SL-enriched domains that compartmentalize cellular processes'. Small rafts can sometimes be stabilized to form larger platforms through protein-protein and protein-lipid interactions. [222] Thus, rafts are much more complex than just membrane phase separation into domains. Moreover, evidence showing that other lipids, such as ceramide [223] and GSLs[50] are able to form lipid domains suggests that non-cholesterol rafts may also exist [220]. Even though there is still considerable controversy regarding the existence and involvement of rafts in the modulation of several cell events and signaling pathways, an increasing number of studies support the importance of lipid domains in membrane organization into functionally distinct compartments[18, 33, 124, 224, 225, 226, 227, 228]. Some examples of these cellular processes include endocytosis[229], membrane fusion (e.g. by the sorting of soluble N-ethylmaleimide-sensitive-factor attachment protein receptor, SNAREs[230]), cellular trafficking[227], apoptosis[231], cell sorting (e.g. of specific membrane protein for the activation of T-cells[232]), and cell migration (e.g. in neuronal cell lines[233]),

etc. Additionally, rafts were also related and implicated with the development of different pathologies, such as Alzheimer´s Disease[234], cancer[235] and infectious diseases[236, 237]. Moreover, the pack defects formed in the boundaries between different membrane phases (e.g. between l_d and l_o) facilitate different cell processes, namely the activity of some proteins, pore formation and lipid flip-flop[3], further suggesting that phase-separation occur in cells.

One of the new challenges regarding rafts is the analysis of the fraction of the l_o phase in a membrane. This phase may occupy the majority of the membrane forming a percolating phase where the l_d is the actual domain, in opposition to the current paradigm. This new hypothesis would explain why some non-raft proteins are also found in clusters, namely due to restricted membrane fraction at l_d phase[220]. Therefore, more studies are required to obtain additional information about the biogenesis of membrane domains, namely rafts.
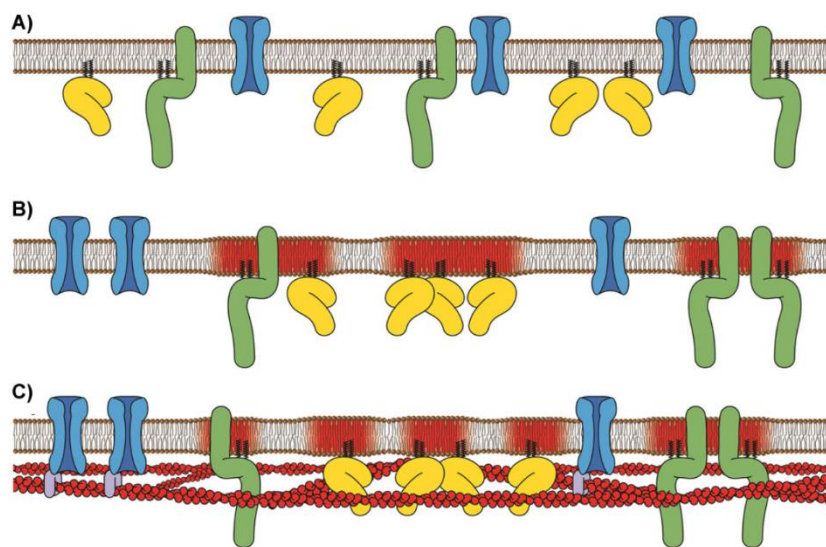
Figure 15 - Evolution of the concept of raft domains and membrane organization
A) In the FMM model (prior to the evidence of membrane lipid aggregates) proteins were randomly distributed in the bilayers; B) the first definition of rafts proposed that proteins were sorted by the formation of large lipid platforms; C) the current best model to describe membrane and rafts organization, and the interplay between membrane proteins with rafts (now recognized as small and dynamic structures) and with the cell cytoskeleton (adapted from[220]).

Regarding GlcCer, as described in sections 6 and 2.3, it is able to segregate into membrane domains [79], and GlcCer-containing domains are involved in the modulation of several cell processes, namely cellular trafficking[81], thus further supporting the involvement of this GSL in the formation of rafts and other biologically active membrane domains. In addition, it is also known that GlcCer affects Chol levels and its distribution in

cells[81], which could reflect GlcCer importance in the modulation of raft properties. Furthermore, the few biophysical studies that addressed the interaction of GlcCer with Chol, reported that GlcCer enriched domains incorporate very low amounts of Chol[206]. This weak interaction was further reported by Maunula et al[79]. However, the addition of other bioactive lipids like SM in the membrane, improved the ability of GlcCer to interact with Chol[79], suggesting that this interaction is dependent on the neighbor lipids. Therefore, understanding the interplay between Chol and GlcCer might shed light into the impact of this lipid on membrane properties and organization, as well as in membrane associated events.

Moreover, the involvement of GlcCer in the modulation of membrane domains formation and properties might be linked to the development of GD. Since that very high GlcCer levels are found in GD patient´s cells, e.g. the temporal lobe of a GD type 2 patient has 10 times more GlcCer than a healthy person[80], studies analyzing the effect of pathological amounts of GlcCer in the membrane biophysical properties, could provide valuable information into the molecular mechanisms that are involved in the development of this disease.

8 Membrane model systems

It is very difficult to directly study in a cell membrane the biophysical effect of a particular lipid. Therefore in order to evaluate the biophysical behavior or the effect of a particular lipid in the properties of a membrane with a defined composition, it is necessary to simplify the complexity of the studied membrane. Therefore, *in vitro* mono- or bilayer lipid structures were developed as a tool to study the individual role and properties of cell membrane components in detail[238]. However, one of the most criticized limitations of model membranes, is related to the lack of cell membranes complexity[36, 239]. The simplicity of model membranes could provide data that could not be extrapolated for the context of a cell[36]. Nevertheless, studies report that membrane models are good predictors of what occurs in a biological membrane [240, 241].

There are 3 main membrane model systems: i) Monolayers; ii) planar bilayers; iii) liposomes and vesicles[3]. I will focus on the model membranes i) and iii), since these are the ones used in this thesis work.

8.1 Monolayers at an air-water surface or Langmuir Films.

Lipids and other amphiphilic molecules, when in contact with an aqueous solvent, form an oriented monolayer with the polar portions (headgroup) facing the water and the apolar (acyl chains) fraction facing the air (Langmuir films). The lipid monolayer or Langmuir film is insoluble in the sub-phase, which is driven by the very low interactions mostly of repulsive nature between the lipid and water[3]. A Langmuir film can be obtained by dispersing a lipid mixture solubilized in a very volatile organic solvent[3]. The studies in monolayers are useful to obtain information about lipid-lipid, lipid-air, lipid-protein interactions and other parameters that drive lateral processes in the membrane, and it also enables the study of the association of different molecules with the membrane[242]. The use of a monolayer, instead of liposomes, has several advantages, such as the control of several parameters that affect lipid structure including lateral pressure and packing state. Additionally, the exact spatial localization of the monolayer at the water-air interface allows the application of imaging techniques that identify and characterize lateral phase separation (in lipid based mixtures), and also recognize protein-lipid interaction sites[242]. One of the main disadvantages is the absence of a second layer, as in the natural membranes, precluding the study of processes that only occur in a bilayer[243]. The study of the monolayers behavior is commonly performed in a Langmuir balance or trough. In this equipment the most frequent study involves the analyses of the variation of the area of the monolayer with pressure (pressure-surface-area isotherms), for more details see section 9.1.

8.2 Liposomes and Vesicles

The first liposomes where described in 1965 by Bangham and colleagues, and were defined as an artificial microscopic lipid bilayer that encloses a central aqueous compartment[244, 245]. Like in the monolayers, the acyl chains of the lipids are protected from water and the polar headgroups are exposed to the aqueous solvent. Due to the higher hydrophobicity of lipids a spherical bilayer, i.e. a liposome, is formed. This occurs since the sphere is the most stable thermodynamic structure, shielding the bilayer acyl chains from the water. Liposomes are very versatile structures, which can be useful either for research (study of membrane biophysics, targeted drug delivery, etc.) or for industrial

purposes (cosmetics, food technology, etc.)[245]. Liposomes can be classified according to their size and number or bilayers (lamellae) (Fig 16A).

-Small unilamellar vesicles - SUVs

These are vesicles with a size ranging from 20 to 100nm[3, 246]. SUVs can be formed by sonication of lipids in an aqueous solution; by an injection of an ethanol lipid mixture into an aqueous solution or even using a French press[3, 245]. Normally these techniques provide a population of vesicles with small and homogenous diameter. SUVs are advantageous, for example, to prepare supported lipid bilayers [247]. Nevertheless, the very small size and high curvature of these vesicles leads to difficulties in the packing of the lipids. Due to the very high membrane curvature, the area occupied by the outer lipid layer is 2x larger than the inner leaflet, thus inducing lipid asymmetry between the bilayers[3]. If the SUVs are stable, i.e. if they do not fuse, the small size of the vesicles could be an advantage making them less prone to light scattering artifacts [248].

-Multilamellar vesicles- MLVs

These vesicles present several lipid bilayers (onion-like structure). Since the size of these vesicles is not controlled in their production, the particle size distribution is high. These vesicles can be prepared by thoroughly drying the appropriate lipid mixture and hydrating the thin film with the appropriate buffer. After the hydration, micrometer MLVs are spontaneously formed[245]. Additionally, several freeze-thaw cycles can be applied to the sample, this step increases the number of unilamellar vesicles, improving the quality of the posterior analysis [249]. The use of MLVs is advantageous due to the very easy production and by providing a good reproducibility in large scale production[250]. The disadvantages are related to several lamelae present in these vesicles (precluding the study of some membrane processes such as permeability and fusion)[250] and to the existence of residual lipid particles with different sizes, which might affect the experimental results[245].

-Large Unilamellar Vesicles- LUVs

These type of bilayers are used in several studies such as, in the development of drug delivery systems. In addition, LUVs comprise one of the most advantageous membrane

model to use, due to its easy production, high reproducibility, stability, size and unilamellar nature[250, 251].

These are basically very similar structures to the MLVs, however, with only one membrane bilayer[245]. These model membranes are also more stable than SUVs[250]. There are several techniques to prepare LUVs, such as detergent dialysis, infusion and reverse evaporation, and extrusion of previously prepared MLVs through a polycarbonate filter, yielding a very homogenous population within the size range of the pore of the filter commonly 100nm[3, 252].

Although less critical than in SUVs, LUVs still have a significant membrane curvature, that is not representative of the cell membrane curvature, which is near zero[251]. In addition, LUVs are not large enough to address lipid phase separation. Hence, other type of model membranes like the giant unilamellar vesicles[253], are required for microscopy studies.

Giant unilamellar vesicles- GUVs

In order to image membrane shape and phase separation, it was necessary to develop bigger vesicles with curvature and size resembling a cell membrane[253] (Fig. 16B). These model membranes can be labeled with numerous probes [254]. GUVs can be formed, among other techniques, by electroformation (with platinum or Indium tin oxide) and gentle hydration[253]. Electroformation is a very expedite technique to produce GUVs. A very small volume of the lipid mixture is spread on platinum wires, which are posteriorly immersed in aqueous buffer allowing the film to swell. An electric field is then applied to the sample, promoting fluctuation in the bilayers, enabling its detachment of the electrode and the formation of lipid vesicles[253]. The vesicles produced by electroformation are larger than the ones produced by other techniques[245, 253]. The vesicles produced in the platinum wires, are freely moving in the solvent. The mobility of the vesicles could bring some problems in qualitative (making it difficult to obtain a good image) and quantitative analysis (compromising the measuring of membrane domains size) done in such models. This problem can be easily overcome by the addition of biotinilated lipids in the lipid mixture and covering the well surface with avidin[254], or by adding a solvent with higher density than the solvent used to form the vesicles, driving the vesicles to sink in the bottom of the support[157].

Membrane models are characterized by several parameters, namely lipid composition, average diameter, size and zeta distribution in the total vesicle population[3]. In the present work, the vesicles were also characterized by their packing properties and phase separation (see section 9 for more information about the characterization techniques).
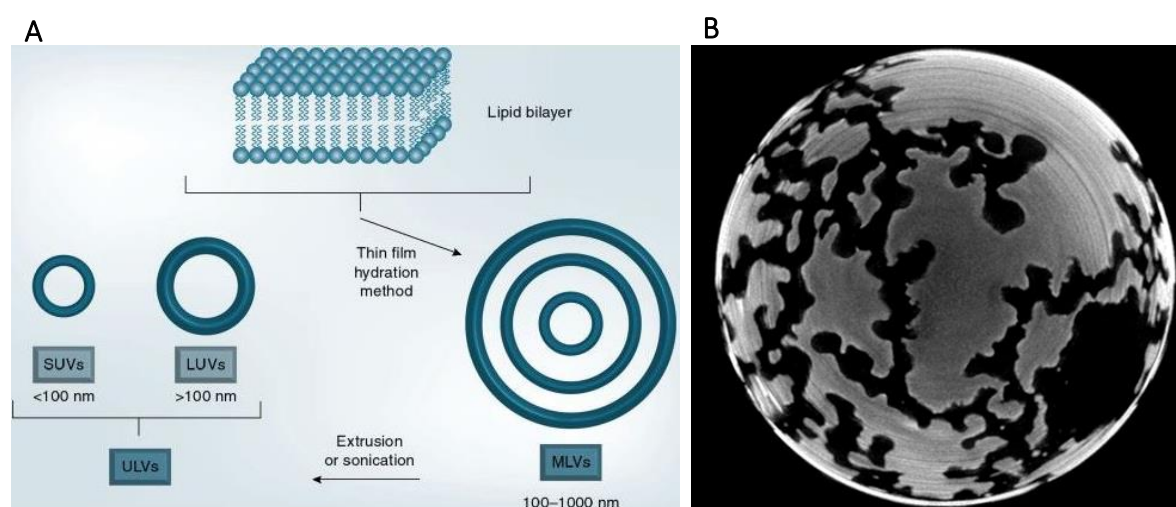
Figure 16 - Membrane Models
A- Schematic Representation of different membrane models (adapted from [246]). B- 3D confocal image of a GUV displaying gel/l_d phase separation, these model membranes generally measure more than 1μm (adapted from[255]) .

9 Membrane Characterization

Several techniques are available to characterize the membrane models or cells. Examples of such techniques are: DSC, Langmuir balance, Spectroscopic and microscopic techniques (confocal, atomic force microscopy (AFM), fluorescence correlation spectroscopy (FCS), FLIM and Förster Resonance Energy Transfer (FRET). According to the chosen technique, which is dependent on a specific parameter, an adequate membrane model must be selected. GUVs are the best models for confocal microscopy and for other microscopic techniques, MLVs are adequate for spectroscopic studies. In the following paragraphs, attention will be focused on the explanation of the methods used in this thesis.

9.1 Characterization of Monolayers- Langmuir balance or trough

A lipid monolayer spread (with the help of a solvent) in a liquid sub-phase is frequently defined as a Langmuir film. The characterization of such films is classically studied in a Langmuir balance. This equipment comprises a trough that is filled with the appropriate

sub-phase, by barriers that control the pressure added to the membranes and a movable float that monitors the surface area of the monolayer. By varying the pressure (π) applied to the membrane, a pressure-area isotherm is determined for the lipid sample (Fig. 17). From the isotherm it is possible to obtain different parameters, namely membrane compressibility[3]. Typically, in an isotherm the evidence of discontinuities, due to phase transitions, are observed as the monolayer is organized under pressure. When low pressure is applied the membrane behaves as a two-dimensional gas phase (the lipid molecules are not interacting) or as a liquid phase (the molecules start to interact), and in a maximum pressure a solid phase is observed (lipid molecules are completely organized). Right after the maximum pressure is obtained the membrane collapses, and the pressure applied to the membrane is no longer controlled. Moreover, the larger the lipids the higher is the minimal surface area[3, 256].

If the monolayer is transferred to a solid surface, this is described as a Langmuir-Blodgett film (in the case of vertical deposition) or Langmuir-Schaefer film (in the case of horizontal deposition)[256]. Moreover, the characterization of the monolayer can be further described, attaching a Brewster Angle Microscope-BAM to the Langmuir trough, providing real time imaging of the monolayer surface (e.g. existence of domains, shape, size)[257]
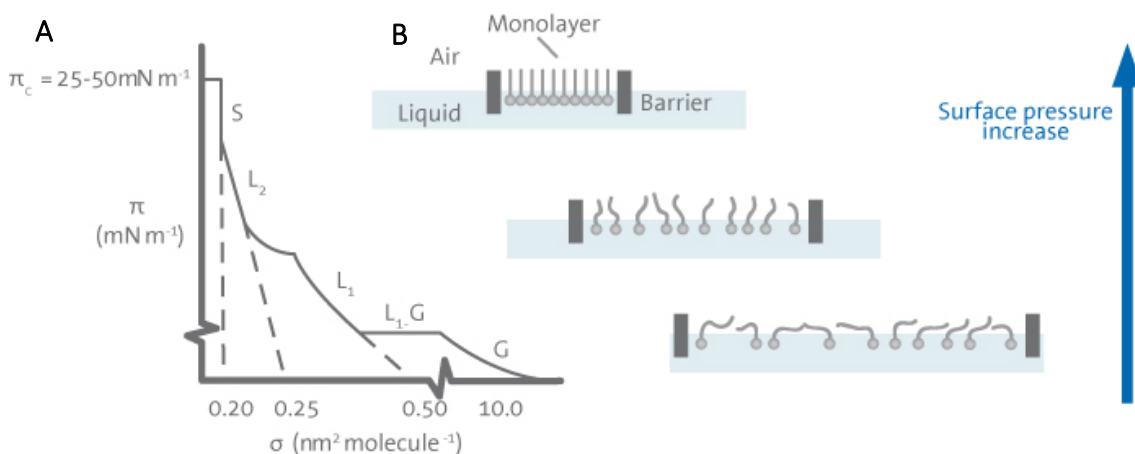
Figure 17 - Characterization of monolayer in Langmuir Through.
A- Surface area-pressure isotherm of a Langmuir film. At lower pressures the monolayer is in a gas phase (G), increasing the pressure the film behaves as a liquid phase (L) or as a solid phase (S), at maximum pressure the film collapses. B- Monolayer organization with different applied pressures[256].

9.2 Electrophoretic and scattered light measurements

These techniques determine the size and surface charge of the analyzed vesicles.

Dynamic Light Scattering (DLS)

Using the Stokes-Einstein equation that correlates the particle size with particle motion, it is possible to make a measurement of particles size in a suspension or emulsion. The Brownian motion of the vesicles in the sample makes the laser light to be scattered with different intensities. The determination of the particle size is based on the correlation between the alteration of light intensity and the particle Brownian movement velocity. Using these two conditions in the framework of the Stokes–Einstein equation is possible to determine the particle size[258]. The particles analyzed by this technique can range from liposomes to molecules[258].

Electrophoretic light scattering (ELS)

Other parameter that is critical in the characterization of vesicles is their electrophoretic mobility, which is directly related to the vesicles zeta potential. Normally a positive or negative zeta is preferred, since it prevents the coalescence of the vesicles and in consequence the formation of aggregates[259].

9.3 Microscopy

Confocal Microscopy - Confocal Laser Scanning Microscopy (CLSM)

Confocal microscopy allows an image acquisition free of focal signals (in this case fluorescence). This is achieved by illuminating the sample with a focused laser beam and using a pinhole aperture in the image plane in front of the photon detector. In this thesis work, only fluorescent samples were used, however, confocal microscopy can also be used for reflective samples. This microscope can be attached with different components, which enhance the quality of the image (e.g. Nipkow disk) or that allow the quantitative analysis of different parameters (e.g. FLIM set-up), however further technical information regarding this subject will be focused on the modulus used throughout this work.

In confocal microscopy, a stepper motor that changes the microscope focus in small steps along the *z*-axis enables the acquisition of a stack of images, at different focal planes. The software of the instrument can stack the captured z-series and constructs a 3D projection of the analyzed sample. Using probes with different colors and affinities for different lipid

phases or cell organelles, allows the follow-up of the model membrane or cell properties and dynamics, in a point or along a certain time.

A brief description will be made about the optics and electronics parts of this equipment. [260].
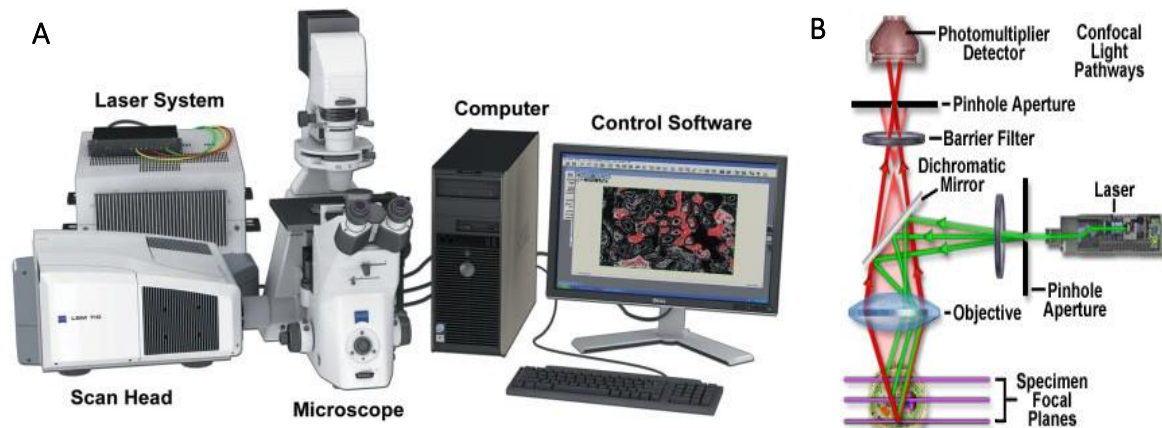
Figure 18 - Confocal laser scanning microscope (CLSM)

A – Basic components of a CLSM (adapted from[260]) . B- Principle of confocal microscopy (adapted from [261])

A confocal microscope is an integrated system with a fluorescence microscope (commonly inverted microscope), multiple laser lights sources, a confocal scan head with optical and electronic equipment (where a pinhole with different apertures is localized), a computer, a monitor for display and software for acquiring, processing and analyzing images (Fig. 18A). Through the computer control a scan head scans a sample with the beam of light from the laser system. At the same time, the scan head also directs the signal from the sample to the pinhole and photomultiplier tube (PMT) (Fig. 18B). The pinhole is a central piece in the confocal microscope, since it excludes the fluorescence signals that arrive from out of focus point, and also the stray light in the optical system. Due to the optical diffraction or resolution limit (200-300nm[220]), qualitative and quantitative analysis performed by confocal microscopy is limited to elements with larger size than the diffraction limit, such as bacteria. Thus, this technique provides information about membranes morphologies, existence of domains and domains sizes and shapes with size >200-300 nm.

Quantitative techniques could complement the confocal microscope, as FRET and FLIM, improving the sample analysis.

9.4 Fluorescence Spectroscopy

The spectroscopic analysis of fluorophores incorporated in membranes, enables the determination of several biophysical properties of the samples in study. Frequently a combination of several probes with different lipid phase partition properties are used. The multiprobe approach enables a detailed analysis of the biophysical behavior of the membranes under study[146]. The different photophysical properties of the fluorophores are used as a fingerprint of lipid phases[146]. In addition, the photophysical characterization of the probes can be carried out by steady-state or time-resolved fluorescence methodology.

Regarding this dissertation, the spectroscopic approaches involved the determination of fluorescence lifetime of the intensity decay, the steady-state anisotropy and the fluorescence emission and excitation spectra of the fluorophores. These concepts will be further developed throughout the next sections.

Fluorescence Lifetime of the Intensity Decay

The fluorescence lifetime of the excited state of a fluorophore is given by the average time (normally within the range of picoseconds or nanoseconds) that the molecule stays in the excited state prior from emitting a photon and returning to the ground state[262]. Lifetime is a statistical average since fluorophores emit randomly through the decay. In other words, some fluorophores will emit almost instantaneously after being excited and others will emit a photon at longer times. This time distribution of emitted photons corresponds to the intensity decay. [262]

The fact that the fluorescence lifetime is independent of the fluorophore, but sensitive to several environmental factors including temperature and polarity, makes this suited to study lipid phase separation[263].

When the lifetime decay is only described by a single exponential, the fluorescence lifetime is obtained directly from the time-dependent intensity (Eq. 1):

$I(t) = I_0 \exp(-t/\tau)$ Eq.1,

where I_0 is the intensity at time 0, and the lifetime (τ) is the inverse of total decay rate. Therefore, the fluorescence lifetime can be determined from the slope of I (t) Vs t, or by fitting the suitable model (time-domain measurement)[262]. However, the fluorophores commonly have a complex decay described by multiple exponentials, and therefore a multi-exponential decay is applied. In this model the intensity decay is assumed as a sum of individual single exponential decays. This is the case of the probes used in this work, like *t*-PnA and N-rhodamine-dipalmitoylphosphatidylethanolamine (Rho-DOPE) that have intensity decays with 3 to 4[177] and 2 to 3[264] exponentials, respectively. Furthermore, probes that partition into more rigid environment will present longer lifetimes then when they are in more fluid environments. This is due to the probe restrictions, which decrease the non-radiative relaxation leading to an increase in the fluorescence lifetime[262, 263]. This is probe dependent, and changes in probes' lifetimes must always be analyzed in relation to the probes' own photophysical characteristics, e.g. propensity to undergo static or dynamic self-quenching[262, 264], phase partition behavior and membrane properties.

Fluorescence excitation and emission spectra

The emission and excitation of a probe reflect the properties of the environment in which the probe is inserted, which can be reported as an alteration in the fluorescence intensity (Fig. 19) (e.g. rigidity of the environment, solvent polarity), or in a shift of the maximum of excitation or emission spectra [262]. For example the quantum yield of *trans*-Parinaric Acid (*t*-PnA) increases significantly when the probe is inserted in a very ordered membrane, as in gel phases. Therefore an increase in order of the environment surrounding *t*-PnA is followed by an increase in the probe fluorescence intensity[265].

Shifts in the spectra are reported, for example, by probes sensitive to environment polarity such as 6-dodecanoyl-2-dimethylaminonaphthalene (Laurdan) (solvatochromatic probe). Which is reflected by a shift in the maximum emission to higher wavelength as the polarity of the medium increases [266]. This occurs since Laurdan presents a dipole moment, between the 2-dimethylamino and the 6-carbonyl residues (in the naphthalene moiety), that increases when this probe is excited leading to the reorientation of the surrounding solvent dipole. This is a consuming energy process, which decreases the excited energy of the probe, driving a red shift of the maximum emission wavelength (solvent relaxation) [266, 267]. Since Laurdan´s naphthalene moiety is

located near the glycerol backbone of the lipid bilayer, therefore in the vicinity of the aqueous environment, it makes this probe sensitive to the bilayer hydration, and in consequence to the lipid phase. When the membrane is in a fluid state (i.e. with higher water content) the solvent relaxation occurs in a higher extent driving a red shift of the probe emission. In opposition, if the probe is inserted in tightly packed membrane, the low amount of water molecules is not enough to cause a decrease of the naphthalene energy, occurring a shift to lower wavelengths[266] (for more details see section 9.5).
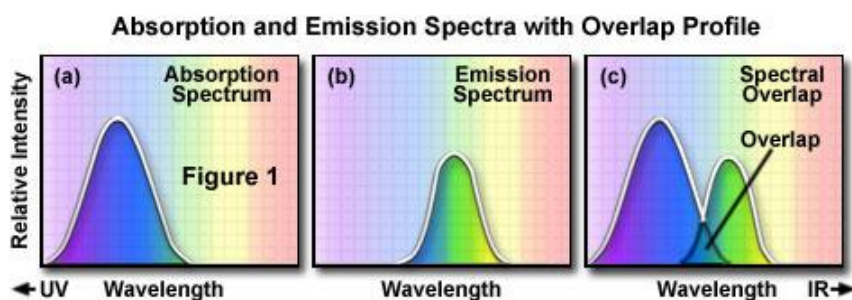
Figure 19 - Excitation (or absorption) and Emission spectra

Representation of the (a) Excitation and (b) Emission spectra of a hypothetic probe. (c) Overlay of the spectra (adapted from[267]). The fluorescence spectra and steady-state anisotropy can be acquired in a spectrofluorimeter[262]. To determine the fluorescence emission spectrum, the wavelength of maximum excitation (commonly the same as the absorption maximum) is usually used. Then the distribution of emission intensity is acquired. Moreover the excitation spectrum is determined in a similar manner; setting the maximum emission wavelength (previously defined), the fluorophore is excited through consecutive wavelengths and the dependence of emission intensity is acquired [262].

Steady State Fluorescence Anisotropy

Anisotropy measurements provide information about protein shape and size, but also about the rigidity of molecular environments[262]. This parameter is based on the principle of photoselective excitation of fluorophores by polarized light (Fig. 20). The probe has a higher ability to absorb photons that are parallel to its transition moment (which as a defined orientation in respect to molecular axis)[262]. Upon excitation with polarized light, only the fluorophores with a parallel dipole with the electric vector of excitation will absorb the photons. The selective excitation results in a partial polarized fluorescence emission. The photons emitted upon excitation of the probe by the polarized light are measured by two linear filters, namely parallel and perpendicular to the direction of the polarized light excitation. The intensities of the emitted light are used to calculate the anisotropy[262]:

$$<r> = (Ivv - G * Ivh)/(Ivv + 2G * Ivh)$$ Eq.3,

I_{VV} and I_{VH} are the emission intensities measured parallel and perpendicular to the vertically polarized excitation, respectively. The G factor is the ratio between the intensities at parallel and perpendicular orientations to the horizontally polarized excitation, thus, G is a setup correction factor for the different sensitivity of the equipment for emitted light at different polarizations[262].

There are several factors that can decrease the anisotropy from its maximum value (0.4), being the probe rotational diffusion one example. If a probe is in a very fluid environment it can freely rotate, which means that upon excitation the emitted light is randomly oriented. In consequence, probes that are in non-viscous environments have very low anisotropies (approximately 0)[262]. In opposition, at more viscous environments (such as in the gel phase) the rotational diffusion of the probe is slower and higher anisotropy values are obtained. Therefore, anisotropy is a sensitive parameter towards lipid organization, reporting with accuracy membrane packing. Moreover, other factors that perturb the rigidity of the environment, namely temperature, will also affect the value of anisotropy.
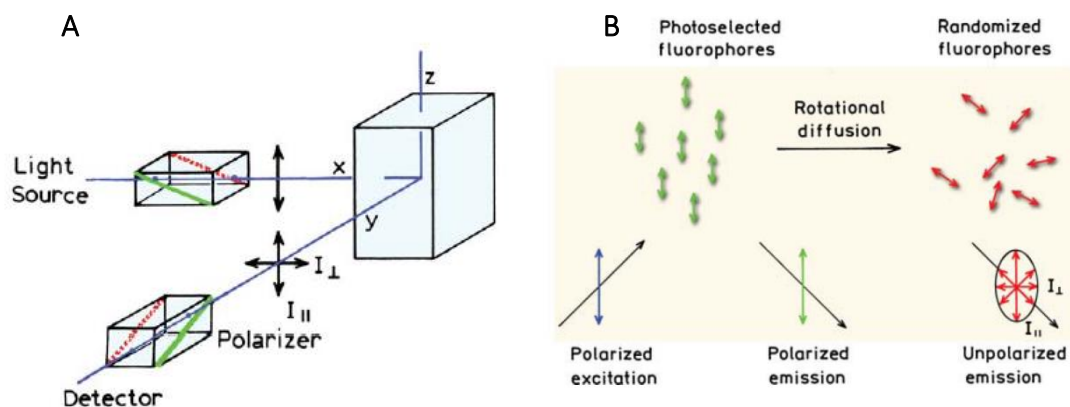
Figure 20 - Anisotropy measurement

A- Schematic representation of the determination of fluorescence anisotropy. B-Impact of the polarized excitation and the rotational diffusion on the anisotropy (polarization of the emission),(adapted from[262]).

Additionally, other non-radiative events can also influence the probe anisotropy, such as Förster Energy transfer (FRET)[262]. This process is based in the transfer of energy from one probe dipole, donor, to other dipole of the same (homo-FRET) or of a distinct probe (hetero-FRET), acceptor. In order to occur FRET, it is essential that the emission spectra

of the donor overlaps with the excitation spectra of the acceptor, the donor and acceptor must be in close proximity (20 to 60 Å), and the donor and acceptor transition dipole must be nearly parallel[262]. For example, Rhodamine-DOPE is a probe that extensively undergoes homo-FRET since it has a small stokes shift, high molar absorption coefficient and high quantum yield[264], enabling a high efficiency of energy migration. In an environment rich in l_o or gel domains, from where Rho is excluded[264], these probe is limited to a small area where the efficiency of energy transfer increases[264], thus Rho anisotropy is expected to decrease when a membrane contains larger fractions of l_o or gel domains[264].

9.5 Fluorophores

The previous referred microscopy and spectroscopy techniques commonly require the use of fluorescent probes, a significant number of fluorophores are available. The selection of the adequate probe depends on the experimental settings. The fluorescent probes used in membrane biophysical characterization have different characteristics and can be divided into three main classes: i) probes that label specific lipid molecules of the membranes[268], ii) probes that rely on the selective partition into distinct membrane phases and/or that are sensitive to alterations in the membrane packing[269], and iii) probes that are sensitive to the environment hydration or dipolar moment[270, 271]. The probes used within the framework of this dissertation include molecules of the two latter classes, namely the t-PnA[269], 1,2-dipalmitoyl-sn-glycero-3-phosphoethanolamine-N-(7-nitro-2-1,3-benzoxadiazol-4-yl) (NBD-DPPE)[272], 1,6-diphenyl-1,3,5-hexatriene (DPH)[273], Rho-DOPE [264] and 6-dodecanoyl-2-dimethylaminonaphthalene (Laurdan)[270], the only solvatochromatic probe used in this work.

The t-PnA and DPH are lipophilic probes. In the first case, t-PnA is very sensitive to local density of lipid bilayers, namely it presents a high partition to and a high quantum yield when in gel domains, which makes this probe suited to identify this tightly packed domains[265]. Moreover, this probe is able to partition into very rigid domains, such as the ones formed by ceramides, from which the majority of probes is excluded[177, 265, 274]. In addition, the steady-state anisotropy and quantum yield of this probe is significantly higher when it is inserted in a solid lipid membrane, which makes t-PnA an excellent probe to detect the gel phase, even when in lower fractions[160, 269]. This probe intensity

decay is described by 3 or 4 exponentials, and the longest lifetime component reflects the order of the highly packed domains[177]. In contrast to the great potential that this probe shows for cuvette spectroscopic studies, t-PnA is not suited for optical microscopy due to the excitation and emission in the UV range[275]. DPH is a probe that partitions equally between l_d, l_o and *gel* phases[139], nonetheless, in the l_o and *gel* phases DPH reports higher steady-state anisotropies and lifetime in comparison to the l_d phase[146]. Moreover, DPH presents almost no fluorescence when it is surrounded by water molecules, whereas the insertion of DPH into membranes significantly increases its fluorescence[276]. The sensitive nature of DPH and its molecular geometry adapted to the membrane structure, promoted the extensive use of this probe to measure membrane fluidity[276].

Rho-DOPE and NDB-DPPE are probes formed through the linkage of a fluorophore (NBD and Rho) to the headgroup of PE phospholipids. The Rho-DOPE preferentially partitions into the l_d phases[264]. Rhodamine probes present a high photostability and emission in visible wavelengths, making them appropriate for microscopy experiments, such as confocal imaging and two-photon microscopy[264].

Moreover, as previously described in section 9.4, due to a small Stoke´s shift, a high molar absorption coefficient and a high quantum yield, when these molecules are closer than a critical radius, energy transfer occurs between them (homo-FRET)[264]. In addition, it is worthy to stress that the Rho-DOPE anisotropy values in membranes have always to be interpreted taking into account the homo-FRET phenomena. It is expected that Rho-DOPE has a higher anisotropy in membranes that present a larger l_d fraction than in the ones with a larger l_o fraction. This occurs because Rho-DOPE molecules are excluded from ordered phases and confined to disordered phases. Therefore, an increase in the area of the l_o phase results in an increase in the surface density of Rho molecules in the l_d phase, allowing a more efficient transference of energy between Rho-DOPE molecules, consequently leading to the decrease of the anisotropy values[264].

Regarding NDB-DPPE, it is a probe sensitive to the environment organization, and in most of the cases the lipid attached to NBD behave as endogenous lipids[272]. When NBD is in an aqueous environment, it presents a weakly fluorescence intensity. In contrast if this probe is located in an hydrophobic environment, its intensity increases significantly[272]. Thus, the fluorescence lifetime of this probe presents a very high sensitivity to environment polarity. This is reflected by the longest lifetime (≈7 ns) when NBD is

involved in a hydrophobic environment in comparison to the short lifetime ($\approx$1 ns) reported by this probe when surrounded by water. This occurs due to the hydrogen bonding established between the probe and the solvent, which increases the non-radiative decay rate[272].

NBD-DPPE partitions preferentially towards l_o phase[177], however, it is excluded from gel phases. This probe is suited to detect and characterize model membranes that contain l_o phases, such as the membranes containing POPC, Chol and SM[177]. It is worthy to mention that this probe has a poor photostability, however, this can be reduced or avoided by the use of low intensity excitation light[272].

Laurdan was also used in this work. It is a solvatochromatic probe, which means that changes in the environment parameters, such as polarity, hydration, and fluidity are reflected in alterations of Laurdan´s spectroscopic properties. Therefore, when in a low viscosity or fluid environment, Laurdan's maximum of emission is centered at 490nm. In opposition, in viscous or packed environment the emission maximum shift to 440nm[277] (Fig. 21A-). The shift of the Laurdan's maximum emission can be quantified by the determination of a ratio, usually defined as generalized polarization (GP), (Fig. 21) Eq. 2:

$$GP = (I440 - I490)/(I440 + I490) \hspace{3cm} Eq.2,$$

The GP values for Laurdan typically range from 0.7 (in the gel phase) to -0.14 (in the fluid phase)[277]. Thereby, this is a useful parameters to be analyzed, when there is a need to characterize the biophysical properties of a membrane[277].
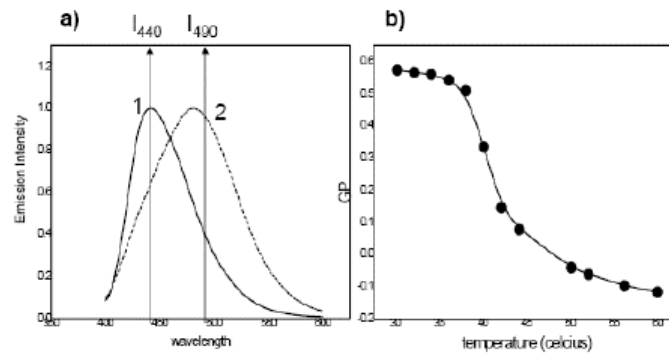
Figure 21 - Laurdan emission spectra and GP

A-Laurdan´s emission spectrum shift from a maximum at 440 nm (typical of membranes with high packing) to a peak at 490nm (typical of fluid membranes) due to different hydration of the membranes. B- Alteration of GP values with temperature (adapted from[266]).

Moreover, Laurdan is virtually insoluble in water, and can partition evenly between specific gel /l_o and l_d phases, and it is excluded from highly packed gel domains[159, 271]. In addition, since this type of probes presents changes in the emission or lifetime ratio in response to the membrane phase where it is inserted, the solvatochromatic probes are adequate for quantitative imaging, as the intensity ratio at two distinct wavelengths directly defines the lipid order[271]. Examples of such analysis are the FLIM measurements and the GP calculation in live cells and tissues[159, 271].

In this work, the global aim is to understand how GlcCer affects membrane biophysical properties. In order to do so, the characterization of GlcCer biophysical behavior was performed in simple fluid membranes, in membranes containing lipids that are typical of membrane domains (Chol and SM), and in whole cell membranes. The study comprised in this dissertation, might shed light over the possible biophysical events beneath GlcCer biological actions, clarifying some of the GlcCer effects in the cell membranes, both in normal and pathological conditions.

10 References

1.   ALBERTS B.; JONHSON A.; LEWIS J.; AL., E. MOLECULAR BIOLOGY OF THE CELL. 4TH EDITION ED.; GARLAND SCIENCE: NEW YORK, 2002.

2.   DEVLIN, T. M. TEXTBOOK OF BIOCHEMISTRY WITH CLINICAL CORRELATIONS SEVENTH ED.; 2011.

3.   GENNIS, R. B. BIOMEMBRANES: MOLECULAR STRUCTURE AND FUNCTION. SPRINGER-VERLAG: NEW YORK, USA, 1989.

4.   DANIELSEN, E. M.; HANSEN, G. H. LIPID RAFTS IN EPITHELIAL BRUSH BORDERS: ATYPICAL MEMBRANE MICRODOMAINS WITH SPECIALIZED FUNCTIONS. BIOCHIM BIOPHYS ACTA 2003, 1617 (1–2), 1-9.

5.   LOMBARD, J. ONCE UPON A TIME THE CELL MEMBRANES: 175 YEARS OF CELL BOUNDARY RESEARCH. BIOL DIRECT 2014, 9 (1), 32.

6.   GORTER, E.; GRENDEL, F. ON BIMOLECULAR LAYERS OF LIPOIDS ON THE CHROMOCYTES OF THE BLOOD. J EXP MED 1924, 41, 439-443.

7.   DANIELLI, J. F.; DAVSON, H. A CONTRIBUTION TO THE THEORY OF PERMEABILITY OF THIN FILMS. J CELL COMP PHYSIOL 1935, 5 (4), 495-508.

8.   ROBERTSON, J. D. THE ULTRASTRUCTURE OF CELL MEMBRANES AND THEIR DERIVATIVES. BIOCHEM SOC SYMP 1959, 16, 3-43.

9.   DA SILVA, P. P.; BRANTON, D. MEMBRANE SPLITTING IN FREEZE-ETCHING: COVALENTLY BOUND FERRITIN AS A MEMBRANE MARKER. J CELL BIOL 1970, 45 (3), 598-605.

10.   FRYE, L. D.; EDIDIN, M. THE RAPID INTERMIXING OF CELL SURFACE ANTIGENS AFTER FORMATION OF MOUSE-HUMAN HETEROKARYONS. J CELL SCI 1970, 7, 319-335.

11.   LIEBERMAN, R. L.; WUSTMAN, B. A.; HUERTAS, P.; POWE, A. C.; PINE, C. W.; KHANNA, R.; SCHLOSSMACHER, M. G.; RINGE, D.; PETSKO, G. A. STRUCTURE OF ACID B-GLUCOSIDASE WITH PHARMACOLOGICAL CHAPERONE PROVIDES INSIGHT INTO GAUCHER DISEASE. NAT CHEM BIOL 2006, 3 (2), 101-107.

12.   SINGER, S. J.; NICOLSON, G. L. THE FLUID MOSAIC MODEL OF THE STRUCTURE OF CELL MEMBRANES. SCIENCE 1972, 175, 720-731.

13.   NICOLSON, G. L. THE FLUID—MOSAIC MODEL OF MEMBRANE STRUCTURE: STILL RELEVANT TO UNDERSTANDING THE STRUCTURE, FUNCTION AND DYNAMICS OF BIOLOGICAL MEMBRANES AFTER MORE THAN 40 YEARS. BIOCHIM BIOPHYS ACTA 2014, 1838 (6), 1451-1466.

14.   TSUJI, A.; OHNISHI, S. RESTRICTION OF THE LATERAL MOTION OF BAND 3 IN THE ERYTHROCYTE MEMBRANE BY THE CYTOSKELETAL NETWORK: DEPENDENCE ON SPECTRIN ASSOCIATION STATE. BIOCHEMISTRY 1986, 25 (20), 6133-6139.

15.   KUSUMI, A.; HYDE, J. S. SPIN-LABEL SATURATION-TRANSFER ELECTRON SPIN RESONANCE DETECTION OF TRANSIENT ASSOCIATION OF RHODOPSIN IN RECONSTITUTED MEMBRANES. BIOCHEMISTRY 1982, 21 (23), 5978-5983.

16.   LINDBLOM, G.; ORÄDD, G. LIPID LATERAL DIFFUSION AND MEMBRANE HETEROGENEITY. BIOCHIM BIOPHYS ACTA 2009, 1788 (1), 234-244.

17.   MURASE, K.; FUJIWARA, T.; UMEMURA, Y.; SUZUKI, K.; IINO, R.; YAMASHITA, H.; SAITO, M.; MURAKOSHI, H.; RITCHIE, K.; KUSUMI, A. ULTRAFINE MEMBRANE COMPARTMENTS FOR MOLECULAR DIFFUSION AS REVEALED BY SINGLE MOLECULE TECHNIQUES. BIOPHYS J 2004, 86 (6), 4075-4093.

18.   SIMONS, K.; IKONEN, E. FUNCTIONAL RAFTS IN CELL MEMBRANES. NATURE 1997, 387, 569-572.

19.   KUSUMI, A.; SAKO, Y.; YAMAMOTO, M. CONFINED LATERAL DIFFUSION OF MEMBRANE RECEPTORS AS STUDIED BY SINGLE PARTICLE TRACKING (NANOVID MICROSCOPY). EFFECTS OF CALCIUM-INDUCED DIFFERENTIATION IN CULTURED EPITHELIAL CELLS. BIOPHYS J 1993, 65 (5), 2021-2040.

20.	Ritchie, K.; Iino, R.; Fujiwara, T.; Murase, K.; Kusumi, A. The fence and picket structure of the plasma membrane of live cells as revealed by single molecule techniques (Review). Mol Membr Biol 2003, 20 (1), 13-18.

21.	Sperotto, M. M.; Mouritsen, O. G. Monte Carlo simulation studies of lipid order parameter profiles near integral membrane proteins. Biophys J 1991, 59 (2), 261-270.

22.	Fujiwara, T.; Ritchie, K.; Murakoshi, H.; Jacobson, K.; Kusumi, A. Phospholipids undergo hop diffusion in compartmentalized cell membrane. J Cell Biol 2002, 157 (6), 1071-1082.

23.	Nicolson, G. L. Cis- and trans- membrane control of cell surface topography. J Supramol Struct 1973, 1 (4-5), 410-416.

24.	Jacobson, K.; Sheets, E.; Simson, R. Revisiting the fluid mosaic model of membranes. Science 1995, 268 (5216), 1441-1442.

25.	Edidin, M.; Kuo, S.; Sheetz, M. Lateral movements of membrane glycoproteins restricted by dynamic cytoplasmic barriers. Science 1991, 254 (5036), 1379-1382.

26.	Edidin, M. Lipids on the frontier: a century of cell-membrane bilayers. Nat Rev Mol Cell Biol 2003, 4 (5), 414-418.

27.	Nelson, D.; Cox, M. Lehninger principles of biochemistry (4th ed.). John Wiley & Sons Inc.: 2005; Vol. 33, p 74-75.

28.	Sutherland, E.; Dixon, B. S.; Leffert, H. L.; Skally, H.; Zaccaro, L.; Simon, F. R. Biochemical localization of hepatic surface-membrane Na+,K+-ATPase activity depends on membrane lipid fluidity. Proc Natl Acad Sci U S A 1988, 85 (22), 8673-8677.

29.	Baenziger, J. E.; Morris, M.-L.; Darsaut, T. E.; Ryan, S. E. Effect of Membrane Lipid Composition on the Conformational Equilibria of the Nicotinic Acetylcholine Receptor. J Biol Chem 2000, 275 (2), 777-784.

30.	Svensson, M.; Mossberg, A.-K.; Pettersson, J.; Linse, S.; Svanborg, C. Lipids as cofactors in protein folding: Stereo-specific lipid−protein interactions are required to form HAMLET (human a-lactalbumin made lethal to tumor cells). Protein Sci 2003, 12 (12), 2805-2814.

31.	Van Meer, G. Cellular lipidomics. EMBO J 2005, 24, 3159-3165.

32.	van Meer, G.; de Kroon, A. I. P. M. Lipid map of the mammalian cell. J Cell Sci 2011, 124 (1), 5-8.

33.	van Meer, G.; Voelker, D. R.; Feigenson, G. W. Membrane lipids: where they are and how they behave. Nat Rev Mol Cell Biol 2008, 9 (2), 112-124.

34.	Westerlund, B.; Slotte, J. P. How the molecular features of glycosphingolipids affect domain formation in fluid membranes. Biochim Biophys Acta 2009, 1788 (1), 194-201.

35.	Jennemann, R. Cell-specific deletion of glucosylceramide synthase in brain leads to severe neural defects after birth. Proc Natl Acad Sci U S A 2005, 102 (35), 12459-12464.

36.	Eeman, M.; Deleu, M. From biological membranes to biomimetic model membranes. Base 2010, 14 (4), 719-736.

37.	Ohvo-Rekilä, H.; Ramstedt, B.; Leppimäki, P.; Peter Slotte, J. Cholesterol interactions with phospholipids in membranes. Prog Lipid Res 2002, 41 (1), 66-97.

38.	van Meer, G.; de Kroon, A. I. P. M. Lipid map of the mammalian cell. J Cell Sci 2010, 124 (1), 5-8.

39.	Lahiri, S.; Futerman, A. H. The metabolism and function of sphingolipids and glycosphingolipids. Cell Mol Life Sci 2007, 64 (17), 2270-2284.

40.	Hannun, Y. A.; Obeid, L. M. Many Ceramides. J Biol Chem 2011, 286 (32), 27855-27862.

41.   Sandhoff, R. Very long chain sphingolipids: Tissue expression, function and synthesis. FEBS Lett 2010, 584 (9), 1907-1913.

42.   Gulbins, E.; Grassmé, H. Ceramide and cell death receptor clustering. Biochim Biophys Acta 2002, 1585 (2–3), 139-145.

43.   Venkataraman, K.; Futerman, A. H. Ceramide as a second messenger: sticky solutions to sticky problems. Trends Cell Biol 2000, 10 (10), 408-412.

44.   Nikolova-Karakashian, M.; Rozenova, K. Ceramide in Stress Response. In Sphingolipids as Signaling and Regulatory Molecules, Chalfant, C.; Poeta, M., Eds.; Springer New York, 2010; Vol. 688, pp 86-108.

45.   Yu, Z.; Nikolova-Karakashian, M.; Zhou, D.; Cheng, G.; Schuchman, E.; Mattson, M. Pivotal role for acidic sphingomyelinase in cerebral ischemia-induced ceramide and cytokine production, and neuronal apoptosis. J Mol Neurosci 2000, 15 (2), 85-97.

46.   Morita, Y.; Perez, G. I.; Paris, F.; Miranda, S. R.; Ehleiter, D.; Haimovitz-Friedman, A.; Fuks, Z.; Xie, Z.; Reed, J. C.; Schuchman, E. H.; Kolesnick, R. N.; Tilly, J. L. Oocyte apoptosis is suppressed by disruption of the acid sphingomyelinase gene or by sphingosine -1-phosphate therapy. Nat Med 2000, 6 (10), 1109-1114.

47.   Pattingre, S.; Bauvy, C.; Levade, T.; Levine, B.; Codogno, P. Ceramide-induced autophagy: To junk or to protect cells? Autophagy 2009, 5 (4), 558-560.

48.   Messner, M. C.; Cabot, M. C. Glucosylceramide in humans. In Sphingolipids as Signaling and Regulatory Molecules; Springer, 2010, pp 154-64.

49.   Hoekstra, D. Membrane dynamics and cell polarity: the role of sphingolipids. J Lipid Res 2003, 44 (5), 869-877.

50.   Hakomori, S.-i. The glycosynapse. Proc Natl Acad Sci U S A 2002, 99 (1), 225-232.

51.   Yamashita, T. Glycosphingolipid Modification: Structural Diversity, Functional and Mechanistic Integration of Diabetes. Diabetes Obes Metab 2011, 35 (4), 309.

52.   Correa-Freire, M. C.; Freire, E.; Barenholz, Y.; Biltonen, R. L.; Thompson, T. E. Thermotropic Behavior of Monoglucocerebroside-Dipalmitoylphosphatidylcholine Multilamellar Liposomes. Biochemistry 1979, 18 (3), 442-445.

53.   Porubsky, S.; Speak, A. O.; Salio, M.; Jennemann, R.; Bonrouhi, M.; Zafarulla, R.; Singh, Y.; Dyson, J.; Luckow, B.; Lehuen, A.; Malle, E.; Müthing, J.; Platt, F. M.; Cerundolo, V.; Gröne, H.-J. Globosides but Not Isoglobosides Can Impact the Development of Invariant NKT Cells and Their Interaction with Dendritic Cells. J Immunol 2012, 189 (6), 3007-3017.

54.   Todeshini, A. R.; Hakomori, S.-i. Functional role of glycosphingolipids and gangliosides in control of cell. Biochim Biophys Acta 2008, 1780, 421-433.

55.   Singh, P.; Paila, Y. D.; Chattopadhyay, A. Role of glycosphingolipids in the function of human serotonin1A receptors. J Neurochem 2012, 123 (5), 716-724.

56.   van Meer, G.; Wolthoorn, J.; Degroote, S. The fate and function of glycosphingolipid glucosylceramide. Phil Trans R Soc B 2003, 358 (1433), 869-873.

57.   Liang, Y.-J.; Yang, B.-C.; Chen, J.-M.; Lin, Y.-H.; Huang, C.-L.; Cheng, Y.-Y.; Hsu, C.-Y.; Khoo, K.-H.; Shen, C.-N.; Yu, J. Changes in Glycosphingolipid Composition During Differentiation of Human Embryonic Stem Cells to Ectodermal or Endodermal Lineages. Stem Cells 2011, 29 (12), 1995-2004.

58.   Hakomori, S.-i. Traveling for the glycosphingolipid path. Glycoconj J 2000, 17 (7), 627-647.

59.   Seddon, J. M.; Templer, R. H. Polymorphism of lipid-water Systems. Elsevier Science B.V.: London 1995; Vol. 1.

60.   Riezman, H.; Hernández-Corbacho, M. J.; Jenkins, R. W.; Clarke, C. J.; Hannun, Y. A.; Obeid, L. M.; Snider, A. J.; Siskind, L. J. Accumulation of Long-Chain Glycosphingolipids during Aging Is Prevented by Caloric Restriction. PloS ONE 2011, 6 (6), e20411.

61.   Warnock, D. E.; Lutz, M. S.; Blackburn, W. A.; Young, W. W.; Baenziger, J. U. Transport of newly synthesized glucosylceramide to the plasma membrane by a non-Golgi pathway. Proc Natl Acad Sci U S A 1994, 91 (7), 2708-2712.

62.   Jennemann, R.; Gröne, H.-J. Cell-specific in vivo functions of glycosphingolipids: Lessons from genetic deletions of enzymes involved in glycosphingolipid synthesis. Prog Lipid Res 2013, 52 (2), 231-248.

63.   Ichikawa, I.; Hirabayashi, Y. Glucosylceramide synthase and glycosphingolipid synthesis. Trends Cell Biol 1998, 8, 198-202.

64.   Liu, Y.-Y.; Li, Y.-T. Ceramide Glycosylation Catalyzed by Glucosylceramide Synthase and Cancer Drug Resistance. Adv Cancer Res 2013, 117, 59-89.

65.   Walden, C. M.; Sandhoff, R.; Chuang, C. C.; Yildiz, Y.; Butters, T. D.; Dwek, R. A.; Platt, F. M.; van der Spoel, A. C. Accumulation of Glucosylceramide in Murine Testis, Caused by Inhibition of beta-Glucosidase 2: Implication For Spermatogenesis. J Biol Chem 2007, 282 (45), 32655-32664.

66.   Nyholm, P.-G.; Pascher, I. Orientation of the Saccharide Chains of Glycolipids at the membrane Surface. Biochemistry 1993, 32, 1225-1234.

67.   Körschen, H. G.; Yildiz, Y.; Raju, D. N.; Schonauer, S.; Bönigk, W.; Jansen, V.; Kremmer, E.; Kaupp, U. B.; Wachten, D. The Non-lysosomal b-Glucosidase GBA2 Is a Non-integral Membrane-associated Protein at the Endoplasmic Reticulum (ER) and Golgi. J Biol Chem 2013, 288 (5), 3381-3393.

68.   Quinn, P. J. The structure of complexes between phosphatidylethanolamine and glucosylceramide: A matrix for membrane rafts. Biochim Biophys Acta 2011, 1808 (12), 2894-2904.

69.   Avanti Polar Lipids. www.avantilipids.com.

70.   Martin, O. C.; Pagano, R. E. Internalization and Sorting of a Fluorescent Analogue of Glucosylceramide to the Golgi Apparatus of Human Skin Fibroblasts: Utilization of Endocytic and Nonendocytic Transport Mechanisms. J Cell Biol 1994, 125, 769-781.

71.   Kolter, T.; Sandhoff, K. Principles of Lysosomal Membrane Digestion: Stimulation of Sphingolipid Degradation by Sphingolipid Activator Proteins and Anionic Lysosomal Lipids. Annu Rev Cell Dev Biol 2005, 21 (1), 81-103.

72.   Zhao, Y.; Ren, J.; Padilla-Parra, S.; Fry, E. E.; Stuart, D. I. Lysosome sorting of b-glucocerebrosidase by LIMP-2 is targeted by the mannose 6-phosphate receptor. Nat Commun 2014, 5.

73.   Hayashi, Y.; Okino, N.; Kakuta, Y.; Shikanai, T.; Tani, M.; Narimatsu, H.; Ito, M. Klotho-related Protein Is a Novel Cytosolic Neutral beta-Glycosylceramidase. J Biol Chem 2007, 282 (42), 30889-30900.

74.   Walden, C. M.; Sandhoff, R.; Chuang, C. C.; Yildiz, Y.; Butters, T. D.; Dwek, R. A.; Platt, F. M.; van der Spoel, A. C. Accumulation of Glucosylceramide in Murine Testis, Caused by Inhibition of beta-Glucosidase 2: IMPLICATIONS FOR SPERMATOGENESIS. J Biol Chem 2007, 282 (45), 32655-32664.

75.   Hayashi, Y.; Okino, N.; Kakuta, Y.; Shikanai, T.; Tani, M.; Narimatsu, H.; Ito, M. Klotho-related Protein Is a Novel Cytosolic Neutral b-Glycosylceramidase. J Biol Chem 2007, 282 (42), 30889-30900.

76.   DVIR, H.; HAREL, M.; McCARTHY, A. A.; TOKER, L.; SILMAN, I.; FUTERMAN, A. H.; SUSSMAN, J. L. X-RAY STRUCTURE OF HUMAN ACID-B-GLUCOSIDASE, THE DEFECTIVE ENZYME IN GAUCHER DISEASE. EMBO REP 2003, 4 (7), 704-709.

77.   VAN DER POEL, S.; WOLTHOORN, J.; VAN DEN HEUVEL, D.; EGMOND, M.; GROUX-DEGROOTE, S.; NEUMANN, S.; GERRITSEN, H.; VAN MEER, G.; SPRONG, H. HYPERACIDIFICATION OF TRANS-GOLGI NETWORK AND ENDO/LYSOSOMES IN MELANOCYTES BY GLUCOSYLCERAMIDE-DEPENDENT V-ATPASE ACTIVITY. TRAFFIC 2011, 12 (11), 1634-1647.

78.   LEIPELT, M.; WARNECKE, D.; ZÄHRINGER, U.; OTT, C.; MÜLLER, F.; HUBE, B.; HEINZ, E. GLUCOSYLCERAMIDE SYNTHASES, A GENE FAMILY RESPONSIBLE FOR THE BIOSYNTHESIS OF GLUCOSPHINGOLIPIDS IN ANIMALS, PLANTS, AND FUNGI. J BIOL CHEM 2001, 276 (36), 33621-33629.

79.   MAUNULA, S.; BJÖRKQVIST, Y. J. E.; SLOTTE, J. P.; RAMSTEDT, B. DIFFERENCES IN THE DOMAIN FORMING PROPERTIES OF N-PALMITOYLATED NEUTRAL GLYCOSPHINGOLIPIDS IN BILAYER MEMBRANES. BIOCHIM BIOPHYS ACTA 2007, 1768 (2), 336-345.

80.   LLOYD-EVANS, E. GLUCOSYLCERAMIDE AND GLUCOSYLSPHINGOSINE MODULATE CALCIUM MOBILIZATION FROM BRAIN MICROSOMES VIA DIFFERENT MECHANISMS. J BIOL CHEM 2003, 278 (26), 23594-23599.

81.   SILLENCE, D. J. GLUCOSYLCERAMIDE MODULATES MEMBRANE TRAFFIC ALONG THE ENDOCYTIC PATHWAY. J LIPID RES 2002, 43 (11), 1837-1845.

82.   UCHIDA, Y.; MURATA, S.; SCHMUTH, M.; BEHNE, M. J.; LEE, J. D.; ICHIKAWA, S.; ELIAS, P. M.; HIRABAYASHI, Y.; HOLLERAN, W. M. GLUCOSYLCERAMIDE SYNTHESIS AND SYNTHASE EXPRESSION PROTECT AGAINST CERAMIDE-INDUCED STRESS. J LIPID RES 2002, 43 (8), 1293-1302.

83.   RHOME, R.; SINGH, A.; KECHICHIAN, T.; DRAGO, M.; MORACE, G.; LUBERTO, C.; POETA, M. D. SURFACE LOCALIZATION OF GLUCOSYLCERAMIDE DURING CRYPTOCOCCUS NEOFORMANS INFECTION ALLOWS TARGETING AS A POTENTIAL ANTIFUNGAL. PLOS ONE 2011, 6 (1), 1-13.

84.   BODENNEC, J. PHOSPHATIDYLCHOLINE SYNTHESIS IS ELEVATED IN NEURONAL MODELS OF GAUCHER DISEASE DUE TO DIRECT ACTIVATION OF CTP:PHOSPHOCHOLINE CYTIDYLYLTRANSFERASE BY GLUCOSYLCERAMIDE. FASEB J 2002.

85.   RICHARD, I.; DUCLOS, J. THE TOTAL SYNTHESES OF D-ERYTHRO-SPHINGOSINE,N-PALMITOYLSPHINGOSINE (CERAMIDE), AND GLUCOSYLCERAMIDE (CEREBROSIDE) VIA AN AZIDOSPHINGOSINE ANALOG. CHEM PHYS LIPIDS 2011, 111, 111-138.

86.   INAFUKU, M.; LI, C.; KANDA, Y.; KAWAMURA, T.; TAKEDA, K.; OKU, H.; WATANABE, H. BETA-GLUCOSYLCERAMIDE ADMINISTRATION (I.P.) ACTIVATES NATURAL KILLER T CELLS IN VIVO AND PREVENTS TUMOR METASTASIS IN MICE. LIPIDS 2012, 47 (6), 581-591.

87.   ABE, A.; WU, D.; SHAYMAN, J. A.; RADIN, N. S. METABOLIC EFFECTS OF SHORT-CHAIN CERAMIDE AND GLUCOSYLCERAMIDE ON SPHINGOLIPIDS AND PROTEIN KINASE C. EUR J BIOCHEM 1992, 210 (3), 765-773.

88.   SCHWERER, B. ANTIBODIES AGAINST GANGLIOSIDES: A LINK BETWEEN PRECEDING INFECTION AND IMMUNOPATHOGENESIS OF GUILLAINBARRÉ SYNDROME. MICROB INFECT 2002, 4 (3), 373-384.

89.   MAGÉRUS-CHATINET, A.; YU, H.; GARCIA, S.; DUCLOUX, E.; TERRIS, B.; BOMSEL, M. GALACTOSYL CERAMIDE EXPRESSED ON DENDRITIC CELLS CAN MEDIATE HIV-1 TRANSFER FROM MONOCYTE DERIVED DENDRITIC CELLS TO AUTOLOGOUS T CELLS. VIROLOGY 2007, 362 (1), 67-74.

90.   MAZZULLI, JOSEPH R.; XU, Y.-H.; SUN, Y.; KNIGHT, ADAM L.; McLEAN, PAMELA J.; CALDWELL, GUY A.; SIDRANSKY, E.; GRABOWSKI, GREGORY A.; KRAINC, D. GAUCHER DISEASE GLUCOCEREBROSIDASE AND A-SYNUCLEIN FORM A BIDIRECTIONAL PATHOGENIC LOOP IN SYNUCLEINOPATHIES. CELL 2011, 146 (1), 37-52.

91. Ramalho-Santos, J.; Lima, J. P. D. The role of target membrane sialic acid residues in the fusion activity of the influenza virus: the effect of two types of ganglioside on the kinetics of membrane merging. Cell Mol Biol Lett 2004, 9, 337-351.

92. Lingwood, C. A.; Branch, D. R. The role of glycosphingolipids in HIV/AIDS. Discov Med 2011, 11 (59), 303-313.

93. Rittershaus, P. C.; Kechichian, T. B.; Allegood, J. C.; Jr, A. H. M.; Hennig, M.; Luberto, C.; Poeta, M. D. Glucosylceramide synthase is an essential regulator of pathogenicity of Cryptococcus neoformans. J Clin Invest 2006, 116, 1651-1659.

94. Sato, T.; Serizawa, T.; Okahata, Y. Binding of influenza A virus to monosialoganglioside (GM3) reconstituted in glucosylceramide and sphingomyelin membranes. Biochim Biophys Acta 1996, 1285 (1), 14-20.

95. Liu, Y.-Y.; Gupta, V.; Patwardhan, G. A.; Bhinge, K.; Zhao, Y.; Bao, J.; Mehendale, H.; Cabot, M. C.; Li, Y.-T.; Jazwinski, S. M. Glucosylceramide synthase upregulates MDR1 expression in the regulation of cancer drug resistance through cSrc and b-catenin signaling. Mol Cancer 2010, 9 (1), 145.

96. Aerts, J. M.; Ottenhoff, R.; Powlson, A. S.; Grefhorst, A.; van Eijk, M.; Dubbelhuis, P. F.; Aten, J.; Kuipers, F.; Serlie, M. J.; Wennekes, T.; Sethi, J. K.; O'Rahilly, S.; Overkleeft, H. S. Pharmacological Inhibition of Glucosylceramide Synthase Enhances Insulin Sensitivity. Diabetes 2007, 56 (5), 1341-1349.

97. Kang, S.; Kim, J.-B.; Heo, T.-H.; Kim, S.-J. Cell cycle arrest in Batten disease lymphoblast cells. Gene 2013, 519 (2), 245-250.

98. Mehta, A. Epidemiology and natural history of Gaucher's disease. Eur J Intern Med 2006, 17, S2-S5.

99. Pampols, T.; Pineda, M.; Giros, M.; Ferrer, I.; Cusi, V.; Chabas, A.; Sanmarti, F.; Vanier, M.; Christomanou, H. Neuronopathic juvenile glucosylceramidosis due to sap-C deficiency: clinical course, neuropathology and brain lipid composition in this Gaucher disease variant. Acta Neuropathol 1999, 97 (1), 91-97.

100. Cox, T. Gaucher disease: clinical profile and therapeutic developments. Biol Targets Ther 2010, 299.

101. Grabowski, G. A. Phenotype, diagnosis, and treatment of Gaucher's disease. Lancet 2008, 372 (9645), 1263-1271.

102. Jmoudiak, M.; Futerman, A. H. Gaucher disease: pathological mechanisms and modern management. Br J Haematol 2005, 129 (2), 178-188.

103. Farfel-Becker, T.; Vitner, E. B.; Kelly, S. L.; Bame, J. R.; Duan, J.; Shinder, V.; Merrill, A. H.; Dobrenis, K.; Futerman, A. H. Neuronal accumulation of glucosylceramide in a mouse model of neuronopathic Gaucher disease leads to neurodegeneration. Hum Mol Gen 2014, 23 (4), 843-854.

104. Mistry, P. K.; Liu, J.; Yang, M.; Nottoli, T.; McGrath, J.; Jain, D.; Zhang, K.; Keutzer, J.; Chuang, W.-L.; Mehal, W. Z.; Zhao, H.; Lin, A.; Mane, S.; Liu, X.; Peng, Y. Z.; Li, J. H.; Agrawal, M.; Zhu, L.-L.; Blair, H. C.; Robinson, L. J.; Iqbal, J.; Sun, L.; Zaidi, M. Glucocerebrosidase gene-deficient mouse recapitulates Gaucher disease displaying cellular and molecular dysregulation beyond the macrophage. Proc Natl Acad Sci U S A 2010, 107 (45), 19473-19478.

105. Fuller, M.; Rozaklis, T.; Lovejoy, M.; Zarrinkalam, K.; Hopwood, J. J.; Meikle, P. J. Glucosylceramide accumulation is not confined to the lysosome in fibroblasts from patients with Gaucher disease. Mol Gen Metab 2008, 93 (4), 437-443.

106.   Elleder, M. Glucosylceramide transfer from lysosomes—the missing link in molecular pathology of glucosylceramidase deficiency: A hypothesis based on existing data. J Inherit Metab Dis 2006, 29 (6), 707-715.

107.   Cox, T. M. Gaucher disease:Clinical profile and therapeutic developments. Biol Targets Ther 2010, 299-313.

108.   Shachar, T.; Bianco, C. L.; Recchia, A.; Wiessner, C.; Raas-Rothschild, A.; Futerman, A. H. Lysosomal storage disorders and Parkinson's disease: Gaucher disease and beyond. Mov Disorders 2011, 26 (9), 1593-1604.

109.   Aureli, M.; Bassi, R.; Loberto, N.; Regis, S.; Prinetti, A.; Chigorno, V.; Aerts, J.; Boot, R.; Filocamo, M.; Sonnino, S. Cell surface associated glycohydrolases in normal and Gaucher disease fibroblasts. J Inherit Metab Dis 2012, 35 (6), 1081-1091.

110.   Eblan, M. J.; Goker-Alpan, O.; Sidransky, E. Perinatal Lethal Gaucher Disease: A Distincti Phenotype Along The Neuropathic Continuum. Fetal Pediatr Pathol 2005, 24 (4-5), 205-222.

111.   Chabás, A.; Cormand, B.; Grinberg, D.; Burguera, J. M.; Balcells, S.; Merino, J. L.; Mate, I.; Sobrino, J. A.; Gonzàlez-Duarte, R.; Vilageliu, L. Unusual expression of Gaucher's disease: cardiovascular calcifications in three sibs homozygous for the D409H mutation. J Med Genet 1995, 32 (9), 740-742.

112.   Liu, J.; Halene, S.; Yang, M.; Iqbal, J.; Yang, R.; Mehal, W. Z.; Chuang, W.-L.; Jain, D.; Yuen, T.; Sun, L.; Zaidi, M.; Mistry, P. K. Gaucher disease gene GBA functions in immune regulation. Proc Natl Acad Sci U S A 2012, 109 (25), 10018-10023.

113.   Mucci, J. M.; Rozenfeld, P. Pathogenesis of Bone Alterations in Gaucher Disease: The Role of Immune System. J Immunol Res 2015, 2015, 6.

114.   Žnidar, I.; Collin-Histed, T.; Niemeyer, P.; Parkkinen, J.; Lauridsen, A.-G.; Zariņa, S.; Cohen, Y.; Manuel, J. The European Gaucher Alliance: a survey of member patient organisations' activities, healthcare environments and concerns. Orphanet J Rare Dis 2014, 9 (1), 134.

115.   Barth, B. M.; Gustafson, S. J.; Young, M. M.; Fox, T. E.; Shanmugavelandy, S. S.; Kaiser, J. M.; Cabot, M. C.; Kester, M.; Kuhn, T. B. Inhibition of NADPH oxidase by glucosylceramide confers chemoresistance. Cancer Biol Ther 2010, 10 (11), 1126-1136.

116.   Rittershaus, P. C.; Kechichian, T. B.; Allegood, J. C.; Merrill, A. H.; Hennig, M.; Luberto, C.; Del Poeta, M. Glucosylceramide synthase is an essential regulator of pathogenicity of Cryptococcus neoformans. J Clin Invest 2006, 116 (6), 1651-1659.

117.   Kartal Yandim, M.; Apohan, E.; Baran, Y. Therapeutic potential of targeting ceramide/glucosylceramide pathway in cancer. Cancer Chemother Pharmacol 2013, 71 (1), 13-20.

118.   Ideta, R.; Sakuta, T.; Nakano, Y.; Uchiyama, T. Orally Administered Glucosylceramide Improves the Skin Barrier Function by Upregulating Genes Associated with the Tight Junction and Cornified Envelope Formation. Biosci Biotechnol Biochem 2011, 75 (8), 1516-1523.

119.   van Lummel, M.; van Blitterswijk, W. J.; Vink, S. R.; Veldman, R. J.; van der Valk, M. A.; Schipper, D.; Dicheva, B. M.; Eggermont, A. M. M.; ten Hagen, T. L. M.; Verheij, M.; Koning, G. A. Enriching lipid nanovesicles with short-chain glucosylceramide improves doxorubicin delivery and efficacy in solid tumors. FASEB J 2010, 25 (1), 280-289.

120.   Duan, J.; Sugawara, T.; Sakai, S.; Aida, K.; Hirata, T. Oral Glucosylceramide Reduces 2,4-Dinitrofluorobenzene Induced Inflammatory Response in Mice by Reducing TNF-Alpha Levels and Leukocyte Infiltration. Lipids 2011, 46 (6), 505-512.

121.	Fujiwara, K.; Kitatani, K.; Fukushima, K.; Yazama, H.; Umehara, H.; Kikuchi, M.; Igarashi, Y.; Kitano, H.; Okazaki, T. Inhibitory effects of dietary glucosylceramides on squamous cell carcinoma of the head and neck in NOD/SCID mice. J Clin Invest 2010, 16 (2), 133-140.

122.	Vill, V.; Vill, V.; Böcker, T.; Thiem, J.; Fischer, F. The stereochemistry of glycolipids. A key for understanding membrane functions? Liq Cryst 2006, 33 (11-12), 1351-1358.

123.	Grassme, H. CD95 Signaling via Ceramide-rich Membrane Rafts. J Biol Chem 2001, 276 (23), 20589-20596.

124.	Simons, K.; Van Meer, G. Lipid sorting in epithelial cells. Biochemistry 1988, 27 (17), 6197-6202.

125.	Edidin, M. The State of Lipid Rafts: From Model Membranes to Cells. Annu Rev Biophys Biomol Struct. 2003, 32 (1), 257-283.

126.	Gupta, G.; Surolia, A. Glycosphingolipids in microdomain formation and their spatial organization. FEBS Lett 2010, 584 (9), 1634-1641.

127.	Janmey, P. A.; Kinnunen, P. K. J. Biophysical properties of lipids and dynamic membranes. Trends Cell Biol 2006, 16 (10), 538-546.

128.	Seddon, J.; Templer, R. Polymorphism of lipid-water Systems. Elsevier: London, 1995; Vol. 1, p 97-160.

129.	Veiga, M. P.; Arrondo, J. L. R.; Goñi, F. M.; Alonso, A. Ceramides in Phospholipid Membranes: Effects on Bilayer Stability and Transition to Nonlamellar Phases. Biophys J 1999, 76 (1), 342-350.

130.	Ruiz-Arguëllo, M. B.; Basáñez, G.; Goñi, F. M.; Alonso, A. Different Effects of Enzyme-generated Ceramides and Diacylglycerols in Phospholipid Membrane Fusion and Leakage. J Biol Chem 1996, 271, 26616-26621.

131.	Tresset, G. The multiple faces of self-assembled lipidic systems. PMC Biophys 2009, 2 (1), 3.

132.	Laboratory, T. C. http://cherezov.scripps.edu/resources.htm.

133.	Hauser, H.; Pascher, I.; Pearson, R. H.; Sundell, S. Preferred conformation and molecular packing of phosphatidylethanolamine and phosphatidylcholine. Biochim Biophys Acta 1981, 650 (1), 21-51.

134.	Bernchou, U.; Midtiby, H.; Ipsen, J. H.; Simonsen, A. C. Correlation between the ripple phase and stripe domains in membranes. Biochim Biophys Acta 2011, 1808 (12), 2849-2858.

135.	Mouritsen, O. G. Life-As a Matter of Fat. Springer-Verlag 2005.

136.	Rubenstein, J. L.; Smith, B. A.; McConnell, H. M. Lateral diffusion in binary mixtures of cholesterol and phosphatidylcholines. Proc Natl Acad Sci U S A 1979, 76 (1), 15-18.

137.	Bakht, O.; Delgado, J.; Amat-Guerri, F.; Acuña, A. U.; London, E. The phenyltetraene lysophospholipid analog PTE-ET-18-OMe as a fluorescent anisotropy probe of liquid ordered membrane domains (lipid rafts) and ceramide-rich membrane domains. Biochim Biophys Acta 2007, 1768 (9), 2213-2221.

138.	Brown, D. A.; London, E. Structure of Detergent-Resistant Membrane Domains: Does Phase Separation Occur in Biological Membranes? Biochem Biophys Res Commun 1997, 240 (1), 1-7.

139.	Baumgart, T.; Hunt, G.; Farkas, E. R.; Webb, W. W.; Feigenson, G. W. Fluorescence probe partitioning between Lo/Ld phases in lipid membranes. Biochim Biophys Acta 2007, 1768 (9), 2182-2194.

140.	Brown, D. A.; London, E. Structure and Function of Sphingolipid- and Cholesterol-rich Membrane Rafts. J Biol Chem 2000, 275 (23), 17221-17224.

141. Grassmé, H.; Riethmüller, J.; Gulbins, E. Biological aspects of ceramide-enriched membrane domains. Prog Lipid Res 2007, 46 (3-4), 161-170.

142. Saxena, K.; Duclos, R. I.; Zimmermann, P.; Schmidt, R. R.; Shipley, G. G. Structure and properties of totally synthetic galacto- and gluco-cerebrosides. J Lipid Res 1999, 40, 839-849.

143. Yeagle, P. The membranes of cells. Academic Press: San Diego, 1987; p 304.

144. Veatch, S.; Keller, S. Miscibility Phase Diagrams of Giant Vesicles Containing Sphingomyelin. Phys Rev Lett 2005, 94 (14).

145. Marsh, D. CRC handbook of lipid bilayers. 1990.

146. Castro, B. M.; de Almeida, R. F. M.; Silva, L. C.; Fedorov, A.; Prieto, M. Formation of Ceramide/Sphingomyelin Gel Domains in the Presence of an Unsaturated Phospholipid: A Quantitative Multiprobe Approach. Biophys J 2007, 93, 1639-1650.

147. Hsueh, Y. W.; Giles, R.; Kitson, N.; Thewalt, J. The Effect of Ceramide on Phosphatidylcholine Membranes: A Deuterium NMR Study. Biophys J 2002, 82, 3089-3095.

148. de Almeida, R. F. M.; Fedorov, A.; Prieto, M. SPhingomyelin/Phosphatidylcholine/Cholesterol Phase Diagram: Boundaries and Composition of Lipid Rafts. Biophys J 2003, 85, 2406-2416.

149. van Meer, G. Dynamic Transbilayer Lipid Asymmetry. Cold Spring Harb Perpect Biol 2011, 3 (5).

150. McConnell, H. M.; Kornberg, R. D. Inside-outside transitions of phospholipids in vesicle membranes. Biochemistry 1971, 10 (7), 1111-1120.

151. Zhang, Y.-M.; Rock, C. O. Membrane lipid homeostasis in bacteria. Nat Rev Micro 2008, 6 (3), 222-233.

152. Aresta-Branco, F.; Cordeiro, A. M.; Marinho, H. S.; Cyrne, L.; Antunes, F.; de Almeida, R. F. M. Gel Domains in the Plasma Membrane of Saccharomyces cerevisiae: Highly Ordered, Ergosterol-Free, and Sphingolipid-Enriched Lipid Rafts. J Biol Chem 2010, 286 (7), 5043-5054.

153. Pinto, S. N.; Laviad, E. L.; Stiban, J.; Kelly, S. L.; Merrill, A. H.; Prieto, M.; Futerman, A. H.; Silva, L. C. Changes in membrane biophysical properties induced by sphingomyelinase depend on the sphingolipid N-acyl chain. J Lipid Res 2014, 55 (1), 53-61.

154. Devaux, P. F. Lipid transmembrane asymmetry and flip-flop in biological membranes and in lipid bilayers. Curr Opin Struct Biol 1993, 3 (4), 489-494.

155. Pomorski, T. Tracking down lipid flippases and their biological functions. J Cell Sci 2004, 117 (6), 805-813.

156. Carreira Ana, C.; Ventura Ana, E.; Varela Ana, R. P.; Silva Liana, C. Tackling the biophysical properties of sphingolipids to decipher their biological roles. Biol Chem 2015, 396 (6-7), 597-609.

157. Pinto, S. N.; Silva, L. C.; Futerman, A. H.; Prieto, M. Effect of ceramide structure on membrane biophysical properties: The role of acyl chain length and unsaturation. Biochim Biophys Acta 2011, 1808 (11), 2753-2760.

158. Levy, M.; Futerman, A. H. Mammalian ceramide synthases. IUBMB Life 2010, NA-NA.

159. Pinto, S. N.; Fernandes, F.; Fedorov, A.; Futerman, A. H.; Silva, L. C.; Prieto, M. A combined fluorescence spectroscopy, confocal and 2-photon microscopy approach to re-evaluate the properties of sphingolipid domains. Biochim Biophys Acta 2013, 1828, 2099-2110.

160. Silva, L.; De Almeida, R. F. M.; Fedorov, A.; Matos, A. P. A.; Prieto, M. Ceramide-platform formation and -induced biophysical changes in a fluid phospholipid membrane. Mol Membr Biol 2006, 23 (2), 137-148.

161. J. Shah, J. A., RI Duclos, AV Rawlings, Z Dong, GG Shipley. Structural and thermotropic properties os synthetic C16:0 (palmitoyl) ceramide: effect of hydration. J Lipid Res 1995, 36, 1936-1944.

162. Pinto, S. N.; Silva, L. C.; de Almeida, R. F. M.; Prieto, M. Membrane Domain Formation, Interdigitation, and Morphological Alterations Induced by the Very Long Chain Asymmetric C24:1 Ceramide. Biophys J 2008, 95 (6), 2867-2879.

163. Chen, H.-C.; Mendelsohn, R.; Rerek, M. E.; Moore, D. J. Fourier transform infrared spectroscopy and differential scanning calorimetry studies of fatty acid homogeneous ceramide 2. Biochim Biophys Acta 2000, 1468 (1–2), 293-303.

164. Carrer, D.; Maggio, B. Phase behavior and molecular interactions in mixtures of ceramide and dipalmitoylphosphatidylcholine. J Lipid Res 1999, 40, 1978-1989.

165. Contreras, F. X. Sphingomyelinase Activity Causes Transbilayer Lipid Translocation in Model and Cell Membranes. J Biol Chem 2003, 278 (39), 37169-37174.

166. Sot, J.; Goñi, F. M.; Alonso, A. Molecular associations and surface-active properties of short- and long-N-acyl chain ceramides. Biochim Biophys Acta 2005, 1711 (1), 12-19.

167. Holopainen, J. M.; Angelova, M. I.; Kinnunen, P. K. J. Vectorial Budding of Vesicles by Asymmetrical Enzymatic Formation of Ceramide in Giant Liposomes. Biophys J 2000, 78, 830-838.

168. Montes, L. R. Membrane Restructuring via Ceramide Results in Enhanced Solute Efflux. J Biol Chem 2002, 277 (14), 11788-11794.

169. Sot, J.; Ibarguren, M.; Busto, J. V.; Montes, L. R.; Goñi, F. M.; Alonso, A. Cholesterol displacement by ceramide in sphingomyelin-containing liquid-ordered domains, and generation of gel regions in giant lipidic vesicles. FEBS Lett 2008, 582 (21-22), 3230-3236.

170. Holopainen, J. M.; Lehtonen, J. Y. A.; Kinnunen, P. K. J. Lipid microdomains in dimyristoylphosphatidylcholine-ceramide liposomes. Chem Phys Lipids 1997, 88, 1-13.

171. Fidorra, M.; Duelund, L.; Leidy, C.; Simonsen, A. C.; Bagatolli, L. A. Absence of Fluid-Ordered/Fluid-Disordered Phase Coexistence in Ceramide/POPC Mixtures Containing Cholesterol. Biophys J 2006, 90 (12), 4437-4451.

172. Goni, F.; Alonso, A. Biophysics of sphingolipids I. Membrane properties of sphingosine, ceramides and other simple sphingolipids. Biochim Biophys Acta 2006, 1758 (12), 1902-1921.

173. Zupancic, E.; Carreira, A. C.; de Almeida, R. F. M.; Silva, L. C. Biophysical Implications of Sphingosine Accumulation in Membrane Properties at Neutral and Acidic pH. The Journal of Physical Chemistry B 2014, 118 (18), 4858-4866.

174. Carrer, D. C.; Schreier, S.; Patrito, M.; Maggio, B. Effects of a Short-Chain Ceramide on Bilayer Domain Formation, Thickness, and Chain Mobililty: DMPC and Asymmetric Ceramide Mixtures. Biophys J 2006, 90 (7), 2394-2403.

175. Ira; Johnston, L. J. Sphingomyelinase generation of ceramide promotes clustering of nanoscale domains in supported bilayer membranes. Biochim Biophys Acta 2008, 1778 (1), 185-197.

176. Ira; Zou, S.; Ramirez, D. M. C.; Vanderlip, S.; Ogilvie, W.; Jakubek, Z. J.; Johnston, L. J. Enzymatic generation of ceramide induces membrane restructuring: Correlated AFM and fluorescence imaging of supported bilayers. J Struct Biol 2009, 168 (1), 78-89.

177. Silva, L. C.; de Almeida, R. F. M.; Castro, B. M.; Fedorov, A.; Prieto, M. Ceramide-Domain Formation and Collapse in Lipid Rafts: Membrane Reorganization by an Apoptotic Lipid. Biophys J 2007, 92 (2), 502-516.

178.   Silva, L. C.; Futerman, A. H.; Prieto, M. Lipid Raft Composition Modulates Sphingomyelinase Activity and Ceramide-Induced Membrane Physical Alterations. Biophys J 2009, 96 (8), 3210-3222.

179.   Castro, B. M.; Prieto, M.; Silva, L. C. Ceramide: A simple sphingolipid with unique biophysical properties. Prog Lipid Res 2014, 54, 53-67.

180.   Corti, M.; Cantù, L.; Brocca, P.; Del Favero, E. Self-assembly in glycolipids. Curr Opin Colloid Interface Sci 2007, 12 (3), 148-154.

181.   Arnulphi, C.; Levstein, P. R.; Ramia, M. E.; Martin, A.; Fidelio, G. D. Ganglioside hydration study 2H-NMR: dependence in temperature and water/lipid ratio. J Lipid Res 1997, 38, 1412-1420.

182.   Zaraiskaya, T.; Jeffrey, K. R. Molecular Dynamics Simulations and 2H NMR Study of the GalCer/DPPG Lipid Bilayer. Biophys J 2005, 88 (6), 4017-4031.

183.   Feng, Y.; Rainteau, D.; Chachaty, C.; Yu, Z.-W.; Wolf, C.; Quinn, P. J. Characterization of a Quasicrystalline Phase in Codispersions of Phosphatidylethanolamine and Glucocerebroside. Biophys J 2004, 86 (4), 2208-2217.

184.   Hakomori, S.-t. Glycosynapses: microdomains controlling carbohydrate-dependent cell adhesion and signaling. An Acad Bras Cienc 2004, 76, 553-572.

185.   Maggio, B.; Fanani, M. L.; Rosetti, C. M.; Wilke, N. Byophisics of sphingolipids II: Glycosphingolipids: An assortment of multiple structural information transducers at the membrane surface. Biochem Biophys Acta 2006, 1758, 1922-1944.

186.   Freire, E.; Bach, D.; Correa-Freire, M.; Miller, I.; Barenholz, Y. Calorimetric investigation of the complex phase behavior of glucocerebroside dispersions. Biochemistry 1980, 19 (16), 3662-3665.

187.   Reed, R. A.; Shipley, G. G. Structure and metastability of N-lignocerylgalactosylsphingosine (cerebroside) bilayers. Biochim Biophys Acta 1987, 896 (2), 153-164.

188.   Maggio, B.; Ariga, T.; Sturtevant, J. M.; Yu, R. K. Thermotropic behavior of binary mixtures of diplamitoylphosphatidylcholine and glycosphingolipids in aqueous dispersions. Biochim Biophys Acta 1985, 818 (1), 1-12.

189.   Thompson, T. E.; Tillack, T. W. Organization of Glycosphingolipids in Bilayers and Plasma Membranes of Mammalian Cells. Annu Rev Biophys Biophys Chem 1985, 14 (1), 361-386.

190.   Rock, P.; Allietta, M.; Young, W. W.; Thompson, T. E.; Tillack, T. W. Ganglioside GM1 and asialo-GM1 at low concentration are preferentially incorporated into the gel phase in two-component, two-phase phosphatidylcholine bilayers. Biochemistry 1991, 30 (1), 19-25.

191.   Morrow, M.; Singh, D.; Lu, D.; Grant, C. Glycosphingolipid phase behaviour in unsaturated phosphatidylcholine bilayers: a 2H-NMR study. Biochem Biophys Acta 1992, 1106, 85-93.

192.   Schifferer, F.; Beitinger, H.; Rahmann, H.; Möbius, D. Effect of calcium and temperature on mixed lipid-valinomycin monolayers A comparison of glycosphingolipids (ganglioside GT1b, sulphatides) and phosphatidylcholine. FEBS Lett 1988, 233 (1), 158-162.

193.   Maggio, B.; Cumar, F. A.; Caputto, R. Surface behaviour of gangliosides and related glycosphingolipids. Biochem. J 1978, 171, 559-565.

194.   Wu, X.; Li, Q.-T. Hydration and stability of sulfatide-containing phosphatidylethanolamine small unilamellar vesicles. Biochim Biophys Acta 1999, 1416 (1–2), 285-294.

195.   Wang, T.-Y.; Silvius, J. R. Sphingolipid Partitioning into Ordered Domains in Cholesterol-Free and Cholesterol-Containing Lipid Bilayers. Biophys J 2003, 84, 367-378.

196.   Sáez-Cirión, A.; Basáñez, G.; Fidelio, G.; Goñi, F. M.; Maggio, B.; Alonso, A. Sphingolipids (galactosylceramide and sulfatide) in lamellar-hexagonal phospholipid phase transitions and in membrane fusion. Langmuir 2000, 16 (23), 8958-8963.

197.   Sarasij, R.; Mayor, S.; Rao, M. Chirality-induced budding: a raft-mediated mechanism for endocytosis and morphology of caveolae? Biophys J 2007, 92 (9), 3140-3158.

198.   Brown, R. E.; Anderson, W. H.; Kulkarni, V. S. Macro-Ripple Phase Formation in Bilayers Composed of Galactosylceramide and Phosphatidylcholine. Biophys J 1995, 68, 1396-1405.

199.   Kulkarni, V. S.; Anderson, W. H.; Brown, R. E. Bilayer Nanotubes and Helical Ribbons Formed by Hydrated Galactosylceramides: Acyl Chain and Headgroup Effects. Biophys J 1995, 69, 1976-1986.

200.   Helfrich, W.; Prost, J. Intrinsic bending force in anisotropic membranes made of chiral molecules. Phys Rev A 1988, 38 (6), 3065-3068.

201.   Archibald, D. D.; Yager, P. Microstructural polymorphism in bovine brain galactocerebroside and its two major subfractions. Biochemistry 1992, 31 (37), 9045-9055.

202.   Kulkarni, V. S.; Boggs, J. M.; Brown, R. E. Modulation of Nanotube Formation by Structural Modifications of Sphingolipids. Biophys J 1999, 77, 319-330.

203.   Suetsugu, S.; Kurisu, S.; Takenawa, T. Dynamic Shaping of Cellular Membranes by Phospholipids and Membrane-Deforming Proteins. Physiol Rev. 2014, 94 (4), 1219-1248.

204.   Li, X.-M.; Momsen, M. M.; Brockman, H. L.; Brown, R. E. Lactosylceramide: Effect of Acyl Chain Structure on Phase Behavior and Molecular Packing. Biophys J 2002, 83 (3), 1535-1546.

205.   Mannock, D. A.; Harper, P. E.; Gruner, S. M.; McElhaney, R. N. The physical properties of glycosyl diacylglycerols. Calorimetric, X-ray diffraction and Fourier transform spectroscopic studies of a homologous series of 1,2-di-O-acyl-3-O-(b-d-galactopyranosyl)-sn-glycerols. Chem Phys Lipids 2001, 111 (2), 139-161.

206.   Slotte, J. P.; Oestman, A. L.; Kumar, E. R.; Bittman, R. Cholesterol interacts with lactosyl and maltosyl cerebrosides but not with glucosyl or galactosyl cerebrosides in mixed monolayers. Biochemistry 1993, 32 (31), 7886-7892.

207.   Klappe, K.; Hinrichs, J. W. J.; Kroesen, B.-J.; Sietsma, H.; Kok, J. W. MRP1 and glucosylceramide are coordinately over expressed and enriched in rafts during multidrug resistance acquisition in colon cancer cells. Int J Cancer 2004, 110 (4), 511-522.

208.   Harzer, K.; Massenkeil, G.; Fröhlich, E. Concurrent increase of cholesterol, sphingomyelin and glucosylceramide in the spleen from non-neurologic Niemann−Pick type C patients but also patients possibly affected with other lipid trafficking disorders. FEBS Lett 2003, 537 (1-3), 177-181.

209.   Perkovic´, S.; McConnell, H. M. Cloverleaf Monolayer Domains. J Phys Chem B 1997, 101, 381-388.

210.   Blanchette, C. D.; Lin, W.-C.; Ratto, T. V.; Longo, M. L. Galactosylceramide Domain Microstructure: Impact of Cholesterol and Nucleation/Growth Conditions. Biophys J 2006, 90 (12), 4466-4478.

211.   Wesołowska, O.; Michalak, J.; Maniewska, J.; Hendrich, A. Giant unilamellar vesicles — a perfect tool to visualize phase separation and lipid rafts in model systems. Acta Biochim Pol 2009, 56 (1), 33-39.

212.	Georgieva, R.; Koumanov, K.; Momchilova, A.; Tessier, C.; Staneva, G. Effect of sphingosine on domain morphology in giant vesicles. J Colloid Interface Sci 2010, 350 (2), 502-510.

213.	Watanabe, C.; Puff, N.; Staneva, G.; Seigneuret, M.; Angelova, M. I. Antagonism and Synergy of Single Chain Sphingolipids Sphingosine and Sphingosine-1-phosphate toward Lipid Bilayer Properties. Consequences for Their Role as Cell Fate Regulators. Langmuir 2014, 30 (46), 13956-13963.

214.	Prenner, E.; Honsek, G.; Hönig, D.; Möbius, D.; Lohner, K. Imaging of the domain organization in sphingomyelin and phosphatidylcholine monolayers. Chem Phys Lipids 2007, 145 (2), 106-118.

215.	Yuan, C.; Furlong, J.; Burgos, P.; Johnston, L. J. The Size of Lipid Rafts: An Atomic Force Microscopy Study of Ganglioside GM1 Domains in Sphingomyelin/DOPC/Cholesterol Membranes. Biophys J 2002, 82 (5), 2526-2535.

216.	Bandekar, A.; Sofou, S. Floret-Shaped Solid Domains on Giant Fluid Lipid Vesicles Induced by pH. Langmuir 2012, 28 (9), 4113-4122.

217.	Grabe, M.; Oster, G. Regulation of Organelle Acidity. J Gen Physiol 2001, 117 (4), 329-44.

218.	Paroutis, P. The pH of the Secretory Pathway: Measurement, Determinants, and Regulation. Physiology 2004, 19 (4), 207-215.

219.	Petelska, A. D.; Naumowicz, M.; Figaszewski, Z. A. Influence of pH on Sphingomyelin Monolayer at Air/Aqueous Solution Interface. Langmuir 2012, 28 (37), 13331-13335.

220.	Owen, D. M.; Magenau, A.; Williamson, D.; Gaus, K. The lipid raft hypothesis revisited – New insights on raft composition and function from super-resolution fluorescence microscopy. BioEssays 2012, 34 (9), 739-747.

221.	Shaw, A. S. Lipid rafts: now you see them, now you don't. Nat Immunol 2006, 7 (11), 1139-1142.

222.	Pike, L. J. Rafts defined: a report on the Keystone symposium on lipid rafts and cell function. J Lipid Res 2006, 47 (7), 1597-1598.

223.	Magenau, A.; Benzing, C.; Proschogo, N.; Don, A. S.; Hejazi, L.; Karunakaran, D.; Jessup, W.; Gaus, K. Phagocytosis of IgG-Coated Polystyrene Beads by Macrophages Induces and Requires High Membrane Order. Traffic 2011, 12 (12), 1730-1743.

224.	Simons, K.; Sampaio, J. L. Membrane Organization and Lipid Rafts. Cold Spring Harb Perpect Biol 2011, 3 (10), a004697-a004697.

225.	Lingwood, D.; Simons, K. Lipid Rafts As a Membrane-Organizing Principle. Science 2010, 327 (5961), 46-50.

226.	Sharma, M.; Celver, J.; Octeau, J. C.; Kovoor, A. Plasma Membrane Compartmentalization of D2 Dopamine Receptors. J Biol Chem 2013, 288 (18), 12554-12568.

227.	Sillence, D.; Platt, F. Glycosphingolipids in endocytic membrane transport. Semin Cell Dev Biol 2004, 15 (4), 409-416.

228.	London, E. Membrane fusion: A new role for lipid domains? Nat Chem Biol 2015, 11 (6), 383-384.

229.	Ewers, H.; Helenius, A. Lipid-Mediated Endocytosis. Cold Spring Harb Perpect Biol 2011, 3 (8), 1-14.

230.	Lafont, F.; Verkade, P.; Galli, T.; Wimmer, C.; Louvard, D.; Simons, K. Raft association of SNAP receptors acting in apical trafficking in Madin–Darby canine kidney cells. Proc Natl Acad Sci U S A 1999, 96 (7), 3734-3738.

231.	George, K. S.; Wu, S. Lipid raft: A floating island of death or survival. Toxicol Appl Pharmacol 2012, 259 (3), 311-319.

232.	Diaz-Rohrer, B. B.; Levental, K. R.; Simons, K.; I., L. Membrane raft association is a determinant of plasma membrane localization. Proc Natl Acad Sci U S A 2014, 111 (23), 8500-8505.

233.	Ando, K.; Obara, Y.; Sugama, J.; Kotani, A.; Koike, N.; Ohkubo, S.; Nakahata, N. P2Y2 Receptor-Gq/11 Signaling at Lipid Rafts Is Required for UTP-Induced Cell Migration in NG 108-15 Cells. J Pharm Exp Ther 2010, 334 (3), 809-819.

234.	Evangelisti, E.; Wright, D.; Zampagni, M.; Cascella, R.; Fiorillo, C.; Bagnoli, S.; Relini, A.; Nichino, D.; Scartabelli, T.; Nacmias, B. Lipid rafts mediate amyloid-induced calcium dyshomeostasis and oxidative stress in Alzheimer's disease. Curr Alzheimer Res 2013, 10 (2), 143-153.

235.	Mierke, C. T.; Bretz, N.; Altevogt, P. Contractile Forces Contribute to Increased Glycosylphosphatidylinositol-anchored Receptor CD24-facilitated Cancer Cell Invasion. J Biol Chem 2011, 286 (40), 34858-34871.

236.	Goldston, A. M.; Powell, R. R.; Temesvari, L. A. Sink or swim: lipid rafts in parasite pathogenesis. Trends Parasitol 28 (10), 417-426.

237.	Nguyen, D. H.; Hildreth, J. E. K. Evidence for Budding of Human Immunodeficiency Virus Type 1 Selectively from Glycolipid-Enriched Membrane Lipid Rafts. J Virol 2000, 74 (7), 3264-3272.

238.	Chan, Y.-H. M.; Boxer, S. G. Model Membrane Systems and Their Applications. Curr Opin Chem Biol 2007, 11 (6), 581-587.

239.	Lagny, T. J.; Bassereau, P. Bioinspired membrane-based systems for a physical approach of cell organization and dynamics: usefulness and limitations. Interface Focus 2015, 5 (4), 1-10.

240.	Peetla, C.; Stine, A.; Labhasetwar, V. Biophysical interactions with model lipid membranes: applications in drug discovery and drug delivery. Mol Pharm 2009, 6 (5), 1264-1276.

241.	Miret, S.; Abrahamse, L.; de Groene, E. M. Comparison of in Vitro Models for the Prediction of Compound Absorption across the Human Intestinal Mucosa. J Biomol Screen 2004, 9 (7), 598-606.

242.	Cruz, A.; Pérez-Gil, J. Langmuir films to determine lateral surface pressure on lipid segregation. In Methods in Membrane Lipids; Springer, 2007, pp 439-457.

243.	Busto, J. V.; Fanani, M. L.; De Tullio, L.; Sot, J.; Maggio, B.; Goñi, F. M.; Alonso, A. Coexistence of Immiscible Mixtures of Palmitoylsphingomyelin and Palmitoylceramide in Monolayers and Bilayers. Biophys J 2009, 97 (10), 2717-2726.

244.	Laouini, A.; Jaafar-Maalej, C.; Limayem-Blouza, I.; Sfar, S.; Charcosset, C.; Fessi, H. Preparation, Characterization and Applications of Liposomes: State of the Art. J Colloid Sci Biotechnol 2012, 1 (2), 147-168.

245.	Jesorka, A.; Orwar, O. Liposomes: Technologies and Analytical Applications. Annu Rev Anal Chem 2008, 1 (1), 801-832.

246.	Pinheiro, M.; Lúcio, M.; Lima, J. L.; Reis, S. Liposomes as drug delivery systems for the treatment of TB. Nanomedicine 2011, 6 (8), 1413-1428.

247.	Richter, R. P.; Brisson, A. R. Following the Formation of Supported Lipid Bilayers on Mica: A Study Combining AFM, QCM-D, and Ellipsometry. Biophys J 2005, 88 (5), 3422-3433.

248.	Torcato, I. M.; Castanho, M. A.; Henriques, S. T. The application of biophysical techniques to study antimicrobial peptides. Spectrosc-Int J 2012, 27 (5-6), 541-549.

249.   Hope, M. J.; Nayar, R.; Mayer, L. D.; Cullis, P. Reduction of liposome size and preparation of unilamellar vesicles by extrusion techniques. 1993; Vol. 1, p 123-139.

250.   Hope, M. J.; Bally, M. B.; Mayer, L. D.; Janoff, A. S.; Cullis, P. R. Generation of multilamellar and unilamellar phospholipid vesicles. Chem Phys Lipids 1986, 40 (2–4), 89-107.

251.   Ma, Y. Characterization of Membrane Permeability and Polymer-Stabilized Model Membranes. ProQuest: 2007.

252.   Hope, M. J.; Bally, M. B.; Webb, G.; Cullis, P. R. Production of large unilamellar vesicles by a rapid extrusion procedure. Characterization of size distribution, trapped volume and ability to maintain a membrane potential. Biochim Biophys Acta 1985, 812 (1), 55-65.

253.   Walde, P.; Cosentino, K.; Engel, H.; Stano, P. Giant vesicles: preparations and applications. ChemBioChem 2010, 11 (7), 848-865.

254.   Sarmento, M. J.; Prieto, M.; Fernandes, F. Reorganization of lipid domain distribution in giant unilamellar vesicles upon immobilization with different membrane tethers. Biochim Biophys Acta 2012, 1818 (11), 2605-2615.

255.   Oglecka, K.; Sanborn, J.; Parikh, A. N.; Kraut, R. S. Osmotic Gradients Induce Bio-reminiscent Morphological Transformations in Giant Unilamellar Vesicles. Front Physiol 2012, 3.

256.   Scientific, B. Langmuir, Langmuir-Blodgett, Langmuir-Schaefer Technique. http://www.biolinscientific.com/technology/l-lb-ls-technique/.

257.   Giner-Casares, J.; Brezesinski, G. Brewster Angle Microscopy (BAM) for in situ characterization of ultrathin films at air/liquid interfaces. Formatex: Badajoz, 2012; Vol. 2, p 1007-1012.

258.   Malvern. Dynamic Light Scattering (DLS). http://www.malvern.com/en/products/technology/dynamic-light-scattering/default.aspx.

259.   Malvern. Electrophoretic Light Scattering (ELS). http://www.malvern.com/en/products/technology/electrophoretic-light-scattering/default.aspx.

260.   Murphy, D. B.; Davidson, M. W. Fundamentals of Light Microscopy and Electronic Imaging. Wiley: 2012.

261.   Olympus. Theory of Confocal Microscopy. http://www.olympusconfocal.com/theory/.

262.   Lakowicz, J. R. 3rd ed.; Springer: New York, 2006.

263.   Berezin, M. Y.; Achilefu, S. Fluorescence Lifetime Measurements and Biological Imaging. Chem Rev 2010, 110 (5), 2641-2684.

264.   Castro, B. M.; de Almeida, R. F. M.; Fedorov, A.; Prieto, M. The photophysics of a Rhodamine head labeled phospholipid in the identification and characterization of membrane lipid phases. Chem Phys Lipids 2012, 165 (3), 311-319.

265.   Sklar, L. A.; Hudson, B. S.; Petersen, M.; Diamond, J. Conjugated polyene fatty acids as fluorescent probes: spectroscopic characterization. Biochemistry 1977, 16 (5), 813-819.

266.   Sanchez, S. A.; Tricerri, M. A.; Gunther, G.; Gratton, E. Laurdan Generalized Polarization: from cuvette to microscope. Formatex: Badajoz, 2007; Vol. 3, p 1007-1014.

267.   Olympus. Overview of Fluorescence Excitation and Emission Fundamentals. http://www.olympusmicro.com/primer/lightandcolor/fluoroexcitation.html.

268.   Merritt, E. A.; Sarfaty, S.; Akker, F. V. D.; L'Hoir, C.; Martial, J. A.; Hol, W. G. J. Crystal structure of cholera toxin B-pentamer bound to receptor GM1 pentasaccharide. Protein Sci 1994, 3 (2), 166-175.

269.   Sklar, L. A.; Miljanich, G. P.; Dratz, E. A. Phospholipid Lateral Phase Separation and the Partition of cis-Parinaric Acid and trans-Parinaric Acid among Aqueous, Solid Lipid, and Fluid Lipid Phases. Biochemistry 1979, 18, 1707-1716.

270.   Parasassi, T.; Stefano, M. D.; Loiero, M.; Ravagnan, G.; Gratton, E. Influence of Cholesterol on Phospholipids Bilayers Phase Domains as Detected by Laurdan Fluorescence. Biophys J 1994, 66, 120-132.

271.   Klymchenko, Andrey S.; Kreder, R. Fluorescent Probes for Lipid Rafts: From Model Membranes to Living Cells. Chem Biol 2014, 21 (1), 97-113.

272.   Haldar, S.; Chattopadhyay, A. Application of NBD-Labeled Lipids in Membrane and Cell Biology. Springer-Verlag: Heidelberg, 2012; Vol. 13, p 37-50.

273.   Shinitzky, M.; Barenholz, Y. Dynamics of the Hydrocarbon Layer in Liposomes of Lecithin and Sphingomyelin Containing Dicetylphosphate. J Biol Chem 1974, 249 (8), 2652-2657.

274.   Nyholm, T. K. M.; Lindroos, D.; Westerlund, B.; Slotte, J. P. Construction of a DOPC/PSM/Cholesterol Phase Diagram Based on the Fluorescence Properties of trans-Parinaric Acid. Langmuir 2011, 27 (13), 8339-8350.

275.   Castro, B. M.; Silva, L. C.; Fedorov, A.; de Almeida, R. F. M.; Prieto, M. Cholesterol-rich Fluid Membranes Solubilize Ceramide Domains: Implcations for the Structure and Dynamics of Mammmalian Intracellular and Plasma Membranes. J Biol Chem 2009, 284 (34), 22978-22987.

276.   Haugland, R. P.; Spence, M. T.; Johnson, I. D. Handbook of Fluorescent Probes and Research Chemicals. 6th ed.; Molecular Probes: Eugene OR, 1996.

277.   Harris, F. M.; Best, K. B.; Bell, J. D. Use of Laurdan fluorescence intensity and polarization to distinguish between changes in membrane fluidity and phospholipid order. Biochem Biophys Acta 2002, 1565, 123-128.

Chapter I

Chapter II

Effect of glucosylceramide on the biophysical properties of fluid membranes

Contents lists available at SciVerse ScienceDirect

Biochimica et Biophysica Acta

journal homepage: www.elsevier.com/locate/bbamem

Effect of glucosylceramide on the biophysical properties of fluid membranes

Ana R.P. Varela [a,b,c], Amélia M.P.S. Gonçalves da Silva [d], Alexander Fedorov [b], Anthony H. Futerman [c], Manuel Prieto [b], Liana C. Silva [a,*]

[a] iMed.UL - Research Institute for Medicines and Pharmaceutical Sciences, Faculdade de Farmácia, Universidade de Lisboa, Av. Prof. Gama Pinto, 1649-003 Lisboa, Portugal
[b] Centro de Química-Física Molecular and Institute of Nanoscience and Nanotechnology, Instituto Superior Técnico, Universidade Técnica de Lisboa, Complexo I, Av. Rovisco Pais, 1049-001 Lisboa, Portugal
[c] Department of Biological Chemistry, Weizmann Institute of Sciences, Rehovot 76100, Israel
[d] Centro de Química Estrutural, Instituto Superior Técnico, Universidade Técnica de Lisboa, Complexo I, Av. Rovisco Pais, 1049-001 Lisboa, Portugal

ARTICLE INFO

ABSTRACT

Glucosylceramide (GlcCer), a relevant intermediate in the pathways of glycosphingolipid metabolism, plays key roles in the regulation of cell physiology. The molecular mechanisms by which GlcCer regulates cellular processes are unknown, but might involve changes in membrane biophysical properties and formation of lipid domains. In the present study, fluorescence spectroscopy, confocal microscopy and surface pressure–area (π–A) measurements were used to characterize the effect of GlcCer on the biophysical properties of model membranes. We show that C16:0-GlcCer has a high tendency to segregate into highly ordered gel domains and to increase the order of the fluid phase. Monolayer studies support the aggregation propensity of C16:0-GlcCer. π–A isotherms of single C16:0-GlcCer indicate that bilayer domains, or crystal-like structures, coexist within monolayer domains at the air–water interface. Mixtures with POPC exhibit partial miscibility with expansion of the mean molecular areas relative to the additive behavior of the components. Moreover, C16:0-GlcCer promotes morphological alterations in lipid vesicles leading to formation of flexible tubule-like structures that protrude from the fluid region of the bilayer. These results support the hypothesis that alterations in membrane biophysical properties induced by GlcCer might be involved in its mechanism of action.

© 2012 Elsevier B.V. All rights reserved.

1. Introduction

Glycosphingolipids (GSLs) are ubiquitous components of eukaryotic cell membranes. GSLs are synthesized by sequential addition of saccharides to the hydroxyl group at the C-1 position of the ceramide (Cer) backbone [1–4]. GSLs are mainly located in the extracellular leaflet of the plasma membrane, where they are involved in several functions such as cell-to-cell interaction and recognition [1,5,6]. Glucosylceramide (GlcCer), one of the simplest GSLs, is widely distributed in mammalian tissues. GlcCer is formed at the cytosolic leaflet of Golgi apparatus by glycosylation of Cer by GlcCer synthase (GCS) [7].

After its synthesis, GlcCer is transported to the luminal side of the Golgi apparatus where is converted into more complex GSLs, or transported by FAPP2 (4-phosphate adaptor protein-2) [8] to the cytoplasmic leaflet of the plasma membrane (PM) or of the endoplasmic reticulum (ER) [9–11]. In the PM, GlcCer may remain on the cytoplasmic leaflet or translocate to the cell surface [12].

GlcCer is an important intracellular messenger that plays key roles in cell maintenance and regulation [13–17]. However, the molecular mechanisms by which GlcCer regulates cellular processes are unknown. GSLs are thought to be involved in the formation of lipid rafts which, because of their specific biophysical properties, can act as signaling platforms [5,6]. In the last decade, much effort has been made to understand the biophysical properties of lipid rafts [18–21]; however, little attention has been given to GlcCer. GlcCer has a high main transition temperature (T_m) and a complex thermotropic phase behavior, with multiple transitions between different stable and metastable phases [22]. Due to their high T_m and extensive hydrogen-bond network, GSLs with small uncharged headgroups are expected to segregate from low T_m phospholipids and form tightly packed domains [23–27], with a higher packing density than sphingomyelin with a similar backbone [28–30]. These observations suggest that GlcCer might promote similar changes to those induced by Cer in the biophysical properties of fluid membranes [31–33]. Previous studies from our group have showed that Cer has a complex phase behavior promoting

Chapter II- Effect of glucosylceramide on the biophysical properties of fluid membranes

1 Abstract

Glucosylceramide (GlcCer), a relevant intermediate in the pathways of glycosphingolipid metabolism, plays key roles in the regulation of cell physiology. The molecular mechanisms by which GlcCer regulates cellular processes are unknown, but might involve changes in membrane biophysical properties and formation of lipid domains. In the present study, fluorescence spectroscopy, confocal microscopy and surface pressure - area (π–A) measurements were used to characterize the effect of GlcCer on the biophysical properties of model membranes. We show that C16:0-GlcCer has a high tendency to segregate into highly ordered gel domains and to increase the order of the fluid phase. Monolayer studies support the aggregation propensity of C16:0-GlcCer. π–A isotherms of single C16:0-GlcCer indicate that bilayer domains, or crystal-like structures, coexist within monolayer domains at the air–water interface. Mixtures with POPC exhibit partial miscibility with expansion of the mean molecular areas relative to the additive behavior of the components. Moreover, C16:0-GlcCer promotes morphological alterations in lipid vesicles leading to formation of flexible tubule-like structures that protrude from the fluid region of the bilayer. These results support the hypothesis that alterations in membrane biophysical properties induced by GlcCer might be involved in its mechanism of action.

2 Introduction

Glycosphingolipids (GSLs) are ubiquitous components of eukaryotic cell membranes. GSLs are synthesized by sequential addition of saccharides to the hydroxyl group at the C-1 position of the ceramide (Cer) backbone[1, 2, 3, 4]. GSLs are mainly located in the extracellular leaflet of the plasma membrane, where they are involved in several functions such as cell-to-cell interaction and recognition[1, 5, 6]. Glucosylceramide (GlcCer), one of the simplest GSLs, is widely distributed in mammalian tissues. GlcCer is formed at the cytosolic leaflet of Golgi apparatus by glycosylation of Cer by GlcCer synthase (GCS) [7]. After its synthesis, GlcCer is transported to the luminal side of the Golgi apparatus where is converted into more complex GSLs, or transported by FAPP2 (4-phosphate adaptor protein-2) [8] to the cytoplasmic leaflet of the plasma membrane (PM) or of the endoplasmic reticulum (ER) [9, 10, 11]). In the PM, GlcCer may remain on the cytoplasmic leaflet or translocate to the cell surface [12].

GlcCer is an important intracellular messenger that plays key roles in cell maintenance and regulation[13, 14, 15, 16, 17]. However, the molecular mechanisms by which GlcCer regulates cellular processes are unknown. GSLs are thought to be involved in the formation of lipid rafts which, because of their specific biophysical properties, can act as signaling platforms [5, 6]. In the last decade, much effort has been made to understand the biophysical properties of lipid rafts [18, 19, 20, 21]; however, little attention has been given to GlcCer. GlcCer has a high main transition temperature (T_m) and a complex thermotropic phase behavior, with multiple transitions between different stable and metastable phases [22]. Due to their high T_m and extensive hydrogen-bond network, GSLs with small uncharged headgroups are expected to segregate from low T_m phospholipids and form tightly packed domains [23, 24, 25, 26, 27], with a higher packing density than sphingomyelin with a similar backbone [28, 29, 30]. These observations suggest that GlcCer might promote similar changes to those induced by Cer in the biophysical properties of fluid membranes[31, 32, 33]. Previous studies from our group have showed that Cer has a complex phase behavior promoting extensive alterations in the biophysical properties of membranes that are dependent both on Cer content and membrane lipid composition, particularly on cholesterol (Chol) content [34, 35, 36].

In the present study, fluorescence spectroscopy, confocal microscopy and surface pressure - area (π–A) measurements were used to characterize lipid lateral distribution, ability to segregate into tightly-packed domains and membrane morphological alterations induced by C16:0-GlcCer in fluid model membranes. Our results show that C16:0-GlcCer has a high tendency to segregate into highly ordered gel domains and to increase the order of the fluid phase, although to a lower extent than the corresponding Cer (C16:0-Cer). Thermodynamic analysis of POPC/ C16:0-GlcCer mixed monolayers indicates (partial) miscibility with positive deviations from the ideal behavior. Moreover, C16:0-GlcCer promotes morphological alterations in lipid vesicles leading to the formation of flexible tubule-like structures that protrude from the fluid membrane.

3 Materials and Methods

3.1 Materials

POPC (1-palmitoyl-2-oleoyl-*sn*-glycero-3-phosphocholine), GlcCer (D-glucosyl-ß-1,1' N-palmitoyl-D-*erythro*-sphingosine), Rho-DOPE (N-rhodamine-dipalmitoylphosphatidylethanolamine) and DOPE-biotin (1,2-dioleoyl-sn-glycero-3-phosphoethanolamine-*N*-(biotinyl)) were from Avanti Polar Lipid (Alabaster, AL). DPH (1,6-diphenyl-1,3,5-hexatriene), *t*-PnA (*trans*-parinaric acid), Laurdan (6-dodecanoyl-2-dimethylaminonaphthalene) and NBD-DPPE (1,2-dipalmitoyl-*sn*-glycero-3-phosphoethanolamine-N-(7-nitro-2-1,3-benzoxadiazol-4yl)) were from Molecular Probes (Leiden, The Netherlands). All organic solvents were UVASOL grade from Merck (Darmstadt, Germany). The concentration of the lipid and of the probes stock solutions were determined as previously described [33].

3.2 Fluorescence spectroscopy

To evaluate the effect of GlcCer on membrane biophysical properties, multilamellar vesicles (MLV) (total lipid concentration of 0.1 mM) were prepared as previously described [33]. The suspension medium was 10 mM sodium phosphate, 150 mM NaCl, 0.1 mM EDTA (pH 7.4). Fluorescence anisotropy of *t*-PnA, DPH and Rho-DOPE, and Laurdan emission spectra (at a probe/lipid ratio of 1/500, 1/200, 1/500 and 1/400, respectively) were measured in a SLM Aminco 8100 series 2 spectrofluorimeter with double excitation and emission monochromators, MC400 (Rochester, NY). All

measurements were performed in 0.5 cm × 0.5 cm quartz cuvettes. The excitation (λ_{exc})/emission (λ_{em}) wavelengths were 320/405 nm for t-PnA; 358/430 nm for DPH; 350/435nm for Laurdan; 570/593 for Rho-DOPE. Constant temperature was maintained using a Julabo F25 circulating water bath controlled with 0.1°C precision directly inside the cuvette with a type-K thermocouple (Electrical Electronic Corp., Taipei, Taiwan). For measurements performed at different temperatures, the heating rate was always below 0.2°C/min. The fluorescence anisotropy $<r>$ was calculated from [37]:

$$<r> = \frac{I_{vv} - GI_{vh}}{I_{vv} + 2GI_{vh}}$$

(Eq. 1)

where the different intensities (I_{ii}) are the steady state vertical and horizontal components of the fluorescence emission with the excitation vertical (I_{vv} and I_{vh}) and horizontal (I_{hv} and I_{hh}) for the emission axis. The latter pair of components is used to calculate the G factor ($G = I_{hv}/I_{hv}$). An appropriate blank was subtracted from each intensity reading before calculation of the anisotropy value.

Laurdan GP (generalized polarization) was determined using [38]:

$$GP = \frac{I_{440} - I_{490}}{I_{440} + I_{490}}$$

(Eq. 2)

where I_{440} and I_{490} are the emission intensities at 440 and 490 nm respectively, reporting the maximum emission in the gel and in the liquid crystalline phase, respectively [38, 39]. Theoretically this parameter varies from +1 to -1, however, experimentally ranges from 0.7 to -0.3 both for pure lipids or mixtures [38].

Time-resolved fluorescence measurements with t-PnA were performed using λ_{exc}=305nm (using a secondary laser of Rhodamine 6G) and λ_{em}=405nm. The experimental decays were analyzed using TRFA software (Scientific Software Technologies Center, Minsk, Belarus).

3.3 Confocal fluorescence microscopy

Giant unilamellar vesicles (GUVs) contained the appropriate lipids, DOPE-biotin (at a biotinylated/non-biotinylated lipid ratio of $1{:}10^{6}$), Rho-DOPE and NBD-DPPE (at a

probe/lipid ratio of 1:500 and 1:200, respectively). These were prepared by electroformation, as previously described[32, 40, 41]. The GUVs were then transferred to 8 well Ibidi® μ-slides that had been previously coated with avidin (at 0.1mg/ml) to improve GUV adhesion to the plate [42]. Confocal fluorescence microscopy was performed using a Leica TCS SP5 (Leica Mycrosystems CMS GmbH, Mannheim, Germany) inverted microscope (DMI6000) with a 63×water (1.2 numerical aperture) apochromatic objective. NBD-DPPE and Rho-DOPE excitation was performed using the 458 nm and 514 nm lines from an Ar⁺ laser, respectively. The emission was collected at 480-530 nm and 530-650 nm, for NBD-DPPE and Rho-DOPE, respectively. Confocal sections of thickness below 0.5 μm were obtained using a galvanometric motor stage. Three-dimensional (3D) projections were obtained using Leica Application Suite-Advanced Fluorescence software.

3.4 Lipid monolayers and surface pressure–area measurements

Surface pressure–area (π–A) isotherm measurements were carried out on a KSV 5000 Langmuir–Blodgett system (KSV Instruments, Helsinki) installed in a laminar flow hood. Procedures for π–A measurements and cleaning care were described elsewhere [43]. Monolayers were spread drop-wise as chloroform solutions using a microsyringe, on the subphase of a buffer solution. Unless specified, the concentration of spreading solution was 0.5 mM. The temperature of the subphase was controlled by water circulation from a thermostat within an error of ±0.1 °C. The barrier speed of symmetric compression was 10 mm min⁻¹ (3.3 Å² molecule⁻¹ min⁻¹). π–A isotherms were measured at least three times from fresh spreading solutions to confirm reproducibility.

The isothermal two-dimensional compressibility modulus, or elastic modulus, is calculated from the π–A isotherms as $C_s^{-1} = -A(\partial A/\partial \pi)_T$.

The Gibbs energy of mixing, ΔG_{mix}, is taken from:

$$\Delta G_{mix}(\pi) = \Delta G_{ideal} + G^E(\pi), \qquad\qquad\qquad \text{(Eq. 3)}$$

where ΔG_{ideal} is the Gibbs energy of ideal mixing at low surface pressure (π→0)

$$\Delta G_{ideal} = RT(X_1 ln\, X_1 + X_2 ln\, X_2), \qquad\qquad \text{(Eq. 4)}$$

and $G^E(\pi)$ is the excess Gibbs energy of mixing:

$$G^E(\pi) = \int A^E(\pi)d\pi, \qquad\qquad\qquad\qquad \text{(Eq. 5)}$$

where $A^E(\pi)$ is the excess area of mixing at the surface pressure π,

$$A^E (\pi) = [A_{12} - (X_1 A_1 + X_2 A_2)],\qquad\qquad\text{(Eq. 6)}$$

and A_{12} is the MMA (Mean Molecular Area) of the mixed monolayer, X_1 and X_2 are the mole fraction of components 1 and 2, respectively, and A_1 and A_2 are the corresponding molecular areas in the single component monolayer at the surface pressure π.

4 Results

4.1 Biophysical properties of POPC/GlcCer mixtures

The effect of C16:0-GlcCer on the properties of the fluid POPC membrane was assessed by following the variation of the photophysical parameters of different probes as a function of C16:0-GlcCer molar fraction (Fig. 1). An increase in C16:0-GlcCer molar fraction leads to an increase in t-PnA fluorescence anisotropy reaching values typical of the gel phase [36], showing that C16:0-GlcCer is able to drive the formation of gel domains (Fig. 1A). This is further supported by the increase in the lifetime of the long component of t-PnA fluorescence intensity decay (Fig. 1B). A long lifetime component > 30ns, as observed for C16:0-GlcCer > 20%, is characteristic of gel domains [35]. It should be stressed that for very high C16:0-GlcCer content (> 90%), t-PnA fluorescence anisotropy decrease, and in addition the error associated with the measurements is high. This might be associated with the formation of crystal-like phases that exclude t-PnA to the aqueous environment, as previously reported for C16:0-Cer [33]. Studies performed by Saxena et al [22] and Dicko *et al* [44] also support the existence of GlcCer crystals. However, the decrease in t-PnA fluorescence anisotropy is not as sharp as observed in POPC/C16:0-Cer mixtures, which suggests that crystal-like structures (that exclude t-PnA) might coexist with lipid bilayers (that incorporate t-PnA). The characterization of crystal-like structures is beyond the scope of the present study, and therefore full characterization of the effect of C16:0-GlcCer in model membranes was only performed for mixtures containing ≤ 90% GlcCer. Moreover, the presence of crystal structures would imply that the lipid mixture is not under a fully hydration regime and therefore, the contribution of water had to be taken into account. Under these conditions, the system would have to be treated has a ternary mixture, where the water concentration would be the third component. Nevertheless, the GlcCer mixtures investigated under the present study encompasses the range of GlcCer at the cell level, even considering the existence of high basal concentrations and pathological conditions.

To further characterize the nature of the gel domains, the fluorescence anisotropy of DPH was determined. Increase in C16:0-GlcCer molar fraction leads to a slight increase in DPH fluorescence anisotropy (Fig. 1C), demonstrating that C16:0-GlcCer forms highly-ordered gel domains similar to Cer-domains, which exclude DPH [33, 45]. Because DPH is excluded from these gel domains, the slight increase in its fluorescence anisotropy induced by C16:0-GlcCer is due to an increase in the order of the coexistent fluid phase. It should be stressed that DPH anisotropy increases in pure GlcCer, suggesting that DPH is not totally excluded from GlcCer membranes, in contrast to the observed for Cer [33, 45]. This observation further supports the hypothesis of coexisting crystal-like structures and lipid bilayers for mixtures containing very high GlcCer molar fractions. The highly-ordered nature of the C16:0-GlcCer gel domains was further confirmed by Laurdan GP (Fig. S1B). Laurdan GP is often used to distinguish between ordered and disordered phases [46]. High GP values are typically obtained in gel phases and low GP values in fluid phases. In POPC/ C16:0-GlcCer mixtures, GP values increase only moderately with C16:0-GlcCer concentration (Fig. S1B) showing that this probe is also partially excluded from these gel domains.

Rho-DOPE displays different behavior: first, this probe is excluded from ordered (gel and liquid ordered) phases and reports mainly alterations in the fluid (disordered) phase [36]; second, Rho-DOPE displays energy homotransfer, which is strongly dependent on the distance between the chromophores. When the molecules are close, energy homotransfer occurs, leading to a decrease in Rho-DOPE fluorescence anisotropy [37]. This behavior allows the detection of the formation of ordered phases (Fig. 1D), since the increase in C16:0-GlcCer content leads to an increase in the fraction of ordered phase and a consequent decrease in the fraction of the fluid phase available for Rho-DOPE distribution. This implies a higher probe surface concentration, with a concomitant decrease of its anisotropy, due to a higher FRET efficiency (Fig. 1D).
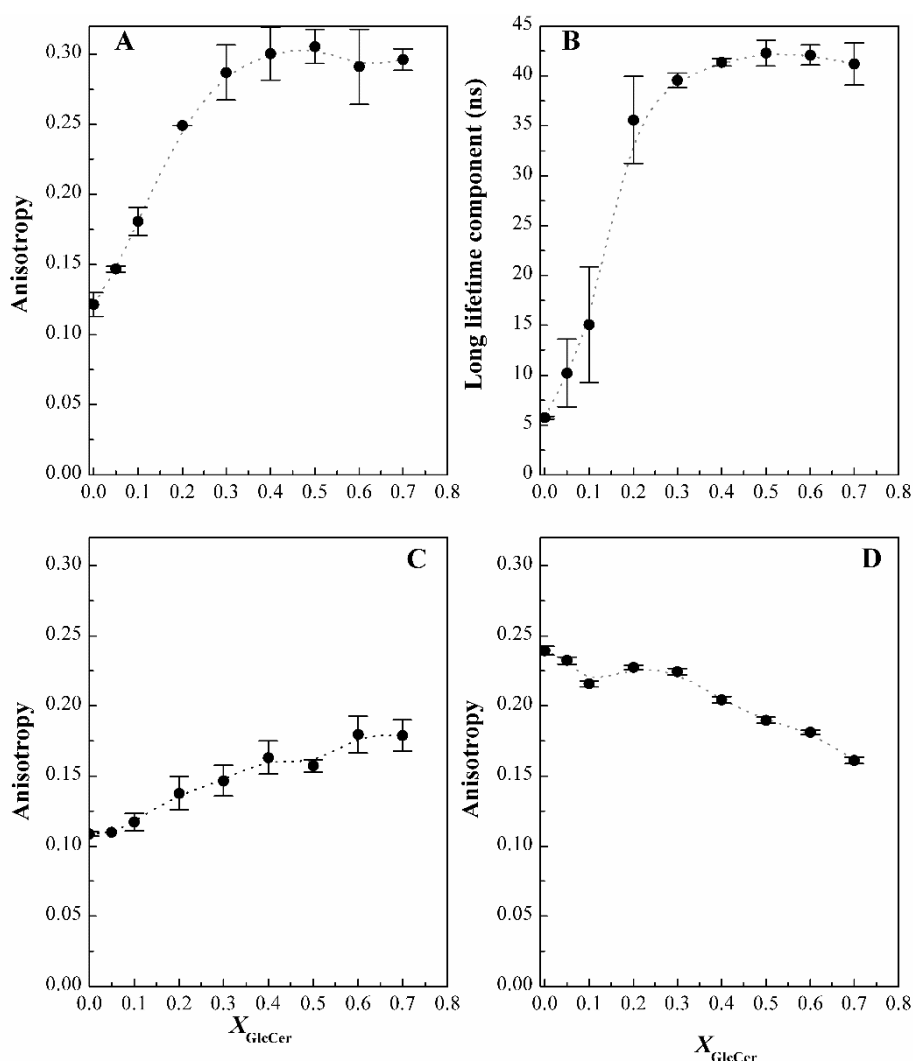
Figure 1 - Biophysical behavior of POPC/ C16:0-GlcCer mixtures.

t-PnA (A) fluorescence anisotropy and (B) long lifetime component of the intensity decay in binary POPC/GlcCer mixtures. Fluorescence anisotropy of (C) DPH and (D) Rho-DOPE in binary POPC/C16:0-GlcCer mixtures. All measurements were performed 24°C. Values are means ± SD of at least 3 independent experiments.

4.2 Thermotropic characterization of POPC/GlcCer mixtures

The variation of *t*-PnA fluorescence anisotropy as a function of temperature was used to characterize the thermotropic behavior of POPC/ C16:0-GlcCer mixtures (Fig. 2). *t*-PnA is a fluorescent polyene fatty acid probe that has high fluorescence sensitivity to lipid local density [47] and a high preference to lipid environments with gel-like properties [47], presenting a partition coefficient of $K_p(g/f)$ = 5 ± 2 [47,48]. This makes *t*-PnA a suitable probe to detect the formation of even small clusters of gel-phase domains [49] and to determine the gel-to-fluid transition temperature [32]. Our results show that mixtures containing 10%

C16:0-GlcCer display a thermotropic behavior similar to POPC. It should be stressed that POPC is fluid in the temperature range of this study ($T_m = -2.9 \pm 1.3°C$ [50]) and therefore the observed decrease in anisotropy is only due to a gradual increase of the membrane fluidity with temperature and not associated to a phase transition. However, increasing C16:0-GlcCer content to >20% induces significant changes in the fluid POPC (Fig. 2A). At low temperatures (up to 24°C), t-PnA anisotropy is higher than in POPC, and in addition an inflection is observed in the curve likely due to the presence of C16:0-GlcCer-enriched gel domains. Slightly increasing the temperature leads to an abrupt decrease in t-PnA anisotropy to values similar to those obtained in pure POPC, reflecting a transition from the gel to the fluid phase which ends at ~34°C. A further increase in the C16:0-GlcCer molar fraction (up to 70%) leads to a shift in the gel-to-fluid transition temperature of the mixtures towards higher values (Fig. 2B). From these data it is possible to determine the temperature at which the melting of gel domains is completed. This corresponds to the midpoint of intersection of the lines describing the initial (gel), intermediate and final (fluid) regimes. Knowing the width of the transition of the pure lipids [22], it is then possible to determine the main transition temperature for each of the mixtures [51], which corresponds to the *liquidus* boundary in the binary POPC/C16:0-GlcCer phase diagram (Fig. 2C). The partial phase diagram shows that C16:0-GlcCer is poorly miscible in the fluid POPC, presenting gel-fluid phase separation at low C16:0-GlcCer content (~10%).
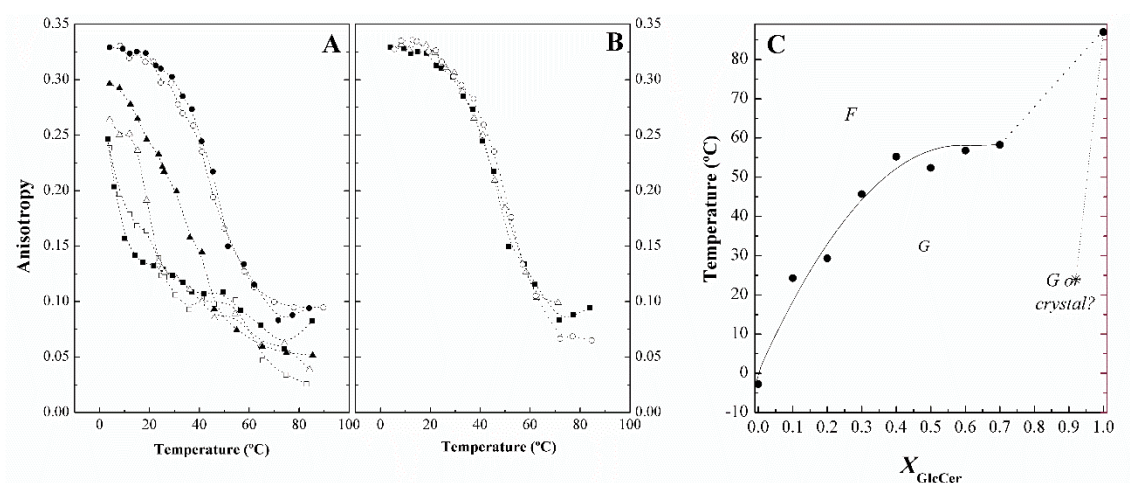
Figure 2- Thermotropic behavior of POPC/ C16:0-GlcCer mixtures.
Steady-state fluorescence anisotropy of t-PnA as a function of temperature in MLVs composed of (A) (■) POPC and POPC containing (□) 10, (△) 20, (▲) 30, (○) 40 and (●) 50 mol% of C16:0-GlcCer. (B) POPC containing (■) 50, (△) 60 and (○) 70 mol% of C16:0-GlcCer. Values are means ± SD of at least 3 independent experiments. (C) POPC/C16:0-

GlcCer partial binary phase diagram. The full line was experimental determined from data in figure 2A and B, and corresponds to the *liquidus* boundary. The dashed lines are the best estimates based on thermodynamic rules and the photophysical parameters of *t*-PnA (see text for further details). Abbreviations correspond to: *F*- fluid phase, *G* - gel phase.

4.3 GlcCer gel domains and membrane morphology

Confocal fluorescence microscopy was used to characterize the size and morphology of the C16:0-GlcCer gel domains and the morphological alterations induced by this GSL. The homogeneous labeling of vesicles containing 10% C16:0-GlcCer (Fig. 3B) shows that for this vesicle composition no gel domains or with a size below the resolution of microscopy are formed, in agreement with the spectroscopy data (Fig. 1). GUVs containing 30% of C16:0-GlcCer display clear gel (dark areas)-fluid (bright areas) phase separation (Fig. 3C-D). The majority of the domains display a polygonal shape, suggesting a lower line tension between gel and fluid phases, as compared to the typical flower-like shapes observed in this case of phase coexistence [40, 52]. The total exclusion of both Rho-DOPE and NBD-DPPE (Fig. S2) from the gel domains further confirm their highly-ordered nature.

In addition to gel domains, alterations in membrane morphology were also observed for GUVs containing ≥ 30% C16:0-GlcCer: tubule-like structures protrude from fluid areas of the vesicles (Fig. 3C and S2). These structures are highly flexible, thin and dynamic.
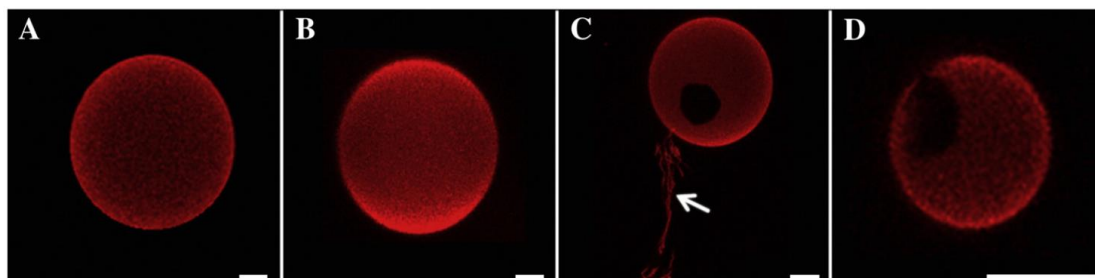
Figure 3 - Confocal fluorescence microscopy of POPC/C16:0-GlcCer mixtures. 3D projection images from 0.4 μm confocal slices of GUVs labeled with Rho-DOPE. The GUVs contain (A) POPC and POPC with (B) 10%, (C) 30% and (D) 40% of C16:0-GlcCer. Flexible tubule-like structures (white arrow) were observed in mixtures containing C16:0-GlcCer ≥ 30 mol%. Scale bar, 5 μm.

4.4 GlcCer-POPC molecular interactions in lipid monolayers

Surface pressure-area measurements were performed to evaluate the molecular interactions between C16:0-GlcCer and POPC in mixed monolayers (Fig. 4). Information about the packing density of the monolayers can be obtained from the determination of the compressibility modulus (C_s^{-1}): the higher the value for C_s^{-1} the lower the interfacial elasticity and the higher the molecular density. Furthermore, C_s^{-1} provides a simple approach to determine the onset and completion surface pressures of possible transitions [53, 54].

At room temperature, POPC displays a behavior expected for a stable monolayer of the 'expanded type', with a limiting molecular area of ~ 60 Å^2 and a C_s^{-1} < 100 mN/m at the collapse pressure of 42 mN m^{-1} (Fig. 4A-B), in agreement with reported data using a similar experimental set up [55, 56]. It is worth to mention that changing the spreading solvent and/or the subphase leads to significant alterations in the π–A isotherm of POPC, as previously reported [57] (Fig. S3A). In contrast, C16:0-GlcCer forms an insoluble monolayer of the 'condensed type': the π–A isotherm of C16:0-GlcCer appears in the range of lower molecular areas 42 − 32 Å^2, from $\pi \approx 0$ until the collapse at 60 mN m^{-1} and displays 250 mN/m < C_s^{-1} < 1000 mN/m at high surface pressures. Similarly to POPC, changes in the spreading solvent leads to significant alterations in the π–A isotherm of C16:0-GlcCer (Fig. S3A).

The shape of π–A isotherms of mixed monolayers changes regularly with the composition and the lift-off area at $\pi \approx 0$ decreases stepwise with increasing content of C16:0-GlcCer, except for C16:0-GlcCer = 10% that appears at slightly larger mean molecular areas (MMA) than the pure POPC (Fig. 4A). Mixed monolayers containing C16:0-GlcCer ≥ 30% display phase separation as shown by the two collapses: a first one occurring at larger MMA, which corresponds to the collapse of the POPC enriched phase, and a second collapse corresponding to a C16:0-GlcCer enriched phase. The maximum compressibility modulus of mixed monolayers also increases gradually with C16:0-GlcCer molar fraction (Fig. 4B), but drops dramatically when the monolayer collapse pressure is reached. For C16:0-GlcCer < 50%, the monolayers are in the expanded type in the whole range of surface pressures (Fig. 4B and S3B). For C16:0-GlcCer ≥ 50 %, there is a gradual transition from a state of nearly constant compressibility in the range of values of liquid-expanded

monolayers (C_s^{-1}< 100 mN/m) at low surface pressures (π <10 mN/m) to a liquid condensed phase (100 mN/m < C_s^{-1}< 250 mN/m) at higher surface pressures below the first collapse (30 mN/m < π < 42 mN/m).

The variation of the MMA with C16:0-GlcCer content (Fig. 4D) exhibits a positive deviation from the additive behavior of components, suggesting partial miscibility with expansion of the MMA. This is further confirmed by the negative Gibbs energy of mixing, ΔG_{mix} (Fig. 4C). As expected, the deviations from the ideal behavior increase with the surface pressure.

The results obtained in POPC/ C16:0-GlcCer mixed monolayers are consistent with data from fluorescence spectroscopy and microscopy, showing that C16:0-GlcCer is only partially miscible in POPC and is able to increase membrane packing density.

5 Discussion

5.1 Properties of GlcCer

The mechanisms by which C16:0-GlcCer changes the biophysical properties of fluid membranes are of importance for understanding how GlcCer is involved in intracellular processes, in physiological and pathological states. In physiological conditions the levels of GlcCer are low compared to the total membrane lipids [58, 59]. However, in pathological states, like in Gaucher disease, GlcCer levels significantly increase in cells, tissues and plasma [60, 61, 62, 63].

Fully hydrated GlcCer, similarly to Cer [33, 64] and GalCer [22], has a complex thermotropic phase behavior and a high main transition temperature (~87°C) [22]. In the present study, it was not possible to characterize pure C16:0-GlcCer by fluorescence spectroscopy methodologies. This is because GlcCer, like ceramides and GalCer, also has a strong tendency to form crystal-like structures [22, 31, 44]. The highly-compact crystal structure leads to the exclusion of the fluorescent probes, which is revealed by the decrease in *t*-PnA fluorescence anisotropy (and lifetime) at very high C16:0-GlcCer molar fractions. It should be stressed that we have previously shown that *t*-PnA displays a similar photophysical behavior in mixtures containing high Cer molar fractions, which was associated with crystal formation as observed by transmission electron microscopy [31]. In the present study, further evidence for crystal formation arose from monolayer studies.

The area occupied per C16:0-GlcCer molecule at the collapse surface pressure (~30 Å^2) is smaller than the expected one based on the molecular structure of C16:0-GlcCer [65]. The estimated area for two closely packed alkyl chains perpendicular to the interface is ~36 Å^2. These results show that C16:0-GlcCer should form 3D multilayer structures, most likely crystals coexisting with the 2D monolayer structure at the air-water interface.
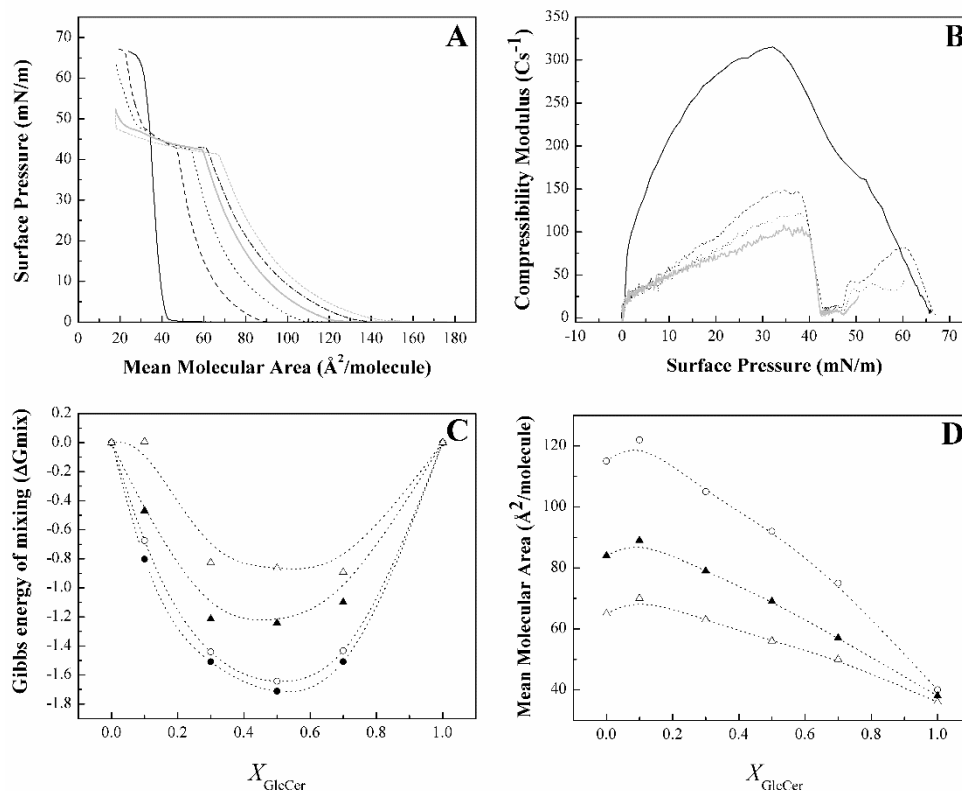
Figure 4 - POPC/ C16:0-GlcCer mixed monolayers.
(A) π–A isotherms of (—·—) POPC, (—) C16:0-GlcCer and POPC with (—·—) 10%, (—) 30%, (···) 50% and (---) 70% of C16:0-GlcCer. (B) Isothermal compressional modulus as a function of surface pressure in (—) GlcCer and POPC with (—) 30%, (···) 50% and (---) 70% of C16:0-GlcCer. (C) Gibbs energy of mixing and (D) Mean molecular area as a function of the GlcCer mole fraction at (O) 5 mN/m, (▲) 20 mN/m and (△) 40 mN/m. (●) ideal Gibbs energy of mixing. Values were determined according to eq. 3.

5.2 Effect of GlcCer on membrane biophysical properties

C16:0-GlcCer has a marked effect on the biophysical properties of fluid POPC membranes. From our data, it is possible to conclude that C16:0-GlcCer is able to drive gel-fluid phase separation, to form highly ordered gel domains, and to increase the order of the POPC fluid phase. Together, this suggests that C16:0-GlcCer induces similar changes in membrane properties to those reported for saturated ceramides [33, 45].

However, this conclusion is not straightforward because higher GlcCer content is required to induce gel-fluid phase separation. Comparison between the *liquidus* boundaries of the phase diagrams reveals that ~10% and ~24% of GlcCer are required to form gel phase at 24°C and 37°C, respectively compared to ~4% and ~10% for saturated ceramides [33, 45]. This shows that GlcCer displays higher miscibility in the fluid phase as compared to saturated ceramides. The difference in the effects of C16:0-Cer and C16:0-GlcCer on membrane biophysical properties allows concluding that the introduction of a glucose moiety in the Cer headgroup creates a packing constraint that prevents GlcCer segregation into gel domains at a lower GSL molar fraction. This effect is comparable to the introduction of a double bond in Cer [32]. Indeed, the results obtained for POPC/ C16:0-GlcCer mixtures display some similarities to those obtained with POPC/C24:1-Cer mixtures. For instance, as shown in Fig. 2C, the initial part of the *liquidus* phase boundary is very similar, demonstrating that the same molar fractions of C16:0-GlcCer and C24:1-Cer are required to drive gel-fluid phase separation [32]. Furthermore, the variation of *t*-PnA fluorescence anisotropy and lifetime in POPC/ C16:0-GlcCer mixtures is comparable to POPC/C24:1-Cer [32], further demonstrating that GlcCer and C24:1-Cer induce similar global alterations in the biophysical properties of fluid membranes.

It was previously demonstrated that GlcCer and GalCer with the same acyl chain structure have similar thermotropic behaviors [22]. Additionally, our results show that the *liquidus* boundary of POPC/ C16:0-GlcCer mixtures is similar to the one reported for C16:0 GalCer/ SOPC (1-stearoyl-2-oleoyl-*sn*-glycero-3-phosphocholine) binary system [66]. This suggests that the overall impact of GalCer and GlcCer on the biophysical properties of simple models of fluid membranes is identical. Certainly, the differences in the headgroup structure of these two lipids will promote subtle changes in lipid organization and membrane properties, that are likely to be enhanced in more complex mixtures, as observed in membranes containing Chol [25].

Regarding the surface-pressure studies, the first collapse of POPC/ C16:0-GlcCer mixed monolayers ($\sim$ 42 mN m^{-1}) is not affected by the composition, further indicating lipid phase separation. The thermodynamic analysis of mixed monolayers at π < 42 mN m^{-1}, shows non-ideal mixing behavior with positive deviations. The molecular interactions between these lipids lead to the expansion of the mean molecular area. A similar behavior was reported for Cer/GlcCer mixtures [65]. The increase of the molecular distances was

ascribed to the increase of dipolar repulsion induced by the molecular dipole hyperpolarization that occurred in the Cer/GlcCer mixed films.

Confocal fluorescence microscopy further confirmed the ability of C16:0-GlcCer to form micron-sized highly-ordered gel domains. Interestingly, these domains did not present the typical flower shape structure characteristic of gel domains [32], but an irregular polygonal- or bean-like structure. Lipid domain shape and size is controlled by several factors including line tension, dipole density and the entropy of distributing molecules between domains [67]. The increase in line tension commonly drives the formation of larger domains with irregular shapes; hydrophobic mismatch at the boundaries of the domains also contributes to an irregular domain shape. This is the case of a typical boundary between a thicker gel phase and a thinner fluid phase. However, some lipids can act as line-active components to minimize the line tension at the boundaries of the domains. POPC is a typical example of a line-active lipid, presenting a saturated chain that preferential interacts with the gel domain boundary and an unsaturated chain that has a preference towards the more disordered fluid phase [68, 69, 70]. Such an interaction stabilizes the interface by reducing the line tension and creating smoother boundaries, such as those observed in this work.

The exclusion of the Rho-DOPE probe from gel phases, as well as the phase diagram depicted in Figure 2C, are further supported from the variation of anisotropy due to homo-FRET described in Figure 1D. Application of Snyder and Freire's model [71] of homo-FRET to our experimental anisotropy values, allows estimation of the expected decrease in the area for Rho-DOPE distribution based on its depolarization. The available area is not the total membrane surface, and the reduction should correspond to the area involved in the formation of gel phase domains. Fig. 5 shows the expected surface area decrease for Rho-DOPE distribution for each POPC/ C16:0-GlcCer mixture that accounts for the experimental depolarization. The values obtained are in agreement with the theoretical values based on the phase diagram, and calculated taking into account the fraction of gel phase of each of the mixtures, and the respective area per molecule of POPC and GlcCer (66.4Å^2 [55] and 40Å^2 [65]). In these calculations, the composition of the fluid was taken from the *liquidus* line of the phase diagram (Fig. 2C) and for the gel composition it was assumed that the solidus boundary is located at ~ 90% C16:0-GlcCer at 24°C, since this is the composition at which exclusion of *t*-PnA from the membranes

starts to occur. There is an excellent agreement for the lower molar fractions of gel phase, which correspond to the lower probe surface densities, and the small deviation at higher FRET efficiencies is inherent to the model used. In fact Snyder and Freire [71] assume that the probes are distributed in a plane, but also consider that the transition moments are isotropically oriented. This is not verified in membranes, since probes are both restricted in their orientations and dynamics, i.e., only allowed to wobble within a cone, and this implies a smaller efficiency for transfer, which is here translated into a higher area. Nevertheless, the good agreement between the theoretical and experimental values further support the proposed phase diagram, particularly the *solidus* boundary that could not be experimentally determined.

It should be stressed that the diagram displayed in Figure 2C is only a partial binary phase diagram for these mixtures and does not exclude the possibility that other phases might be present, including non-lamellar phases [72] that could not be assessed by the methodologies employed in the present study. These, however, are likely to form at higher temperatures, far from physiological conditions [22]. Previous studies also suggest that GSL can form stoichiometric complexes with phospholipids with properties intermediate between gel and ordered phase resembling, to a certain extent, a liquid-ordered raft like structure[12, 73]. While we do not rule out their existence, with our experimental approach it is not possible to conclude about their formation. Nevertheless, our study clearly shows that GlcCer mixes only partially in the fluid phospholipid segregating into a highly-ordered GlcCer-enriched gel phase. The characteristics of this phase can however change in the presence of other lipids, as previously observed for mixtures containing Cer and Chol. Indeed, taking into account the similarity between the phases formed by GlcCer and Cer, one might hypothesized that increasingly amounts of Chol will hindered the formation of a highly-ordered GlcCer-enriched gel phase by increasing the solubility of this GSL in the Chol-enriched liquid-ordered phase [34].
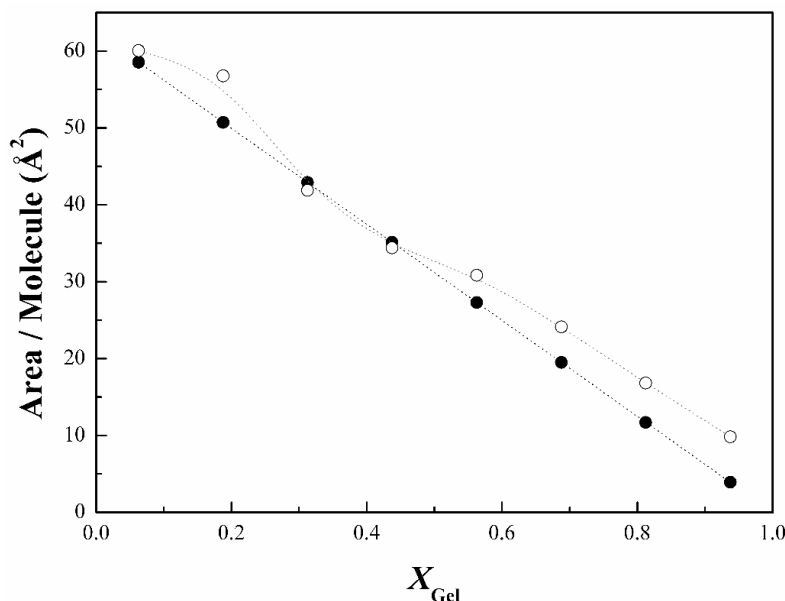
Figure 5 - Variation in the fluid surface area available for Rho-DOPE distribution. (○) Values were calculated according to the Snyder and Freire model [71]. This model considers a random distribution of the fluorophores. For the calculations the following parameters were used: Förster radius, R_0 = 57.7Å [74]; [Rho-DOPE] = 0.2μM; an areas per molecule of 40 Å^2 [65] and 66.4 Å^2 [55] were used for C16:0-GlcCer and POPC, respectively; and the numerical constants, α, were taken from [71] for an R_0/L = 4, where L is the distance of closest approach between fluorophores; (●) values were calculated from the phase diagram (Fig. 2C) taking into account the fraction of gel phase of each of the mixtures and the respective area per molecule of POPC and C16:0-GlcCer (see text for details).

5.3 GlcCer promotes morphological alterations

Increased C16:0-GlcCer concentration also promotes major changes in GUVs, including the formation of flexible-like tubular structures (Fig. 3 and S2). The formation of such tubules might occur spontaneously in response to an increase in membrane tension upon gel domain formation. In addition, it is known that lipid phase separation might drive changes in membrane curvature that affect not only the lateral organization of lipids, but also the transbilayer distributions of lipid mixtures [75]. This asymmetric lipid distribution will enhance the differences in the spontaneous membrane curvature promoted by each of the lipids, which might finally lead to the protrusion of tubule-like structures to prevent further membrane deformation and to restore membrane tension. Chiral lipids, such as GlcCer and GalCer, also have a higher tendency to drive tubule formation due to the intrinsic bending force arising from chirality [76]. It was also shown that the formation of tubule-like structures might arise from transbilayer chain interdigitation. However, this

mechanism is likely to be more important in membranes containing lipids with asymmetric chains, as C24:0- and C24:1-Cer [32], where the acyl chain is much longer than the sphingoid base, or in membranes composed of lipids with strong chain mismatch [31]. Since none of these situations occurs in the mixtures under study, it is unlikely that interdigitation governs tubule formation in POPC/ C16:0-GlcCer mixtures. Another possible mechanism underlying tubule formation is the presence of a tilted phase. X-ray studies have shown that GSL forms tilted phases in order to accommodate the sugar moiety and to account for the extensive H-bond network [77]. In addition, formation of a macro-rippled phase by GalCer has been reported [78]. It was hypothesized that the presence of a tilted phase, together with the inherent chirality of GalCer and the increased lipid misalignment, is responsible for surface defects from where GalCer tubules would form [79]. Such a mechanism would also explain tubule formation in POPC/ C16:0-GlcCer membranes.

From our microscopy studies, it is not possible to draw clear conclusions about the nature of the tubules formed by POPC/ C16:0-GlcCer mixtures [80]. Mutz et al have shown that C24:1-GlcCer forms rigid needle-like structures that project away from the glycolipid mass. These structures are different from the highly flexible structures observed in the present study. This could be due to the different acyl chain structure of the GlcCer species. For instance, it was shown that GalCer is able to form different tubule-like structures, depending on its structure and environment [81, 82], including ribbons, lipid tubules and cochleate cylinders. Analysis of the structural features that control GalCer nanotube formation revealed that longer monounsatured GalCer has a higher tendency to form stable nanotubes, while shorter-chain GalCer (C18) formed a variety of structures [79].

6 Conclusions and biological implications

Biological membranes are complex structures where interactions among the different membrane components are responsible for cell function. However, to understand these interactions, it is necessary to use simplified models, where the effect of a particular component can be evaluated. In the present study, it was possible to assess the mode by which C16:0-GlcCer changes the biophysical properties of fluid membranes.

Our results show that C16:0-GlcCer promotes extensive alterations in the membrane, driving the formation of highly-ordered gel domains. Formation of such domains might have strong implications on cell processes, including in the sorting of lipids and proteins into or out of the domains, and consequent activation of signaling cascades. Moreover, it has been shown that GSLs at the cell surface are active participants in cell-to-cell communication and recognition[83, 84, 85]. These processes might be facilitated by the formation of flexible structures that protrude from the membrane, such as those observed in this simple mixtures. Whether the formation of C16:0-GlcCer domains and/or tubule-like structures is enhanced or inhibited in biological membranes is unknown, but will certainly depend on the interactions with the other membrane components and might even constitute a mechanism by which the cell turn on and off specific processes. These evidences may provide new insights into the molecular mechanisms by which the accumulation of GlcCer leads to alterations in cellular processes under pathological states, such as observed in Gaucher disease.

7 Acknowledgments

8 References

1.   MAGGIO, B.; FANANI, M. L.; ROSETTI, C. M.; WILKE, N. BYOPHISICS OF SPHINGOLIPIDS II: GLYCOSPHINGOLIPIDS: AN ASSORTMENT OF MULTIPLE STRUCTURAL INFORMATION TRANSDUCERS AT THE MEMBRANE SURFACE. BIOCHEM BIOPHYS ACTA 2006, 1758, 1922-1944.
2.   SILVA, L. C.; FUTERMAN, A. H.; PRIETO, M. LIPID RAFT COMPOSITION MODULATES SPHINGOMYELINASE ACTIVITY AND CERAMIDE-INDUCED MEMBRANE PHYSICAL ALTERATIONS. BIOPHYS J 2009, 96 (8), 3210-3222.

3.   Gramlich, G.; Zhang, J.; Winterhalter, M.; Nau, W. M. A long-lived amphiphilic fluorescent probe studied in POPC air–water monolayer and solution bilayer systems. Chem Phys Lipids 2001, 113, 1-9.

4.   Maccioni, H. J. F.; Quiroga, R.; Ferrari, M. L. Cellular and molecular biology of glycosphingolipid glycosylation. J Neurochem 2011, no-no.

5.   Hall, A. Role of glycolipids in lipid rafts : A view through atomistic molecular dynamics simulations with galactosylceramide. J Phys Chem B 2010, 114, 7797-7807.

6.   Hakomori, S.-t. Glycosynapses: microdomains controlling carbohydrate-dependent cell adhesion and signaling. An Acad Bras Cienc 2004, 76, 553-572.

7.   Becker, K. A.; Riethmuller, J.; Luth, A.; Doring, G.; Kleuser, B.; Gulbins, E. Acid Sphingomyelinase Inhibitors Normalize Pulmonary Ceramide and Inflammation in Cystic Fibrosis. Am J Respir Cell Mol Biol 2009, 42 (6), 716-724.

8.   D'Angelo, G.; Polishchuk, E.; Tullio, G. D.; Santoro, M.; Campli, A. D.; Godi, A.; West, G.; Bielawski, J.; Chuang, C.-C.; van der Spoel, A. C.; Platt, F. M.; Hannun, Y. A.; Polishchuk, R.; Mattjus, P.; De Matteis, M. A. Glycosphingolipid synthesis requires FAPP2 transfer of glucosylceramide. Nature 2007, 449 (7158), 62-67.

9.   Halter, D.; Neumann, S.; van Dijk, S. M.; Wolthoorn, J.; de Maziere, A. M.; Vieira, O. V.; Mattjus, P.; Klumperman, J.; van Meer, G.; Sprong, H. Pre- and post-Golgi translocation of glucosylceramide in glycosphingolipid synthesis. J Cell Biol 2007, 179 (1), 101-115.

10.   van Meer, G.; Wolthoorn, J.; Degroote, S. The fate and function of glycosphingolipid glucosylceramide. Phil Trans R Soc B 2003, 358 (1433), 869-873.

11.   Lannert, H.; Bünning, G.; Jeckel, D.; Wieland, F. T. Lactosylceramide is synthesized in the lumen of the Golgi apparatus. FEBS Lett 1994, 342 (1), 91-96.

12.   Quinn, P. J. The structure of complexes between phosphatidylethanolamine and glucosylceramide: A matrix for membrane rafts. Biochim Biophys Acta 2011, 1808 (12), 2894-2904.

13.   Messner, M. C.; Cabot, M. C. Glucosylceramide in humans. Adv Exp Med Biol 2010, 688, 154-64.

14.   Walden, C. M.; Sandhoff, R.; Chuang, C. C.; Yildiz, Y.; Butters, T. D.; Dwek, R. A.; Platt, F. M.; van der Spoel, A. C. Accumulation of Glucosylceramide in Murine Testis, Caused by Inhibition of beta-Glucosidase 2: Implication For Spermatogenesis. J Biol Chem 2007, 282 (45), 32655-32664.

15.   Bodennec, J. Phosphatidylcholine synthesis is elevated in neuronal models of Gaucher disease due to direct activation of CTP:phosphocholine cytidylyltransferase by glucosylceramide. FASEB J 2002.

16.   Lloyd-Evans, E. Glucosylceramide and Glucosylsphingosine Modulate Calcium Mobilization from Brain Microsomes via Different Mechanisms. J Biol Chem 2003, 278 (26), 23594-23599.

17.   Sillence, D. J. Glucosylceramide modulates membrane traffic along the endocytic pathway. J Lipid Res 2002, 43 (11), 1837-1845.

18.   Simons, K.; Ikonen, E. Functional rafts in cell membranes. Nature 1997, 387, 569-572.

19.   Lingwood, D.; Simons, K. Lipid Rafts As a Membrane-Organizing Principle. Science 2010, 327 (5961), 46-50.

20.   Cremesti, A. E.; Goni, F.; Kolesnick, R. Role of sphingomyelinase and ceramide in modulating rafts: do biophysical properties determine biologic outcome? FEBS Lett 2002, 531, 47-53.

21. EDIDIN, M. THE STATE OF LIPID RAFTS: FROM MODEL MEMBRANES TO CELLS. ANNU REV BIOPHYS BIOMOL STRUCT. 2003, 32 (1), 257-283.

22. SAXENA, K.; DUCLOS, R. I.; ZIMMERMANN, P.; SCHMIDT, R. R.; SHIPLEY, G. G. STRUCTURE AND PROPERTIES OF TOTALLY SYNTHETIC GALACTO- AND GLUCO-CEREBROSIDES. J LIPID RES 1999, 40, 839-849.

23. THOMPSON, T. E.; TILLACK, T. W. ORGANIZATION OF GLYCOSPHINGOLIPIDS IN BILAYERS AND PLASMA MEMBRANES OF MAMMALIAN CELLS. ANNU REV BIOPHYS BIOPHYS CHEM 1985, 14 (1), 361-386.

24. WESTERLUND, B.; SLOTTE, J. P. HOW THE MOLECULAR FEATURES OF GLYCOSPHINGOLIPIDS AFFECT DOMAIN FORMATION IN FLUID MEMBRANES. BIOCHIM BIOPHYS ACTA 2009, 1788 (1), 194-201.

25. MAUNULA, S.; BJÖRKQVIST, Y. J. E.; SLOTTE, J. P.; RAMSTEDT, B. DIFFERENCES IN THE DOMAIN FORMING PROPERTIES OF N-PALMITOYLATED NEUTRAL GLYCOSPHINGOLIPIDS IN BILAYER MEMBRANES. BIOCHIM BIOPHYS ACTA 2007, 1768 (2), 336-345.

26. MORROW, M.; SINGH, D.; LU, D.; GRANT, C. GLYCOSPHINGOLIPID PHASE BEHAVIOUR IN UNSATURATED PHOSPHATIDYLCHOLINE BILAYERS: A 2H-NMR STUDY. BIOCHEM BIOPHYS ACTA 1992, 1106, 85-93.

27. MAGGIO, B.; CARRER, D. C.; FANANI, M. L.; OLIVEIRA, R. G.; ROSETTI, C. M. INTERFACIAL BEHAVIOR OF GLYCOSPHINGOLIPIDS AND CHEMICALLY RELATED SPHINGOLIPIDS. CURR OPIN COLLOID INTERFACE SCI 2004, 8 (6), 448-458.

28. LI, X.-M.; SMABY, J. M.; MOMSEN, M. M.; BROCKMAN, H. L.; BROWN, R. E. SPHINGOMYELIN INTERFACIAL BEHAVIOR: THE IMPACT OF CHANGING ACYL CHAIN COMPOSITION. BIOPHYS J 2000, 78 (4), 1921-1931.

29. LI, X.-M.; MOMSEN, M. M.; BROCKMAN, H. L.; BROWN, R. E. LACTOSYLCERAMIDE: EFFECT OF ACYL CHAIN STRUCTURE ON PHASE BEHAVIOR AND MOLECULAR PACKING. BIOPHYS J 2002, 83 (3), 1535-1546.

30. SMABY, J. M.; KULKARNI, V. S.; MOMSEN, M.; BROWN, R. E. THE INTERFACIAL ELASTIC PACKING INTERACTIONS OF GALACTOSYLCERAMIDES, SPHINGOMYELINS, AND PHOSPHATIDYLCHOLINES. BIOPHYS J 1996, 70, 886-877.

31. PINTO, S. N.; SILVA, L. C.; FUTERMAN, A. H.; PRIETO, M. EFFECT OF CERAMIDE STRUCTURE ON MEMBRANE BIOPHYSICAL PROPERTIES: THE ROLE OF ACYL CHAIN LENGTH AND UNSATURATION. BIOCHIM BIOPHYS ACTA 2011, 1808 (11), 2753-2760.

32. PINTO, S. N.; SILVA, L. C.; DE ALMEIDA, R. F. M.; PRIETO, M. MEMBRANE DOMAIN FORMATION, INTERDIGITATION, AND MORPHOLOGICAL ALTERATIONS INDUCED BY THE VERY LONG CHAIN ASYMMETRIC C24:1 CERAMIDE. BIOPHYS J 2008, 95 (6), 2867-2879.

33. SILVA, L.; DE ALMEIDA, R. F. M.; FEDOROV, A.; MATOS, A. P. A.; PRIETO, M. CERAMIDE-PLATFORM FORMATION AND -INDUCED BIOPHYSICAL CHANGES IN A FLUID PHOSPHOLIPID MEMBRANE. MOL MEMBR BIOL 2006, 23 (2), 137-148.

34. CASTRO, B. M.; SILVA, L. C.; FEDOROV, A.; DE ALMEIDA, R. F. M.; PRIETO, M. CHOLESTEROL-RICH FLUID MEMBRANES SOLUBILIZE CERAMIDE DOMAINS: IMPLCATIONS FOR THE STRUCTURE AND DYNAMICS OF MAMMMALIAN INTRACELLULAR AND PLASMA MEMBRANES. J BIOL CHEM 2009, 284 (34), 22978-22987.

35. CASTRO, B. M.; DE ALMEIDA, R. F. M.; SILVA, L. C.; FEDOROV, A.; PRIETO, M. FORMATION OF CERAMIDE/SPHINGOMYELIN GEL DOMAINS IN THE PRESENCE OF AN UNSATURATED PHOSPHOLIPID: A QUANTITATIVE MULTIPROBE APPROACH. BIOPHYS J 2007, 93 (5), 1639-1650.

36. SILVA, L. C.; DE ALMEIDA, R. F. M.; CASTRO, B. M.; FEDOROV, A.; PRIETO, M. CERAMIDE-DOMAIN FORMATION AND COLLAPSE IN LIPID RAFTS: MEMBRANE REORGANIZATION BY AN APOPTOTIC LIPID. BIOPHYS J 2007, 92 (2), 502-516.

37. LAKOWICZ, J. R. 3RD ED.; SPRINGER: NEW YORK, 2006.

38.   SANCHEZ, S. A.; TRICERRI, M. A.; GUNTHER, G.; GRATTON, E. LAURDAN GENERALIZED POLARIZATION: FROM CUVETTE TO MICROSCOPE. FORMATEX: BADAJOZ, 2007; VOL. 3, P 1007-1014.

39.   CISTOLA, D.; HAMILTON, J. A.; JACKSON, D.; SMALL, D. M. IONIZATION AND PHASE BEHAVIOR OF FATTY ACIDS IN WATER: APPLICATION OF THE GIBBS PHASE RULE. BIOCHEMISTRY 1988, 27, 1881-1888.

40.   DE ALMEIDA, R. F. M.; BORST, J.; FEDOROV, A.; PRIETO, M.; VISSER, A. J. W. G. COMPLEXITY OF LIPID DOMAINS AND RAFTS IN GIANT UNILAMELLAR VESICLES REVEALED BY COMBINING IMAGING AND MICROSCOPIC AND MACROSCOPIC TIME-RESOLVED FLUORESCENCE. BIOPHYS J 2007, 93 (2), 539-553.

41.   HAUGLAND, R. P.; SPENCE, M. T.; JOHNSON, I. D. HANDBOOK OF FLUORESCENT PROBES AND RESEARCH CHEMICALS. 6TH ED.; MOLECULAR PROBES: EUGENE OR, 1996.

42.   SARMENTO, M. J.; PRIETO, M.; FERNANDES, F. REORGANIZATION OF LIPID DOMAIN DISTRIBUTION IN GIANT UNILAMELLAR VESICLES UPON IMMOBILIZATION WITH DIFFERENT MEMBRANE TETHERS. BIOCHIM BIOPHYS ACTA 2012, 1818 (11), 2605-2615.

43.   GONÇALVES DA SILVA, A. M.; ROMÃO, R. I. S. MIXED MONOLAYERS INVOLVING DPPC, DODAB AND OLEIC ACID AND THEIR INTERACTION WITH NICOTINIC ACID AT THE AIR–WATER INTERFACE. CHEM PHYS LIPIDS 2005, 137 (1-2), 62-76.

44.   DICKO, A. INTERACTIONS BETWEEN GLUCOSYLCERAMIDE AND GALACTOSYLCERAMIDE I3 SULFATE AND MICROSTRUCTURES FORMED. BIOCHIM BIOPHYS ACTA 2003, 1613 (1-2), 87-100.

45.   ALMEIDA, R. F. M.; LOURA, L. M. S.; PRIETO, M. MEMBRANE LIPID DOMAINS AND RAFTS: CURRENT APPLICATIONS OF FLUORESCENCE LIFETIME SPECTROSCOPY AND IMAGING. CHEM PHYS LIPIDS 2009, 157, 61-77.

46.   BAGATOLLI, L. A.; GRANTON, E.; FIDELIO, G. D. WATER DYNAMICS IN GSL AGGREGATES STUDIED BY LAURDAN FLUORESCENCE. BIOPHYS J 1998, 75, 331-341.

47.   SKLAR, L. A.; HUDSON, B. S.; PETERSEN, M.; DIAMOND, J. CONJUGATED POLYENE FATTY ACIDS AS FLUORESCENT PROBES: SPECTROSCOPIC CHARACTERIZATION. BIOCHEMISTRY 1977, 16 (5), 813-819.

48.   HUDSON, D. L. H. B.; LUDESHER, R. D.; RUGGIERO, A.; COONEY- FREED, A.; CAVALIER, S. A. FLUORESCENCE PROBE STUDIES OF PROTEINS AND MEMBRANES. ALAN R. LISS: NEW YORK, 1986.

49.   MATEO, C. R.; BROCHON, J.-C.; LILLO, M. P.; ACUÑA, A. U. LIPID CLUSTERING IN BILAYERS DETECTED BY THE FLUORESCENCE KINETICS AND ANISOTROPY OF TRANS-PARINARIC ACID. BIOPHYS J 1993, 65, 2237-2247.

50.   HUANG, C. MIXED-CHAIN PHOSPHOLIPIDS AND INTERDIGITATED BILAYER SYSTEMS. KLIN WOCHENSCHR 1990, 68 (3), 149-165.

51.   MABREY, S.; STURTEVANT, J. M. INVESTIGATION OF PHASE TRANSITIONS OF LIPIDS AND LIPID MIXTURES BY HIGH SENSITIVITY DIFFERENTIAL SCANNING CALORIMETRY. PROC NATL ACAD SCI U S A 1976, 73, 3862-3866.

52.   HOLOPAINEN, J. M.; BROCKMAN, H. L.; BROWN, R. E.; KINNUNEN, P. K. J. INTERFACIAL INTERACTIONS OF CERAMIDE WITH DIMYRISTOYLPHOSPHATIDYLCHOLINE: IMPACT OF THE N-ACYL CHAIN. BIOPHYS J 2001, 80, 765-775.

53.   SMABY, J. M.; KULKARNI, V. S.; MOMSEN, M.; BROWN, R. E. THE INTERFACIAL ELASTIC PACKING INTERACTIONS OF GALACTOSYLCERAMIDES, SPHINGOMYELINS, AND PHOSPHATIDYLCHOLINES. BIOPHYS J 1996, 70, 868-877.

54.   MATTI, V.; SÄILY, J.; RYHÄNEN, S. J.; HOLOPAINEN, J. M.; BOROCCI, S.; MANCINI, G.; KINNUNEN, P. K. J. CHARACTERIZATION OF MIXED MONOLAYERS OF PHOSPHATIDYLCHOLINE AND A DICATIONIC GEMINI SURFACTANT SS-1 WITH A LANGMUIR BALANCE: EFFECTS OF DNA. BIOPHYS J 2001, 81, 2135-2143.

55.   CHIU, S. W.; JAKOBSSON, E.; SUBRAMANIAM, S.; SCOTT, H. L. COMBINED MONTE CARLO AND MOLECULAR DYNAMICS SIMULATION OF FULLY HYDRATED DIOLEYL AND PALMITOYL-OLEYL PHOSPHATIDYLCHOLINE LIPID BILAYERS. BIOPHYS J 1999, 77, 2462-2469.

56.   Schwarz, G.; Wackerbauer, G.; Taylor, S. E. Partitioning of a nearly insoluble lipid monolayer into its aqueous subphase. Colloids Surf A Physicochem Eng Asp 1996, 111 (1–2), 39-47.

57.   Weis, I.; Welzel, P. B.; Bähr, G.; Schwarz, G. Equations of state for POPX lipids at the air/water interface. A comprehensive study. Chem Phys Lipids 2000, 105 (1), 1-8.

58.   van Meer, G.; de Kroon, A. I. P. M. Lipid map of the mammalian cell. J Cell Sci 2010, 124 (1), 5-8.

59.   van Meer, G.; Voelker, D. R.; Feigenson, G. W. Membrane lipids: where they are and how they behave. Nat Rev Mol Cell Biol 2008, 9 (2), 112-124.

60.   Jmoudiak, M. F., Anthony H. Gaucher disease: pathological mechanisms and modern management. Br J Haematol 2005, 129, 178-188.

61.   Groener, J. Plasma glucosylceramide and ceramide in type 1 Gaucher disease patients: Correlations with disease severity and response to therapeutic intervention. Biochim Biophys Acta 2008, 1781 (1-2), 72-78.

62.   Fuller, M.; Rozaklis, T.; Lovejoy, M.; Zarrinkalam, K.; Hopwood, J. J.; Meikle, P. J. Glucosylceramide accumulation is not confined to the lysosome in fibroblasts from patients with Gaucher disease. Mol Gen Metab 2008, 93 (4), 437-443.

63.   Matti, V.; Säily, J.; Ryhänen, S. J.; Holopainen, J. M.; Borocci, S.; Mancini, G.; Kinnunen, P. K. J. Characterization of Mixed Monolayers of Phosphatidylcholine and a Dicationic Gemini Surfactant SS-1 with a Langmuir Balance: Effects Of DNA. Biophys J 2001, 81, 2135-2143.

64.   J. Shah, J. A., RI Duclos, AV Rawlings, Z Dong, GG Shipley. Structural and thermotropic properties os synthetic C16:0 (palmitoyl) ceramide: effect of hydration. J Lipid Res 1995, 36, 1936-1944.

65.   Maggio, B. Favorable and unfavorable lateral interactions of ceramide, neutral glycosphingolipids and gangliosides in mixed monolayers. Chem Phys Lipids 2004, 132 (2), 209-224.

66.   Lu, D.; Singh, D.; Morrow, M. R.; Grant, C. W. M. Effect of Glycosphingolipid Fatty Acid Chain Length on Behavior in Unsaturated Phosphatidylcholine Bilayers: A 2H NMR Study. Biochemistry 1993, 32, 290-297.

67.   Lee, D. W.; Minb, Y.; Dharc, P.; Ramachandrand, A.; Israelachvilia, J. N.; Zasadzinskif, J. A. Relating domain size distribution to line tension and molecular dipole density in model cytoplasmic myelin lipid monolayers   Proc Natl Acad Sci U S A 2011, 108, 9425-9430.

68.   Yamamoto, T.; Brewster, R.; Safran, S. A. Chain ordering of hybrid lipids can stabilize domains in saturated/ hybrid/ cholesterol lipid membranes. Europhys Lett 2010, 91, 1-6.

69.   Brewster, R.; Safran, S. A. Line Active Hybrid Lipids Determine Domain Size in Phase Separation of Saturated and Unsaturated Lipids. Biophys J 2010, 98 (6), L21-L23.

70.   Brewster, R.; Pincus, P. A.; Safran, S. A. Hybrid Lipids as a Biological Surface-Active Component. Biophys J 2009, 97 (4), 1087-1094.

71.   Taute, A.; Wätzig, K.; Simons, B.; Lohaus, C.; Meyer, H. E.; Hasilika, A. Presence of detergent-resistant microdomains in lysosomal membranes. Biochem Biophys Res Commun 2002, 298, 5-9.

72.   Veiga, M. P.; Arrondo, J. L. R.; Goñi, F. M.; Alonso, A. Ceramides in Phospholipid Membranes: Effects on Bilayer Stability and Transition to Nonlamellar Phases. Biophys J 1999, 76 (1), 342-350.

73.   Feng, Y.; Rainteau, D.; Chachaty, C.; Yu, Z.-W.; Wolf, C.; Quinn, P. J. Characterization of a Quasicrystalline Phase in Codispersions of Phosphatidylethanolamine and Glucocerebroside. Biophys J 2004, 86 (4), 2208-2217.

74.   SNYDER, B.; FREIRE, E. FLUORESCENCE ENERGY TRANSFER IN TWO DIMENSIONS - A NUMERIC SOLUTION FOR RANDOM AND NONRANDOM DISTRIBUTIONS. BIOPHYS J 1982, 40, 137-148.

75.   SACKMANN, E. MEMBRANE BENDING ENERGY CONCEPT OF VESICLE- AND CELL-SHAPES AND SHAPE-TRANSITIONS. FEBS LETT 1994, 346 (1), 3-16.

76.   HELFRICH, W.; PROST, J. INTRINSIC BENDING FORCE IN ANISOTROPIC MEMBRANES MADE OF CHIRAL MOLECULES. PHYS REV A 1988, 38 (6), 3065-3068.

77.   BITBOL, A.-F.; FOURNIER, J.-B.; ANGELOVA, M. I.; PUFF, N. DYNAMICAL MEMBRANE CURVATURE INSTABILITY CONTROLLED BY INTERMONOLAYER FRICTION. JOURNAL OF PHYSICS: CONDENSED MATTER 2011, 23 (28), 284102.

78.   BROWN, R. E.; ANDERSON, W. H.; KULKARNI, V. S. MACRO-RIPPLE PHASE FORMATION IN BILAYERS COMPOSED OF GALACTOSYLCERAMIDE AND PHOSPHATIDYLCHOLINE. BIOPHYS J 1995, 68, 1396-1405.

79.   PABST, G.; DANNER, S.; KARMAKAR, S.; DEUTSCH, G.; RAGHUNATHAN, V. A. ON THE PROPENSITY OF PHOSPHATIDYLGLYCEROLS TO FORM INTERDIGITATED PHASES. BIOPHYS J 2007, 93 (2), 513-525.

80.   MUTZ, M.; SERVUSS, R.-M.; HELFRICH, W. GIANT MEMBRANES OF SWOLLEN PHOSPHATIDYLETHANOLAMINES AND GLYCOLIPIDS. J PHYS FRANCE 1990, 51, 2557-2570.

81.   VANIER, M. T. LIPID CHANGES IN NIEMANN-PICK DISEASE TYPE C BRAIN: PERSONAL EXPERIENCE AND REVIEW OF THE LITERATURE. NEUROCHEM RES 1999, 24, 481-489.

82.   ARCHIBALD, D. D.; YAGER, P. MICROSTRUCTURAL POLYMORPHISM IN BOVINE BRAIN GALACTOCEREBROSIDE AND ITS TWO MAJOR SUBFRACTIONS. BIOCHEMISTRY 1992, 31 (37), 9045-9055.

83.   DEGROOTE, S.; WOLTHOORN, J.; VANMEER, G. THE CELL BIOLOGY OF GLYCOSPHINGOLIPIDS. SEMIN CELL DEV BIOL 2004, 15 (4), 375-387.

84.   HAKOMORI, S. STRUCTURE, ORGANIZATION, AND FUNCTION OF GLYCOSPHINGOLIPIDS IN MEMBRANE. CURR OPIN HEMATOL 2003, 10 (1), 16-24.

85.   KARLSSON, K.-A. ANIMAL GLYCOLIPIDS AS ATTACHMENT SITES FOR MICROBES. CHEM PHYS LIPIDS 1986, 42 (1–3), 153-172.

9 Supporting Material for: Effect of glucosylceramide on the biophysical properties of fluid membranes
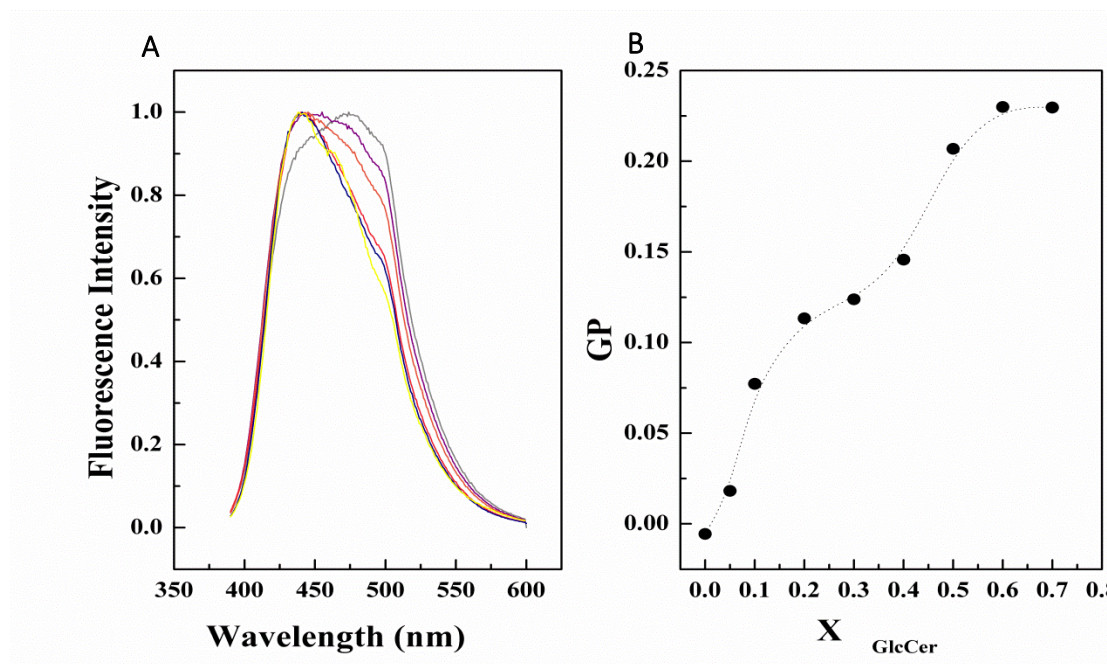
Figure S1 - Laurdan (A) emission spectra and (B) GP values in POPC/GlcCer mixtures. (A) Vesicles were composed of (grey) POPC and POPC containing (purple) 10, (orange) 20, (pink) 30, (blue) 40 and (yellow) 50 mol% of GlcCer. All measurements were performed at 24°C.
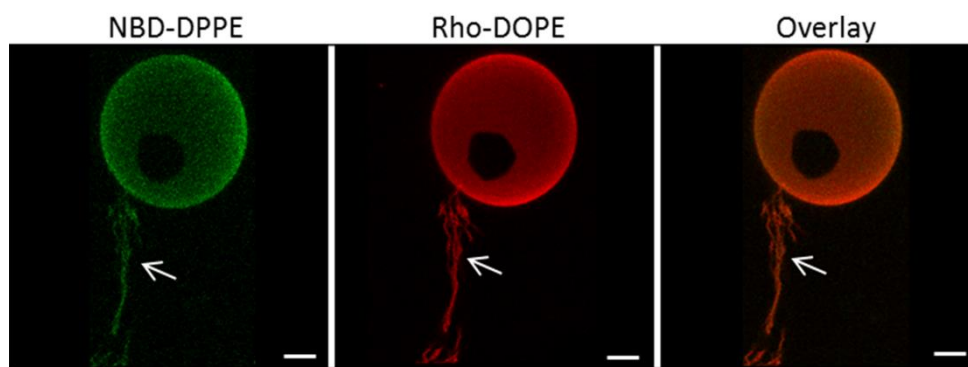
Figure S2- Confocal fluorescence microscopy of POPC/GlcCer mixtures.
3D projection images from 0.4 μm confocal slices of GUVs labeled with (green) NBD-DPPE and (red) Rho-DOPE. The GUVs contain 30% GlcCer. Scale bar, 5 μm.
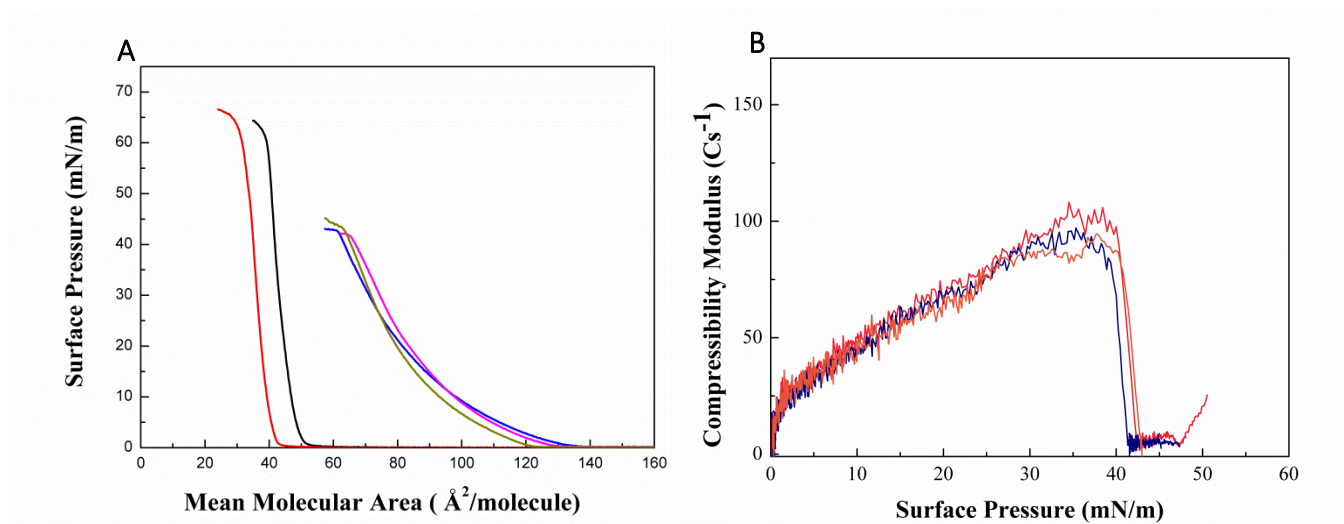
Figure S3 – Solvent and GlcCer effect in the membrane packing

(A) π–A isotherms of (green, blue, pink) POPC and (red, black) C16:0-GlcCer using (red, blue, pink) Chloroform, (black) Chloroform/Methanol/Water (2:1:0.15), or (green) Chloroform/Methanol (4:1) as the spreading solvent and (red, black, blue) PBS buffer at pH 7.4 or (pink) water as subphase. (B) Isothermal compressibility modulus as a function of surface pressure in (orange) POPC and POPC with (blue) 10% and (red) 30% of GlcCer.

Chapter III

Influence of the intracellular membrane pH on Sphingolipid organization and membrane biophysical properties

Varela A.R.P.., Gonçalves da Silva A., Fedorov A., Futerman A., Prieto M., Silva L.C.

Chapter III

Langmuir

Influence of Intracellular Membrane pH on Sphingolipid Organization and Membrane Biophysical Properties

Ana R. P. Varela,[†,‡,§] Amélia M. P. S. Gonçalves da Silva,[∥] Alexander Fedorov,[‡] Anthony H. Futerman,[§] Manuel Prieto,[‡] and Liana C. Silva*,[†]

[†]iMed.UL, Faculdade de Farmácia, Universidade de Lisboa, Avenida Professor Gama Pinto, 1649-003 Lisboa, Portugal

[‡]Centro de Química-Física Molecular and Institute of Nanoscience and Nanotechnology, Instituto Superior Técnico and [∥]Centro de Química Estrutural, Instituto Superior Técnico, Universidade de Lisboa, Avenida Rovisco Pais, 1049-001 Lisboa, Portugal

[§]Department of Biological Chemistry, Weizmann Institute of Science, Rehovot 76100, Israel

Ⓢ *Supporting Information*

ABSTRACT: Glucosylceramide (GlcCer) is a signaling lipid involved in the regulation of several cellular processes. It is present in different organelles, including the plasma membrane, Golgi apparatus, endoplasmic reticulum, and lysosomes. Accordingly, GlcCer is exposed to different pH environments in each organelle, which may lead to alterations in its properties and lateral organization and subsequent biological outcome. In this study, we addressed the effect of pH on the biophysical behavior of this lipid and other structurally related sphingolipids (SLs). Membranes composed of POPC (1-palmitoyl-2-oleoyl-*sn*-glycero-3-phosphocholine) and C16-GlcCer, sphingomyelin, and different acyl chain ceramides were characterized by fluorescence spectroscopy, confocal microscopy, and surface pressure–area measurements under neutral and acidic conditions. The results show that changing the pH from 7.4 to 5.5 has a larger impact on C16-GlcCer-containing membranes compared to other SLs. In addition, acidification mainly affects the organization and packing properties of the GlcCer-enriched gel phase, suggesting that the interactions established by the glucose moiety, in the GlcCer molecule, are those most affected by the increase in the acidity. These results further highlight the role of GlcCer as a modulator of membrane biophysical properties and will possibly contribute to the understanding of its biological function in different organelles.

1. INTRODUCTION

SLs are internalized by a combination of clathrin- and nonclathrin-mediated endocytic pathways and transported between cell organelles by vesicular and nonvesicular mechanisms.[1,2] Upon transport between intracellular membranes, SLs are exposed to a progressive change in pH,[3−5] from neutral, ~7.4, in the plasma membrane (PM) to acidic, ~5, in the lysosomal lumen.[5,6] Acidification of the lumen of intracellular organelles is achieved by a proton-pumping vacuolar-type ATPase (V-ATPase) in combination with ion channels and transporters.[7] Progressive luminal acidification along the endocytic pathway is crucial for correct intracellular trafficking and allows for proper sorting of proteins and lipids.[1,7,8]

Evidence exists that SLs (mainly glycosphingolipids (GSLs)) can modulate cellular pH, probably by interfering with V-ATPase activity.[9−11] In this context, it was recently shown that GlcCer depletion or accumulation affects V-ATPase activity,[9,12] suggesting that this lipid might function as a regulator of V-ATPase. This is supported by increased values of endolysosomal pH observed in lymphoblasts from patients with Gaucher Disease (GD), a metabolic disease characterized by GlcCer accumulation.[9] It was suggested that altered levels of GlcCer

might disturb membrane structure and lipid lateral organization and perturb the conformation of V-ATPase, resulting in pH changes that might alter the cellular trafficking of the proton pump, leading to a cascade of events that could impair cell function.[1,13,14] Other studies have demonstrated that GlcCer affects membrane biophysical properties,[15] supporting a role of GlcCer on the modulation of membrane properties, and consequent alteration of membrane organization. Similar evidence was obtained for sphingomyelin (SM)[16] and ceramides,[17,18] inasmuch as these lipids may exert their biological action through formation of lipid domains with distinct packing properties.[19] Even though many studies address the impact of these lipids on membrane biophysical properties,[20,21] literature regarding the effect of pH on the organization of these SLs is scarce.

In this study, we investigate the role of acidification on the biophysical properties of GlcCer and other SLs. The SLs were selected according to the following criteria: (i) Neutral (Cer and GlcCer) and zwitterionic (SM); (ii) SLs presenting the

Chapter III- Influence of intracellular membrane pH on sphingolipid organization and membrane biophysical properties

1 Abstract

Glucosylceramide (GlcCer) is a signaling lipid involved in the regulation of several cellular processes. It is present in different organelles, including the plasma membrane, Golgi apparatus, endoplasmic reticulum, and lysosomes. Accordingly, GlcCer is exposed to different pH environments in each organelle, which may lead to alterations in its properties and lateral organization and subsequent biological outcome. In this study, we addressed the effect of pH on the biophysical behavior of this lipid and other structurally related sphingolipids (SLs). Membranes composed of POPC (1-palmitoyl-2-oleoyl-sn-glycero-3-phosphocholine) and C16-GlcCer, sphingomyelin and different acyl chain ceramides were characterized by fluorescence spectroscopy, confocal microscopy and surface pressure - area measurements under neutral and acidic conditions. The results show that changing the pH from 7.4 to 5.5 has a larger impact on C16-GlcCer-containing membranes compared to other SLs. In addition, acidification mainly affects the organization and packing properties of the GlcCer-enriched gel phase, suggesting that the interactions established by the glucose moiety, in the GlcCer molecule, are those most affected by the increase in the acidity. These results further highlight the role of GlcCer as a modulator of membrane biophysical properties and will possibly contribute to the understanding of its biological function in different organelles.

2. Introduction

SLs are internalized by a combination of clathrin- and nonclathrin-mediated endocytic pathways and transported between cell organelles by vesicular and nonvesicular mechanisms[1, 2]. Upon transport between intracellular membranes, SLs are exposed to a progressive change in pH [3, 4, 5], from neutral ,~7.4, in the plasma membrane (PM) to acidic ,~5, in the lysosomal lumen[5, 6]. Acidification of the lumen of intracellular organelles is achieved by a proton-pumping vacuolar-type ATPase (V-ATPase) in combination with ion channels and transporters[7]. The progressive luminal acidification along the endocytic pathway is crucial for correct intracellular trafficking and allows for proper sorting of proteins and lipids [1, 7, 8].

Evidence exists that SLs (mainly glycosphingolipids (GSLs)) can modulate cellular pH, probably by interfering with V-ATPase activity[9, 10, 11]. In this context, it was recently shown that GlcCer depletion or accumulation affects V-ATPase activity[9, 12], suggesting that this lipid might function as a regulator of V-ATPase. This is supported by increased values of endolysosomal pH observed in lymphoblasts from patients with Gaucher Disease (GD), a metabolic disease characterized by GlcCer accumulation[9]. It was suggested that altered levels of GlcCer might disturb membrane structure and lipid lateral organization, and perturb the conformation of V-ATPase, resulting in pH changes that might alter the cellular trafficking of the proton pump, leading to a cascade of events that could impair cell function[1, 13, 14]. Other studies have demonstrated that GlcCer affects membrane biophysical properties [15], supporting a role of GlcCer on the modulation of membrane properties, and consequent alteration of membrane organization. Similar evidence was obtained for sphingomyelin (SM)[16] and ceramides [17, 18], inasmuch as these lipids may exert their biological action through formation of lipid domains with distinct packing properties[19]. Even though many studies address the impact of these lipids on membrane biophysical properties[20, 21], literature regarding the effect of pH on the organization of these SLs is scarce.

In this study, we investigate the role of acidification on the biophysical properties of GlcCer and other SLs. The SLs were selected according to the following criteria: i) Neutral (Cer and GlcCer) and zwitterionic (SM); ii) SLs presenting the same acyl chain structure but different headgroups (C16-Cer, -GlcCer and -SM); iii) SLs presenting different acyl

chains (C16, C24:1-Cer) and the same headgroup (Figure 1). Our results indicate that membrane properties are influenced by pH, which mainly affects the organization and packing of the gel phase domains formed by these SLs. This effect is more pronounced in C16-GlcCer containing membranes compared to other SLs, likely due to alterations in the H-bonding network and/or protonation state of the glucose moiety in the GlcCer molecules.

A

B

C

D
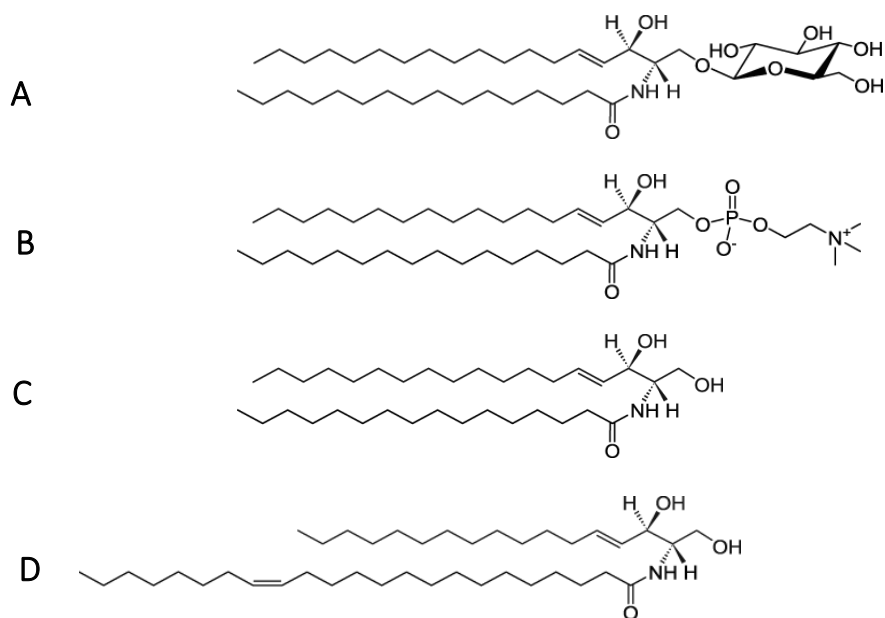
Figure 1-. Structures of the studied SLs.
(A) C16-GlcCer, (B) C16-SM, (C) C16-Cer and (D) C24:1-Cer.

3 Materials and Methods

3.1 Materials

POPC (1-palmitoyl-2-oleoyl-*sn*-glycero-3-phosphocholine), C16-GlcCer (D-glucosyl-ß-1,1' N-palmitoyl-D-erythro-sphingosine), C16-SM (N-palmitoyl-D-erythro-sphingosylphosphorylcholine), C16-Cer (N-palmitoyl-D-erythro-sphingosine), C24:1-Cer (N-nervonoyl-D-erythro-sphingosine), Rho-DOPE (N-rhodamine-dipalmitoylphosphatidylethanolamine), and 1,2-dioleoyl-*sn*-glycero-3-phosphoethanolamine-N-(biotinyl) (DOPE-biotin) were from Avanti Polar Lipids (Alabaster, AL). DPH (1,6-diphenyl-1,3,5-hexatriene), *t*-PnA (*trans*-parinaric acid), and NBD-DPPE (1,2-dipalmitoyl-sn-glycero-3-phosphoethanolamine-N-(7-nitro-2-1,3-

benzoxadiazol-4yl)) were from Molecular Probes (Leiden, The Netherlands). All organic solvents were UVASOL grade from Merck (Darmstadt, Germany).

3.2 Fluorescence Spectroscopy

To evaluate the effect of pH on the biophysical properties of model membranes containing POPC and different SLs, multilamellar vesicles (MLV) (total lipid concentration of 0.1 mM) were prepared as previously described [17]. The suspension medium was PBS buffer (10 mM sodium phosphate, 150 mM sodium chloride, and 0.1 mM EDTA (pH 7.4)) or citrate-phosphate buffer (100mM citric acid and 200 mM sodium phosphate (pH 5.5)). Fluorescence anisotropy of t-PnA, DPH, and Rho-DOPE were measured in a SLM Aminco 8100 series 2 spectrofluorimeter with double excitation and emission monochromators, MC400 (Rochester, NY). All measurements were performed in 0.5 cm × 0.5 cm quartz cuvettes. The excitation (λ_{exc})/emission (λ_{em}) wavelengths were 320/405 nm for t-PnA; 358/430 nm for DPH, and 570/593 for Rho-DOPE. The probe/lipid ratios used were 1/500, 1/200 and 1/500 for t-PnA, DPH and Rho-DOPE, respectively. Constant temperature was maintained using a Julabo F25 circulating water bath controlled with 0.1°C precision directly inside the cuvette with a type-K thermocouple (Electrical Electronic Corp., Taipei, Taiwan). For measurements performed at different temperatures, the heating rate was always below 0.2°C/min. The fluorescence anisotropy $<r>$ was calculated as[22]:

$$<r> = \frac{Ivv - GIvh}{Ivv + 2GIvh}$$
(Eq. 1)

where the different intensities (I_{ii}) are the steady state vertical and horizontal components of the fluorescence emission with the excitation vertical (Ivv and Ivh) and horizontal (Ihv and Ihh) to the emission axis. The latter pair of components is used to calculate the G factor (G= Ihv/Ihh). An appropriate blank was subtracted from each intensity reading before calculation of the anisotropy value.

Time-resolved fluorescence measurements with t-PnA were performed by the single photon timing technique with a laser pulse excitation[23] adjusted to the λ_{exc}=305nm (using

a secondary laser of Rhodamine 6G[24]) and λ_{em}=405nm. The experimental decays were analyzed using TRFA software (Scientific Software Technologies Center, Minsk, Belarus).

3.3 Confocal Fluorescence Microscopy

Giant unilamellar vesicles (GUVs) were prepared with the appropriate lipids, DOPE-biotin (at a biotinylated/non-biotinylated lipid ratio of $1:10^6$), Rho-DOPE and NBD-DPPE) (at a probe/lipid ratio of 1:500 and 1:200, respectively). These were formed by electroformation, as previously described[25, 26, 27]. The GUVs were then transferred to 8-well Ibidi® μ-slides that had been previously coated with avidin (at 0.1mg/ml) to improve GUV adhesion to the plate [28]; PBS or citrate-phosphate were added to create a neutral (7.4) or acidic (5.5) environment, respectively. Confocal fluorescence microscopy was performed using a Leica TCS SP5 (Leica Mycrosystems CMS GmbH, Mannheim, Germany) inverted microscope (DMI6000) with a 63×water (1.2 numerical aperture) apochromatic objective. NBD-DPPE and Rho-DOPE excitation was performed using the 458 nm and 514 nm lines from an Ar^+ laser, respectively. The emission was collected at 480-530 and 530-650 nm, for NBD-DPPE and Rho-DOPE, respectively. Confocal sections of thickness below 0.5 μm were obtained using a galvanometric motor stage. Three-dimensional (3D) projections were obtained using Leica Application Suite-Advanced Fluorescence software.

3.4 Lipid monolayers and Surface Pressure-Area Measurements

Surface pressure–area (π–A) isotherm measurements were carried out on a KSV 5000 Langmuir–Blodgett system (KSV Instruments, Helsinki) installed in a laminar flow hood. Procedures for π–A measurements and cleaning care were described elsewhere[29]. Monolayers were spread drop-wise as chloroform solutions, using a glass microsyringe, on a subphase composed of a buffer solution (PBS or citrate-phosphate) at pH 7.4 or 5.5. Unless specified, the volume and concentration of spreading solution was 100μL and 0.5 mM, respectively. The temperature of the subphase was 24°C ± 1°C, controlled by water circulation from a thermostat within an error of ± 0.1 °C. The barrier speed of symmetric compression was 10 mm min−1 (3.3 $Å^2$ molecule^{-1} min^{-1}). π–A isotherms were measured at least three times from fresh spreading solutions to confirm reproducibility.

The isothermal two-dimensional compressibility modulus (Cs^{-1}), or elastic modulus, is calculated from the π-A isotherms as

$$Cs^{-1} = -A(\partial A / \partial \pi)T. \qquad \text{(Eq. 2)}$$

The Gibbs energy of mixing, ΔGmix, is taken from:

$$\Delta Gmix\ (\pi) = \Delta Gideal + GE(\pi), \qquad \text{(Eq. 3)}$$

where ΔG_{ideal} is the Gibbs energy of ideal mixing at low surface pressure (π → 0)

$$\Delta Gideal = RT(X1\ln X1 + X2\ln X2), \qquad \text{(Eq. 4)}$$

and $G^E(\pi)$ is the excess Gibbs energy of mixing:

$$GE(\pi) = \int AE(\pi)d\,\pi, \qquad \text{(Eq. 5)}$$

where $A^E\,(\pi)$ is the excess area of mixing at the surface pressure π,

$$AE\,(\pi) = [A12 - (X1\,A1 + X2\,A2)], \qquad \text{(Eq. 6)}$$

and A_{12} is the MMA (mean molecular area) of the mixed monolayer, X_1 and X_2 are the mole fraction of components 1 and 2, respectively, and A_1 and A_2 are the corresponding molecular areas in the single component monolayer at the surface pressure π.

4 Results

4.1 Thermotropic studies

To evaluate the effect of neutral and acidic environments on the properties of membranes containing neutral or zwitterionic SLs, the thermotropic behavior of mixtures of C16-SM and C16-GlcCer was characterized. Our previous study demonstrated that *t*-

PnA is a suitable probe to report the gel-to-fluid phase transition of POPC/GlcCer mixtures[15], and therefore, it was used in the present study to evaluate differences in the thermotropic properties of these mixtures in response to acidic pH (Figure 2A and 2B). At lower temperatures (< 15°C), mixtures containing ≥ 20 mol% of C16-GlcCer present gel phase at both neutral and acidic pH. This is apparent by the very high t-PnA anisotropy values, typical of gel phase[30]. Increasing the temperature leads to a sharp decrease in the anisotropy of the probe (in both environments) to values typical of the fluid phase. The temperature at which t-PnA anisotropy abruptly decreases and the temperature at which the melting of the gel phase is complete are dependent on both C16-GlcCer content and pH (Figure 2A, 2B, and 2D). At neutral pH, t-PnA anisotropy is higher, demonstrating that C16-GlcCer gel domains are more ordered and thermally stable in this pH compared to acidic pH (Figure 2D).

The thermotropic characterization of POPC/C16-SM mixtures was performed using DPH (Figure 2C). This probe displays a partition coefficient ($Kp^{g/f}$) of ~ 1 into a SM-enriched gel phase[15], and therefore is a suitable probe to report the effect of pH on the thermotropic properties of these mixtures. Note that, DPH cannot be used to study the properties of mixtures containing GlcCer or ceramides, due to its strong exclusion from the gel domains formed by these lipids[15, 17]. As shown in Figure 2C, the thermotropic properties of POPC/C16-SM mixtures are not markedly affected by changes in membrane pH environment. These results suggest that alteration in pH have a stronger impact on the thermotropic behavior of C16-GlcCer.
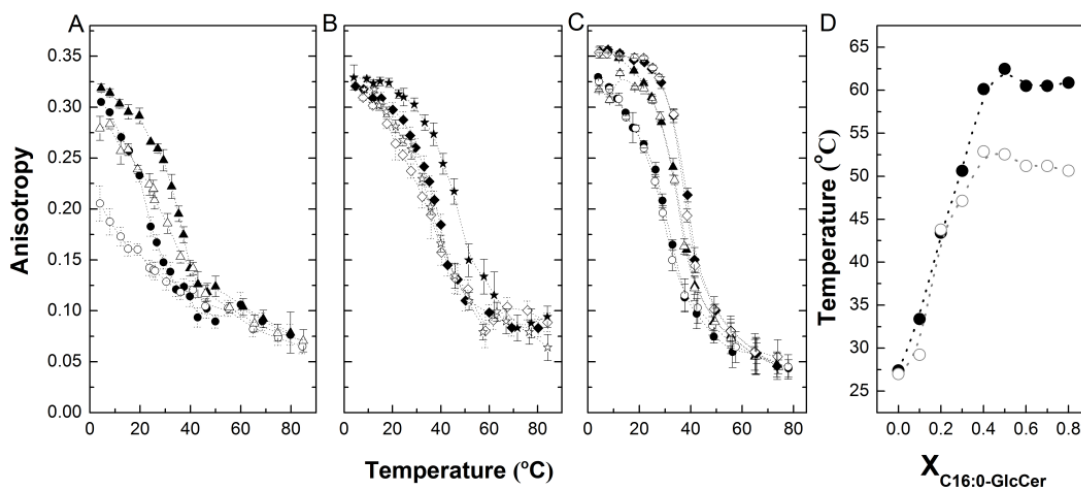
Figure 2 - Thermotropic behavior of POPC/C16-GlcCer and POPC/C16-SM mixtures in neutral and acidic environments.

Steady-state fluorescence anisotropy performed at pH 7.4 (solid symbols) and 5.5 (open symbols) of (A , B) *t*-PnA and (C) DPH as a function of temperature in MLVs composed of (A , B) POPC containing (●, ○) 10, (▲,△) 20, (◆,◇) 30, and (★,✷) 50   mol% of C16-GlcCer and (C) POPC containing (●, ○) 60, (▲,△) 80, and (◆,◇) 90 mol% of C16-SM. (D) Temperature at which the melting of C16-GlcCer-enriched gel domains is complete. Some values might be superimposed. Values are means ± SD of at least 3 independent experiments.

4.2 Spectroscopic characterization of the gel phase

The effect of pH environment on the properties of the gel phase in membranes containing different SLs was assessed by following the variation of the fluorescence anisotropy and fluorescence intensity decay of *t*-PnA as a function of SL molar fraction (Figure 3). Figure 3A shows the variation of *t*-PnA fluorescence anisotropy in POPC/C16-GlcCer mixtures at neutral and acidic pH. In agreement with our previous report[15], increasing the C16-GlcCer molar fraction leads to an increase in *t*-PnA fluorescence anisotropy toward values typical of gel phase, showing that this GSL is able to drive formation of gel domains at both pH values. Moreover, the results show that *t*-PnA anisotropy is higher at neutral pH, indicating a higher membrane order and/or gel phase fraction, in agreement with the thermotropic data presented above.

To further characterize the effect of pH on the properties of the gel phase formed in the POPC/SL mixtures, *t*-PnA fluorescence intensity decay was measured. Qualitative information about the packing properties and the fraction of the gel phase can be obtained by analysis of the lifetime components (τ_i) of *t*-PnA fluorescence intensity decay (Figure 3B) and amplitude (α_i) of the decay components (Figure 3C). Specifically, we have shown that formation of a SL-enriched gel phase can be evaluated by the appearance of a very long lifetime component on *t*-PnA intensity decay[31, 32, 33]. In mixtures containing C16-GlcCer, the long lifetime component of *t*-PnA displays a similar trend of variation at neutral and acidic pH. However, the longer lifetime component of *t*-PnA measured at pH 7.4 suggests that the packing of the C16-GlcCer gel phase is tighter at neutral pH compared to acidic pH (Figure 3B). Furthermore, the extent of gel phase formation is larger at neutral pH, as shown by the higher amplitude associated with the long lifetime component of *t*-PnA fluorescence intensity decay (Figure 3C).
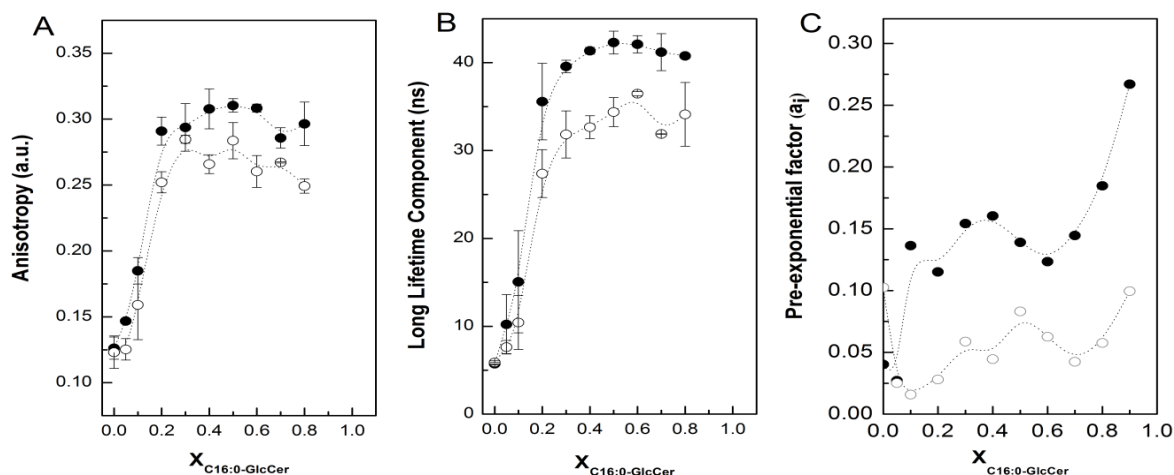
Figure 3 - Influence of membrane pH environment on the biophysical properties of POPC/GlcCer mixtures.
(A) Fluorescence anisotropy, (B) long lifetime component and (C) pre-exponential factors (amplitude) of the long lifetime component of *t*-PnA intensity decay in binary POPC/GlcCer mixtures. All measurements were performed at 24°C, in neutral (solid symbols) or acidic (open symbols) environment. Values are means ± SD of at least 3 independent experiments.

To evaluate if pH-mediated alterations on membrane properties were specific to C16-GlcCer or a common phenomenon to other SLs, *t*-PnA fluorescence anisotropy was measured in binary mixtures composed of POPC and C16-Cer (Figure 4A), C24:1-Cer (Figure 4B) or C16-SM (Figure 4C). The results show that *t*-PnA anisotropy only reports minor alterations on membrane organization when the aqueous environment is acidified. In addition, neither the phase behavior nor the packing properties of mixtures containing ceramides (Figures 4D and 4E) is affected by membrane pH environment, except for mixtures containing > 50 mol% C24:1-Cer, where a slightly tighter packing (longer lifetime component) at neutral pH is observed (Figure 4E). Figure 4F shows that the packing properties of POPC/C16-SM model membranes are influenced by the pH, especially when the C16-SM content increases above 30 mol%. Interestingly, at ~ 28 mol% of C16-SM a gel/fluid phase separation is observed for these binary mixtures [31], suggesting that changes in membrane pH have a stronger impact on the properties of the gel phase than on the fluid phase. It is worth to mentioning that ceramides have a strong tendency to drive gel/fluid phase separation and form tightly packed domains [17, 26] but apparently these ceramide-enriched gel domains are not markedly affected by changes in pH.
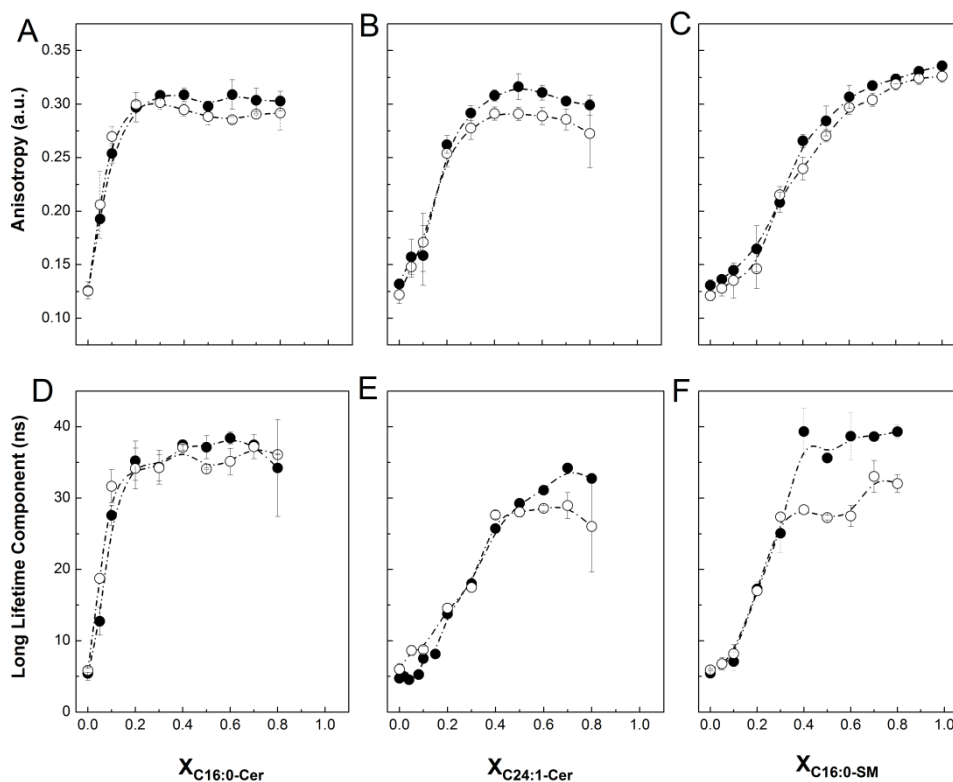
Figure 4. Influence of membrane pH environment on the biophysical properties of the gel phase.
(A-C) Fluorescence anisotropy and (D-F) long lifetime component of *t*-PnA intensity decay in binary POPC/SL mixtures. (A, D) POPC/C16-Cer; (B, E) POPC/C24:1-Cer and (C, F) POPC/C16-SM mixtures. All measurements were performed at 24°C in neutral (solid symbols) or acidic (open symbols) environment. Values are means ± SD of at least 3 independent experiments.

4.3 Spectroscopic characterization of the fluid phase

Alterations of the biophysical properties of the fluid phase were studied using DPH and Rho-DOPE. These probes are known to have a very low partition into C16-GlcCer[15] and Cer-enriched domains[17], and therefore, alterations in their photophysical properties are mainly due to changes occurring in the fluid phase.

DPH fluorescence anisotropy is similar in POPC/C16-GlcCer mixtures at acidic and neutral pH (Figure 5A) and only very minor differences were observed, suggesting a stronger effect of the pH in the organization/properties of the gel phase. This is further supported by the similar anisotropy values of Rho-DOPE, a probe that is completely excluded from the tightly packed GlcCer-gel domains[15], in the different environments (Figure 5A). It

should be stressed that Rho-DOPE anisotropy decreases with the increase of the gel fraction. This is due to electronic energy transfer that occurs between the Rho-DOPE molecules (homo-FRET), which becomes more efficient with the proximity of the chromophores. This decrease is directly related to the reduction in the area available (fluid phase) for the distribution of Rho-DOPE [34], as we previously showed for POPC/C16-GlcCer mixtures at neutral pH [15].

The anisotropy of Rho-DOPE and DPH was also unaltered by acidification of POPC/C16-SM (Figure 5B), POPC/C24:1-Cer (Figure 5C) or POPC/C16-Cer (Figure S1, Supporting Material) mixtures. These results suggest that the biophysical properties of the fluid phase in these mixtures are not strongly affected by pH variation. Note that, for mixtures containing C16-SM, DPH equally incorporates into the gel and the fluid phases, thus reporting the overall properties of these binary mixtures. Moreover, Rho-DOPE anisotropy decreases to a much lower extent upon gel formation in POPC/C16-SM mixtures, showing that the probe is not fully excluded from this gel phase and further supporting the less ordered packing properties of C16-SM-enriched gel phase [33], compared to a C16-GlcCer gel phase.
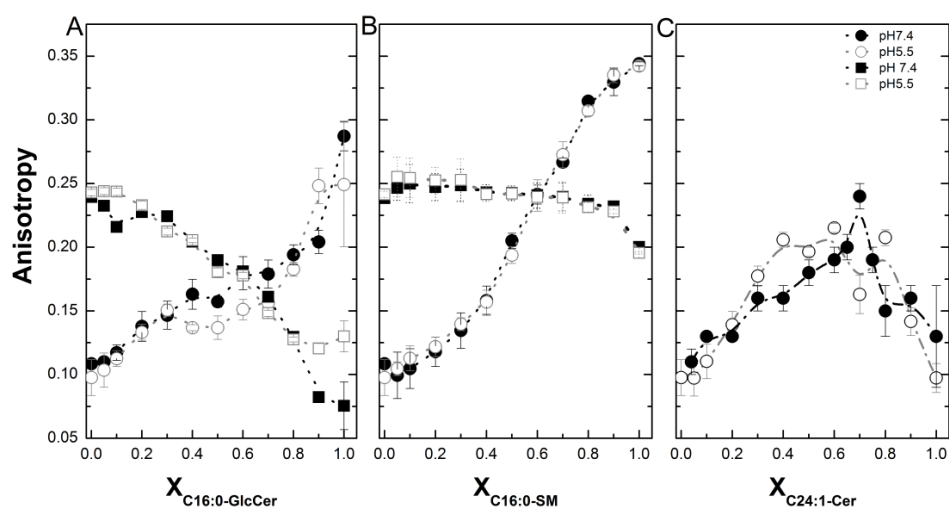
Figure 5 - Influence of membrane pH environment on the biophysical properties of the fluid phase.
Steady-state fluorescence anisotropy of (squares) Rho-DOPE and (circles) DPH in binary mixtures of POPC containing (A) C16-GlcCer, (B) C16-SM and (C) C24:1-Cer. All measurements were performed at 24°C, at pH 7.4 (solid symbols) and pH 5.5 (open

symbols). Some values might be superimposed. Values are means ± SD of at least 3 independent experiments.

4.4 Monolayer studies

To obtain additional information regarding lipid-lipid and lipid-solvent interactions, Langmuir monolayer studies were performed. The dependence of the surface area on the pH can thus be studied by surface pressure-area measurements in lipid monolayers. Figure 6A-C shows representative π-A isotherms of monolayers composed of POPC and C16-GlcCer at neutral (as described in our previous work [15]) and acidic pH. The shape of the isotherms is similar in neutral and acidic subphases. However, at acidic pH (dashed lines), all POPC/C16-GlcCer mixtures display a more expanded behavior compared to neutral pH. This is apparent from the larger lift-off area ($\pi \approx 0$) and mean molecular area (MMA) at the collapse pressures of POPC/C16-GlcCer mixtures in acidic environments. As an example, the lift-off area and MMA at the collapse pressure decrease, respectively, from ~ 140 Å^2 and ~ 70 Å^2, at pH 5.5 to ~ 127 Å^2 and ~ 62 Å^2 at pH 7.4 for mixtures containing 30 mol% of C16-GlcCer (Figure 6B, curves 7 and 8). The pressure at which the collapse occurs is essentially independent of the pH, except for 100% GlcCer, where the collapse occurred at a slightly higher pressure at neutral pH (~ 65 mN/m) compared to acidic pH (~ 60 mN/m). Figure 6A-C further shows that at acidic pH the lift-off ($\pi \approx 0$) area decreases with the increase in C16-GlcCer molar fraction, except for the mixture containing 10 mol% of C16-GlcCer (Figure 6C, curve 10), which is more expanded than pure POPC (Figure 6C, curve 12) in the same pH environment. The same behavior was previously reported for these mixtures at neutral pH[15] (curves 9 and 11, respectively).

Mixtures containing C16-Cer are insensitive to the membrane environment (Figure 6D) and only minor differences are observed in the lift-off area, collapse pressure and MMA at the collapse pressure. In contrast, isotherms of mixtures containing C24:1-Cer, display a pH dependent behavior (Figure 6E): the lift-off area and the MMA at the collapse pressure increase at acidic pH, showing that the monolayer is less packed at pH 5.5. Finally, the isotherms of model membranes containing C16-SM (Figure 6F) also exhibited a pH sensitive behavior; however, the more condensed mixed monolayers were formed at the acidic pH, as shown by the smaller lift-off area and MMA at the collapse pressure.

This behavior contrasts with the other studied SLs, but is consistent with previous reports for these mixtures[35], where it was suggested that the higher protonation of the environment could promote stronger interactions between the lipid headgroups and the subphase or/and between the lipids in the monolayer [36].
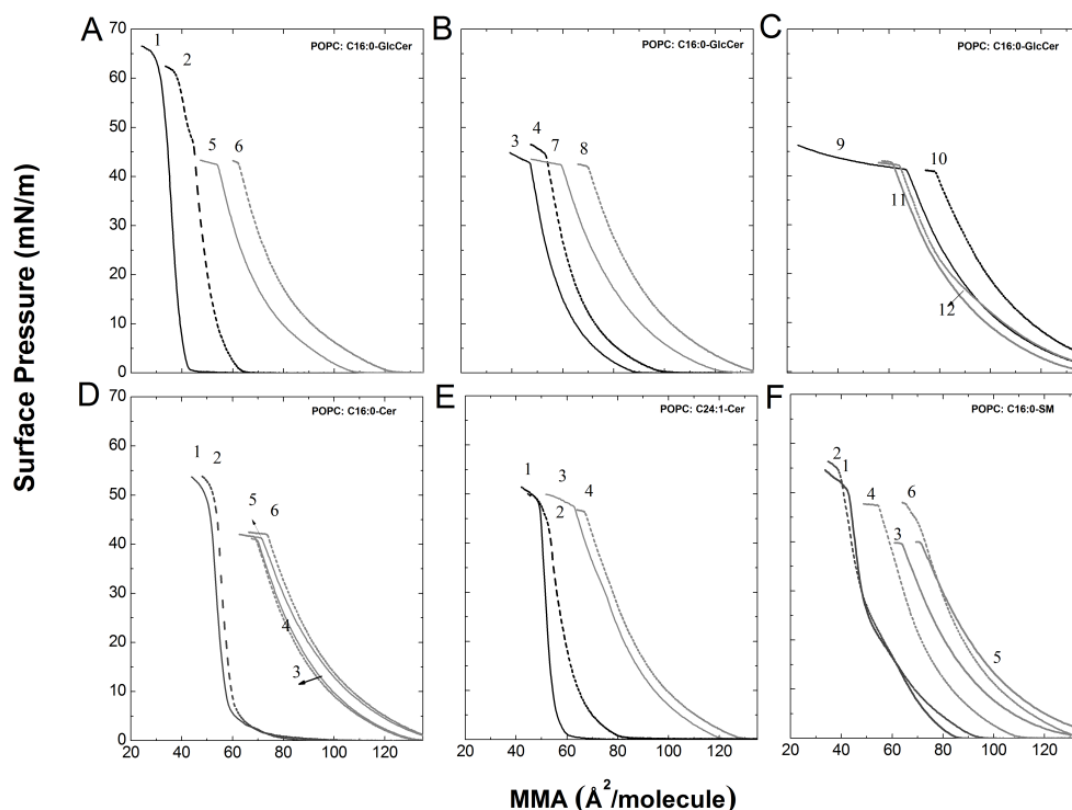
Figure 6. Influence of pH on π-A isotherms of mixed monolayers.
π-A isotherms of (A-C) POPC/C16-GlcCer, (D) POPC/C16-Cer, (E) POPC/C24:1-Cer and (F) POPC/C16-SM monolayers). In (A-C) isotherms numbered 1 and 2 represent the pure SL and 3-10 represent mixed monolayers of POPC with (3,4) 70, (5, 6) 50, (7, 8) 30, and (9, 10) 10 mol% of C16-GlcCer. Finally, isotherms 11 and 12 represent the pure phospholipid. (D-F) isotherms numbered 1 and 2 represent the pure SL and 3-6 represent mixed monolayers of POPC containing (3, 4) 30 and (5, 6) 10 mol% of SL. All measurements were performed at 24°C at pH 7.4 (full lines) or 5.5 (dashed lines).

The compressibility modulus (Cs^{-1}) (Eq. 3, Table 1 and Figure S2, Supporting Information), the excess area (A^E) (Figure 7A and 7B), and the free energy of mixing (ΔG_{mix}) (Figures 7C and 7D) were determined to further characterize the monolayers under study.

The Cs^{-1} allows identification of two-dimensional phase transitions and provides information regarding molecular interactions: the higher the Cs^{-1}, the lower the interfacial elasticity[36, 37]. The Cs^{-1} of C16-GlcCer mixed-monolayers is essentially identical at neutral and acidic pH. However, pure C16-GlcCer samples were sensitive to the higher protonation of the solvent exhibiting a decrease in the Cs^{-1} values indicating the more elastic nature of the lipid monolayers at acidic pH (Table 1 and Figure S2A Supporting Information). In addition, the results show that membrane elasticity decreases with increasing content of C16-GlcCer, as evidenced by the increase of the maximum of compressibility modulus with C16-GlcCer content, independently of the pH (Table 1 and Figure S2, Supporting Information).

Table 1. Effect of the SL structure and pH environment on the maximum compressibility modulus (Cs^{-1}) and respective MMA.

	pH 7.4		pH5.5	
Sample	Max Cs^{-1}(mN/m)	MMA($Å^2$/molecule)	Max Cs^{-1}(mN/m)	MMA($Å^2$/molecule)
POPC (PC)	94.55	65.06	102	71.12
PC:C16-GlcCer (90:10)	97.11	71.64	101.127	80.7
PC: C16-GlcCer (70:30)	105.88	61.84	115.35	72.55
PC: C16-GlcCer (50:50)	122.47	56.16	131.19	65.96
PC: C16-GlcCer (30:70)	148	49	160	55.7
C16-GlcCer	315	35.95	267	46.98
PC: C24:1-Cer (70:30)	116.8	77.89	118.259	70.88
C24:1-Cer	460	52.31	249.17	55.6
PC:C16-SM (90:10)	94.97	76.38	126.46	74.88
PC:C16-SM (70:30)	92.45	71.62	117.93	63.36
C16-SM	201.98	45.95	149.32	44.16

Similarly to C16-GlcCer, C24:1-Cer -monolayers display less elasticity at neutral pH and with increasing C24:1-Cer content, as shown by the higher Cs^{-1} (Table 1 and Figure S2B,

Supporting Information). An opposite behavior is observed for C16-SM-mixed-monolayers, where an increase in the elasticity is observed at neutral pH, especially at higher pressures (Table1 and Figure S2C, Supporting Information). Comparison of the Cs^{-1} between C16-GlcCer, C24:1-Cer and C16-SM monolayers, with the same molar fraction of SL (30 mol%), shows that the packing density decreases in the order C24:1-Cer (117 mN/m) > C16-GlcCer (105 mN/m) > C16-SM (93 mN/m) at neutral pH, whereas at acidic pH C16-GlcCer is less elastic than C24:1-Cer.

The variation of MMA with C16-GlcCer molar fraction exhibits a positive deviation from the additive behavior of the components (A^E >0) showing that the mixtures have a non-ideal mixing behavior (Figure 7A). This further shows that the interaction between the components is weaker than between each component itself. In addition, the larger A^E at acidic pH further confirms the more expanded nature of these monolayers in this environment (Figure 7A). C16-SM mixed monolayers also display a positive deviation from additive behavior at both pH, but in contrast with C16-GlcCer mixed monolayers, the larger A^E is observed at neutral pH (Figure 7B).

To compare the global effect of the neutral and acidic environment on the mixtures, the MMA at the maximum Cs^{-1} ($MMA_{max\ Cs-1}$) was determined at pH 7.4 and 5.5 for the same lipid composition. From analysis of Table 1, it is clear that higher $MMA_{max\ Cs-1}$ are observed at pH 5.5 for C16-GlcCer-mixed and pure monolayers, while C16-SM-mixed and pure - monolayers exhibit the opposite behavior. This further supports that the acidification of the environment expands membranes containing C16-GlcCer and increases the packing of membranes containing C16-SM.

The stability of the mixed monolayers was evaluated by the excess free energy of mixing (G^E) and free energy of mixing (ΔG_{mix}) (Figure 7C, D and 7E, F, respectively). C16-GlcCer mixed monolayers display mainly positive G^E values implying that the attractive interactions decrease in these mixtures (Figure 7C). However, at lower surface pressures and acidic pH, G^E is close to zero (ideal behavior) for most of the studied mixtures. C16-SM mixed monolayers in acidic pH exhibit attractive forces between the components, as shown by the negative G^E values (Figure 7D). In contrast, in a neutral subphase G^E is positive (at higher pressures) or close to neutrality, evidencing that repulsive forces become dominant (Figure 7D). These results show that lipid-lipid interactions in C16-SM

mixed monolayers are determined by both the subphase composition and the surface pressure. Mixed monolayers containing 30 mol% of C24:1-Cer exhibit a negative or close
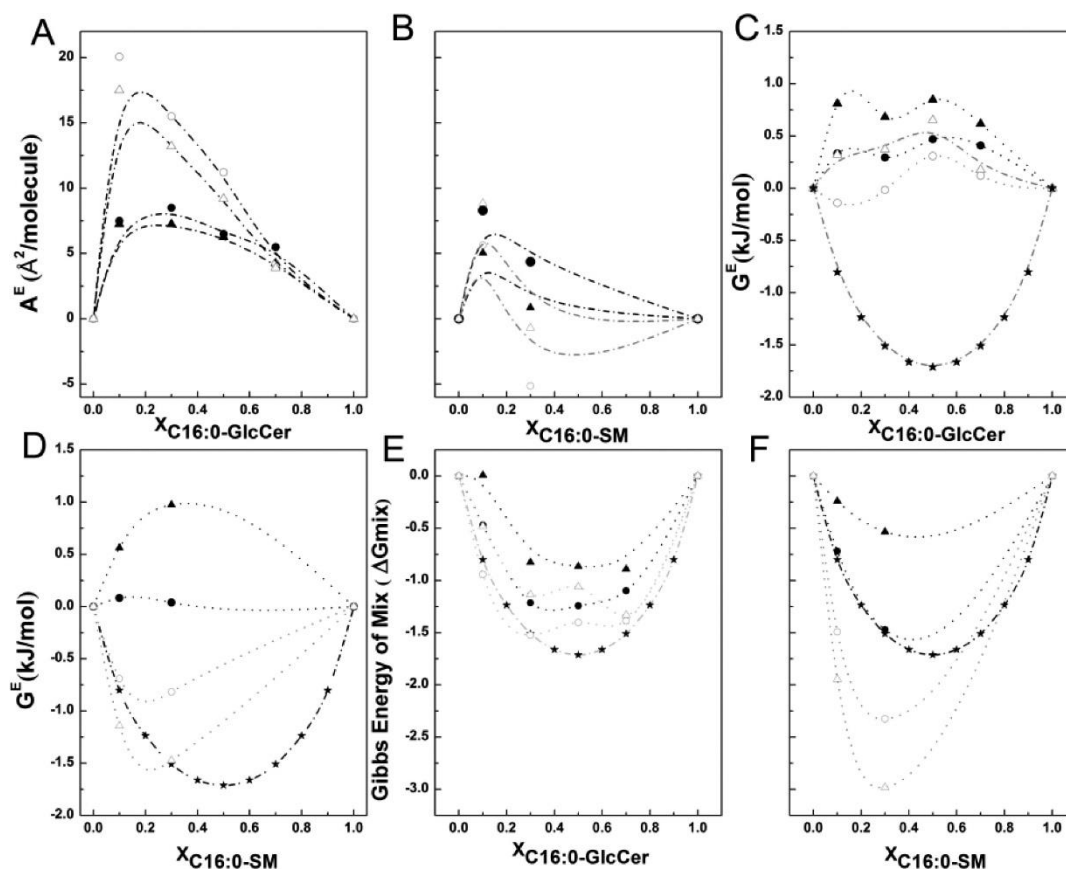
Figure 7. Characterization of the biophysical behavior of mixed monolayers at pH 7.4 and 5.5.

The monolayers characterization was performed at 24 °C at pH 7.4 (solid symbols) or 5.5. (open symbols) at (●, ○) 20 and (▲, △) 40 mN/m. (A, B) Excess area, (C, D) excess energy of mixing and (E, F) free energy of mixing of (A, C, E) C16-GlcCer and (B, D, F) C16-SM monolayers and mixed monolayers. (E, F) Solid star (★) corresponds to the ideal Gibbs energy of mixing.

to neutral G^E showing that attractive forces are dominant (Figure S3, Supporting Information). However, at higher surface pressures and neutral pH, G^E becomes positive and thus, repulsive forces between the components are now dominant. The negative values of ΔG_{mix} obtained in all the studied mixtures (Figures 7E, 7F and Figure S3B, Supporting Information) imply that the mixtures are more stable than the pure components and confirm their partial miscibility; the only exception is the mixture with 10 mol% of C16-SM, where ΔG_{mix} is almost zero at 20 mN/m. The more negative values

of ΔG_{mix} in acidic environment, suggest that both C16-GlcCer and C16-SM mixed monolayers are more stable in this subphase.

4.5. Effect of pH on gel domain shape and size

GUVs composed of POPC and the different SLs (Figure 8) were studied by confocal fluorescence microscopy in order to visualize the impact of membrane environment on (i) domain size, (ii) domain morphology, (iii) the extent of gel-fluid phase separation and (iv) membrane morphological alterations.

Despite the intrinsic heterogeneity of GUV population[28], some differences were observed between GlcCer-containing mixtures at neutral and acidic pH (Figures 8A and S4, Supporting Information), particularly regarding the shape of the domains: the majority of the vesicles displayed polygonal-shape domains at pH 7.4; while flower-like/branched shape domains were dominant at pH 5.5. The morphologic alterations induced by C16-GlcCer, such as the tubules, also exhibit different properties depending on the environment: at neutral pH they are highly flexible (Figures 8AIV and S4III, Supporting Information), while at acidic pH the structures are rigid (Figures 8AVIII and S4VII, Supporting Information). The latter structures resemble those already described for very-long acyl chain ceramides[18, 26] (Figure 8B II, 8BIII, 8BVI and 8BVII). The microscopy results further confirm that C16-GlcCer gel domains are sensitive to membrane pH.

pH acidification had no major effect on the organization of GUVs containing C16-Cer (Figure 8B I and 8BV) or C16-SM (Figure 8B IV and 8BVIII), which displayed flower-like and branched shape domains, respectively, regardless of pH. GUVs containing C24:1-Cer displayed a very heterogeneous population at both pHs, precluding any correlation between membrane environment and changes occurring in the shape/size of the domains and membrane morphology. Nevertheless, it should be stressed that strong morphological alterations including the formation of rigid, needle-like tubules, were observed at both pHs. In addition, the domains formed by C24:1-Cer did not completely exclude Rho-DOPE, as shown by the slight fluorescence intensity arising from the darker regions of the vesicles (e.g., Figure 8BII and 8BIII), and which reflects the looser packing of C24:1-Cer-gel domains compared to those formed by C16 -GlcCer or -Cer [18, 26].
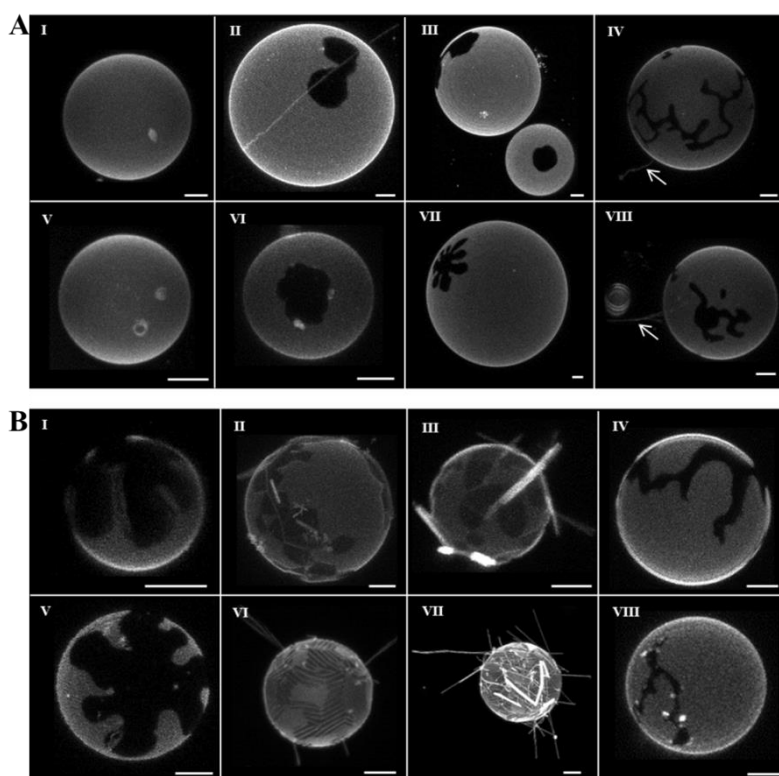
Figure 8 - Characterization of the effect of pH by confocal fluorescence microscopy. 3D projection images from 0.4 µm confocal slices of GUVs labeled with Rho-DOPE. (A) Images are shown for vesicles containing POPC with (I, V) 10, (II, VI) 20 and (III,IV,VII,VIIi) 30 mol% C16-GlcCer. Tubule-like structures (white arrows in IV and VIII) were observed in mixtures containing C16-GlcCer ≥ 30 mol%. (B) Images are shown for vesicles containing POPC with 30 mol% of (I, V) C16-Cer, (II, III, VI, VII) C24:1-Cer and (IV, VIII) C16-SM. All measurements were performed at 24 °C at pH 7.4 (I-IV) or 5.5 (V-VIII). Scale bar, 5 µm.

5 Discussion

5.1 POPC/C16-GlcCer Mixtures

Our studies, performed using multiple biophysical methods, demonstrated that GlcCer-induced changes on membrane biophysical properties are pH dependent. Acidification resulted in alterations of the organization of GlcCer-enriched gel domains, at the level of both the lipid packing and the extent of the gel phase, as observed by the variation of the photophysical parameters of the gel-phase probe t-PnA and confirmed by confocal microscopy and monolayer studies. The effect of pH on the properties of POPC or POPC mixed with the other SLs was less pronounced, suggesting that changes in pH might be

mainly affecting the link between ceramide and the sugar residue and/or the hydrogen bonds between glucose and the surrounding environment. Alterations in the intra- and intermolecular H-bonding network could alter the orientation of the glucose moiety at the membrane interface, with a strong impact in the order of the hydrophobic core of the lipid mixtures[38383838]. In addition, since changes in pH were shown to have a major impact on the gel phase, acidification might mainly affect the van der Waals and hydrogen-bond interactions that maintain the gel phase in such a tightly packed state. These interactions, particularly the H-bonding network, do not exist to such a high extent in the fluid phase, and therefore, this phase is less affected by pH. This is supported by confocal microscopy, where pH-induced alterations were mainly noticed on gel domains and at the interface between the gel and the fluid phase. Despite the intrinsic heterogeneity of the GUV population, the majority of the domains observed at pH 7.4 had a polygonal shape[15], while at pH 5.5 'flower-like' and 'dendritic-like' domains were dominant. The equilibrium shape of the domains is a result of three major forces: line tension at the domain boundary, dipolar repulsion inside the domains, and domain-domain interactions[39]. Alteration of any of these factors results in domain shape changes. Moreover, alterations in the hydrogen bonds between the glucose headgroup and the neighbor lipids and/or the surrounding medium, as it might occur in response to pH changes, might also influence the shape of the gel domains. This is further supported by data showing that round-like/polygonal domains have a tighter packing of hydrophobic chains and higher immiscibility in the fluid phase due to efficient hydrogen bonding, which promotes a lower line tension at the domain boundaries. In contrast, in the more complex branched, networks or 'flower-like' domains, the dipole-dipole repulsion forces are dominant[40, 41]. Accordingly, domain shape transformations could also be promoted by alterations in the equilibrium of glucose (de)protonation. Glucose has a $pK_a \sim 12$[42], meaning that glucose is mainly in its acidic state at both environments. However, in an acidic environment with more hydrogen ions in solution, the equilibrium is shifted to the acid state and a protonation of the hydroxyl group might occur[42]. Protonation would also affect dipole-dipole repulsions and so change the shape of the gel domains, but it would also contribute to a decrease in the extent of gel-phase formation and to more expanded monolayers exhibiting larger miscibility with POPC.

Our results demonstrated that pH also affects the morphology of the vesicles. Flexible-like tubular structures were observed in mixtures containing ≥ 30 mol% C16-GlcCer at pH 7.4 [15]. Identical tubular structures were visualized at pH 5.5, although, these appear to be stiffer. Several factors can contribute to GlcCer-tubule formation, such as the chirality of this lipid (which increases bending force), the presence of a tilted phase (to better accommodate the glucose and the tension created by the H-bonding network) and the possibility, similar to GalCer, that the nature of the tubules is dependent on the acyl chain length of the lipid and of the environment, such as temperature and degree of hydration[43,44]. This together with the fact that GlcCer can form a large hydrogen-bond network with the solvent, demonstrate that GlcCer-containing membranes might be very sensitive to alterations in the environment. As mentioned above, these alterations could shift the hydrogen-bond network, affecting lipid organization in the bilayers and consequently promoting formation of more stiffer tubules at more acidic pH.[45]

5.2 POPC/Sphingomyelin and POPC/Ceramide mixtures

Even though alterations in pH resulted in stronger changes on the organization/properties of membranes containing GlcCer, changes in the properties of C24:1-Cer-containing membranes were also observed upon acidification. Similarly to C16-GlcCer, C24:1-Cer formed a more expanded monolayer in an acidic environment and C24:1-Cer-enriched gel domains were less packed at pH 5.5 compared to pH 7.4. However, larger molar fractions of C24:1-Cer were required in order to detect significant changes on membrane properties, particularly by fluorescence spectroscopy studies. This might be related to the properties of the C24:1-Cer gel phase, which, according to the binary phase diagram for this mixture (POPC/C24:1-Cer)[26], mainly consists of a partially interdigitated gel phase that displays a looser packing compared to a C16-GlcCer gel[15]. Accordingly, the interactions among C24:1-Cer molecules might not be as strong as those between C16-GlcCer molecules and therefore, much less affected by changes in pH. In monolayers, chain interdigitation is not possible, however, the phenomenon observed in monolayers that in bilayers enables interdigitation, is the 'mushroom' to 'brush' transition[46]. According to this theory, at low pressure and SL content, the long acyl chains of C24:1-Cer protrude from the monolayer acquiring a mushroom state. Upon increasing

the pressure and levels of C24:1-Cer, the protruding acyl chains are nearer and attracted toward each other by van der Waal's interactions, adopting a more condensed regime similar to a brush[46]. A change in membrane environment, such as acidification, might affect the interactions between the acyl chains of C24:1-Cer, which would result in differences in the condensation of the monolayers at pH 7.4 and 5.5, as observed for monolayers containing 30 mol% of C24:1-Cer. In a bilayer, the interactions among the acyl chains would be much less affected by changes in pH.

The packing properties of POPC/C16-SM mixtures also changed upon acidification. Studies performed with the gel phase probe *t*-PnA suggest that the gel phase is more tightly packed at neutral pH. However, monolayer studies suggest the opposite: C16-SM monolayer and mixed monolayers are more condensed and less elastic at acidic pH. These apparently contradictory results might be explained based on the preferential interactions that occur between the lipids in the monolayers. Determination of the excess free energy of mixing (G^E) shows that upon acidification there is a change from repulsive to attractive forces among the components. These attractive forces contribute to an overall tighter packing of the lipids in the monolayer, while the repulsive forces contribute to a less condensed monolayer, as observed at neutral pH[35]. From these monolayer studies it is, however, not possible to conclude anything about the packing properties of the gel phase. The overall attractive forces might be enhanced at lower pH, but the packing of the gel phase might be higher at neutral pH as suggested by spectroscopy. Interestingly, the thermotropic studies and spectroscopic studies with probes that do not have a strong preference toward the gel phase suggest that the overall packing of POPC/C16-SM mixtures is not strongly affected by the pH. This indicates that in monolayers changes in pH might mainly affect the overall interactions between the lipids and the subphase, as previously suggested [35].

From our results it can be concluded that acidification has a major effect on the interactions between the lipids forming the gel phase, probably at the level of the H-bonding network. However, the highly ordered C16-Cer-enriched gel domains seem to be unaffected by these changes. Indeed, none of the techniques used in the present study were able to detect alterations on the properties of POPC/C16-Cer mixtures upon change in pH. It can thus be inferred that the interactions that take place among C16-Cer molecules are stronger and more stable to environmental changes. From a biological

perspective this is an interesting finding since it implies that highly ordered ceramide-enriched domains under different physiological conditions could serve as signaling platforms in the PM as well as in intracellular membranes.

6 Conclusions and Biological Implication

This study highlights the different biophysical properties of SLs with small structural changes, and the effect of pH on their properties. It demonstrates that lipid packing is altered in response to pH changes, particularly in C16-GlcCer-containing membranes. GlcCer can be found both in the PM and in the lysosome and the sensitivity to the environment could be an inherent mechanism to modulate the packing properties of this lipid according to its function in each organelle[6, 47, 48]. Since GlcCer is a neutral lipid, the notion that it could be sensitive to pH was unexpected; we suggest that the increase in the protonation of the solvent may perturb the hydrogen bonds between glucose and the aqueous environment and change the hydration of the glucose headgroup, potentially leading to alterations in the membrane order. We suggest that at pH 7.4, a pH typical of the plasma membrane, GlcCer packs tighter with other GSLs or other lipids, as in lipid rafts, conferring higher stability to the membrane domains. This packing would be disturbed during the endolysosomal pathway, where the pH drop would affect the GlcCer hydrogen bonds with the aqueous medium and/or with the other lipids.

Another important scenario is Gaucher Disease, where accumulation of GlcCer within the lysosome is observed [49]. The increased GlcCer levels in GD might potentiate formation of tightly packed GlcCer-gel domains in the lysosomal membrane. This would result in changes on the overall properties of the membrane, which would not occur under normal physiological conditions. These might compromise the activity of important proteins, such as the V-ATPase [9, 50] and globally contribute to pathology development.

An optimal lipid selection confers optimal rigidity and elasticity to promote a proper rheology to the concerned membrane function; this allows the proteins to fold properly and offers an adequate matrix for the lateral movement of the proteins along the membrane[51]. The effect of a decrease in pH on the biophysical behavior of most of the lipids in this study demonstrates that this parameter can be crucial for global lipid organization and consequently on protein sorting and trafficking.

In conclusion, the biophysical properties observed either when changing the chemical structure or mediated by acidification of the pH might be involved in modulating the different biological roles of SLs in different organelles. Moreover, the biophysical properties of GlcCer, together with evidence that this lipid is directly involved in pH regulation, might be crucial in understanding its regulatory roles in cell biology.

7 Acknowledgments

8 References

1.   Sillence, D.; Platt, F. Glycosphingolipids in endocytic membrane transport. Semin Cell Dev Biol 2004, 15 (4), 409-416.

2.   Funato, K.; Riezman, H. Vesicular and nonvesicular transport of ceramide from ER to the Golgi apparatus in yeast. J Cell Biol 2001, 155 (6), 949-960.

3.   Futerman, A. Intracellular trafficking of sphingolipids: Relationship to biosynthesis. Biochim Biophys Acta 2006, 1758 (12), 1885-1892.

4.   Halter, D.; Neumann, S.; van Dijk, S. M.; Wolthoorn, J.; de Maziere, A. M.; Vieira, O. V.; Mattjus, P.; Klumperman, J.; van Meer, G.; Sprong, H. Pre- and post-Golgi translocation of glucosylceramide in glycosphingolipid synthesis. J Cell Biol 2007, 179 (1), 101-115.

5.   Grabe, M.; Oster, G. Regulation of Organelle Acidity. J Gen Physiol 2001, 117 (4), 329-44.

6.   Paroutis, P. The pH of the Secretory Pathway: Measurement, Determinants, and Regulation. Physiology 2004, 19 (4), 207-215.

7.   Futai, M.; Oka, T.; Sun-Wada, G.; Moriyama, Y.; Kanazawa, H.; Wada, Y. Luminal Acidification of Diverse Organelles by V-ATPase in Animal Cells. J Exp Biol 2000, 203, 107-116.

8.   Spiegel, S.; Milstien, S. Sphingosine-1-phosphate: an enigmatic signalling lipid. Nat Rev Mol Cell Biol 2003, 4 (5), 397-407.

9.   Sillence, D. J. Glucosylceramide modulates endolysosomal pH in Gaucher disease. Mol Gen Metab 2013.

10.   Yamaguchi, M.; Kasamo, K. Modulation of Proton Pumping across Proteoliposome Membrane Reconstituted with Tonoplast H+-ATPase from Cultured Rice (Oryza sativa L. var. Boro) Cells Acyl Steryl Glucoside and Steryl Glucoside. Plant Cell Physiology 2002, 43 (7), 816-822.

11.   Yamaguchi, M.; Kasamo, K. Modulation in the Activity of Purified Tonoplast H+-ATPase by Tonoplast Glycolipids Prepared From Cultured Rice (Oryza sativa L. var. Boro) Cells. Plant Cell Physiology 2001, 42 (5), 516-523.

12.   van der Poel, S.; Wolthoorn, J.; van den Heuvel, D.; Egmond, M.; Groux-Degroote, S.; Neumann, S.; Gerritsen, H.; van Meer, G.; Sprong, H. Hyperacidification of Trans-Golgi Network and Endo/Lysosomes in Melanocytes by Glucosylceramide-Dependent V-ATPase Activity. Traffic 2011, 12 (11), 1634-1647.

13.   Joly, E.; Lafourcade, C.; Sobo, K.; Kieffer-Jaquinod, S.; Garin, J.; van der Goot, F. G. Regulation of the V-ATPase along the Endocytic Pathway Occurs through Reversible Subunit Association and Membrane Localization. PLoS ONE 2008, 3 (7), e2758.

14.   Vruchte, D. t. Accumulation of Glycosphingolipids in Niemann-Pick C Disease Disrupts Endosomal Transport. J Biol Chem 2004, 279 (25), 26167-26175.

15.   Varela, A. R. P.; Gonçalves da Silva, A. M. P. S.; Fedorov, A.; Futerman, A. H.; Prieto, M.; Silva, L. C. Effect of glucosylceramide on the biophysical properties of fluid membranes. Biochim Biophys Acta 2013, 1828 (3), 1122-1130.

16.   Liu, Y.-Y.; Han, T.-Y.; Giuliano, A. E.; Cabot, M. C. Expression of Glucosylceramide Synthase, Converting Ceramide to Glucosylceramide, Confers Adriamycin Resistance in Human Breast Cancer Cells. J Biol Chem 1999, 274 (2), 1140-1146.

17.   Silva, L.; De Almeida, R. F. M.; Fedorov, A.; Matos, A. P. A.; Prieto, M. Ceramide-platform formation and -induced biophysical changes in a fluid phospholipid membrane. Mol Membr Biol 2006, 23 (2), 137-148.

18.   Pinto, S. N.; Silva, L. C.; Futerman, A. H.; Prieto, M. Effect of ceramide structure on membrane biophysical properties: The role of acyl chain length and unsaturation. Biochim Biophys Acta 2011, 1808 (11), 2753-2760.

19.   Johnny, S.; Liana, C. S.; Anthony, H. F. Ceramide-containing membranes: the interface between biophysics and biology. Trends Glycosci Glyc 2008, 20 (116), 297-313.

20.   Li, X.-M.; Smaby, J. M.; Momsen, M. M.; Brockman, H. L.; Brown, R. E. Sphingomyelin Interfacial Behavior: The Impact of Changing Acyl Chain Composition. Biophys J 2000, 78 (4), 1921-1931.

21.   Deguchi, H.; Fernández, J.; Pabinger, I.; Heit, J. A.; Griffin, J. H. Plasma glucosylceramide deficiency as potential risk factor for venous thrombosis and modulator of anticoagulant protein C pathway. Blood 2001, 97 (7), 1907-1914.

22.   Lakowicz, J. R. 3rd ed.; Springer: New York, 2006.

23.   Birch, D. S.; Imhof, R. Time-Domain Fluorescence Spectroscopy Using Time-Correlated Single-Photon Counting. In Topics in Fluorescence Spectroscopy, Lakowicz, J., Ed.; Springer US, 2002; Vol. 1, pp 1-95.

24.   de Almeida, R. F. M.; Fedorov, A.; Prieto, M. SPhingomyelin/Phosphatidylcholine/Cholesterol Phase Diagram: Boundaries and Composition of Lipid Rafts. Biophys J 2003, 85, 2406-2416.

25.   de Almeida, R. F. M.; Borst, J.; Fedorov, A.; Prieto, M.; Visser, A. J. W. G. Complexity of Lipid Domains and Rafts in Giant Unilamellar Vesicles Revealed by Combining Imaging and Microscopic and Macroscopic Time-Resolved Fluorescence. Biophys J 2007, 93 (2), 539-553.

26.   Pinto, S. N.; Silva, L. C.; de Almeida, R. F. M.; Prieto, M. Membrane Domain Formation, Interdigitation, and Morphological Alterations Induced by the Very Long Chain Asymmetric C24:1 Ceramide. Biophys J 2008, 95 (6), 2867-2879.

27.   Haugland, R. P.; Spence, M. T.; Johnson, I. D. Handbook of Fluorescent Probes and Research Chemicals. 6th ed.; Molecular Probes: Eugene OR, 1996.

28.   Sarmento, M. J.; Prieto, M.; Fernandes, F. Reorganization of lipid domain distribution in giant unilamellar vesicles upon immobilization with different membrane tethers. Biochim Biophys Acta 2012, 1818 (11), 2605-2615.

29.   Gonçalves da Silva, A. M.; Romão, R. I. S. Mixed monolayers involving DPPC, DODAB and oleic acid and their interaction with nicotinic acid at the air–water interface. Chem Phys Lipids 2005, 137 (1-2), 62-76.

30.   Silva, L. C.; de Almeida, R. F. M.; Castro, B. M.; Fedorov, A.; Prieto, M. Ceramide-Domain Formation and Collapse in Lipid Rafts: Membrane Reorganization by an Apoptotic Lipid. Biophys J 2007, 92 (2), 502-516.

31.   Castro, B. M.; de Almeida, R. F. M.; Silva, L. C.; Fedorov, A.; Prieto, M. Formation of Ceramide/Sphingomyelin Gel Domains in the Presence of an Unsaturated Phospholipid: A Quantitative Multiprobe Approach. Biophys J 2007, 93 (5), 1639-1650.

32.   Sklar, L. A.; Dratz, E. A. Analysis of membrane bilayer asymmetry using parinaric acid fluorescent probes. FEBS Lett 1980, 118 (2), 308-310.

33.   Pinto, S. N.; Fernandes, F.; Fedorov, A.; Futerman, A. H.; Silva, L. C.; Prieto, M. A combined fluorescence spectroscopy, confocal and 2-photon microscopy approach to re-evaluate the properties of sphingolipid domains. Biochim Biophys Acta 2013, 1828, 2099-2110.

34.   de Almeida, R. F. M.; Loura, L. M. S.; Fedorov, A.; Prieto, M. Lipid Rafts have Different Sizes Depending on Membrane Composition: A Time-resolved Fluorescence Resonance Energy Transfer Study. J Mol Biol 2005, 346, 1109-1120.

35.   Petelska, A. D.; Naumowicz, M.; Figaszewski, Z. A. Influence of pH on Sphingomyelin Monolayer at Air/Aqueous Solution Interface. Langmuir 2012, 28 (37), 13331-13335.

36.   Smaby, J. M.; Kulkarni, V. S.; Momsen, M.; Brown, R. E. The Interfacial ELastic Packing Interactions of Galactosylceramides, Sphingomyelins, and Phosphatidylcholines. Biophys J 1996, 70, 886-877.

37.   Harland, C. W.; Bradley, M. J.; Parthasarathy, R. Phospholipid bilayers are viscoelastic. Proc Natl Acad Sci U S A 2010, 107, 19146-19150.

38.   Nyholm, P.-G.; Pascher, I. Orientation of the Saccharide Chains of Glycolipids at the membrane Surface: Conformational Analysis of the Glucose-Ceramide and the Glucose-Glyceride Linkages Using Molecular Mechanics (MM3). Biochemistry 1993, 32, 1225-1234.

39.   Vega Mercado, F.; Maggio, B.; Wilke, N. Modulation of the domain topography of biphasic monolayers of stearic acid and dimyristoyl phosphatidylcholine. Chem Phys Lipids 2012, 165 (2), 232-237.

40.   Holopainen, J. M.; Brockman, H. L.; Brown, R. E.; Kinnunen, P. K. J. Interfacial Interactions of Ceramide with Dimyristoylphosphatidylcholine: Impact of the N-Acyl Chain. Biophys J 2001, 80, 765-775.

41.   Perkovic´, S.; McConnell, H. M. Cloverleaf Monolayer Domains. J Phys Chem B 1997, 101, 381-388.

42.   Collins, P.; Ferrier, R. Monosaccharides. Jonh Wiley & Sons: Chichester, UK, 1995, p 41.

43.   Kulkarni, V. S.; Boggs, J. M.; Brown, R. E. Modulation of Nanotube Formation by Structural Modifications of Sphingolipids. Biophys J 1999, 77, 319-330.

44.   Kulkarni, V. S.; Anderson, W. H.; Brown, R. E. Bilayer Nanotubes and Helical Ribbons Formed by Hydrated Galactosylceramides: Acyl Chain and Headgroup Effects. Biophys J 1995, 69, 1976-1986.

45.   Mannock, D. A.; Harper, P. E.; Gruner, S. M.; McElhaney, R. N. The physical properties of glycosyl diacylglycerols. Calorimetric, X-ray diffraction and Fourier transform spectroscopic studies of a homologous series of 1,2-di-O-acyl-3-O-(b-d-galactopyranosyl)-sn-glycerols. Chem Phys Lipids 2001, 111 (2), 139-161.

46.   Holopainen, J. M.; Brockman, H. L.; Brown, R. B.; Kinnunen, P. K. J. Interfacial Interactions of Ceramide with Dimyristoylphosphatidylcholine: Impact of the N-Acyl Chain. Biophys J 2001, 80, 765-775.

47.   Messner, M. C.; Cabot, M. C. Glucosylceramide in humans. Adv Exp Med Biol 2010, 688, 154-64.

48.   van Meer, G.; Wolthoorn, J.; Degroote, S. The fate and function of glycosphingolipid glucosylceramide. Phil Trans R Soc B 2003, 358 (1433), 869-873.

49.   Grabowski, G. A. Phenotype, diagnosis, and treatment of Gaucher's disease. Lancet 2008, 372 (9645), 1263-1271.

50.   M., Y.; Kasamo, K. Modulation in the Activity of Purified Tonoplast H+- ATPase by Tonoplast Glycolipids Prepared from Cultured Rice (Oryza sativa L. var. Boro) Cells. Plant Cell Physiology 2001, 42 (5), 516-523.

51.   Espinosaa, G.; López-Monterob, I.; Monroya, F.; Langevina, D. Shear rheology of lipid monolayers and insights on membrane fluidity. Proc Natl Acad Sci U S A 2011, 108 (15), 6008-6013.

9 Supporting Material for: Influence of intracellular membrane pH on sphingolipid organization and membrane biophysical properties
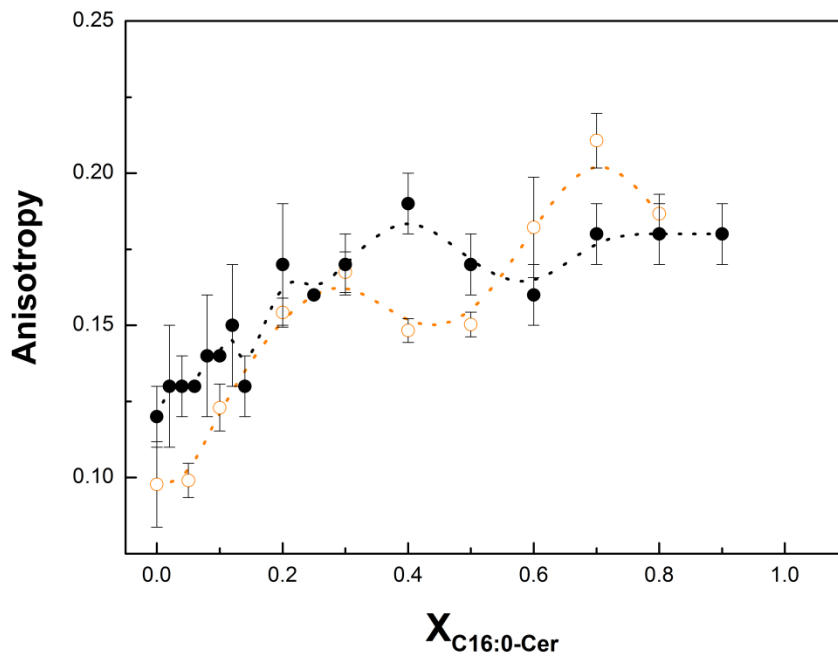
Figure S1 - Steady-state fluorescence anisotropy of DPH in MLVs composed by increasing molar fractions of C16-Cer in POPC.
The values were measured at (black) pH 7.4 or at (orange) pH 5.5. Values are means ± SD of at least 3 independent experiments.
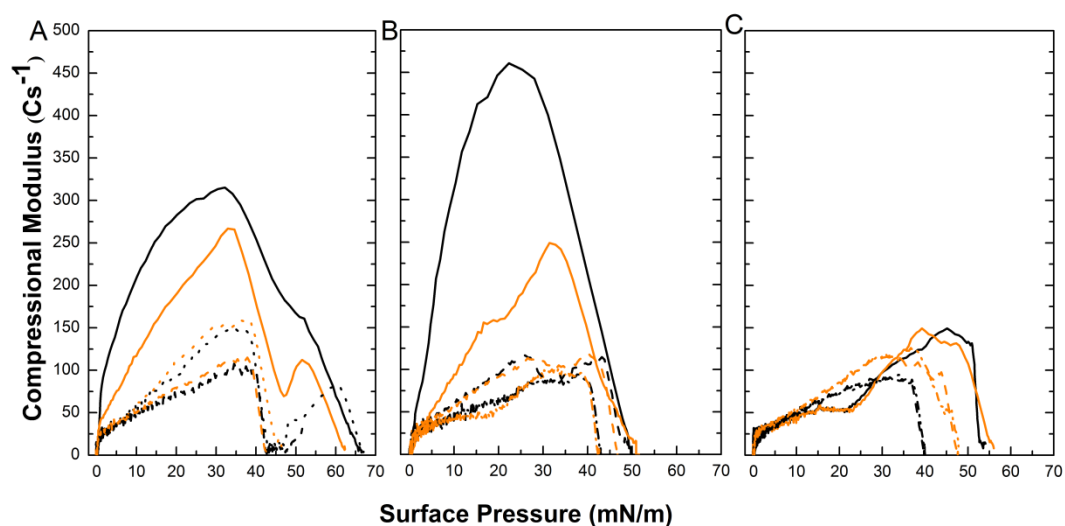
Figure S2- POPC / C16-GlcCer, -C16-Cer, -C16-SM and C24:1-Cer mixed monolayers at pH 7.4 and 5.5.

(A-C) Isothermal compressional modulus as a function of surface pressure in (A) (—) C16-GlcCer and POPC with (---) 30 and (···) 70 mol% of C16-GlcCer. (B) (—) C24:1-Cer, (·-··-··) POPC and (---) POPC with 30 mol% C24:1-Cer. (C) (—) C16-SM and POPC with (-···--···-) 10 and (---) 30 mol% of SM. Measurements were made at (black) pH 7.4 and (orange) 5.5.
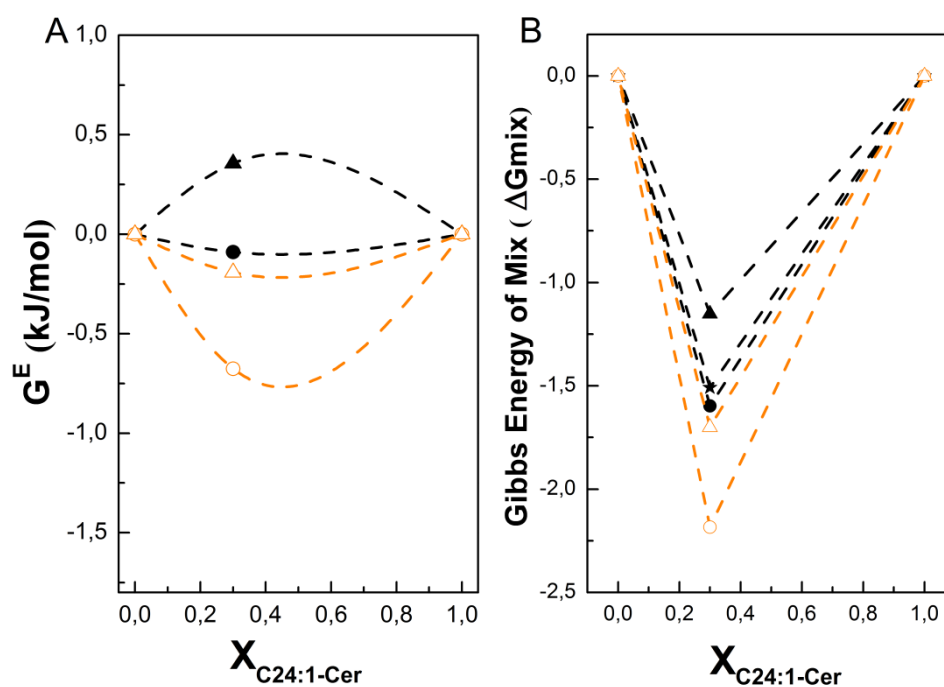
Figure S3 – Characterization of C24:1-Cer mixed monolayers

POPC/C24:1-Cer (A) excess free energy of mixing and (B) free energy of mixing at (●, ○) 20 and (▲△) 40 mN/m, (★) ideal Gibbs energy of mixing. Values were determined according to Eq. 4.The full black symbols represent the pH7.4, and the empty orange symbols the pH5.5.
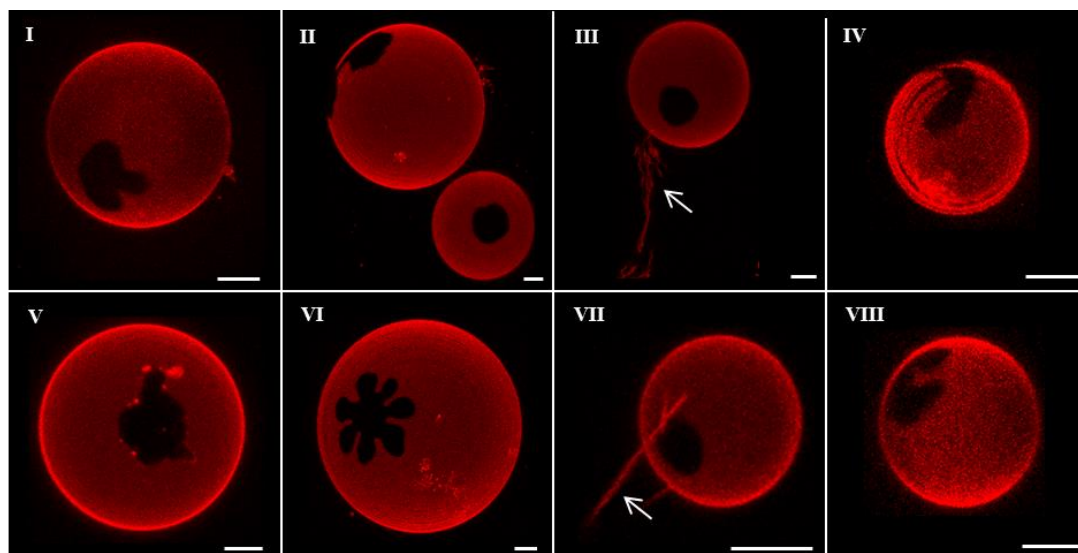
Figure S4 - Confocal fluorescence microscopy of POPC/C16-GlcCer mixtures.
3D projection images from 0.4 μm confocal slices of GUVs labeled with (red) Rho-DOPE. The GUVs contain (I, V) 20, (II, III, VI, VII) 30 and (IV, VIII) 40 mol% of C16-GlcCer.The vesicles were prepared in a neutral (I-IV) or an acidic (V-VIII) environment. Scale bar, 5 μm.

Chapter IV

Glucosylceramide reorganizes cholesterol-containing domains in a fluid phospholipid membrane

Chapter IV

Glucosylceramide reorganizes cholesterol-containing domains in a fluid phospholipid membrane

Ana R.P. Varela,[1,2,3] André Sá Couto,[1] Aleksander Fedorov,[2] Anthony H. Futerman,[3] Manuel Prieto,[2] and Liana C. Silva[1],*

[1] **iMed.ULisboa** – Research Institute for Medicines, Faculdade de Farmácia, Universidade de Lisboa, Av. Prof. Gama Pinto, 1649-003 Lisboa, Portugal

[2] **Centro de Química-Física Molecular and Institute of Nanoscience and Nanotechnology**, Instituto Superior Técnico, Universidade de Lisboa, Av. Rovisco Pais, 1049-001 Lisboa, Portugal

[3] **Department of Biological Chemistry**, Weizmann Institute of Science, Rehovot 76100, Israel

*Corresponding author:

Liana C. Silva, Research Institute for Medicines (iMed.ULisboa), Faculdade de Farmácia, Universidade de Lisboa, Av. Professor Gama Pinto, 1649-003 Lisbon - Portugal Tel: + 351 217 946 400 (ext 14204), Fax: + 351 217 937 703, Email:lianacsilva@ff.ulisboa.pt

Keywords: fluorescence spectroscopy and microscopy, gel domains, sphingolipids, ternary phase diagram

Running Title: Glucosylceramide/Cholesterol interplay

Chapter IV- Glucosylceramide reorganizes cholesterol-containing domains in a fluid phospholipid membrane

1 Abstract

Glucosylceramide (GlcCer), one of the simplest glycosphingolipids, plays key roles in physiology and pathophysiology. It has been suggested that GlcCer modulates cellular events by forming specialized domains. The present study investigates the interplay between GlcCer and cholesterol (Chol), an important lipid involved in the formation of liquid-ordered (l_o) phases. Using fluorescence microscopy and spectroscopy, dynamic and electrophoretic light scattering, we characterized the interaction between these lipids in different pH environments. A quantitative description of the phase behavior of the ternary unsaturated phospholipid/Chol/GlcCer mixture is presented. The results demonstrate coexistence between lo/liquid-disordered (l_d) phases. However, the extent of l_o/l_d phase separation is sparse, mainly due to the ability of GlcCer to segregate into tightly packed gel domains. As a result, the phase diagram of these mixtures is characterized by an extensive 3-phase coexistence region of fluid (l_d-phospholipid-enriched)/l_o (Chol-enriched)/gel (GlcCer-enriched). Moreover, the results showed that upon acidification GlcCer solubility in the lo phase is increased, leading to a larger l_o/l_d coexistence region. Quantitative analyses allowed determination of the differences in the composition of the phases at neutral and acidic pH. These results predict the impact of GlcCer on domain formation and membrane organization in complex biological membranes, and provide the background to unravel the relationship of the biophysical properties of GlcCer and its biological action.

2 Introduction

Membrane lipids play an active role in diverse cellular events, including cell growth, differentiation and migration [1, 2]. Sphingolipids (SLs) are an important lipid class and consists of a number of bioactive lipid species, ranging from sphingoid backbones to more complex glycosphingolipids (GSLs) [3]. Even though the existence of lipid domains is still highly controversial, several studies have linked the bioactive roles of SLs to their ability to form specialized domains that, due to their distinct lipid and protein composition, display different biophysical properties. The most common examples are lipid raft domains [4] and ceramide-platforms [5]. While ceramide-platforms display properties typical of the gel phase [6, 7], lipid raft domains are described as l_o regions – an intermediate state between the gel (or solid ordered, s_o) and the fluid (liquid-disordered, l_d) phases. Accordingly, the lipids in the l_o phase have a high degree of conformational order of the acyl chains, similar to the gel phase, but a fast translational mobility, as in the fluid phase [8]. Favorable interactions between sphingolipids (SLs) and cholesterol (Chol) are one of the underlying principles of lipid rafts [4].

GSLs are an important subgroup of SLs that have also been implicated in membrane domain formation [9, 10]. Structurally, these lipids consist of a ceramide backbone, linked via an ester bond to one or more sugar residues. GSLs are normally found in the outer leaflet of the plasma membrane where they exert some of their biological roles, such as cell-cell communication and act as receptors for pathogens [11]. GlcCer, one of the simplest GSLs, is present in different concentrations in mammalian tissues, reaching up to 95.34 ±1.77 pmol/mg (~ 0,0069% of total lipids) in mouse spleen [12]. In comparison to other important membrane lipids GlcCer levels are quite low. For example, it was reported that Cer levels in the spleen are normally about 148.08 ±14.01 pmol/mg, (~0.0082% of total lipids)[12], while SM levels vary from 2 to 15 % of the total lipids, depending on the analyzed tissue [13]. GlcCer is an important regulator of a number of cellular events, including calcium homeostasis [14] and endocytic trafficking [15]. Even though much evidence links the physiological roles of this lipid to its biophysical properties, only a few studies have addressed the impact of GlcCer on membrane properties. We and others have previously reported that GlcCer causes significant changes on the biophysical properties of fluid model membranes, such as an increase in membrane order and formation of highly-ordered gel domains [16, 17, 18, 19]. These alterations are related to the high melting

temperature (T_m) of this lipid [20], its small uncharged headgroup and its ability to function both as a donor and an acceptor for H-bond formation, which together contribute to its low miscibility in fluid phases and segregation into domains with a high packing density [17, 18]. Moreover, GlcCer promotes strong morphological alterations in vesicles, driving tubular structure formation [16]. These structural alterations are enhanced upon acidification of the membrane environment, even though the ability of GlcCer to form tightly-packed gel domains is decreased [21]. However, little is known about the effect of this lipid on more complex membrane mixtures. Studies performed in membranes containing cholesterol (Chol) or Chol/sphingomyelin (SM) suggested that GlcCer has a low tendency to associate with sterol-enriched domains[18, 22]. However, in resemblance to what has been described for ceramide [23], such interplay might depend on the content of each of the lipids. To further elucidate this issue, we have now performed a thorough study that provides the framework to understand the interplay between GlcCer and Chol under different conditions. Thus, we now investigate these interactions using mixtures composed of different GlcCer/Chol molar ratios in a fluid phospholipid matrix. The biophysical properties and phase behavior of ternary POPC (1-palmitoyl-2-oleoyl-*sn*-glycero-3-phosphocholine)/Chol/GlcCer mixtures were characterized using an array of biophysical methodologies. Partial ternary phase diagrams were determined to quantitatively describe the phase behavior of these mixtures. The results show that even though GlcCer displays a strong tendency to separate into GlcCer-enriched gel domains, it is also able to interact with Chol and form domains displaying l_o properties. These interactions are more favorable at acidic pH, likely due to the decreased ability of GlcCer to form gel domains [21].

3 Materials and methods

3.1 Materials

POPC, C16-GlcCer (D-glucosyl-ß-1,1' N-palmitoyl-D-erythro-sphingosine), Rho-DOPE (N-rhodamine-dipalmitoylphosphatidylethanolamine) and 1,2-dioleoyl-sn-glycero-3-phosphoethanolamine-N-(biotinyl) (DOPE-biotin) were from Avanti Polar Lipids (Alabaster, AL). *t*-PnA (trans-parinaric acid) and NBD-DPPE (1,2-dipalmitoyl-sn-glycero-3-phosphoethanolamine-N-(7-nitro-2-1,3-benzoxa-diazol-4yl)) were from Molecular

Probes (Leiden, The Netherlands). Chol was from Sigma-Aldrich (St. Louis, MO). All organic solvents were UVASOL grade from Merck (Darmstadt, Germany).

3.2 Methods

3.2.1 Liposome preparation

Multilamellar vesicles (MLV) and large unilamellar vesicles (LUVs) (total lipid concentration of 0.1 mM) containing the lipids and probes were prepared as previously described [24]. The suspension medium used was PBS (10 mM sodium phosphate, 150 mM sodium chloride and 0.1 mM EDTA, pH 7.4) or citrate-phosphate buffer (100mM citric acid and 200 mM sodium phosphate, pH 5.5). The concentration of C16-GlcCer and Chol stock solutions were determined gravimetrically with a high precision balance (Metler Toledo UMT2, Greifensee, Switzerland), while the concentration of POPC stock solution was determined by phosphorus analysis [25]. The concentration of the stock solutions of the probes was determined spectrophotometrically using ε (t-PnA, 299.4nm, ethanol) = 89 x $10 M^{-1}cm^{-1}$[26], ε(NBD, 458 nm, chloroform) =21 x 10^3 $M^{-1}cm^{-1}$[27] and ε(Rho-DOPE, 559 nm, chloroform) = 95 x 10^3 $M^{-1}cm^{-1}$[27].

3.2.2 Fluorescence Spectroscopy

Fluorescence anisotropy of t-PnA was measured in a SLM Aminco 8100 series 2 spectrofluorimeter with double excitation and emission monochromators MC400 (Rochester, NY). All measurements were performed at room temperature in 0.5 cm × 0.5 cm quartz cuvettes. t-PnA excitation (λ_{exc})/emission (λ_{em}) wavelengths were 320/405 nm and the probe/lipid ratio used was 1/500. A constant temperature was maintained using a Julabo F25 circulating water bath controlled with 0.1ºC precision directly inside the cuvette with a type-K thermocouple (Electrical Electronic Corp., Taipei, Taiwan).

Time-resolved fluorescence measurements with t-PnA were performed by the single photon timing technique with a laser pulse excitation [28] adjusted to λ_{exc}= 305nm (using a secondary laser of Rhodamine 6G [29]) and λ_{em}= 405nm. The experimental decays were analyzed using TRFA software (Scientific Software Technologies Center, Minsk, Belarus).

3.2.3 Confocal Fluorescence Microscopy

Giant unilamellar vesicles (GUVs) were prepared by electroformation[30, 31] using the appropriate lipids, DOPE-biotin (at a biotinylated/non-biotinylated lipid ratio of $1:10^6$), Rho-DOPE and NBD-DPPE (at a probe/lipid ratio of 1:500 and 1:200, respectively). The GUVs were then transferred to 8-well Ibidi® μ-slides that had been previously coated with avidin (at 0.1mg/ml) to improve GUV adhesion to the plate [32]; PBS or citrate-phosphate were then added to create a neutral (7.4) or acidic (5.5) environment, respectively. Confocal fluorescence microscopy was performed using a Leica TCS SP5 (Leica Mycrosystems CMS GmbH, Mannheim, Germany) inverted microscope (DMI6000) with a 63×water (1.2 numerical aperture) apochromatic objective. NBD-DPPE and Rho-DOPE excitation was performed using the 458 nm and 514 nm lines from an Ar^+ laser, respectively. The emission was collected at 480-530 and 530-650 nm, for NBD-DPPE and Rho-DOPE, respectively. Confocal sections of thickness below 0.4 μm were obtained using a galvanometric motor stage. Three-dimensional (3D) projections were obtained using Leica Application Suite-Advanced Fluorescence software.

3.2.4 Dynamic Light Scattering (DLS) Measurements

The mean diameter and polydispersity index (PdI) of the vesicles were determined by dynamic light scattering analysis on a Zetasizer Nano S (Malvern Instruments, UK). Size measurement was made using patented NIBS (non-invasive back scatter) technology. Samples were placed in 12mm square polystyrene cuvettes and then in a chamber maintained at 25ºC. Data analysis was performed by the accompanying software (Zetasizer Software® 7.03) and expressed as an average size or as a size distribution by intensity. The polydispersion index (PdI) for each sample was also calculated using the same software. In each experiment, measurements were performed in triplicate.

3.2.5 Electrophoretic Light scattering measurements (Zeta-potential determination)

Zeta potential (ZP) was determined by electrophoretic mobility on a ZetaSizer Nano Z equipment (Malvern Instruments, UK) using M3-PALS technology. Samples were placed in clear disposable zeta cells and then in a chamber maintained at 25°C. Data analysis was

performed by the accompanying software (Zetasizer Software® 7.03). In each experiment, measurements were performed in triplicate.

4 Results

4.1 POPC/Chol mixtures

We first characterized the effect of pH on the biophysical and surface charge properties of binary POPC/Chol mixtures. Increasing the Chol content of the mixtures lead to an increase in the fluorescence anisotropy of t-PnA (Fig. 1A), consistent with the formation of a Chol-enriched l_o phase [29]. This is further supported by the increase in the mean fluorescence lifetime (Fig. 1B) and long lifetime component of t-PnA fluorescence intensity decay towards values typical of a l_o-phase (Fig. 1C). Both fluorescence anisotropy and lifetime of t-PnA were higher at pH 7.4 (Fig. 1A-C), suggesting that there is a global decrease in the order of the membrane upon acidification.
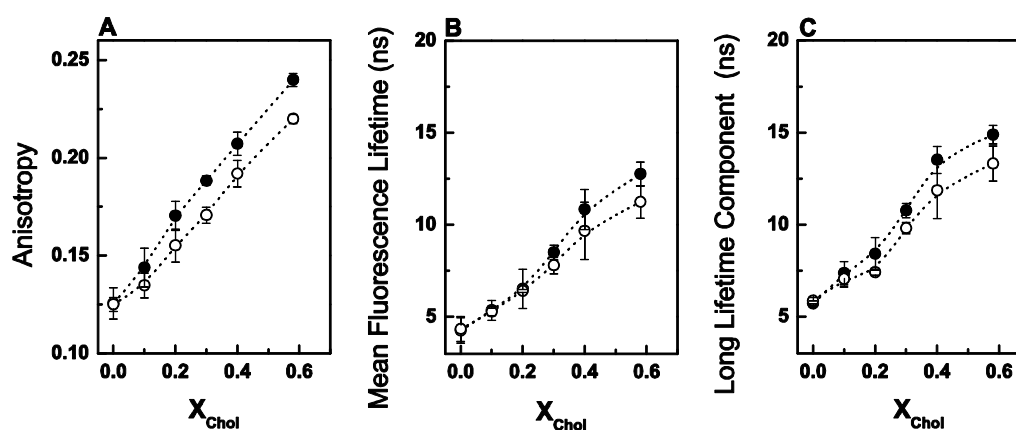
Figure 1 - Biophysical characterization of POPC/Chol mixtures at different pH values.

t-PnA (A) fluorescence anisotropy, (B) mean fluorescence lifetime and (C) long lifetime component of the intensity decay in binary POPC/Chol mixtures. Measurements were performed at neutral (solid symbols) and acidic (open symbols) pHs. Values are means ± SD of at least 3 independent experiments.

Further characterization using DLS revealed that only a slight increase, from ~125 to ~140nm, in the average size of the vesicles is observed upon increasing Chol content (Fig. S1A). Values for acidic conditions are similar, although slightly higher. This is further confirmed by the analysis of scattering intensities and PdI (Fig. S1B-D). Mixtures

containing 40 mol% Chol are the exception, inasmuch as they displayed a tendency to aggregate and/or fuse, as demonstrated by the high scattered light intensity recorded in the range 3.5-6.5μm (Fig. S1B-C). However, this corresponded to only a small percentage of aggregated vesicles (data not shown). Analysis of the zeta potential of the vesicles showed that at neutral pH, a significant decrease in the net surface charge of the vesicles occurred after addition of Chol in the mixtures (Fig. S1E). In contrast, no variation was observed upon acidification of the mixtures (Fig. S1E).

We further characterized the POPC/Chol mixtures by confocal microscopy, using NBD-DPPE and Rho-DOPE as probes for different lipid phases (Fig. S2). NBD-DPPE has a similar partition between the l_d and l_o phases [33], whereas Rho-DOPE is a probe that is typically excluded from l_o phases [30]. NBD-DPPE and Rho-DOPE uniformly labeled the POPC/Chol vesicles, suggesting that no l_d/l_o phase separation occurs in POPC/Chol mixtures (Fig. S2). The difficulty in the identification of POPC/Chol-enriched l_o domain was already reported by us [29], and the existence of phase separation in this lipid mixture is a subject of intensive debate [34, 35, 36, 37]. Nonetheless, a significant number of experimental and theoretical data supports POPC/Chol phase separation into l_d/l_o domains [29, 35, 38, 39, 40, 41]. The factors that might be hindering the identification of the l_o phase by fluorescence microscopy could be: *i*) a domain size smaller than the diffraction limit, in resemblance to l_o domains formed by DPPC/Chol that display a size in the range of 20nm [42]; and/or *ii*) the looser packing of the POPC/Chol-enriched l_o phase, which is less ordered than a Chol/SM-enriched l_o phase [23, 29], enabling the partition of Rho-DOPE into the more ordered fluid phase, preventing the identification of the two phases using the NBD/Rho fluorescent probes pair [43].

Interestingly, our microscopy studies further revealed that POPC/Chol mixtures displayed a higher tendency to aggregate at acidic pH, suggesting that these mixtures are less stable upon acidification. This is not observed at neutral pH probably due to the more negative surface charge of the vesicles which increases electrostatic repulsion, preventing vesicle aggregation.

To study the interplay between Chol and C16-GlcCer, two strategies were employed: *i*) the POPC content of the mixtures was held constant and the ratio between C16-GlcCer and Chol was altered and *ii*) the ratio between POPC and Chol was kept constant and the content of C16-GlcCer was increased.

4.2 Ternary mixtures with different C16-GlcCer/Chol ratios

In the first set of experiments, the POPC concentration was 40 or 70 mol% and the ratio of C16-GlcCer and Chol was varied. The results demonstrated an increase in *t*-PnA fluorescence anisotropy (Fig. 2A), mean fluorescence lifetime (Fig. 2B) and long lifetime component (Fig. 2C) upon increasing C16-GlcCer content, demonstrating the ability of this lipid to increase the packing of the fluid membrane. Membrane order is higher at neutral pH compared to acidic pH, as shown by the higher anisotropy and lifetime at pH 7.4. This is in agreement with our previous study showing that C16-GlcCer forms more tightly packed domains at neutral pH [16].
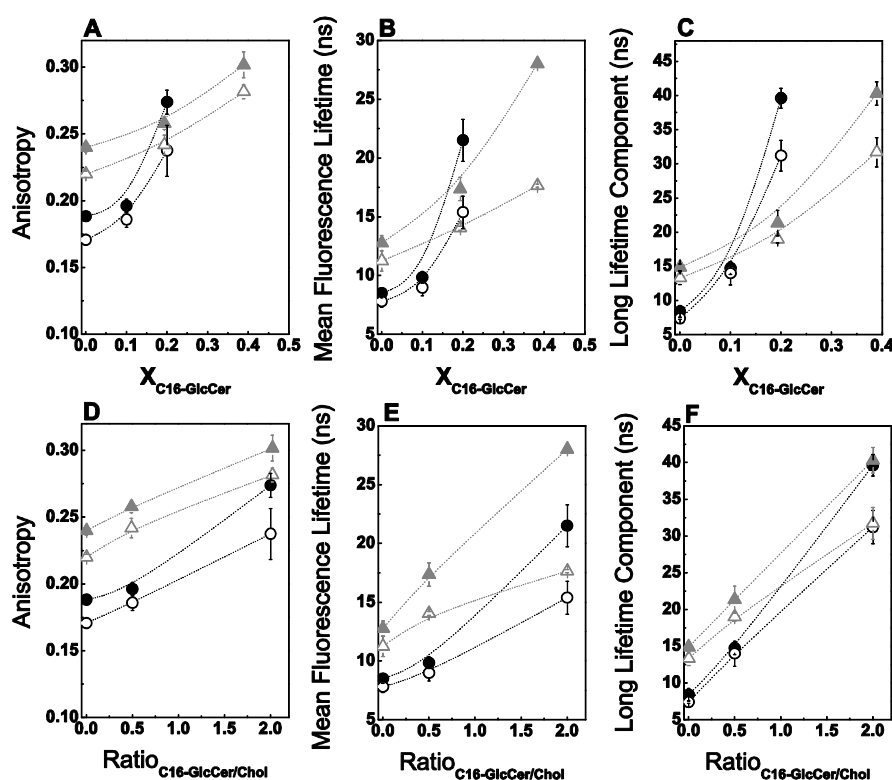
Figure 2 - Biophysical behavior of POPC/Chol/C16-GlcCer mixtures containing a constant POPC composition.

t-PnA (A, D) fluorescence anisotropy, (B, E) mean fluorescence lifetime and (C, F) long component of *t*-PnA intensity decay in ternary POPC/Chol/C16-GlcCer mixtures, as a function of (A-C) C16-GlcCer molar fraction or (D-F) C16-GlcCer-to-Chol ratio. The mixtures contain 40 (triangles) or 70 (circles) mol% of POPC. Measurements were performed at pH 7.4 (solid symbols) and at pH 5.5 (open symbols). Values are means ± SD of at least 3 independent experiments.

To test whether the increase in packing was dependent on C16-GlcCer levels or also modulated by the interplay between C16-GlcCer and Chol, the data were plotted as a function of the GlcCer/Chol ratio (Fig. 2D-F). For the same POPC content, an increase in the ratio of C16-GlcCer/Chol resulted in an almost linear increase in the anisotropy and fluorescence lifetime of *t*-PnA, illustrating that the membrane becomes more ordered as the C16-GlcCer content is increased. Comparison between mixtures containing different POPC content, showed that upon decreasing the POPC content, there was a strong increase in fluorescence anisotropy (Fig. 2D) and mean fluorescence lifetime (Fig. 2E) of *t*-PnA irrespective of the C16-GlcCer/Chol ratio, while the long lifetime component of *t*-PnA was similar for mixtures containing a higher C16-GlcCer/Chol ratio (Fig. 2F). The fluorescence anisotropy and mean fluorescence lifetimes are ensemble average values that depend on the partition properties of the probe towards the different phases present in the lipid mixtures, as well as on the fraction of each phase. In contrast, the long lifetime component provides information about the packing properties of the more ordered phases and is independent on the amount of phase that is present. Therefore, these results suggest that upon decreasing the POPC content, there is an increase in the fraction of the ordered phase (Fig. 2D, E). However, the packing properties of the mixtures are similar (Fig. 2F), suggesting that for these particular mixtures, only the fraction of the ordered phase changes, and therefore should correspond to a tie-line in the phase diagram.

For the ternary mixtures where C16-GlcCer content exceeds that of Chol, both the anisotropy and lifetime of *t*-PnA are high and typical of a C16-GlcCer-enriched gel phase [16]. This is further supported by the detailed analysis of the lifetime components of *t*-PnA fluorescence intensity decay (Fig. S3): the presence of gel-fluid phase separation is characterized by the requirement of a fourth component to describe the fluorescence intensity decay of the probe (Fig. S3)[23, 33]. The lower long lifetime component at pH 5.5 (Fig. 2C, F and Fig. S3B) further supports the evidence that membrane packing is decreased upon acidification [21].

To further characterize these mixtures, fluorescence microscopy studies were performed (Fig. 3). Increasing the C16-GlcCer content of the mixtures drives phase separation into ordered (dark) and disordered (bright) regions. The irregular shape of the domains, together with the exclusion of the probes from those areas suggests that they correspond

to gel-phase domains, in agreement with the spectroscopy data (Fig. 2 and S3). The effect of the pH on the shape and size of the domains was not significant. However, a strong tendency for vesicular fusion and tubule formation was observed at acidic pH in vesicles containing ≥20 mol% of C16-GlcCer (Figs. 3 and S4)
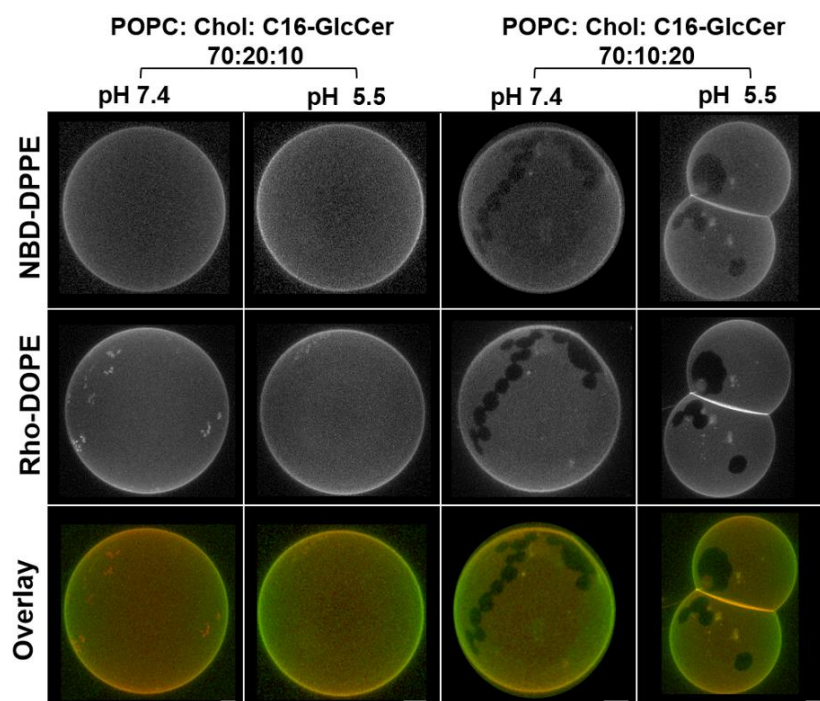
Figure 3 - Confocal fluorescence microscopy of POPC/Chol/C16-GlcCer mixtures containing constant POPC levels.
3D projection images from 0.4 μm confocal slices of POPC/Chol/C16-GlcCer GUVs labelled with NBD-DPPE and Rho-DOPE at neutral and acidic pH. Scale bar, 5 μm.

To better characterize the size heterogeneity of the vesicle population, DLS was performed (Fig. S5). An increase in the mean diameter of the vesicles was observed at acidic pH, particularly for mixtures containing 40% POPC (Fig. S5A). This was accompanied by high scattering intensities (I/I0) recorded in the range of 0.5–5.5 μm (Fig. S5B, C), demonstrating that at acidic pH, the vesicles have a higher tendency to fuse, and/or form tubular structures that result in an increased PdI (Fig. S5D). In addition, the results showed that both the mean diameter (Fig. S5A) and PdI (Fig. S5D) increased upon elevation of C16-GlcCer content in the mixtures, particularly at pH 5.5. To test whether this effect was mainly due to the presence of C16-GlcCer, binary POPC/C16-GlcCer mixtures were also analyzed (Fig. S6). As for the ternary POPC/Chol/C16-GlcCer mixtures,

increasing C16-GlcCer content of the binary POPC/C16-GlcCer mixtures resulted in an increase in the mean diameter of the vesicles (Fig. S6A). However, the shift in the scattering intensity towards a larger vesicle population (Fig. S6B-C) and the elevation of the PdI of the vesicles (Fig. S6D) are higher at pH 5. These results are consistent with an increased ability of the vesicles to alter their shape (Fig. 3) and undergo tubule formation (Fig. S4) upon increasing C16-GlcCer content[16, 21]. Even though the formation of tubules, along with vesicle fusion could affect the hydrodynamic analysis of the vesicles, the results are further confirmed by the microscopy data. The higher instability of both the binary and ternary lipid vesicles at acidic pH might be a consequence of a change in the surface charge upon changing the pH environment (Fig. S5E and S6E). Indeed, at acidic pH the net surface charge is close to neutral, which results in a decrease in the electrostatic repulsive forces between the vesicles, favoring their aggregation.

Since the binary and ternary results exhibit a similar behavior, we suggest that C16-GlcCer is the main element affecting the membrane properties.

4.3 Ternary mixtures with constant POPC/Chol ratio

In the second set of experiments, the ratio between POPC/Chol was kept constant in order to mimic a binary mixture, with 25 and 75% of l_o phase. The composition of these mixtures was determined based on the POPC/Chol phase diagram [29], and correspond to POPC/Chol molar ratios of 79/21and 62/38, respectively. The content of C16-GlcCer in these mixtures was then varied from 0 to 30 mol% and the studies performed at both neutral and acidic pH. In the absence of C16-GlcCer and for mixtures containing 10 mol% C16-GlcCer, t-PnA fluorescence anisotropy (Figs. 4A,B) and mean fluorescence lifetime (Figs. 4C, D) were higher for mixtures where the POPC/Chol ratio mimicked 75% of l_o phase, reflecting the larger l_o phase fraction of these mixtures compared to a POPC/Chol ratio mimicking 25% of the l_o phase [29, 38]. Moreover, both t-PnA fluorescence anisotropy and mean fluorescence lifetime steadily increased upon increasing the content of C16-GlcCer in both sets of ternary mixtures, irrespective of the pH. In addition, the photophysical parameters of t-PnA showed a larger variation in mixtures containing lower Chol content, i.e., mixtures with a POPC/Chol ratio mimicking 25% of l_o phase, demonstrating that C16-GlcCer induces stronger changes in a membrane containing a

larger fraction of l_d phase. No significant differences in the global order of the membrane were detected between the two sets of ternary mixtures when C16-GlcCer was ≥20 mol%, as shown by the similar t-PnA fluorescence anisotropy (Figs. 4A, B) and mean fluorescence lifetime (Figs. 4C, D) values. However, the packing properties of the more ordered phase changed upon varying the lipid composition of the mixtures (Figs. 4E, F). In the absence of C16-GlcCer, the long lifetime component of t-PnA fluorescence intensity decay was similar for the two sets of ternary mixtures, showing identical packing properties of the l_o phase, as would be anticipated for mixtures located within the same tie-line [29]. Upon increasing C16-GlcCer content, the lifetime component of t-PnA became longer and increased to a higher extent for those mixtures containing lower Chol content. The results suggest that the extent of gel-fluid phase separation is higher in mixtures where the POPC-to-Chol ratio mimics 25% of the l_o-phase compared to mixtures where the POPC/Chol ratio mimics 75% of the l_o-phase. Analysis of the lifetime components of t-PnA fluorescence intensity decay further supports this conclusion, as shown by the increase in the pre-exponential associated to the longest lifetime component (Fig. S7A, C, E, G) and the requirement of four components to describe the fluorescence intensity decay of t-PnA for mixtures containing ≥20 mol% C16-GlcCer, which are indicative of gel-fluid phase separation (Fig. S7 B, D, F, H).
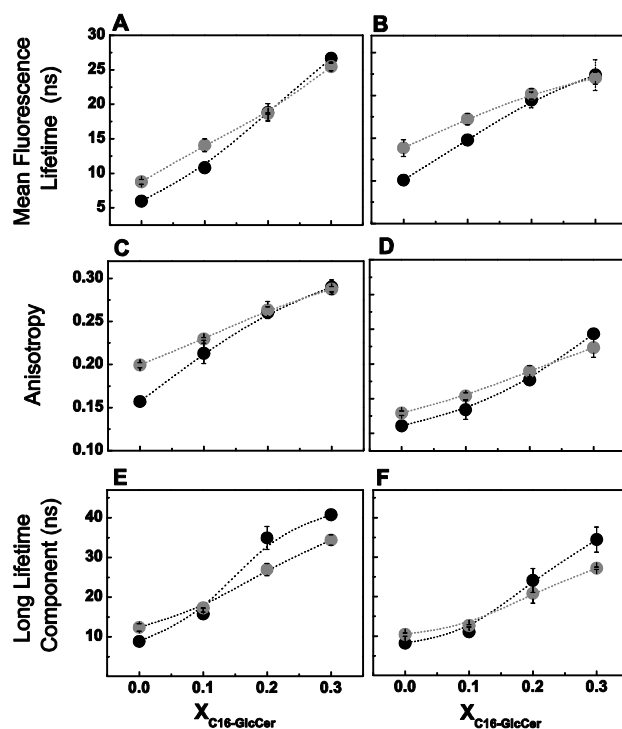
Figure 4 - Biophysical characterization of POPC/Chol/C16-GlcCer mixtures containing a constant POPC/Chol ratio.

t-PnA (A, B) fluorescence anisotropy, (C, D) mean fluorescence lifetime and (E, F) long lifetime component of the intensity decay in ternary POPC/Chol/C16-GlcCer mixtures containing POPC/Chol ratios mimicking 25 (black circles) and 75 (gray circles) mol% of an l_o phase. Measurements were performed at (A, C, E) neutral and (B, D, F) acidic pH. Values are means ± SD of at least 3 independent experiments.

The effect of C16-GlcCer on the global membrane order and packing properties of the mixtures is more pronounced at neutral pH compared to acidic pH (Fig. 4 and S8), as shown by the higher fluorescence anisotropy (Figs. S8A, D), mean fluorescence lifetime (Figs. S8B, E) and longer lifetime component of the *t*-PnA fluorescence intensity decay (Figs. S8C, F). These results are consistent with the higher ability of C16-GlcCer to change membrane packing properties at neutral pH compared to acidic pH [21].

Microscopy studies further supported the conclusions taken from spectroscopy studies: the extent of gel-fluid phase separation was higher for mixtures containing ≥20 mol% C16-GlcCer when the POPC/Chol ratio mimicked 25% of the l_o-phase (Fig. 5A) compared to 75% of the l_o-phase (Fig. 5B). In addition, l_d/l_o phase separation was also observed in ternary mixtures containing lower C16-GlcCer content and/or higher Chol content (Fig. 5,

mixtures with 10mol% of C16-GlcCer). This is shown by the presence of round-shape domains that only partially exclude the probes. These results suggest that C16-GlcCer interacts with Chol to form a more tightly packed l_o-phase that can be distinguished by fluorescence microscopy using NBD-DPPE and Rho-DOPE as probes. Phase separation into l_d, l_o and gel phases was observed for mixtures containing 20 and 30 mol% of C16-GlcCer and a POPC/Chol ratio mimicking 25% of l_o-phase (Fig. 5A). Indeed, a layer enriched in the NBD-DPPE probe surrounding the gel domain was observed, suggesting that this l_o-enriched phase in the interface of the gel and fluid phase, promotes a subtle transition avoiding the high line tension arising from a typical gel-fluid phase separation.
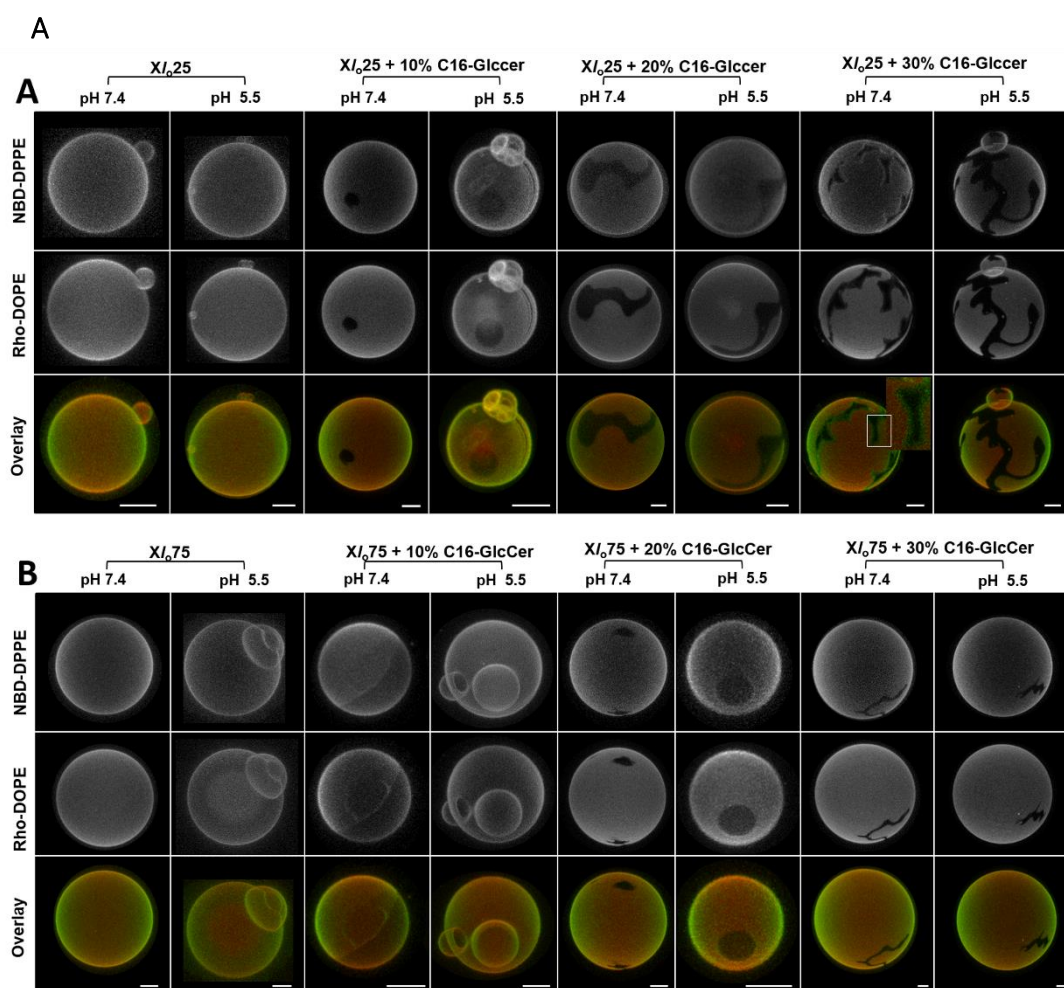
Figure 5 - Confocal fluorescence microscopy of POPC/Chol/C16-GlcCer GUVs containing a constant POPC/Chol ratio.
3D projection images from 0.4 μm confocal slices of GUVs containing POPC/Chol ratios mimicking 25 and 75 mol% of the l_o phase and increasing molar fractions of C16-GlcCer. GUVs were labelled with NBD-DPPE and Rho-DOPE. Studies were performed at neutral and acidic pH. Scale bar, 5 μm.

A stronger tendency for vesicle aggregation, fusion and tubule formation was again observed at acidic pH (Fig. 5 and Fig. S4). Analyses of the vesicle population by DLS showed a higher mean diameter (Figs. S9A) and PdI of the vesicles (Figs. S9B), and an increase in the scattering intensity in the range of 0.5–6 µm at acidic pH compared to neutral pH (Figs. S9C-F). In addition, the differences were more pronounced upon increasing C16-GlcCer content of the mixtures at pH 5.5, which might be related to the ability of C16-GlcCer to induce shape transformation of the vesicles under acidic conditions. The higher instability of the vesicle population at acidic pH might also be related to a decreased electrostatic repulsion between vesicles due to a net surface charge close to neutrality (Fig. S9G). The results further demonstrate that at neutral pH the net surface charge is negative, contributing to a higher electrostatic repulsion and preventing a strong interaction between the vesicles that would contribute to their aggregation and/or fusion.

5 Discussion

GlcCer has been implicated in the formation of lipid domains, particularly the so-called lipid raft domains, but the interplay between GlcCer and Chol has not been studied in detail. The present work aimed at providing further insight into the interactions between these two key membrane lipids and how they change the biophysical properties of fluid phospholipid membranes. Moreover, it also aimed to evaluate how these interactions are modified by environmental factors, such as changes in pH, considering that accumulation of GlcCer in acidic compartments occurs under pathological conditions, particularly in Gaucher Disease [44]. Increased levels of GlcCer might lead to alterations in membrane properties and compromise the integrity of the lysosomal membrane. Thus, it is important to understand the biophysical behavior of this lipid under conditions that mimic its subcellular distribution.

5.1 Qualitative analysis of the interplay between GlcCer/Chol

Overall, our results demonstrated that ternary mixtures containing a higher Chol/GlcCer ratio display properties typical of the l_o phase, while decreasing the ratio between these lipids leads to gel-fluid phase separation. This behavior resembles that observed for

mixtures containing Chol and ceramides, although a larger amount of GlcCer is required to induce gel phase formation compared to mixtures containing ceramides [23]. Previous studies performed by Maunula et al. [17] in a mixture containing Chol and GlcCer showed that GlcCer partitioning into sterol-enriched domains was low. These results are consistent with those obtained in the present study, since mixtures containing a high GlcCer/Chol ratio, such as the one used by Maunula et al. [17], display a strong tendency to form gel domains.

The ability of GlcCer to induce gel-fluid phase separation on the ternary mixtures was reduced upon acidification of the environment, similarly to that observed in POPC/GlcCer mixtures [21]. Moreover, GlcCer-induced vesicle aggregation and shape transformation were increased at pH 5.5, as shown both by microscopy and vesicle size analysis. This tendency is most likely associated with the overall surface charge of the vesicles, which is close to neutrality at acidic pH. The same behavior was observed for vesicles containing ≥20 mol% Chol, where an increased aggregation and decreased electronegativity of the vesicles was observed. Previous studies have also shown that liposomes containing Chol were prone to fuse and aggregate at acidic pH [45, 46].

Interestingly, mixtures containing Chol, GlcCer or both lipids showed a concentration dependent decrease in the overall surface charge of the vesicles, even though no change in the net charge of these lipids is expected, since the pKa of the acidic groups of Chol and GlcCer is ~16 and 12 [21, 47], respectively. Note that, no significant changes in the surface charge of POPC vesicles were observed when changing from neutral to acid pH indicating that variation in the zeta potential is related to the Chol- and GlcCer-vesicle composition.

It is assumed that the usual pKa of a fatty acid in water shifts from pKa ~5 to pKa ~7 upon interaction with a membrane, reflecting the strong change in the environment. However, since the hydroxyl group is not near the double conjugated bonds, it is not expected that alterations in the ionization state of the probe that could occur at pH 5.5 would affect the fluorescence properties of this lipid probe. However, ionization could influence the probe location in the membrane, which could result in changes in its photophysical properties, particularly in its fluorescence anisotropy and lifetime. According to the Perrin equation, anisotropy combines information on both the fluorescence lifetime and the medium viscosity/rigidity and, in addition, it is not based on absolute fluorescence intensities,

which would be probe concentration dependent, and more prone to error. Therefore, to check whether the ionization state of the probe was influencing either probe location and/or its photophysical properties, we evaluated the trend of variation of t-PnA fluorescence anisotropy upon varying the pH, as well as buffer composition in mixtures containing different GlcCer molar ratios. Under these conditions, both the ionic strength and the cation/anion concentration of the citrate-phosphate buffer increases as the pH increases (Supplementary Table 1). Moreover, citrate-phosphate buffer at pH 7.4 is significantly different from PBS buffer at the same pH. However, the anisotropy of t-PnA in mixtures prepared with these buffers is identical (Fig. S10) irrespective of the lipid composition of the mixtures. This shows that changes observed in t-PnA anisotropy upon changing the pH of the ternary POPC/Chol/GlcCer mixtures are not due pH variation or to compositional differences of the buffer. Moreover, an increase in t-PnA anisotropy with increase in buffer pH is only observed for mixtures displaying gel-fluid phase transition, i.e. containing 30 mol% GlcCer. This further supports the assumption that changes in pH environment are mainly affecting the organization of GlcCer molecules involved in the formation of the gel phase, as we have previously suggested [21]. Therefore, our results suggest that important alterations take place at the surface of the vesicles upon changing the pH.

It was recently reported that increasing the Chol content in POPC/Chol mixtures results in an increase in the electronegativity of the vesicles, which was explained based on a decreased binding of Na^+ ions to the surface of the vesicles [48]. This phenomenon was due to the lower ability of Na^+ ions to interact with Chol hydroxyl (OH) groups compared to phosphatidylcholine (PC) headgroups. Moreover, the authors further suggested that the increased association between Chol-OH groups and PC-headgroups and increased membrane hydrophobicity upon Chol content elevation also contributed to an overall decrease in the number of binding sites for cations [48]. It is possible that similar alterations take place in GlcCer-containing vesicles, particularly when considering the strong ability of GlcCer to establish an H-bond network. Increased H-bonding will contribute to a decrease in the layer of positive ions (such as Na^+ or H^+) interacting with the vesicle surface. These observations might also help explaining why the ability of GlcCer and Chol to increase the order of the membranes is decreased at acidic pH. Indeed, under acidic conditions, the surface charge of Chol, GlcCer and Chol/GlcCer-containing mixtures is

close to that obtained for POPC vesicles, suggesting that the number of ions bound to the surface is constant. This suggests that the polar groups of Chol and GlcCer experience conformational changes that might contribute to their lower exposure and/or compromised ability to establish H-bonds with the phospholipids, in agreement with our previous study [21]. It is possible that increase in H^+ content, as observed at acidic pH might contribute to a higher extent in H-bond network between the lipids and the solvent in detriment of lipid-lipid H-bonds. This would certainly contribute to a decrease in the packing of the lipids and therefore a decrease in the overall membrane order upon acidification.

5.2 Determination of a ternary POPC/Chol/GlcCer partial phase diagram

Our results, together with previous data, allow determining the partial ternary phase diagram that quantitatively describes the interplay between GlcCer and Chol in a fluid POPC matrix. POPC/Chol [29] and POPC/GlcCer [16] binary phase diagrams were used to establish the boundaries that define the l_d/l_o (gray triangles) and gel/fluid phase (black triangles) separation for these binary mixtures (Fig. 6). Moreover, thermodynamic principles such as the phase rule and limitations to the 2-phase/1-phase boundaries imposed by the Gibbs energy minimum principle [49, 50], were taken into account. All the experimental data were analyzed and the fraction of each phase present in a given mixture was determined, as described in [51]. This methodology considers the partition coefficient (K_p) of the probe between each phase, the experimental photophysical parameters of the probe in each pure phase, as well as in the lipid mixtures displaying phase coexistence. The methodology is explained in detail in the appendix section of Castro et al [51] and in Supplementary Information.

Table 1 shows a summary of the partition coefficients of t-PnA towards a given phase. K_p was determined using the variation of the fluorescence anisotropy and/or mean fluorescence lifetime of t-PnA as a function of the phase fraction in the indicated binary mixtures (see Supplementary Information). $K_p^{g/lo}$ was obtained by the ratio of the $K_p^{g/ld}$ and $K_p^{lo/ld}$ of t-PnA [51]. The values indicate that t-PnA has a very high preference towards the GlcCer-enriched gel phase in comparison to the l_d and l_o phases.

Table 1 - Partition coefficient of *t*-PnA in different lipid mixtures and between different phases.

Lipid Mixtures	pH 7.4	pH 5.5
$K_p^{g//d}$ in POPC/C16-GlcCer	4.70±0.00050	2.47±0.01000
$K_p^{lo//ld}$ in POPC/Chol	0.14±0.00016	0.14±0.00006
$K_p^{g//lo}$ in POPC/Chol/C16-GlcCer	34.40	17.64

Using the different K_p values, it was possible to determine the fraction of each phase for all the mixtures that were studied (Supplementary Table 2). As could be anticipated, mixtures presenting lower Chol content, such as those mimicking 25% of l_o phase, have larger fraction of the gel phase. The fraction of gel phase was always lower at pH 5.5 compared to pH 7.4.

Upon determination of the phase fractions, an iterative method was used to estimate the boundaries of the partial ternary phase diagram [52]. Briefly, different configurations for a phase diagram of the type shown in Fig. 6 were assayed, and the phase fractions and compositions computed. These were compared to the experimental values. The iteration that provided the smaller maximal difference between the experimental data and the calculated values is shown in Fig. 6 (see Supplementary Information for additional details). Note that only the left part of the diagram was experimentally assessed since this corresponds to more physiological conditions, i.e., high phospholipid content and low-to-medium Chol and GlcCer content. This area of the diagram consists of 4 different regions corresponding to relatively small areas of i) POPC-enriched fluid (l_d) and ii) POPC-enriched fluid + GlcCer-enriched gel (l_d + *gel*); iii) an intermediate POPC-enriched l_d + Chol-enriched l_o (l_d + l_o) region and iv) a large POPC-enriched l_d + Chol-enriched l_o + GlcCer-enriched gel (l_d + l_o + *gel*). This region, defined by a broad tie-triangle, denotes the relatively high immiscibility between the three lipid components. The tie-lines inside the tri-triangle were determined by analysis of the experimental data, particularly by the fluorescence spectroscopy measurements. Indeed, the three samples (*a*, *b* and *c*) crossed by the tie-line display identical packing properties, as shown by similar *t*-PnA long lifetime component for the three mixtures at pH 7.4 (~ 40 ns) and pH 5.5 (~ 32 ns). The same was observed for the second tie-line, crossing samples *d* and *e*, where *t*-PnA long lifetime

component of the mixtures was ~ 34 ns and ~ 27 ns, at pH 7.4 and 5.5, respectively. This evidence shows that the properties of the phases are identical for the different mixtures in each of the tie-lines and only the fraction of the phases is changing (Supplementary Table 2), which is in agreement with the definition of a tie-line.

The right side of the diagram was not experimentally determined. However using thermodynamic considerations, it is possible to predict the orientation of the boundaries. The two phase region should cross the ternary phase with a similar slope and extend inside the three phase region [49, 50]. Therefore, in order to respect geometric constraints imposed by the presence of the three phase region, the points that define the top and lower right of the tie-triangle connect the right side of the ternary diagram, with a line displaying a positive slope [50]. However, it is not possible to predict the composition at which g/l_o phase coexistence occurs for Chol/GlcCer mixtures, and therefore those boundaries are merely illustrative (Fig. 6).
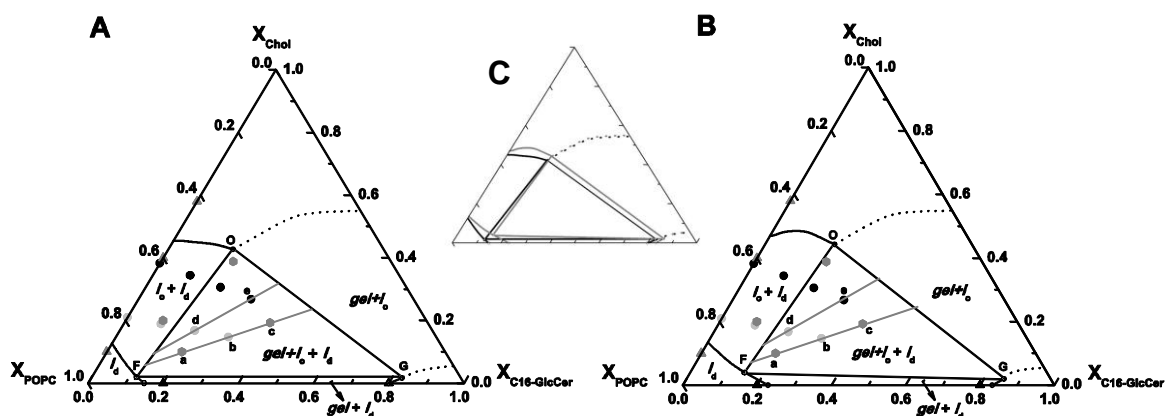
Figure 6 - Partial ternary phase diagram of POPC/Chol/C16-GlcCer mixtures. POPC/Chol/C16-GlcCer partial ternary phase diagrams, at 24ºC, at (A) neutral and (B) acidic pH. The diagrams were determined using the photophysical properties of t-PnA and microscopy data. Solid symbols are experimental data of the following mixtures: POPC/Chol (gray triangles); POPC/GlcCer (black triangles); POPC/Chol/C16-GlcCer ternary systems with constant POPC fraction (dark gray hexagons); POPC/Chol/C16-GlcCer with constant POPC/Chol ratio mimicking 25 (light gray circles) and 75 mol% of the l_o phase (black circles). The boundaries of the tie-triangle and of the coexisting l_o+l_d phase were based in the mathematical analysis of the experimental data (see Table 2 and Supplementary Information). The data from POPC/GlcCer were taken from [16], and the data from POPC/Chol mixtures were complemented by [29]. The dashed lines in the right side of the ternary diagrams are just illustrative of the possible boundaries of the $gel + l_o$ phase. (C) Overlap of the diagrams shows a shift of the tie-triangle to higher GlcCer molar

fractions at acidic pH (in gray) compared to neutral pH (in black). All the lines have a strong experimental basis and are thermodynamically consistent.

Compared to POPC/SM/Chol mixtures [29], this diagram presents a smaller region with l_o/l_d phase coexistence. It can therefore be concluded that GlcCer has a lower miscibility in the l_o phase compared to SM. This is likely due to both the high melting temperature of GlcCer and its stronger tendency to segregate into tightly-packed gel domains [16, 18, 20]. Comparison between POPC/Chol/C16-GlcCer and POPC/Chol/C16-Cer partial phase diagrams allows concluding that the presence of the glucose moiety in the headgroup of GlcCer increases the miscibility of GlcCer in the l_o phase compared to Cer [7, 23]. This suggests that significant levels of GlcCer might be involved in the formation of l_o domains in more complex biological membranes. However, very small fractions of Cer are sufficient to perturb the biophysical properties of l_o domains and drive gel-fluid phase separation [33]. Indeed, the POPC/Chol/C16-Cer phase diagram [23, 53] exhibits relevant differences in comparison to the POPC/Chol/C16-GlcCer ternary phase diagram. While the solubility of C16-Cer in a Chol-enriched fluid phase was minimal leading to a very large gel/fluid phase separation region, GlcCer is capable to interact with Chol forming l_o phase [23]. The differences in the behavior between the two lipids may probably be due to the nature of the interaction of Cer and GlcCer with the neighboring lipids. C16-Cer promotes very strong intermolecular bonds, forming domains with a very high packing density [23, 54, 55], which hinders the incorporation of Chol in the membrane. In contrast, the size of the sugar residue in C16-GlcCer might preclude the formation of domains with an equivalent packing density, which might facilitate the interaction of GlcCer with Chol [17, 21].

It is worth mentioning that even a minor alteration in the headgroup of the SLs, is enough to significantly alter the interplay established between the SL and Chol. For example in comparison with galactosylceramide (GalCer), which only differs from GlcCer regarding the position of the OH group, GlcCer-enriched domains are able to incorporate more Chol. This is probably due to the strength of the intermolecular interactions which are stronger in GalCer, hindering Chol incorporation into GalCer-enriched domains [17].

The effect of the pH on the interplay between POPC/Chol and GlcCer was also translated into a ternary phase diagram. Comparison of the two diagrams shows a slightly broader coexistence between the l_o/l_d phase at acidic pH. This shows that GlcCer miscibility in the

l_o phase is increased upon acidification, and suggests that the l_o domains can accommodate higher levels of GlcCer under acidic conditions without significantly changing the properties of the l_o-phase (Fig. 6B). In a biological context, the subtle differences in the phase behavior of the mixtures at different pH could be enough to induce a large perturbation in membrane organization, particularly considering that alterations in membrane packing and organization are accompanied by a strong tendency to induce membrane fusion/aggregation upon acidification. From a biological perspective such alterations might impact a number of membrane fusion events, including those associated to vesicle trafficking [56, 57]. In other words, in a complex system like a natural cell membrane, a slight change in membrane properties could have a cascade effect, leading to membrane distortions affecting, for instance, protein conformation and ultimately altering cell responses.

6 Conclusions and Biological Relevance

GlcCer is one of several bioactive lipids that modulate cell signaling, possibly by formation of membrane domains. The rationale for designing this study was the lack of systematic biophysical analyses exploring the interactions between GlcCer and another critical lipid involved in lipid domain formation, namely Chol.

The ternary POPC/Chol/GlcCer phase diagram obtained in this study complements previous studies using similar mixtures [22] and will be a valuable tool in the future, for instance in studies that aim to quantitatively analyze alterations of the phase behavior of these mixtures upon interaction with relevant molecules, such as proteins or drugs. Phase diagrams are also indispensable for studies that address lipid-protein interactions and protein partitioning into lipid domains. These phase diagrams will aid in the understanding of how the interplay between these lipids might affect the distribution and sorting of different proteins. The qualitative and quantitative analysis of the phase properties of these mixtures constitutes a further step towards understanding the lipid-lipid interactions and membrane biophysical properties in complex biological membranes. As an example, comparison between these and other SL/Chol-phase diagrams [23, 29] might allow prediction of the biophysical changes that occur in membrane properties upon metabolic conversion of one SL species into another. Since several SL species are involved in signaling events, integrative analysis between biophysical and

biological studies might help elucidate the link between the biophysical properties of these lipids and their biological functions.

7 Author Contributions:

The authors contributed with the following work: L.C.S. conceived the study. L.C.S. and A.R.P.V. designed the experiments. A.R.P.V., A.S.C., A.F. and L.C.S. performed the experiments and data analysis. All authors discussed the results and the implications. A.R.P.V., A.H.F., M.P. and L.C.S. wrote the manuscript.

8 Acknowledgments

9 References

1.   Okazaki, T.; Bell, R. M.; Hannun, Y. A. Sphingomyelin turnover induced by vitamin D3 in HL-60 cells. Role in cell differentiation. J Biol Chem 1989, 264 (32), 19076-19080.

2.   Spiegel, S.; Milstien, S. Sphingosine-1-phosphate: an enigmatic signalling lipid. Nat Rev Mol Cell Biol 2003, 4 (5), 397-407.

3.   Hannun, Y. A.; Obeid, L. M. Principles of bioactive lipid signalling: lessons from sphingolipids. Nat Rev Mol Cell Biol 2008, 9 (2), 139-150.

4.   Simons, K.; Ikonen, E. Functional rafts in cell membranes. Nature 1997, 387, 569-572.

5.   Gulbins, E.; Li, P. L. Physiological and pathophysiological aspects of ceramide. Am J Physiol Regul Integr Comp Physiol 2006, 290 (1), R11-R26.

6.   Castro, B. M.; Prieto, M.; Silva, L. C. Ceramide: A simple sphingolipid with unique biophysical properties. Prog Lipid Res 2014, 54, 53-67.

7.   Goñi, F. M.; Alonso, A. Effects of ceramide and other simple sphingolipids on membrane lateral structure. Biochim Biophys Acta 2009, 1788 (1), 169-177.

8.   de Almeida, R. F.; Marquês, J. T.; Silva, L. C. Biophysics of Lipid Rafts and Their Interplay with Ceramide: Studies in Model Systems and Biological Insights. In Lipid Rafts Properties, Controversies and Roles in Signal Transduction, Sillence, D., Ed.; Nova Science Publishers, Inc: New York, 2014, pp 21-36.

9.   Hakomori, S.-i. Glycosynaptic microdomains controlling tumor cell phenotype through alteration of cell growth, adhesion, and motility. FEBS Lett 2010, 584 (9), 1901-1906.

10.   Parton, R. G. Ultrastructural Localization of Gangliosides; GM1 is Concentrated in Caveolae. J Histochem Cytochem 1994, 42, 155-166.

11.   Degroote, S.; Wolthoorn, J.; Vanmeer, G. The cell biology of glycosphingolipids. Semin Cell Dev Biol 2004, 15 (4), 375-387.

12.   Zhang, W.; Quinn, B.; Barnes, S.; Grabowski, G.; Sun, Y. Metabolic Profiling and Quantification of Sphingolipids by Liquid Chromatography-Tandem Mass Spectrometry. J Glycomics Lipidomics 2013, 3 (107), 2153-0637.1000107.

13.   Ramstedt, B.; Slotte, J. P. Membrane properties of sphingomyelins. FEBS Lett 2002, 531 (1), 33-37.

14.   Lloyd-Evans, E. Glucosylceramide and Glucosylsphingosine Modulate Calcium Mobilization from Brain Microsomes via Different Mechanisms. J Biol Chem 2003, 278 (26), 23594-23599.

15.   Sillence, D. J. Glucosylceramide modulates membrane traffic along the endocytic pathway. J Lipid Res 2002, 43 (11), 1837-1845.

16.   Varela, A. R. P.; Gonçalves da Silva, A. M. P. S.; Fedorov, A.; Futerman, A. H.; Prieto, M.; Silva, L. C. Effect of glucosylceramide on the biophysical properties of fluid membranes. Biochim Biophys Acta 2013, 1828 (3), 1122-1130.

17.   Maunula, S.; Björkqvist, Y. J. E.; Slotte, J. P.; Ramstedt, B. Differences in the domain forming properties of N-palmitoylated neutral glycosphingolipids in bilayer membranes. Biochim Biophys Acta 2007, 1768 (2), 336-345.

18.   Westerlund, B.; Slotte, J. P. How the molecular features of glycosphingolipids affect domain formation in fluid membranes. Biochim Biophys Acta 2009, 1788 (1), 194-201.

19.   Maggio, B.; Carrer, D. C.; Fanani, M. L.; Oliveira, R. G.; Rosetti, C. M. Interfacial behavior of glycosphingolipids and chemically related sphingolipids. Curr Opin Colloid Interface Sci 2004, 8 (6), 448-458.

20.   Saxena, K.; Duclos, R. I.; Zimmermann, P.; Schmidt, R. R.; Shipley, G. G. Structure and properties of totally synthetic galacto- and gluco-cerebrosides. J Lipid Res 1999, 40, 839-849.

21.   Varela, A. R. P.; Gonçalves da Silva, A. M. P. S.; Fedorov, A.; Futerman, A. H.; Prieto, M.; Silva, L. C. Influence of Intracellular Membrane pH on Sphingolipid Organization and Membrane Biophysical Properties. Langmuir 2014, 30 (14), 4094-4104.

22.   Slotte, J. P.; Oestman, A. L.; Kumar, E. R.; Bittman, R. Cholesterol interacts with lactosyl and maltosyl cerebrosides but not with glucosyl or galactosyl cerebrosides in mixed monolayers. Biochemistry 1993, 32 (31), 7886-7892.

23.   Castro, B. M.; Silva, L. C.; Fedorov, A.; de Almeida, R. F. M.; Prieto, M. Cholesterol-rich Fluid Membranes Solubilize Ceramide Domains: Implcations for the Structure and Dynamics of Mammmalian Intracellular and Plasma Membranes. J Biol Chem 2009, 284 (34), 22978-22987.

24.   Almeida, P. F. F.; Pokorny, A.; Hinderliter, A. Thermodynamics of membrane domains. Biochim Biophys Acta 2005, 1720 (1–2), 1-13.

25.   McClare, C. W. F. An accurate and convenient organic phosphorus assay. Analytical Biochemistry 1971, 39 (2), 527-530.

26.   Sklar, L. A.; Hudson, B. S.; Petersen, M.; Diamond, J. Conjugated polyene fatty acids as fluorescent probes: spectroscopic characterization. Biochemistry 1977, 16 (5), 813-819.

27.   Haugland, R. P.; Spence, M. T.; Johnson, I. D. Handbook of Fluorescent Probes and Research Chemicals. 6th ed.; Molecular Probes: Eugene OR, 1996.

28.   Birch, D. S.; Imhof, R. Time-Domain Fluorescence Spectroscopy Using Time-Correlated Single-Photon Counting. In Topics in Fluorescence Spectroscopy, Lakowicz, J., Ed.; Springer US, 2002; Vol. 1, pp 1-95.

29.   de Almeida, R. F. M.; Fedorov, A.; Prieto, M. Sphingomyelin/Phosphatidylcholine/Cholesterol Phase Diagram: Boundaries and Composition of Lipid Rafts. Biophys J 2003, 85, 2406-2416.

30.   de Almeida, R. F. M.; Borst, J.; Fedorov, A.; Prieto, M.; Visser, A. J. W. G. Complexity of Lipid Domains and Rafts in Giant Unilamellar Vesicles Revealed by Combining Imaging and Microscopic and Macroscopic Time-Resolved Fluorescence. Biophys J 2007, 93 (2), 539-553.

31.   Pinto, S. N.; Silva, L. C.; de Almeida, R. F. M.; Prieto, M. Membrane Domain Formation, Interdigitation, and Morphological Alterations Induced by the Very Long Chain Asymmetric C24:1 Ceramide. Biophys J 2008, 95 (6), 2867-2879.

32.   Sarmento, M. J.; Prieto, M.; Fernandes, F. Reorganization of lipid domain distribution in giant unilamellar vesicles upon immobilization with different membrane tethers. Biochim Biophys Acta 2012, 1818 (11), 2605-2615.

33.   Silva, L. C.; de Almeida, R. F. M.; Castro, B. M.; Fedorov, A.; Prieto, M. Ceramide-Domain Formation and Collapse in Lipid Rafts: Membrane Reorganization by an Apoptotic Lipid. Biophys J 2007, 92 (2), 502-516.

34.   Veatch, S. L.; Keller, S. L. Separation of Liquid Phases in Giant Vesicles of Ternary Mixtures of Phospholipids and Cholesterol. Biophys J 2003, 85 (5), 3074-3083.

35.   Frazier, M. L.; Wright, J. R.; Pokorny, A.; Almeida, P. F. F. Investigation of Domain Formation in Sphingomyelin/Cholesterol/POPC Mixtures by Fluorescence Resonance Energy Transfer and Monte Carlo Simulations. Biophys J 2007, 92 (7), 2422-2433.

36.   Veatch, S.; Keller, S. Miscibility Phase Diagrams of Giant Vesicles Containing Sphingomyelin. Phys Rev Lett 2005, 94 (14).

37.	Goñi, F. M.; Alonso, A.; Bagatolli, L. A.; Brown, R. E.; Marsh, D.; Prieto, M.; Thewalt, J. L. Phase diagrams of lipid mixtures relevant to the study of membrane rafts. Biochim Biophys Acta 2008, 1781 (11–12), 665-684.

38.	de Almeida, R. F. M.; Loura, L. M. S.; Fedorov, A.; Prieto, M. Lipid Rafts have Different Sizes Depending on Membrane Composition: A Time-resolved Fluorescence Resonance Energy Transfer Study. J Mol Biol 2005, 346, 1109-1120.

39.	Reyes Mateo, C.; Ulises Acuña, A.; Brochon, J. C. Liquid-crystalline phases of cholesterol/lipid bilayers as revealed by the fluorescence of trans-parinaric acid. Biophys J 1995, 68 (3), 978-987.

40.	Thewalt, J. L.; Bloom, M. Phosphatidylcholine: cholesterol phase diagrams. Biophys J 1992, 63 (4), 1176-1181.

41.	Palmieri, B.; Yamamoto, T.; Brewster, R. C.; Safran, S. A. Line active molecules promote inhomogeneous structures in membranes: Theory, simulations and experiments. Adv Colloid Interface Sci 2014, 208, 58-65.

42.	Edidin, M. Lipids on the frontier: a century of cell-membrane bilayers. Nat Rev Mol Cell Biol 2003, 4 (5), 414-418.

43.	Castro, B. M.; de Almeida, R. F. M.; Fedorov, A.; Prieto, M. The photophysics of a Rhodamine head labeled phospholipid in the identification and characterization of membrane lipid phases. Chem Phys Lipids 2012, 165 (3), 311-319.

44.	Jmoudiak, M.; Futerman, A. H. Gaucher disease: pathological mechanisms and modern management. Br J Haematol 2005, 129 (2), 178-188.

45.	Hazemoto, N.; Harada, M.; Suzuki, S.; Kaiho, F.; Haga, M.; Kato, Y. Effect of Phosphatidylcholine and Cholesterol on pH-Sensitive Liposomes. Chem Pharm Bull 1993, 41 (6), 1003-1006.

46.	Bailey, A. L.; Monck, M. A.; Cullis, P. R. pH-Induced destabilization of lipid bilayers by a lipopeptide derived from influenza hemagglutinin. Biochim Biophys Acta 1997, 1324 (2), 232-244.

47.	Dewick, P. M. Acids and Bases. In Essentials of Organic Chemistry: For Students of Pharmacy, Medicinal Chemistry and Biological Chemistry, Dewick, P. M., Ed.; John Wiley & Sons, Inc.: Hoboken, 2006, pp 120-164.

48.	Magarkar, A.; Dhawan, V.; Kallinteri, P.; Viitala, T.; Elmowafy, M.; Róg, T.; Bunker, A. Cholesterol level affects surface charge of lipid membranes in saline solution. Sci. Rep. 2014, 4.

49.	Rhines, F. N. Phase diagrams in metallurgy: their development and application; McGraw-Hill 1956.

50.	Baker, H. ASM handbook: Alloy phase diagrams; ASM International 1992.

51.	Castro, B. M.; de Almeida, R. F. M.; Silva, L. C.; Fedorov, A.; Prieto, M. Formation of Ceramide/Sphingomyelin Gel Domains in the Presence of an Unsaturated Phospholipid: A Quantitative Multiprobe Approach. Biophys J 2007, 93, 1639-1650.

52.	Bates, D. M.; Watts, D. G. Nonlinear Regression: Iterative Estimation and Linear Approximations. In Nonlinear Regression Analysis and Its Applications; John Wiley & Sons, Inc., 2008, pp 32-66.

53.	Sot, J.; Ibarguren, M.; Busto, J. V.; Montes, L. R.; Goñi, F. M.; Alonso, A. Cholesterol displacement by ceramide in sphingomyelin-containing liquid-ordered domains, and generation of gel regions in giant lipidic vesicles. FEBS Lett 2008, 582 (21-22), 3230-3236.

54.   Pinto, S. N.; Silva, L. C.; Futerman, A. H.; Prieto, M. Effect of ceramide structure on membrane biophysical properties: The role of acyl chain length and unsaturation. Biochim Biophys Acta 2011, 1808 (11), 2753-2760.

55.   Carrer, D. C.; Härtel, S.; Mónaco, H. L.; Maggio, B. Ceramide modulates the lipid membrane organization at molecular and supramolecular levels. Chem Phys Lipids 2003, 122 (1-2), 147-152.

56.   Paroutis, P. The pH of the Secretory Pathway: Measurement, Determinants, and Regulation. Physiology 2004, 19 (4), 207-215.

57.   Riemann, A.; Ihling, A.; Schneider, B.; Gekle, M.; Thews, O. Impact of Extracellular Acidosis on Intracellular pH Control and Cell Signaling in Tumor Cells. In Oxygen Transport to Tissue XXXV, Van Huffel, S.; Naulaers, G.; Caicedo, A.; Bruley, D. F.; Harrison, D. K., Eds.; Springer New York, 2013; Vol. 789, pp 221-228.

10 Supporting Material for: Glucosylceramide reorganizes cholesterol-containing domains in a fluid phospholipid membrane

10.1 Supplementary Figures
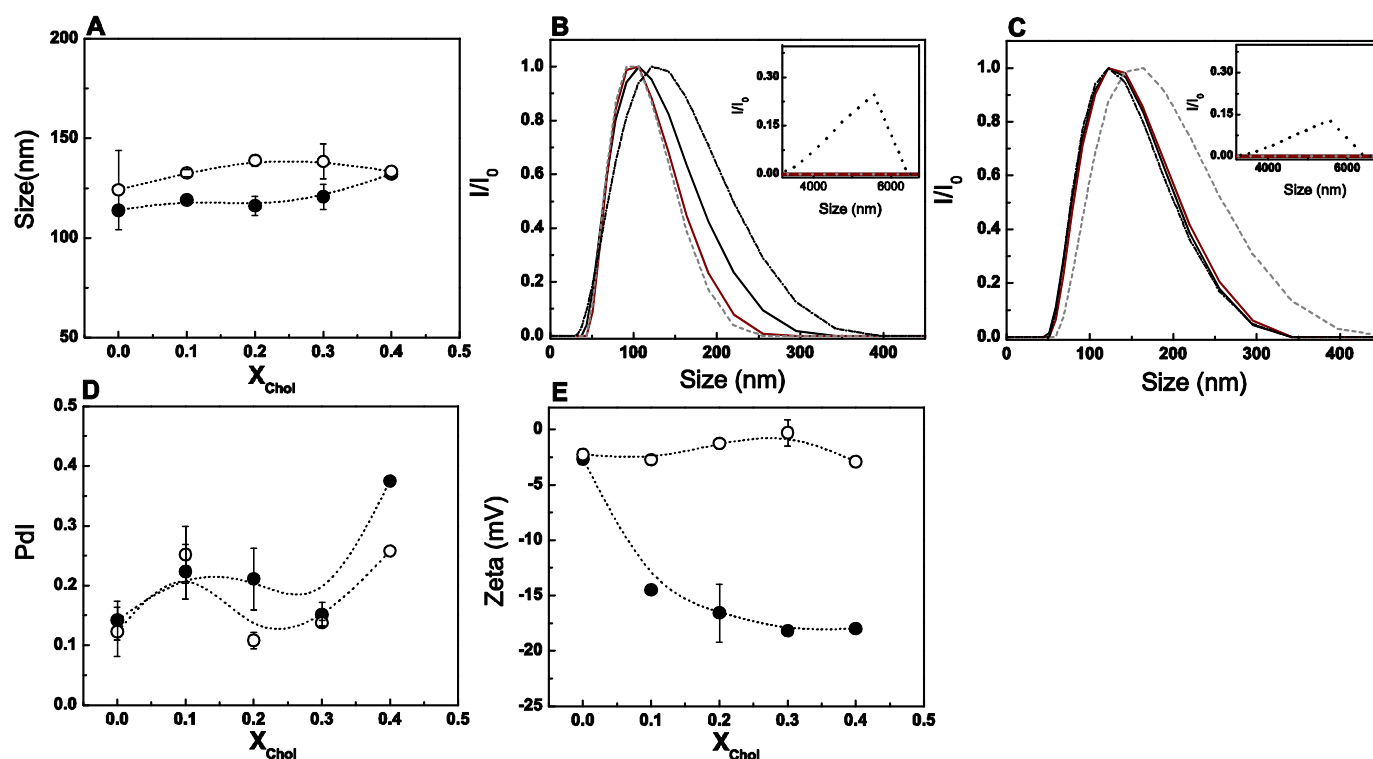
Figure S1 - **Characterization of POPC/Chol binary mixtures by electrophoretic and dynamic light scattering measurements.**

Average size of POPC/Chol LUVs at neutral (solid symbols) and acidic (open symbols) pH. (B, C) Normalized scattered light intensity of LUVs composed by POPC with 10 (—), 20 (—), 30 (---), 40 (-.-.-) and 58 (—) mol% of Chol at (B) pH 7.4 and (C) 5.5. Inset shows vesicle population with sizes in the order of microns. These liposomes represent a very small population of the sample. This was confirmed by the disappearance of the very high size band, when the number of the vesicles was considered instead of the scattering intensity (data not shown). (D) Polidispersity index (PdI) and (E) ζ-potential of POPC/Chol LUVs at neutral (solid symbols) and acidic (open symbols) pH. Values are means ± SD of at least 3 independent experiments.
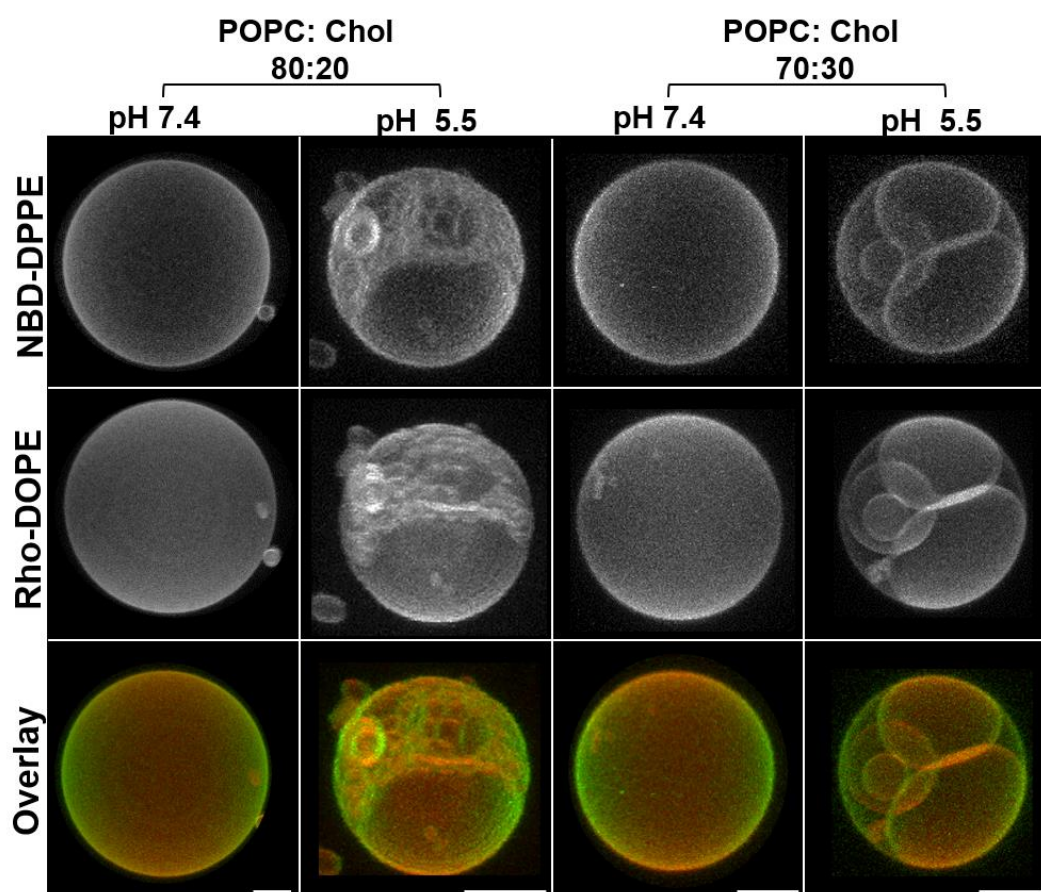
Figure S2 - Confocal fluorescence microscopy of POPC/Chol mixtures.

3D projection images from confocal slices (0.4 µm) of POPC/Chol GUVs labelled with NBD-DPPE and Rho-DOPE at neutral and acidic pH. Scale bar, 5 µm
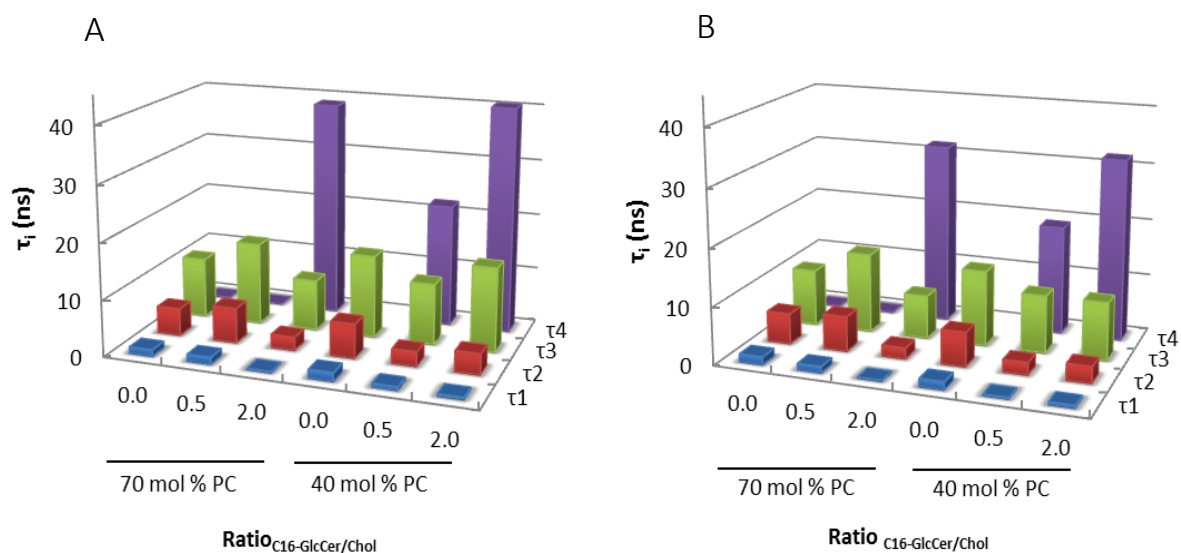
Figure S3 - Lifetime components of *t*-PnA fluorescence intensity decay in mixtures of POPC/Chol/C16-GlcCer with different C16-GlcCer/Chol ratios.

Variation of the lifetime components of *t*-PnA fluorescence intensity decay in POPC/Chol/C16-GlcCer. The mixtures contain 40 and 70 mol% of POPC. Measurements were performed at (A) pH 7.4 and (B) pH 5.5.Values are means of at least 3 independent experiments.
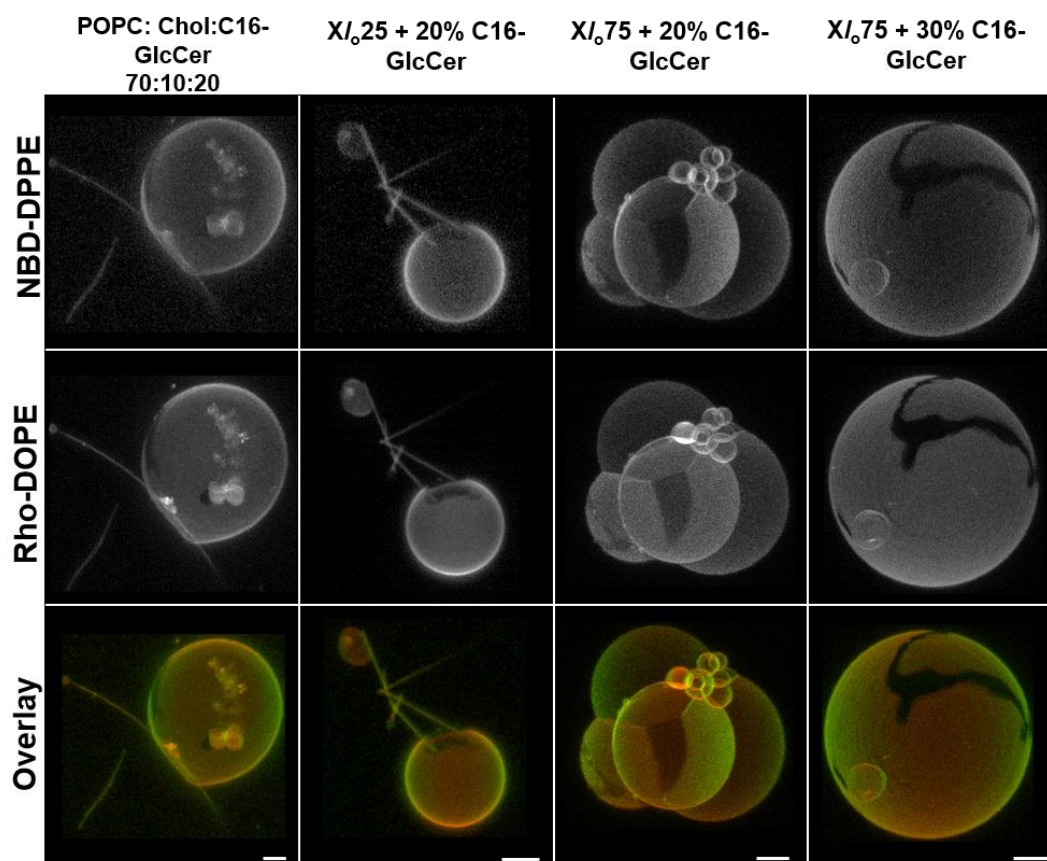
Figure S4 - Morphological alterations of POPC/Chol/C16-GlcCer mixtures at acidic pH.

3D projection images from 0.4 μm confocal slices of POPC/Chol/C16-GlcCer GUVs labelled with NBD-DPPE and Rho-DOPE. Scale bar, 5 μm.
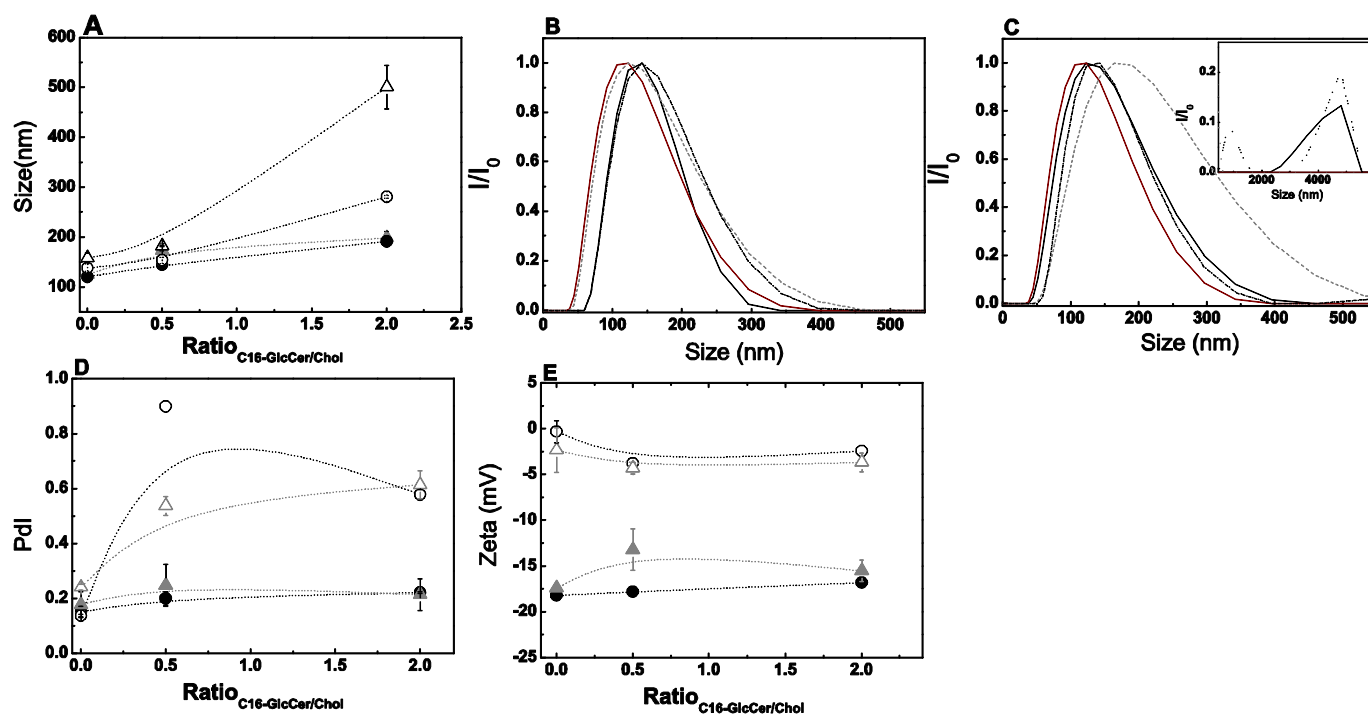
Figure S5 - Characterization of POPC/Chol/C16-GlcCer mixtures by electrophoretic and dynamic light scattering measurements.

(A) Average size of POPC/Chol/GlcCer LUV containing 40 (triangles) and 70 (circles) mol% of POPC at pH 7.4 (solid symbols) and 5.5 (open symbols). (B, C) Normalized scattered light intensity of LUVs containing 40/40/20 (—), 40/20/40 (---), 70/20/10 (—), and 70/10/20 (-.-.-) of POPC/Chol/GlcCer, respectively, at (B) pH 7.4 and (C) pH 5.5. Inset shows vesicle population with sizes in the order of microns. (D) PdI and (E) ζ-potential of POPC/Chol/C16-GlcCer mixtures. Symbols are the same as in (A).
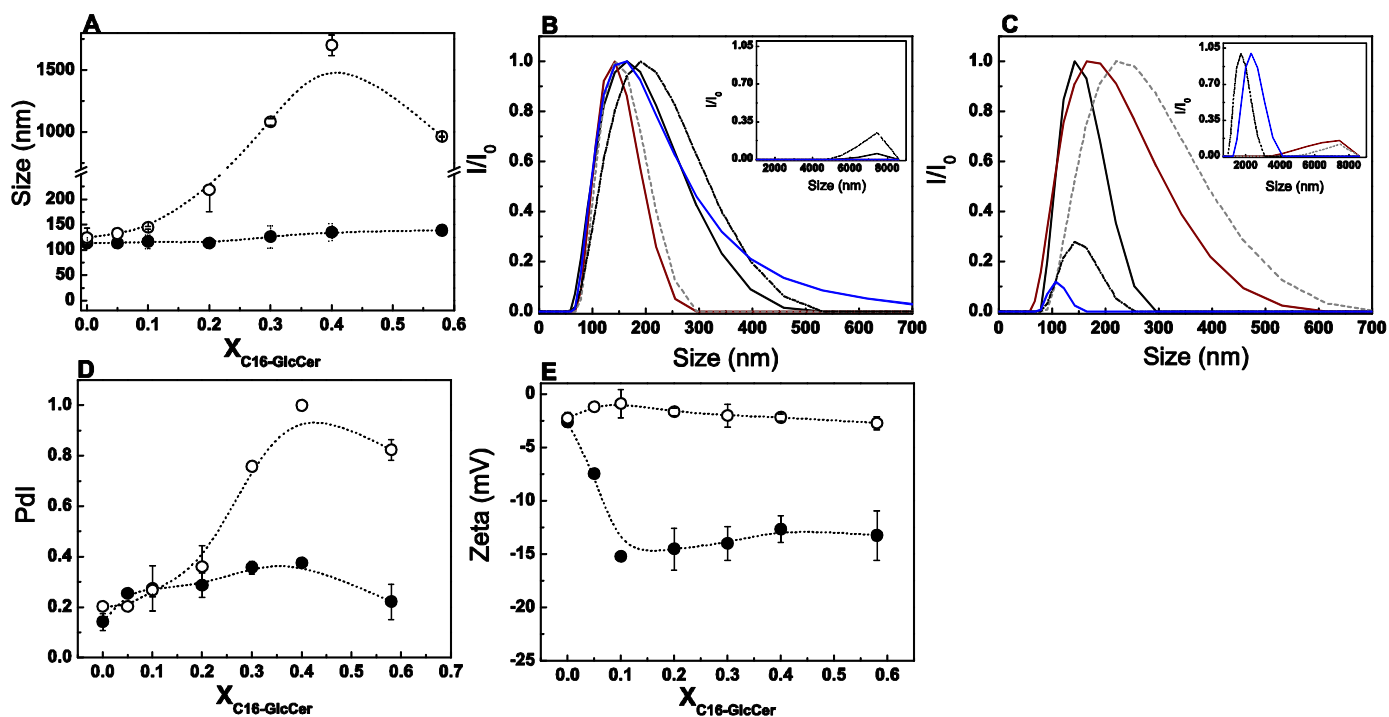
Figure S6. Characterization of POPC/C16-GlcCer binary mixtures by electrophoretic and dynamic light scattering measurements.

(A) Vesicle average size of POPC/C16-GlcCer LUVs at neutral (solid symbols) and acidic (open symbols) pH. (B, C) normalized scattered light intensity of LUVs composed by POPC 10(—), 20(—), 30(---), 40(-.-.-) and 58 (—) mol% of C16-GlcCer, at (B) pH 7.4 and (C) 5.5. Inset shows vesicle population with sizes in the order of microns. (D) PdI and (E) ζ-potential of POPC/C16-GlcCer LUVs at neutral (solid symbols) and acidic (open symbols) pH. Values are means ± SD of at least 3 independent experiments.

.
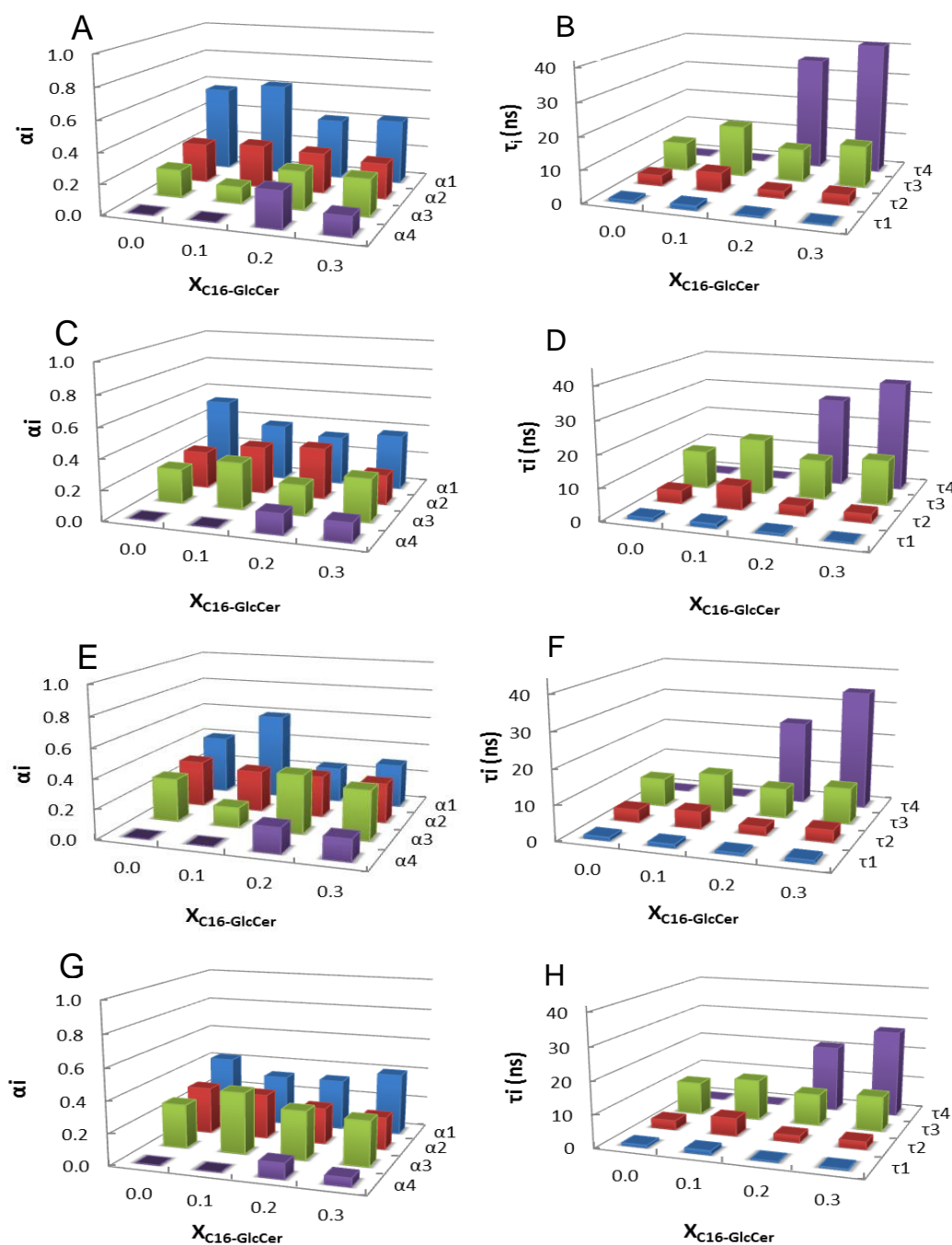
Figure S7. Analysis of *t*-PnA fluorescence intensity decay in POPC/Chol/C16-GlcCer mixtures with constant POPC/Chol ratio.

Variation of the pre-exponential factors and lifetime components of *t*-PnA fluorescence intensity decay, in POPC/Chol/C16-GlcCer ternary mixtures with a POPC/Chol ratio mimicking 25 (A, B, E, F) and 75 (C, D, G, H) mol% of l_o, and increasing molar fractions of C16-GlcCer. Measurements were performed at (A-D) pH 7.4 and (E-H) pH 5.5. Values are means of at least 3 independent experiments.
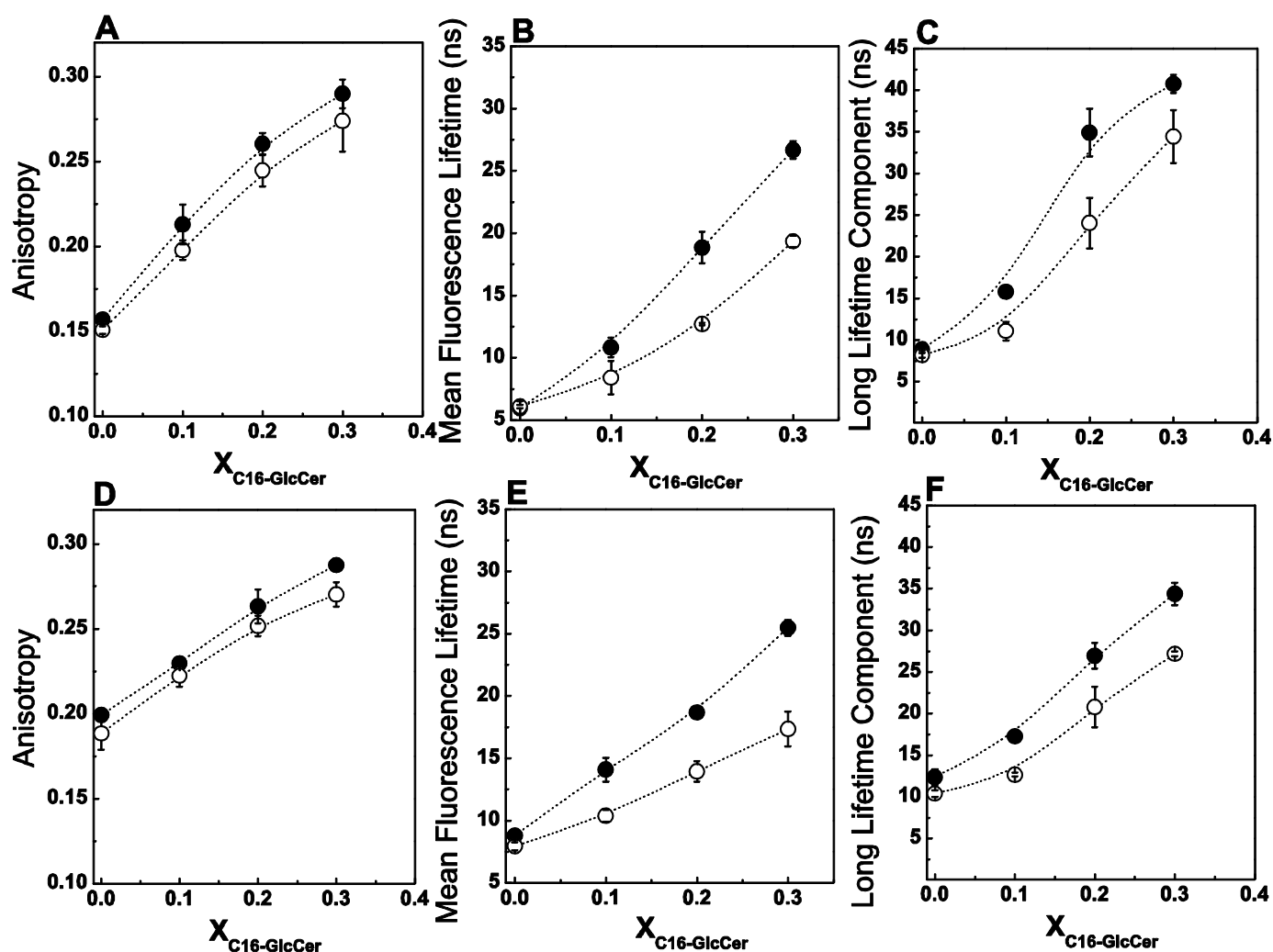
Figure S8- pH influence in the biophysical behavior of POPC/Chol/GlcCer membranes containing different l_o fractions.

t-PnA (A, D) fluorescence anisotropy, (B, E) mean fluorescence lifetime and (C, F) long lifetime component of the intensity decay in ternary POPC/Chol/C16-GlcCer mixtures containing POPC/Chol ratios mimicking (A-C) 25 and (D-F) 75 mol% of l_o phase. Measurements were performed at neutral (solid symbols) and acidic (open symbols) pH. Values are means ± SD of at least 3 independent experiments.
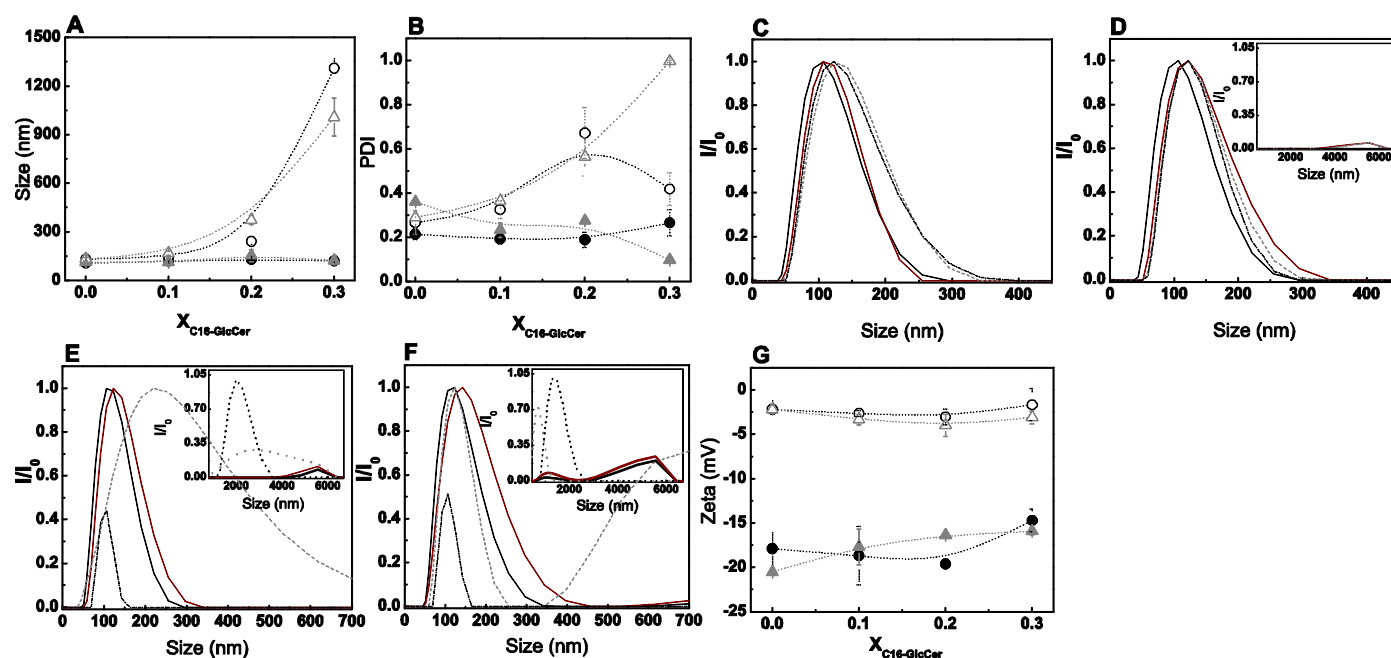
Figure S9 - Characterization of POPC/Chol/C16-GlcCer LUVs containing constant POPC/Chol ratio by electrophoretic and dynamic light scattering measurements.

(A)Vesicle average size and (B) PdI of POPC/Chol/C16-GlcCer LUVs with POPC/Chol ratios mimicking 25(circles) and 75(triangles) mol% of l_o, at neutral (solid symbols) and acidic (open symbols) pH. (C-F) Normalized scattered light intensity of LUVs containing a POPC/Chol ratio mimicking (C, E) 25 and (D, F) 75 mol% of l_o with 0 (—), 10 (—), 20 (---) and 30 (-.-.-) mol% of C16-GlcCer at (C,D) neutral or (E, F) acidic pH. Inset shows vesicle population with sizes in the order of microns. (G) ζ-potential of POPC/Chol/C16-GlcCer LUVs with POPC/Chol ratios mimicking 25(circles) and 75(triangles) mol% of l_o, at neutral (solid symbols) and acidic (open symbols) pH. Values are means ± SD of at least 3 independent experiments.
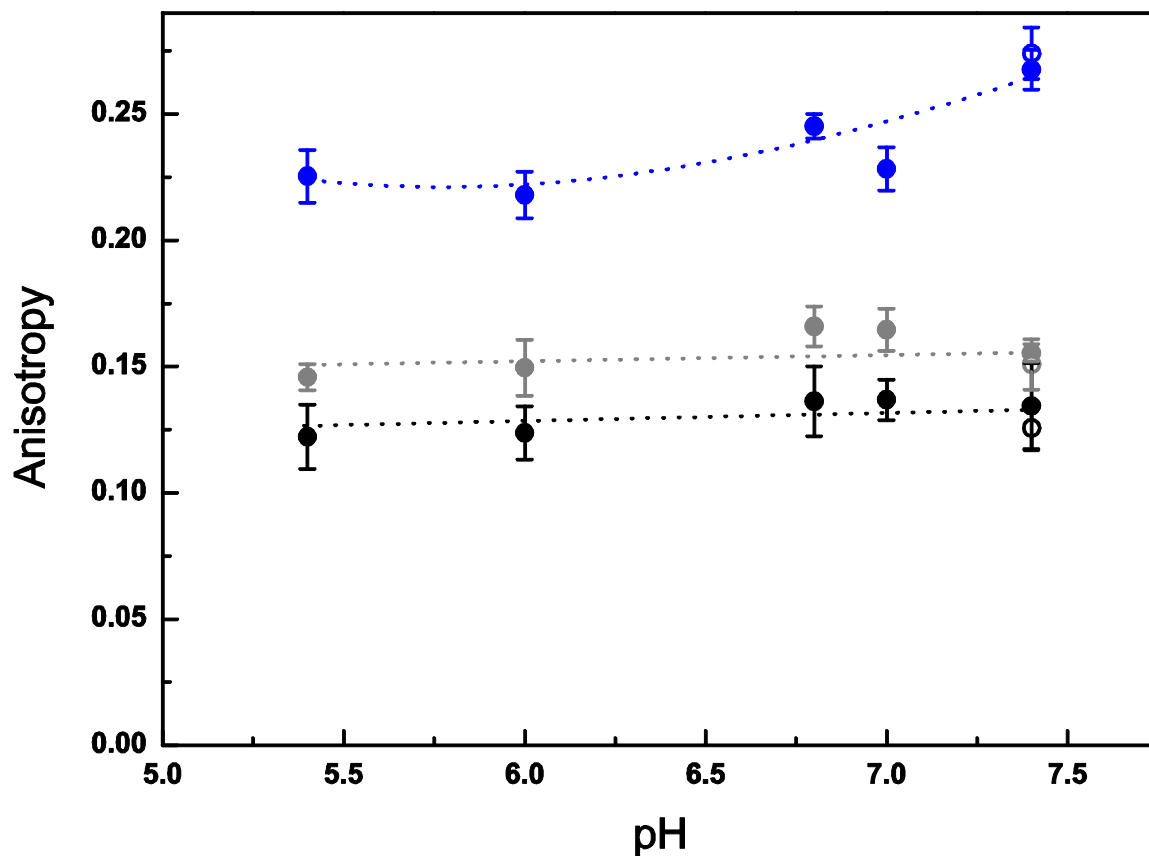
Figure S10 - Influence of pH in the biophysical properties of POPC/C16-GlcCer lipid mixtures
Variation of *t*-PnA fluorescence anisotropy in mixtures containing POPC (black), and POPC with 5 (gray) and 30 (blue) mol% of GlcCer. The lipid mixtures are in citrate-phosphate buffers at different pH (solid circles) or in PBS (open circles)

10.2 Supplementary Tables

Table S1 - Ions concentrations and ionic strength of the different buffers used in the study. The ions concentration was calculated taking into account the concentration of the components of each buffer. The Ionic strength was directly determined in the buffers, using an osmometer.

pH	Total Cation concentration (M)		Total Anion concentration (M)	Ionic Strength (mOsmol/Kg)
	Citrate-Phosphate buffer			
	Na$^+$	H$^+$	PO$_4^{3-}$	
5.40	0.22	0.11	0.11	286.00
6.00	0.25	0.13	0.13	283.00
6.80	0.31	0.15	0.15	326.00
7.00	0.33	0.16	0.16	333.00
7.40	0.36	0.18	0.18	350.00
	PBS buffer			
	Na$^+$	H$^+$	PO$_4^{3-}$ + Cl$^-$	
7.40	0.17	0.01	0.16	291.00
	0.18			

Table S2 - Molar fractions of POPC-rich, Chol-rich and GlcCer-rich phases (l_d, l_o and gel, respectively) in ternary POPC/Chol/C16-GlcCer mixtures.

The l_d, l_o and gel fractions were obtained from t-PnA mean fluorescence lifetime measurements (Fig. 3B, 3E, 5C and 5D), using the formalisms described in the Supplementary Information below.

	$X_{C16\text{-}GlcCer}$		pH 7.4			pH 5.5		
			X_{ld}	X_{lo}	X_{gel}	X_{ld}	X_{lo}	X_{gel}
X_{lo}	0.25	0.1	0.58	0.42	0.00	0.54	0.46	0.00
		0.2	0.55	0.40	0.05	0.51	0.44	0.05
		0.3	0.47	0.34	0.20	0.44	0.39	0.17
	0.75	0.1	0.32	0.68	0.00	0.33	0.67	0.00
		0.2	0.30	0.67	0.04	0.31	0.65	0.04
		0.3	0.27	0.61	0.12	0.29	0.61	0.10
X_{POPC}	0.70	0.1	0.59	0.42	0.00	0.54	0.46	0.00
		0.2	0.69	0.22	0.08	0.66	0.24	0.10
	0.40	0.2	0.12	0.86	0.02	0.13	0.84	0.03
		0.4	0.40	0.29	0.30	0.47	0.41	0.13

11 Supplementary information

11.1 Determination of the fraction and composition of each phase for a three-phase situation of the POPC/Chol/C16-GlcCer ternary system

A. To calculate the fraction of each phase in POPC/Chol/C16-GlcCer mixtures we used a methodology previously developed by us [51]:

First, the partition coefficient (K_p) of t-PnA towards a GlcCer-enriched gel phase and a Chol-enriched l_o phase was determined using t-PnA photophysical parameters obtained for the binary POPC/C16-GlcCer [16] and POPC/Chol mixtures (Fig. 1), respectively, accordingly to the following equations:

From mean fluorescent lifetime, $< \tau >$

$$< \tau > = (< \tau >_g K_p X_g + \ \overline{\tau}_f /\overline{\tau}_g < \tau >_f X_f)/K_p X_g + \overline{\tau}_f/\overline{\tau}_g X_f) \qquad \text{Eq. 1}$$

and from steady-state fluorescent anisotropy, $<r>$

$$< r > = (< r >_g K_p X_g + \ \overline{\tau}_f /\overline{\tau}_g < r >_f X_f)/K_p X_g + \overline{\tau}_f/\overline{\tau}_g X_f \qquad \text{Eq. 2}$$

where X_i is the phase fraction, $< \tau >_i$, $\overline{\tau}_f$, and $<r>_i$, are the mean fluorescence lifetime, the lifetime weighted quantum yield and the steady-state fluorescence anisotropy of t-PnA, in phase i, respectively. K_p is obtained by fitting the equations to the data as a function of X_i.

B - The photophysical properties of t-PnA were used to calculate the fraction of light emitted from the C16-GlcCer-rich gel phase ($FL_{C16-GlcCer}$), as described in [51]:

$$< \tau > = FL_{C16-GlcCer} <\tau>_{C16-GlcCer} + FL_{non\ C16-GlcCer} <\tau>_{nonC16-GlcCer} \qquad \text{Eq. 3}$$

where $<\tau>$ is the mean fluorescence lifetime obtained for these mixtures, $<\tau>_{C16-GlcCer}$ is the probe mean fluorescence lifetime in a C16-GlcCer-rich gel phase, $FL_{nonC16-GlcCer} = (1-FL_{C16-GlcCer})$ is the fraction of emitted light from all the C16-GlcCer poor phases, and $<\tau>_{nonC16-GlcCer}$ is the probe mean fluorescence lifetime in C16-GlcCer poor phases. In this ternary system the probe´s mean fluorescence lifetime in the C16-GlcCer poor phases is the value obtained in the absence of C16-GlcCer, and is given by:

$$< \tau >_{\text{nonC16-GlcCer}} = FL'_{\text{Chol}} < \tau >_{\text{Chol}} + FL'_{\text{POPC}} < \tau >_{\text{POPC}} \qquad \text{Eq. 4}$$

where FL'_i and $<\tau>_i$ are the fraction of light emitted and the probe's mean fluorescence lifetime, respectively, in a Chol-rich l_o (i = Chol) and POPC-rich fluid phase (i = POPC) taken from the binary POPC/Chol mixtures. Using the fraction of light emitted from the Chol-rich and POPC-rich (1-FL'_{Chol}) phases (Eq. 4) and the total fraction of light emitted from the C16-GlcCer-poor phases (Eq. 3) it is then possible to calculate the fraction of light emitted from the Chol- and POPC- rich phases in ternary POPC/Chol/C16-GlcCer mixtures, FL_i using:

$$FL_i = FL'_i (1 - FL_{\text{C16-GlcCer}}) \qquad \text{Eq. 5}$$

where i = Chol or POPC.

The K_p between two phases, α and β, $K_p^{\,\alpha/\beta}$ is given by:

$$K_p^{\frac{\alpha}{\beta}} = \frac{\chi_\alpha}{\chi_\beta} \frac{X_\alpha}{X_\beta} \qquad \text{Eq. 6}$$

where χ_i is the fraction of probe in phase i = α or β, respectively.

The ratio of emitted light fraction from two phases, α and β, is given by:

$$FL_\alpha / FL_\beta = \frac{\chi_\alpha}{\chi_\beta} \frac{\overline{\tau_\alpha}}{\overline{\tau_\beta}} \qquad \text{Eq. 7}$$

Assuming equal molar absorption coefficients in both phases, where FL_i is the fraction of emitted light from the phase i, $\chi_{i,}$ is the fraction of probe in phase i, and $\overline{\tau}_i$ is the probe lifetime-weighted quantum yield in phase i (i = α and β).

Solving equation 6 for the ratio of the probe fraction in each phase (χ_α/χ_β), and replacing in equation 7, the following equation is obtained:

$$FL_\alpha / FL_\beta = K_p^{\alpha/\beta} \frac{X_\alpha}{X_\beta} \frac{\overline{\tau_\alpha}}{\overline{\tau_\beta}} \qquad \text{Eq. 8}$$

The molar fraction ratio of each phase, α and β, (X_α/X_β) is calculated from equation 8. From the last equation the $X_{\text{C16-GlcCer}}/X_{\text{POPC ratio}}$ is calculated.

Knowing the $X_{\text{C16-GlcCer}}/X_{\text{POPC}}$ and $X_{\text{Chol}}/X_{\text{POPC}}$ for the mixtures under study, the POPC-rich phase fraction is obtained, since $X_{\text{C16-GlcCer}} + X_{\text{Chol}} + X_{\text{POPC}} = 1$.

11.2 Determination of the tie-triangle boundaries

Taking into account the phase fractions of the experimental samples, the pure l_o phase (taken from the POPC/Chol binary phase diagram [29]) and pure gel phase (taken from the POPC/GlcCer binary phase diagram [16]), it was possible to calculate the boundaries of the tie-triangle using our previous established iterative method [51]. To estimate the boundaries of the tie-triangle, the phase fraction of each mixture were used (see Table 2) and the lever rule, which is valid inside the tie-triangle, was applied based on the following considerations: inside the tie-triangle the composition of each phase can be calculated by drawing a straight line from each corner of the tie-triangle through each experimental point to its intersection with the opposite side (i.e., to calculate the X_{ld} of point a, a line is drawn from point F through point a to its intersection with the opposite side, a', the X_{ld} is calculated by the ratio between the distances $\overline{aa'}$ and $\overline{Fa'}$ (see Figure S8)).

11.3 Determination of the l_o/l_d phase boundaries

The limits of l_o/l_d phase coexistence were determined taking into account POPC/Chol and POPC/C16-GlcCer binary systems and also the experimental points that corresponded to mixtures displaying l_o/l_d phase coexistence. The lever-rule is also applied to this region of the phase diagram, and the the l_o+l_d boundaries can be calculated, using the determined tie-lines. To calculate the length and direction of the tie-lines, several thermodynamic considerations were taken into account: *i*) the tie-lines must connect the upper and lower boundary of l_o+l_d phase and simultaneously pass through the experimental points; *ii*) the ratio between the distance of the lower boundary to a specific composition and the total length of the tie line should correspond to the l_o fraction of the sample; *iii*) due to thermodynamic restrictions tie lines should never cross and should present a fanwise trend between the lateral boundaries of the phase in question (see Fig S8, black lines in the l_o+l_d phase) [49]. Fig. S11 shows two possible tie-lines in the l_o+l_d phase. Quantitative determination of the phase fraction of the studied mixtures using these two tie-lines

retrieves similar values, suggesting that these tie-lines correspond to the uncertainty associated to our method.
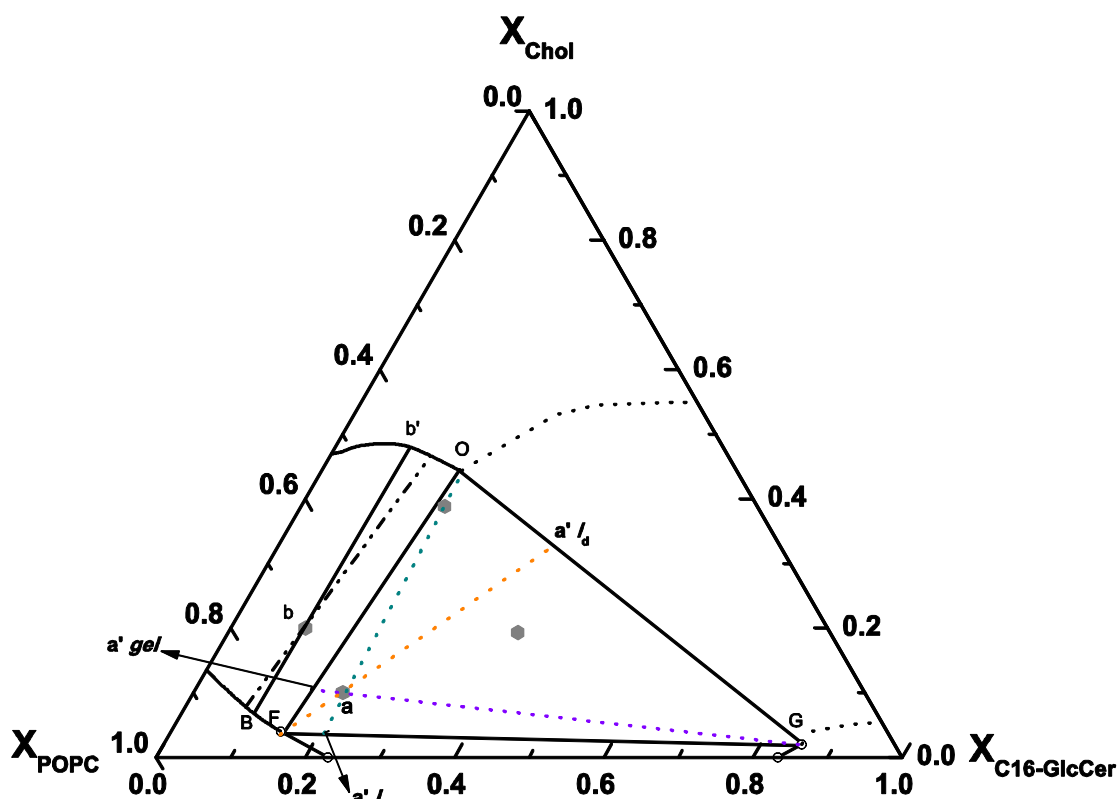
Figure S11 - Determination of the phase fractions and phase boundaries of POPC/Chol/C16-GlcCer ternary phase diagram.

POPC/Chol/C16-GlcCer ternary phase diagram (pH 5.5). The tie-lines (black lines) in the l_o+l_d phase, allowed the determination of the upper boundary of the l_o+l_d phase. Determination of the phase fractions inside the tie-triangle were performed as described in the supporting text. The three lines exemplify the method used for the determination of the l_d (orange), l_o (green) and gel (purple) phase fraction of the ternary mixture a.

Supporting References

1.   CASTRO, B. M.; DE ALMEIDA, R. F. M.; SILVA, L. C.; FEDOROV, A.; PRIETO, M. FORMATION OF CERAMIDE/SPHINGOMYELIN GEL DOMAINS IN THE PRESENCE OF AN UNSATURATED PHOSPHOLIPID: A QUANTITATIVE MULTIPROBE APPROACH. BIOPHYS J 2007, 93, 1639-1650.
2.   VARELA, A. R. P.; GONÇALVES DA SILVA, A. M. P. S.; FEDOROV, A.; FUTERMAN, A. H.; PRIETO, M.; SILVA, L. C. EFFECT OF GLUCOSYLCERAMIDE ON THE BIOPHYSICAL PROPERTIES OF FLUID MEMBRANES. BIOCHIM BIOPHYS ACTA 2013, 1828 (3), 1122-1130.
3.   DE ALMEIDA, R. F. M.; FEDOROV, A.; PRIETO, M. SPHINGOMYELIN/PHOSPHATIDYLCHOLINE/CHOLESTEROL PHASE DIAGRAM: BOUNDARIES AND COMPOSITION OF LIPID RAFTS. BIOPHYS J 2003, 85, 2406-2416.
4.   RHINES, F. N. PHASE DIAGRAMS IN METALLURGY: THEIR DEVELOPMENT AND APPLICATION; MCGRAW-HILL1956.

Glucosylceramide induced biophysical changes in artificial and cell membranes

Chapter V

Glucosylceramide-induced biophysical changes in artificial and cell membranes

Ana R.P. Varela[a,b,c], André Sá Couto[a], Aleksander Fedorov[b], Anthony H. Futerman[c], Manuel Prieto[b], Liana C. Silva[a,*]

[a] **iMed.ULisboa** – Research Institute for Medicines, Faculdade de Farmácia, Universidade de Lisboa, Av. Prof. Gama Pinto, 1649-003 Lisboa, Portugal

[b] **Centro de Química-Física Molecular and Institute of Nanoscience and Nanotechnology**, Instituto Superior Técnico, Universidade de Lisboa, Av. Rovisco Pais, 1049-001 Lisboa, Portugal

[c] **Department of Biological Chemistry**, Weizmann Institute of Science, Rehovot 76100, Israel

Corresponding author: Liana C. Silva, iMed.UL, Faculdade de Farmácia Universidade de Lisboa, Av. Prof. Gama Pinto, 1649-003 Lisboa, Portugal. Tel: + 351 217 946 400 (ext 14204), email: lianacsilva@ff.ul.pt

Keywords:

Lipid domains, Membrane organization, Gaucher Disease

Chapter V- Glucosylceramide-induced biophysical changes in artificial and cell membranes

1 Abstract

Glucosylceramide (GlcCer) is an active player in the regulation of different cellular events. Moreover, GlcCer is also a key modulator of membrane biophysical properties, which might be linked to the mechanism of its biological action. With the aim to analyze the impact of GlcCer in membranes that are compositionally closer to a cell membrane, we studied the interplay between GlcCer and complex artificial membranes containing 1-palmitoyl-2-oleoyl-*sn*-glycero-3-phosphocholine (POPC), Sphingomyelin (SM) and Cholesterol (Chol). Using an array of biophysical methodologies we showed that at lower GlcCer-to-Chol ratios, GlcCer stabilizes the SM/Chol-enriched liquid-ordered domains. However, upon decreasing the Chol content of the membrane, GlcCer significantly increased membrane order through the formation of gel domains. Changes in pH acidification disturbed the packing properties of GlcCer- containing membranes, leading to an increase in membrane fluidity and reduced membrane electronegativity, which consequently increase vesicle aggregation. To address the biophysical impact of GlcCer in biological membranes, studies were performed in wild-type fibroblasts and fibroblasts with GBA mutation for type I Gaucher Disease. The results showed that a decreased membrane fluidity occurred in cells containing higher levels of GlcCer, such as the cells from patients with Gaucher Disease. This suggests that pathological elevated levels of GlcCer change membrane biophysical properties and might compromise membrane-associated cellular events.

2 Introduction

Glucosylceramide is an ubiquitous lipid in mammalian cells and has vital roles in cell maintenance and survival [1, 2]. It is one of the simplest glycosphingolipid (GSL) and a precursor of complex ones [1]. Moreover, the synthesis and degradation of GlcCer controls the levels of 'free' ceramide [3, 4], an important signaling lipid. In addition, GlcCer has been implicated in lipid domain formation, and therefore it is also suggested that GlcCer modulates a number of signaling events, including the activation the of APC: protein S (acting as cofactor) inhibiting coagulation [5] and affecting cell proliferation (generally acting as a pro-mitotic agent) [6]. The exact molecular mechanisms underlying the biological actions of GlcCer remain elusive. However, an increasing body of evidence supports that GlcCer is an important player in the modulation of membrane biophysical properties since it increases membrane order [7, 8] and promotes tubule formation [8], which might trigger GlcCer-mediated biological actions.

GlcCer is structurally similar to ceramides, only differing in the glucose moiety present at the headgroup. It is therefore not surprising that this GSL also displays a strong tendency to change the biophysical and structural properties of fluid model membranes [8, 9]. In analogy to ceramides [10, 11], GlcCer is able to form tightly-packed gel domains in a fluid POPC bilayer [8]. However, significant differences in the biophysical behavior of GlcCer and ceramides with the same acyl chain length have already been reported, which includes a higher tendency of GlcCer to promote shape changes of the membrane [9]. The similarities between GlcCer and ceramide-induced changes in membrane properties can also be extended to more complex membranes containing Chol, where the increasing content of Chol decreases the ability of these lipids to form gel type domains. Even though GlcCer showed low ability to participate in the formation of sterol-enriched domains [12], the miscibility of GlcCer in the liquid ordered (l_o) phase is still higher compared to that of ceramide [13, 14, 15]. In addition, literature reports that the addition of SM, or other glycosphingolipids (as LacCer), improved Chol/GlcCer miscibility [16] probably due to packing defects formed in the domains due the presence of different headgroups. In the previous chapter we have evaluated, in a quantitative manner, the interplay between those two lipids - Chol and GlcCer - in a fluid phospholipid membrane. In this study, it was possible to conclude that GlcCer and Chol are able to form domains with l_o phase properties. However, compared to the canonical sphingomyelin (SM)/Chol mixture, the

extent of l_o/liquid disordered (l_d) phase separation was smaller, due to the stronger ability of GlcCer to segregate into gel domains. In addition, GlcCer-induced biophysical changes are pH-dependent: a decreased ability to drive gel-fluid phase separation and increased tendency to induce membrane morphological alterations is observed upon acidification [9], suggesting that alterations in pH environment, such as those occurring along the endolysosomal pathway, might be enough to alter membrane organization and biophysical properties of membrane regions enriched in GlcCer.

As a step towards the understanding of the biophysical impact of GlcCer in biomembranes, we performed studies in artificial membranes with increasing lipid complexity. The interplay between GlcCer and mixtures containing different molar fractions of POPC/SM/Chol was evaluated by fluorescence spectroscopy, microscopy and dynamic light scattering. Our results showed that GlcCer associates with SM to drive gel-fluid phase separation, but it also interacts with both SM/Chol to increase the extent of l_o phase, particularly when the Chol content of the mixtures is increased. Moreover, changing the pH environment strongly decreased GlcCer ability to increase membrane order and drive gel-fluid separation. Our results further support the hypothesis that in biological membranes local elevation in GlcCer levels, might result in strong alterations in membrane structure and packing properties.

The impact of GlcCer in cell processes, demands a constant regulation of GlcCer synthesis and degradation. A decrease in GlcCer degradation, generally due to a deficiency in β-glucosidase, promotes an accumulation of GlcCer, primarily in the lysosome and later extending to the whole cell, leading to cell and tissue dysfunction [17, 18]. This pathological mechanism is known as Gaucher Disease (GD) [17]. It still remains to be elucidated whether accumulation of this lipid triggers changes in the biophysical properties of biological membranes. To further test this hypothesis, biophysical studies were also performed in fibroblasts derived from patients with GD type I. The results showed a significant increase in the membrane order of fibroblasts derived from GD patients compared to control, showing that GlcCer accumulation due to impaired lysosomal degradation alters the biophysical properties of the membranes, in agreement with the data obtained from artificial membranes.

3 Materials and methods

3.1 Materials

POPC, C16-GlcCer (D-glucosyl-ß-1,1' N-palmitoyl-D-erythro-sphingosine), C16-SM (N-palmitoyl-D-erythro-sphingosylphosphorylcholine), Rho-DOPE (N-rhodamine-dipalmitoylphosphatidylethanolamine) and 1,2-dioleoyl-sn-glycero-3-phosphoethanolamine-N-(biotinyl) (DOPE-biotin) were from Avanti Polar Lipids (Alabaster, AL). t-PnA (trans-parinaric acid) and NBD-DPPE (1,2-dipalmitoyl-sn-glycero-3-phosphoethanolamine-N-(7-nitro-2-1,3-benzoxadiazol-4yl)) were from Molecular Probes (Leiden, The Netherlands). Cholesterol was purchased from Sigma-Aldrich (Steinheim, Germany). All organic solvents were UVASOL grade from Merck (Darmstadt, Germany).

3.2 Methods

3.2.1 Liposome Preparation

The spectroscopic studies were performed in multilamellar vesicles (MLV) containing POPC/C16-SM/Chol and POPC/C16-SM/Chol/C16-GlcCer. MLVs were prepared as previously described [10]. Particle size analysis [19] and zeta potential were determined using large unilamellar vesicles (LUVs). The LUVs were prepared from the previously formed MLVs by the extrusion technique described by Hope et al [20]. The total lipid concentration of the vesicles was 0.1 mM.

For the microscopy studies, giant unilamellar vesicles (GUVs) were prepared by electroformation using the appropriate lipids; DOPE-biotin (at a biotinylated/non-biotinylated lipid ratio of $1:10^6$), Rho-DOPE and NBD-DPPE (at a probe/lipid ratio of 1:500 and 1:200, respectively), as previously described [21, 22]. The GUVs were then transferred to 8-well Ibidi® μ-slides that had been previously coated with avidin (at 0.1mg/ml) to improve GUV adhesion to the plate [22].

MLVs, LUVs and GUVs suspension medium was PBS buffer (10 mM sodium phosphate, 150 mM sodium chloride and 0.1 mM EDTA, pH 7.4) or citrate-phosphate buffer (100mM citric acid and 200 mM sodium phosphate, pH 5.5). The latter buffer was used to evaluate if the biophysical properties of the lipid mixtures were pH-sensitive.

3.2.2 Fluorescence Spectroscopy

Fluorescence anisotropy of t-PnA, was measured in a SLM Aminco 8100 series 2 spectrofluorimeter with double excitation and emission monochromators, MC400 (Rochester, NY). All measurements were performed in 0.5 cm × 0.5 cm quartz cuvettes. t-PnA excitation (λ_{exc})/emission (λ_{em}) wavelengths were 320/405 nm and the probe/lipid ratio was 1/500. Constant temperature was maintained using a Julabo F25 circulating water bath controlled with 0.1ºC precision directly inside the cuvette with a type-K thermocouple (Electrical Electronic Corp., Taipei, Taiwan). The fluorescence anisotropy $<r>$ was calculated as [23]:

$$< r >= \frac{Ivv - GIvh}{Ivv + 2GIvh} \qquad \text{(Eq. 1)}$$

where the different intensities (I_{ii}) are the steady state vertical and horizontal components of the fluorescence emission with the excitation vertical (Ivv and Ivh) and horizontal (Ihv and Ihh) to the emission axis. The latter pair of components is used to calculate the G factor ($G= Ihv/Ihh$). An appropriate blank was subtracted from each intensity reading.

Time-resolved fluorescence measurements with t-PnA were performed by the single photon timing technique with a laser pulse excitation [24] at λ_{exc}=305nm (using a secondary laser of Rhodamine 6G [25]) and λ_{em}=405nm. The experimental decays were analyzed using TRFA software (Scientific Software Technologies Center, Minsk, Belarus).

3.2.3 Confocal Fluorescence Microscopy

Confocal fluorescence microscopy was performed using a Leica TCS SP5 (Leica Mycrosystems CMS GmbH, Mannheim, Germany) inverted microscope (DMI6000) with a 63×water (1.2 numerical aperture) apochromatic objective. NBD-DPPE and Rho-DOPE excitation was performed using the 458 nm and 514 nm lines from an Ar^+ laser, respectively. The emission was collected at 480-530 and 530-650 nm, for NBD-DPPE and Rho-DOPE, respectively. Confocal sections of thickness below 0.4 µm were obtained using a galvanometric motor stage. Three-dimensional (3D) projections were obtained using Leica Application Suite-Advanced Fluorescence software.

3.2.4 Particle size analysis

The mean diameter and polydispersity index (PdI) of the vesicles were determined by dynamic light scattering analysis on a Zetasizer Nano S equipment (Malvern Instruments, UK). Size measurement was performed using patented NIBS (non-invasive back scatter) technology. Samples were placed in 12mm square polystyrene cuvettes and then in a chamber maintained at 25ºC. The data analysis was performed by the accompanying software (Zetasizer Software® 7.03) and expressed as an average size or as a size distribution by intensity. The PdI for each sample was also calculated using the same software. In each experiment, the measurements were performed in triplicate.

3.2.5 Electrophoretic Light scattering measurements

Zeta potential (ZP) was determined by electrophoretic mobility on a ZetaSizer Nano Z equipment (Malvern Instruments, UK) using M3-PALS technology. Samples were placed in clear disposable zeta cells and then in a chamber maintained at 25ºC. Data analysis was performed using Zetasizer Software® 7.03. Measurements were performed in triplicate for each sample.

3.2.6 Cell culture and biophysical characterization of fibroblasts

Wild-type and GD type I (N370S/N370S)-derived fibroblasts were grown in DMEM medium supplemented with 10% fetal bovine serum, 2% antibiotics (100IU/ml penicillin, 100μg/ml streptomycin), 1% non-essential aminoacids and 1% sodium pyruvate at 37°C in 5% carbon dioxide. Upon reaching the adequate confluence, the fibroblasts were suspended, counted, and t-Pna was added to a final concentration of 2μM per 1×10^6 cells/mL. The anisotropy measurements with t-PnA were performed in a FluoroLog spetrofluorimeter (Horiba Jobin-Yvon, NJ, USA), using 320 nm/405 nm as $\lambda_{exc}/\lambda_{em}$ wavelengths. For each sample, at least 10 anisotropy measurements were performed. t-PnA fluorescence intensity decay measurements, were performed in a FluoroLog spectrofluorimeter (Horiba Jobin-Yvon, NJ, USA) and were obtained by the time-correlated single photon timing technique using a NanoLED pulsed laser diode of 295 nm. The experimental decays were analyzed using TRFA software. The intrinsic cell fluorescence (background) was subtracted from all the data, by using a blank (cells without t-PnA) prepared and measured under exactly the same conditions as the samples.

4 Results

4.1 Studies in model membranes

4.1.1 Rationale for the selection of the mixtures

In the present work we extended a previous study of the biophysical impact of C16-GlcCer on the properties of model membranes, now considering increasing lipid complexity. Since it is hypothesized that GlcCer is a lipid involved in lipid domain formation, including the so-called raft domains, we selected well-characterized POPC/SM/Chol mixtures, mimetic of raft domains in model membranes [25]. Six different ternary mixtures in the l_o/l_d phase co-existence region, that span the tie-line that crosses the 1:1:1 composition on the ternary POPC/SM/Chol phase diagram, were used (Table 1, Supplementary Fig. 1). According to the lever rule, the composition of the phases is the same in each of these mixtures, only the fraction of each phase changes. This enables to better rationalize the biophysical effects of GlcCer in these mixtures. Therefore, to study the interplay between GlcCer and these lipid components, the ratio between POPC/SM/Chol was kept constant to mimic the composition of the mixtures taken from the tie-line, and C16-GlcCer molar fraction was increased (Table 1). Different methodologies were then used to evaluate the biophysical properties of these mixtures.

Table 1 Composition of the studied mixtures.

				POPC/C16-SM/Chol mixtures								
Without C16-GlcCer					With 5 mol% C16-GlcCer				With 10 mol% C16-GlcCer			
X_{POPC}	X_{C16-SM}	X_{Chol}	$X_{C16-GlcCer}$	X_{lo}	X_{POPC}	X_{C16-SM}	X_{Chol}	$X_{C16-GlcCer}$	X_{POPC}	X_{C16-SM}	X_{Chol}	$X_{C16-GlcCer}$
0.72	0.23	0.05	0	0	0.68	0.22	0.048	0.05	0.64	0.21	0.045	0.1
0.6	0.26	0.14	0	0.26	0.6	0.25	0.130	0.05	0.54	0.24	0.130	0.1
0.45	0.3	0.25	0	0.51	0.43	0.28	0.240	0.05	0.41	0.27	0.230	0.1
0.34	0.33	0.33	0	0.84	0.32	0.31	0.320	0.05	0.31	0.29	0.300	0.1
0.25	0.35	0.4	0	0.98	0.24	0.33	0.380	0.05	0.23	0.31	0.360	0.1
0.15	0.37	0.48	0	1	0.14	0.36	0.450	0.05	0.14	0.34	0.430	0.1

4.1.2 Characterization of the mixtures by fluorescence spectroscopy

From our previous studies, we have identified *t*-PnA as a suitable probe to detect alterations promoted by C16-GlcCer on membrane biophysical properties. Fig 1 shows

the variation of t-PnA fluorescence anisotropy (Fig. 1A), mean fluorescence lifetime (Fig. 1B) and long lifetime component of the fluorescence intensity decay (Fig. 1C) in POPC/SM/Chol mixtures in the absence and presence of different C16-GlcCer content. Increasing C16-GlcCer content of the mixtures leads to an increase in the fluorescence anisotropy and mean fluorescence lifetime of t-PnA, irrespective of the composition of the mixtures, showing that C16-GlcCer increases membrane order. This effect is more pronounced for mixtures containing low Chol and low SM content, i.e., for mixtures where the l_o-phase fraction is up to 51% (Table 1), compared to mixtures containing high Chol and SM content, showing that the effect of C16-GlcCer on the properties of membranes containing a large fraction of l_o phase is smaller. This effect is similar to what has been previously reported for ceramide [14, 26], where a decreased ability to segregate into tightly-packed gel domains alongside with increased miscibility in the l_o phase was observed upon increasing the l_o fraction of the mixtures [13, 14].

This is further confirmed by the decrease in the long lifetime component of t-PnA fluorescence intensity decay (Fig. 1C, Supplementary Fig. 2C, E). Nonetheless, even in mixtures containing large l_o fraction, the long lifetime component of t-PnA is very high and close to values typical of a gel phase (above 30 ns [27]). Moreover, four components were required to describe the fluorescence intensity decay of the probe, suggesting that GlcCer ability to segregate into gel domains is not completely abolished upon increasing the Chol and SM content of the quaternary mixtures at neutral pH.

Similar effects were observed when these mixtures were characterized at acidic pH: the effect of C16-GlcCer on the packing properties of the mixtures is higher in the low Chol/low SM range (Fig. 1D-F). However, under acidic conditions, GlcCer-induced gel-fluid phase separation is abolished in mixtures containing larger fractions of the l_o phase, as shown by the decrease in the long lifetime component of t-PnA below values typical of the gel phase [27] (Fig 1F), and the disappearance of the fourth component of the analysis of the fluorescence intensity decay of the probe (Supplementary Fig 2D, F).

The results further showed an overall decrease in the packing of the mixtures at acidic pH compared to neutral pH. Moreover, C16-GlcCer-induced gel domain formation is strongly decreased at acidic pH, particularly in mixtures containing the lowest C16-GlcCer content, as shown by the long lifetime component of t-PnA values below 30ns. Decreased

C16-GlcCer-enriched gel-domain formation has been previously observed in mixtures of POPC/C16-GlcCer [9] and POPC/Chol/C16-GlcCer upon acidification (Chapter IV) .
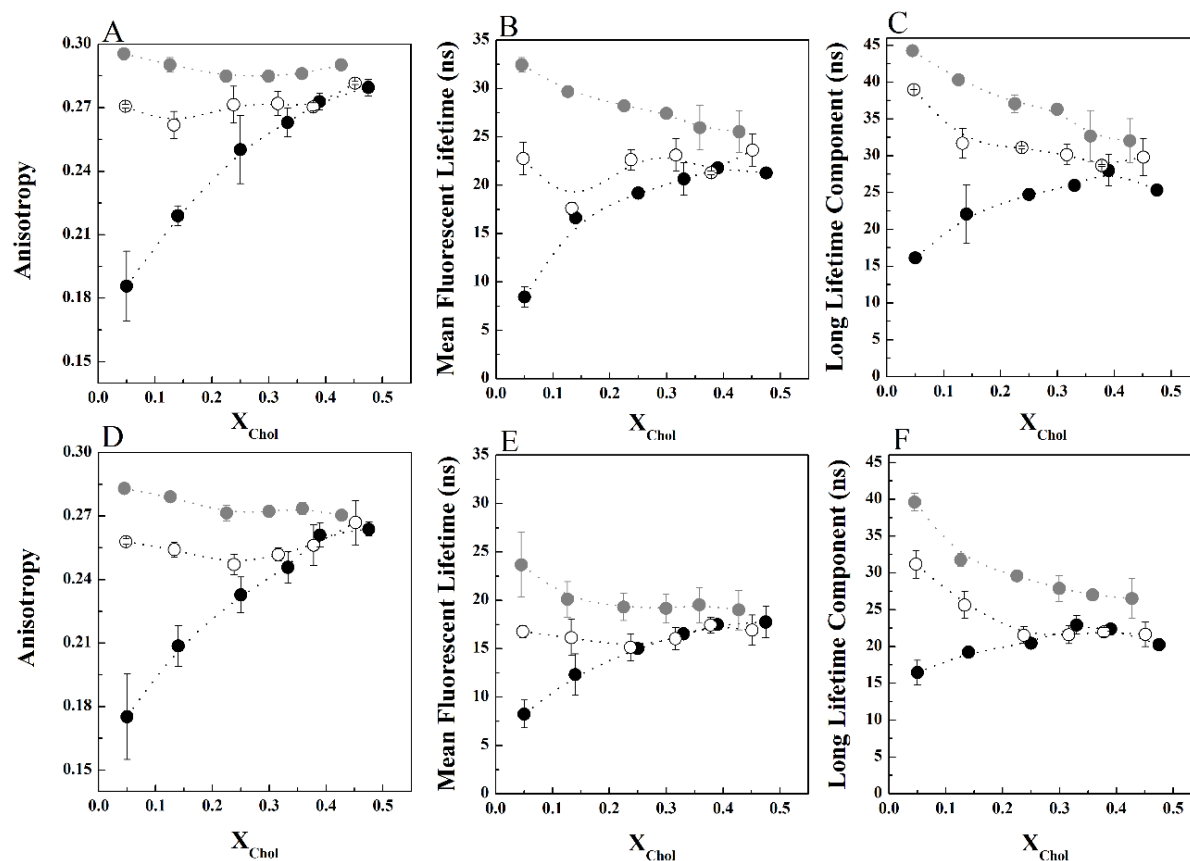
Figure 1 - Biophysical properties of of POPC/C16-SM/Chol/C16-GlcCer at different pH. *t*-PnA (A, D) fluorescence anisotropy, (B, E) mean fluorescence lifetime and (C,F) long lifetime component of the intensity decay in POPC/C16-SM/Chol mixtures containing 0 (solid black circles), 5 (open circles) and 10 (solid grey circles) mol% of C16-GlcCer. Measurements were performed at (A-C) pH 7.4 and (D-F) 5.5. Values are means ± SD of at least 3 independent experiments.

4.1.3 Fluorescence microscopy studies

Fluorescence microscopy studies were performed to further characterize the biophysical properties of the mixtures, as well as structural alterations of the vesicles. To perform these studies two fluorescent probes were used: NBD-DPPE that is excluded from the gel phase, but has a strong partition into the l_o-phase [28], and Rho-DOPE that is excluded both from the gel and the l_o phases [29]. Accordingly, gel phase regions can be distinguished as

dark areas that exclude both probes, bright regions are assigned to the l_d phase, while the l_o-enriched phase correspond to areas that incorporate NBD probe, but exclude Rho. Similarly to observed by fluorescence spectroscopy, analysis of the vesicles by fluorescence microscopy showed that C16-GlcCer drives an extensive gel-fluid phase separation in vesicles containing low Chol content (Fig. 2A and S3A), as shown by the dark regions with irregular shapes [30]. The extent of phase separation is larger upon increasing C16-GlcCer content, irrespective of pH environment (Fig. 2 and S3) Note that, in the absence of C16-GlcCer, the ternary mixtures with low Chol content do not present l_o/l_d phase separation under the microscope according to what is expected for this particular ternary mixture, since the l_o domains ate too small to be detected[28]. (Fig. S3). For ternary mixtures containing a larger l_o phase fraction (Table 1 and Fig. 2A), l_o/l_d phase separation is observed, at least in neutral pH, and the extent of phase separation increases
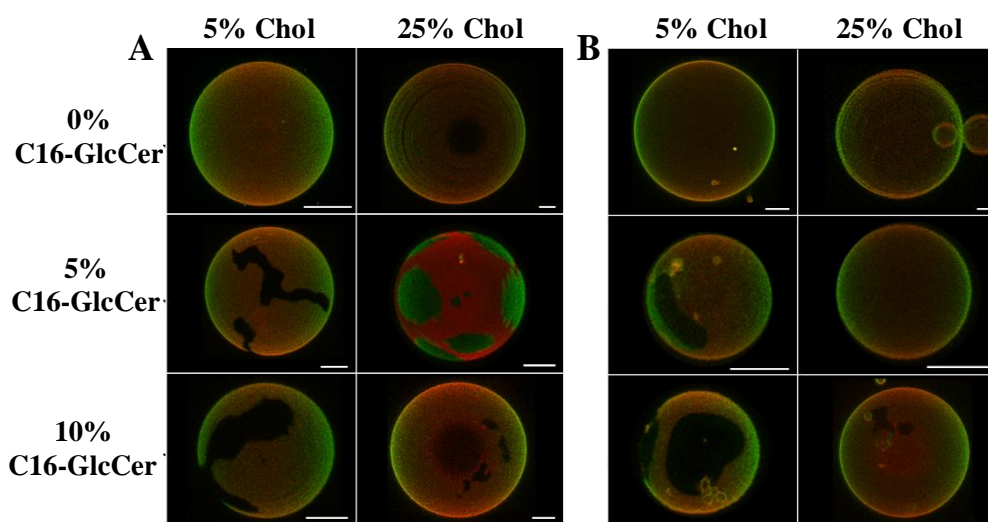
Figure 2 - Confocal fluorescence microscopy of POPC/C16-SM/Chol and POPC/C16-SM/Chol/C16-GlcCer mixtures.
3D projection images from 0.4 μm confocal slices of POPC/C16-SM/Chol GUVs in the absence and presence of 5 and 10 mol% of C16-GlcCer. Images correspond to the overlay of the NBD-DPPE (green) and Rho-DOPE (red) channels. Images were taken at (A) neutral (7.4) and (B) acidic (5.5) pH. Scale bar, 5 μm.

with increasing Chol and SM content of the mixtures, in agreement with previous observations [14]. Upon adding C16-GlcCer to the ternary mixtures with high l_o fraction, C16-GlcCer-induced gel domain formation is no longer observed, which is also confirmed

by the lower values or even the absence of a fourth component in *t*-PnA lifetime decay (Fig. S2). However, in opposition to what would be anticipated [31], l_o-enriched domains displayed irregular interfaces, suggesting that these might result from the presence of a small fraction of gel phase and/or due to the formation of a phase with intermediate properties between the gel and the l_o-phase. This would also justify why the long lifetime component of *t*-PnA (Fig 1 C and F) presented values close to or slightly above of the fingerprint of a gel phase [14].

The effects of C16-GlcCer in mixtures containing larger Chol and SM content studied under acidic conditions were much less pronounced (Fig.2B and S3B), in agreement with data obtained from spectroscopy (Fig.1 and Supplementary 2).

No significant alterations were observed in the morphology of the vesicles, irrespective of their lipid composition, except in the mixtures studied under acidic conditions which displayed a higher tendency to aggregate (Fig. S3).

4.1.4 Dynamic and electrophoretic light scattering studies

To gain further insight into the properties of the vesicles, dynamic and electrophoretic light scattering studies were performed. At neutral pH no significant variation in the average size of the vesicles was observed upon changing the composition of the ternary mixtures (~115nm) (Fig. 3A, B). However, a slight increase in the average size was observed when the GlcCer content of the quaternary mixtures was increased (~135nm and ~150 nm with 5 and 10 mol% of GlcCer, respectively) (Figs 3A, C and D). This is likely due to a higher tendency for vesicle aggregation due to the alteration of the surface charge of the vesicles, which shift to neutrality as the GlcCer content of the vesicles increases (Fig. 3E). In the absence of GlcCer, the electronegativity of the mixtures induces an electrostatic repulsion of the vesicles, preventing vesicle aggregation. Indeed, analysis of the PdI of the mixtures showed a slight increase in the PdI with the increase in GlcCer molar fraction (Fig. 3F), supporting the higher tendency of these mixtures to self-aggregate.
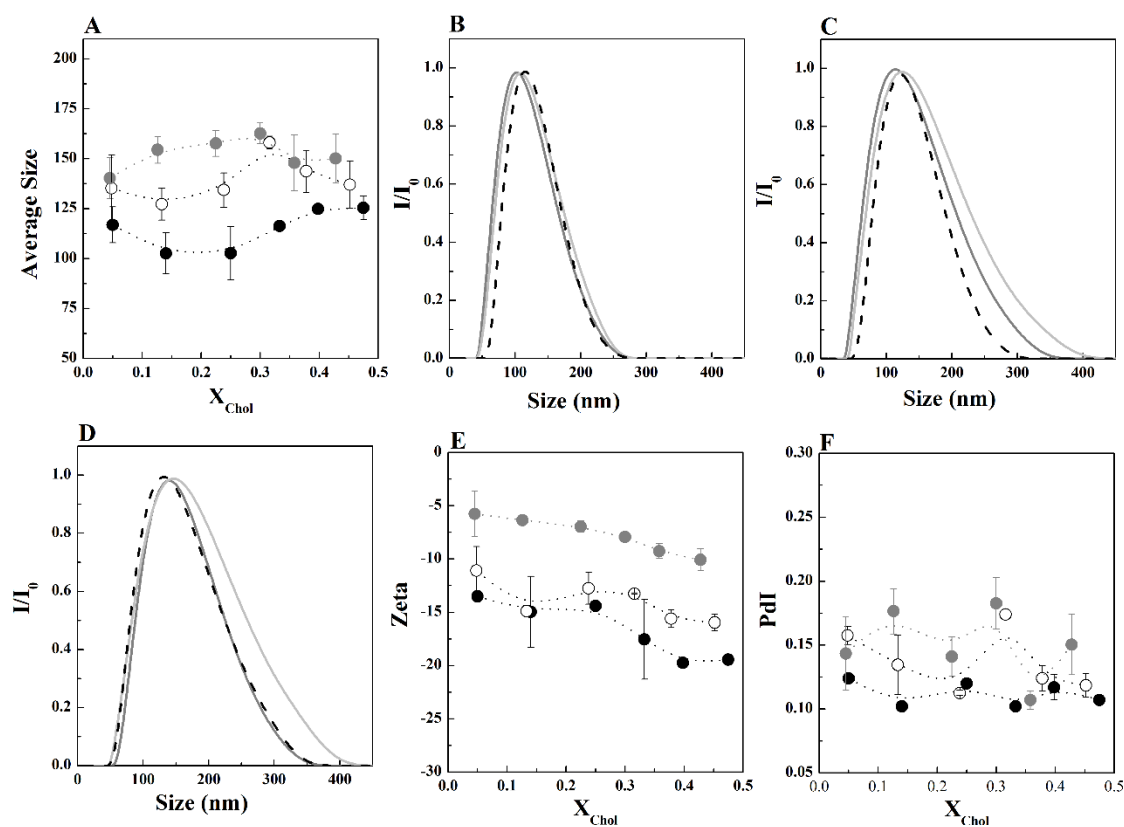
Figure 3 - Characterization of POPC/C16-SM/Chol/C16-GlcCer mixtures by electrophoretic and dynamic light scattering measurements, under neutral conditions.
(A) Average size; (E) ζ- potential of LUVs and (F) PdI composed by POPC/C16-SM/Chol mixtures, containing 0 (black solid symbols), 5 (open circles) and 10 (grey solid circles) mol% of C16-GlcCer. (B-D) Normalized scattered light intensity of POPC/C16-SM/Chol/C16-GlcCer LUVs containing (B) 14 (—),33 (—), 48 (---) mol% of Chol and 0 mol% of GlcCer; (C) 13 (—),32 (—),45 (---) mol% of Chol and 5 mol% of C16-GlcCer; and (D) 13 (—), 30 (—),43 (---) mol% of Chol and 10 mol% of C16-GlcCer. Values are means ± SD of at least 3 independent experiments.

An increase in the average size of the vesicles was also observed under acidic conditions (Fig. 4A), but the extent of variation of the different parameters is larger compared to the one verified in neutral conditions. A larger increment in the average size and PdI (Fig. 4A and B) of the vesicles was observed upon increasing Chol and SM content of the mixtures. Likewise, increasing C16-GlcCer content of the mixtures also contributed to an overall increase in the size of the vesicles (Fig.4A, C-E). This higher tendency to aggregate is probably due to a global surface charge close to neutrality that minimizes the repulsion between the vesicles (Fig. 4F).
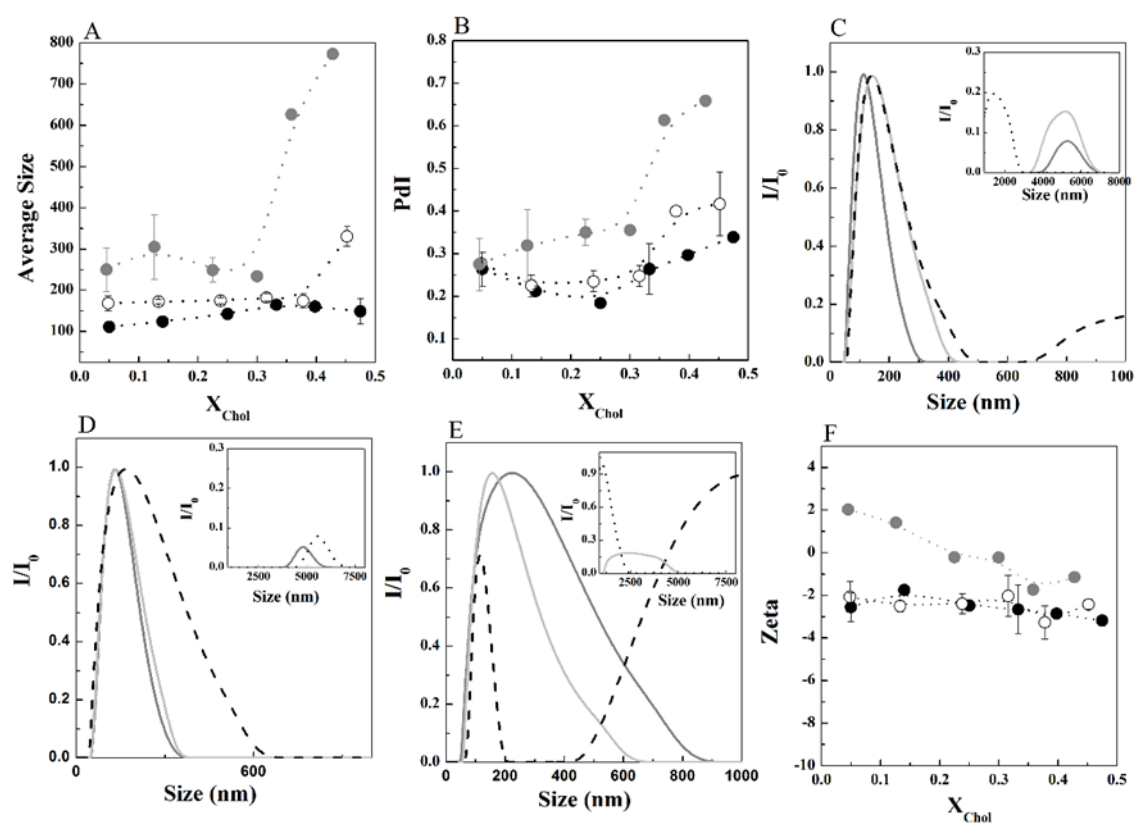
Figure 4 - Characterization of POPC/C16-SM/Chol/C16-GlcCer mixtures by electrophoretic and dynamic light scattering measurements, at acidic pH.(5.5)

(A) Average size; (B) PdI and (F) ζ- potential of POPC/C16-SM/Chol LUVs containing 0 (black solid circles) , 5 (open circles) and 10 (grey solid circles) mol% of C16-GlcCer. (C-E) Normalized scattered light intensity of POPC/C16-SM/Chol/C16-GlcCer LUVs containing (C) 14 (—),33 (—), 48 (---) mol% of Chol and 0 mol% of GlcCer; (D) 13 (—),32 (—),45 (---) mol% of Chol and 5 mol% of C16-GlcCer; and (E) 13 (—), 30 (—),43 (---) mol% of Chol and 10 mol% of C16-GlcCer. Inset shows vesicle population with sizes in the order of microns. Values are means ± SD of at least 3 independent experiments.

4.2 Studies in living cells

To study the biophysical impact of GlcCer in biological membranes and evaluate whether GlcCer is able to increase the packing of membranes from living cells, a fibroblast cell line derived from patients with GD type I (N370S/N370S) was selected and compared to primary wild type human skin fibroblasts. Fig. 5 shows that t-PnA fluorescence anisotropy (Fig. 5A) and mean fluorescence lifetime (Fig. 5B) are higher in mutant fibroblasts, suggesting an overall increase in membrane order compared to control fibroblasts. These

results are compatible with an ordering effect promoted by increased content of GlcCer, in accordance with the model membrane data. This is further confirmed by the strong increase in the long lifetime component of the fluorescence intensity decay of *t*-PnA in GD fibroblasts to values close to the fingerprint of the gel phase (Fig. 5C). These results clearly show that accumulation of GlcCer influences the packing properties of biological membranes.
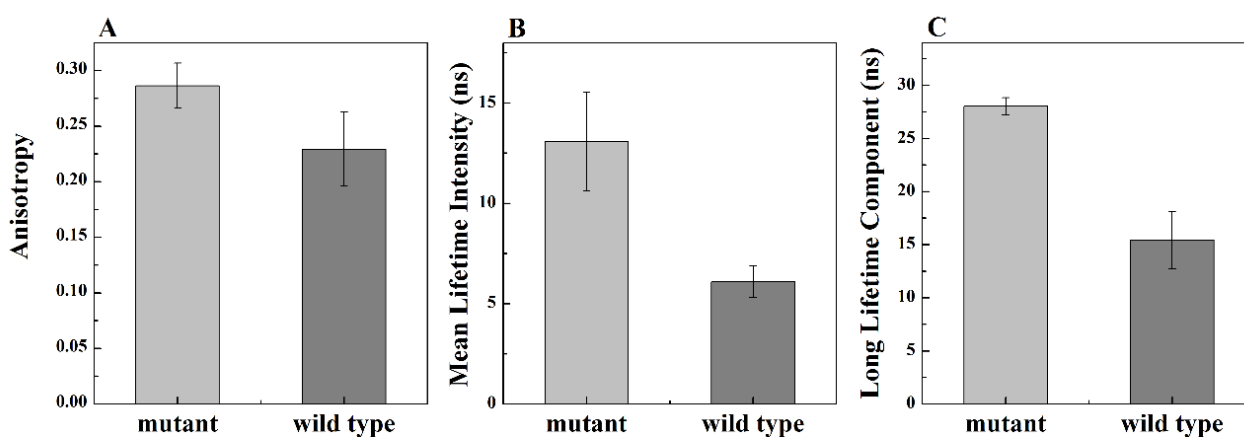
Figure 5 - Biophysical characterization of wt and GD type I mutant fibroblasts.

t-PnA (A) fluorescence anisotropy, (B) mean fluorescence lifetime and (C) long lifetime component of the intensity decay in GD type I mutant (light grey) and wild type fibroblasts (dark grey). Values are means ± SD of at least 3 independent experiments.

5 Discussion

5.1 Interplay between GlcCer and lipid components of model raft domains

It is hypothesized that the biophysical changes induced by GlcCer underlie its biological actions, but the molecular mechanisms that connect the biophysical and biological roles of this lipid remain to be elucidated. The aim of the present study was to provide further insight into the biophysical properties of GlcCer and its interplay with key lipids.

In resemblance to ceramides, GlcCer displays a high tendency to segregate into domains with gel properties, mainly due to its relatively small polar headgroup, high gel-to-fluid melting temperature and ability to function both as donor and acceptor for H-bonding [8]. GlcCer is also able to interact with Chol and participate in the formation of l_o phase – a phase that defines the biophysical features of the so-called raft domains[32, 33]. Compared

to SM, GlcCer is however less prone to segregate into l_o-phase. In contrast, lower levels of GlcCer are required to drive gel-fluid phase separation (in chapter IV). In this study we expanded our knowledge on the biophysical effects of GlcCer, by investigating the interactions between GlcCer and mixtures with lipid composition able to form model lipid raft domains.

This study showed that GlcCer increases the order of the membranes, irrespective of their lipid composition. However, the types of phases induced by GlcCer are strongly dependent on the Chol and SM content of the mixtures. Accordingly, in mixtures containing lower Chol content (up to 35 mol%), GlcCer induces gel-fluid phase separation. Interestingly, in binary POPC/GlcCer and ternary POPC/Chol/GlcCer mixtures (see previous chapter), the same content of GlcCer (5 and 10 mol%) is not enough to induce gel-domain formation [8]. Indeed, 15 and 20 mol% of GlcCer are required to drive gel domain formation in the binary [8] and ternary mixtures (chapter IV), respectively. These results suggest that in the presence of SM the miscibility of GlcCer in the fluid phase is decreased, probably due to association between SM and GlcCer that together contribute to gel-domain formation. This may result from the establishment of an efficient H-bond network between these two lipids. Similar interactions have already been reported for mixtures containing SM and ceramide in the absence and presence of Chol[34, 35], suggesting that this might be a common feature to different SLs.

The ability of GlcCer and SM to phase separate into gel domains is strongly balanced by increased levels of Chol. Indeed, a key biophysical property of Chol, and which has been considered as one of its most important features, is the ability to abolish the gel-fluid phase transition of lipids, by promoting the formation of the intermediate state l_o phase [13, 36]. Therefore, it is not unexpected that mixtures containing more Chol display lower ability to form gel domains. However, the effect of GlcCer in these mixtures is still remarkable: the presence of GlcCer induces not only an increase in the packing properties of the l_o-phase but also an increase in the extent of this ordered phase, particularly in those mixtures displaying intermediate levels of l_o-phase. A previous study suggested that sterol-enriched domains could only accommodate a small amount of GlcCer [12], which would contradict our evidence. However, in that study sphingomyelin was not present in the mixture. Maunula et al. reported that SM can promote pack defects in GlcCer enriched domains, promoting the incorporation of Chol and, in addition, it is also

reported that cerebrosides do not readily interact with Chol when they are the only sphingolipid in the membrane[16, 37]. Moreover, the proportion between the neutral cerebroside, SM and Chol is also important, since it reflects the interaction between these lipids. An example is the study by Björkvist et al. where the biophysical behavior of lipid mixtures with GalCer/SM/Chol was studied in vesicles containing higher content of both GalCer and SM compared to Chol. Under the experimental conditions employed by the authors, where mixtures containing 30 mol% of GalCer and SM and 9 mol% of Chol were used, it is not surprising that GalCer and SM would interact and segregate into gel-enriched domains and only a small fraction of the GSL would be present in the sterol-enriched l_o domains [38].

Ceramides are also able to increase the order of the l_o-phase [13, 14, 39]. However, their ability to increase the size and fraction of l_o phase domains was not significant compared to the observed in the present study. These results therefore highlight how two structurally similar lipids might cause different changes in membrane organization and properties, suggesting that interconversion between ceramide and GlcCer might result in specific alterations in the biophysical properties of the membranes.

Our results further show that changes in pH environment also promote significant alterations in the organization and in the physical and electrostatic properties of membranes enriched in GlcCer. In the present study we further confirmed the decreased ability of GlcCer to induce gel domain formation, and increase the order of the membrane under acidic conditions, irrespective of the lipid composition of the mixtures. These observations are in agreement with our previous studies in simpler model membranes [9]. These differences in the packing properties and membrane organization might arise from alterations in the H-bonding network established between GlcCer molecules, neighbor lipids and water molecules [16, 40], and by the alteration of the orientation of the glucose moiety at the membrane interface [41] as previously suggested [9]. Moreover, an increase in the overall surface charge of the vesicles from electronegative to neutral upon acidification, indicates a shift from electron to proton association with the lipid groups at the membrane surface. Since no significant changes in the overall charge of the lipid constituents of the mixtures are expected [9, 42, 43, 44], it can be hypothesized that alterations in the surface charge might also be driven by changes in the orientation of the lipid headgroups[45], alterations in H-bonding states and lipid organization which would also

contribute to a lower packing of the lipids and/or ability to form tightly-packed gel domains.

5.2 Influence of GlcCer in cell membrane biophysical properties

Even though a vast number of studies have been made to understand the cellular role of GlcCer, particularly regarding GD [2, 7, 46, 47, 48, 49], little attention has been given to the biophysical effects of this important signaling lipid. GlcCer is thought to be associated with lipid domains, from where it might exert its biological roles through the alteration in membrane biophysical properties [8]. Until now, biophysical studies that addressed the impact of GlcCer, were only performed in simpler model membranes. These model membranes studies are fundamental to understand the interplay between different lipids and to provide the adequate tools to understand the biophysical impact of a given lipid in the extremely complex biological membranes. In this and in our previous studies, it was shown that GlcCer changes the biophysical properties of fluid model membranes containing distinct lipid composition. Particularly, increase in the content of GlcCer results in membrane ordering, either due to the formation of a GlcCer-enriched gel phase or GlcCer-enriched l_o-phase, depending on the lipid composition of the artificial membranes. Using the photophysical fingerprints of t-PnA, it was also possible to assess the effect of GlcCer in membranes of living cells, through comparison of the biophysical properties between cells carrying a mutation homozygote for the N370S, thus characteristic of GD type I, and wild type fibroblasts. The results allowed concluding that enrichment in GlcCer, as observed in mutant Gaucher fibroblasts leads to an increase in the order of the membrane. These results are consistent with the data obtained in model membranes that predict an increase in the packing properties of the membrane upon increasing GlcCer content. Moreover, the very long lifetime component of t-PnA fluorescence intensity decay shows that regions that display properties resembling a gel-like phase are present in GD mutant cells. Whether these are driven by GlcCer ability to segregate into gel domains or due to association between GlcCer and other membrane lipids prone to form gel phases, such as ceramides [10], SM (as shown in the present study) [27] or even saturated phospholipids [50], is at present not known. The interactions that occur in cell membranes are complex, involving different lipids and proteins, which, in addition to GlcCer accumulation, will be important determinants in the development of GD

pathophysiology. Nevertheless, the results obtained in the present study point towards a change in the biophysical properties of the membrane, which certainly influence diverse cellular processes, including lipid and protein trafficking, sorting and recycling [51, 52,53] that can ultimately impair cell function. Further investigation of the biophysical changes associated to accumulation of GlcCer in GD might therefore contribute to the understanding of the molecular mechanisms underlying this complex disease.

6 Conclusions and Biological Implications

The biophysical study of POPC/C16-SM/ Chol/ C16-GlcCer mixtures enabled to confirm several aspects regarding the effect of GlcCer in the organization of membranes (either natural or artificial). Coherently and complementing previous reports [8], the present study allowed to confirm that even in more complex membranes, GlcCer increases membrane packing properties, although this property is modulated by Chol levels. The ability of GlcCer to stabilize l_o domains further supports the role of this lipid in the formation of membrane specialized domains. This further suggests that GlcCer-mediated biological action might be linked to lipid domain formation and GlcCer-induced biophysical changes. This might have important consequences, particularly taking into account that an abnormal increase in GlcCer, such as observed in GD, drives significant alterations in the packing properties of biological membranes. The increased membrane rigidity observed in cells from GD patients might disturb several cellular processes, which could underlie some of the mechanisms involved in the triggering of GD.

The present study further highlights the use of synthetic biology approaches, such as the artificial membranes used in this work, to obtain important insights regarding the effects of individual lipid components in their more complex biomembranes environment.

7 Acknowledgements

8 References

1.   DEGROOTE, S.; WOLTHOORN, J.; VANMEER, G. The cell biology of glycosphingolipids. SEMIN CELL DEV BIOL 2004, 15 (4), 375-387.

2.   VAN MEER, G.; WOLTHOORN, J.; DEGROOTE, S. The fate and function of glycosphingolipid glucosylceramide. PHIL TRANS R SOC B 2003, 358 (1433), 869-873.

3.   LIU, Y.-Y.; HAN, T.-Y.; GIULIANO, A. E.; CABOT, M. C. Expression of Glucosylceramide Synthase, Converting Ceramide to Glucosylceramide, Confers Adriamycin Resistance in Human Breast Cancer Cells. J BIOL CHEM 1999, 274 (2), 1140-1146.

4.   HANNUN, Y. A.; LUBERTO, C. Ceramide in the eukaryotic stress response. TRENDS CELL BIOL 10 (2), 73-80.

5.   DEGUCHI, H.; FERNÁNDEZ, J.; PABINGER, I.; HEIT, J. A.; GRIFFIN, J. H. Plasma glucosylceramide deficiency as potential risk factor for venous thrombosis and modulator of anticoagulant protein C pathway. BLOOD 2001, 97 (7), 1907-1914.

6.   DATTA, S.; RADIN, N. Stimulation of liver growth and DNA synthesis by glucosylceramide. LIPIDS 1988, 23 (5), 508-510.

7.   MESSNER, M. C.; CABOT, M. C. Glucosylceramide in humans. ADV EXP MED BIOL 2010, 688, 154-64.

8.   VARELA, A. R. P.; GONÇALVES DA SILVA, A. M. P. S.; FEDOROV, A.; FUTERMAN, A. H.; PRIETO, M.; SILVA, L. C. Effect of glucosylceramide on the biophysical properties of fluid membranes. BIOCHIM BIOPHYS ACTA 2013, 1828 (3), 1122-1130.

9.   VARELA, A. R. P.; GONÇALVES DA SILVA, A. M. P. S.; FEDOROV, A.; FUTERMAN, A. H.; PRIETO, M.; SILVA, L. C. Influence of Intracellular Membrane pH on Sphingolipid Organization and Membrane Biophysical Properties. LANGMUIR 2014, 30 (14), 4094-4104.

10.   SILVA, L.; DE ALMEIDA, R. F. M.; FEDOROV, A.; MATOS, A. P. A.; PRIETO, M. Ceramide-platform formation and -induced biophysical changes in a fluid phospholipid membrane. MOL MEMBR BIOL 2006, 23 (2), 137-148.

11.   PINTO, S. N.; SILVA, L. C.; FUTERMAN, A. H.; PRIETO, M. Effect of ceramide structure on membrane biophysical properties: The role of acyl chain length and unsaturation. BIOCHIM BIOPHYS ACTA 2011, 1808 (11), 2753-2760.

12.   SLOTTE, J. P.; OESTMAN, A. L.; KUMAR, E. R.; BITTMAN, R. Cholesterol interacts with lactosyl and maltosyl cerebrosides but not with glucosyl or galactosyl cerebrosides in mixed monolayers. BIOCHEMISTRY 1993, 32 (31), 7886-7892.

13.   CASTRO, B. M.; SILVA, L. C.; FEDOROV, A.; DE ALMEIDA, R. F. M.; PRIETO, M. Cholesterol-rich Fluid Membranes Solubilize Ceramide Domains: Implcations for the Structure and Dynamics of Mammmalian Intracellular and Plasma Membranes. J BIOL CHEM 2009, 284 (34), 22978-22987.

14.   SILVA, L. C.; DE ALMEIDA, R. F. M.; CASTRO, B. M.; FEDOROV, A.; PRIETO, M. Ceramide-Domain Formation and Collapse in Lipid Rafts: Membrane Reorganization by an Apoptotic Lipid. BIOPHYS J 2007, 92 (2), 502-516.

15.   ALI, M. R.; CHENG, K. H.; HUANG, J. Ceramide Drives Cholesterol Out of the Ordered Lipid Bilayer Phase into the Crystal Phase in 1-Palmitoyl-2-oleoyl-sn-glycero-3-phosphocholine/Cholesterol/Ceramide Ternary Mixtures†. BIOCHEMISTRY 2006, 45 (41), 12629-12638.

16.   MAUNULA, S.; BJÖRKQVIST, Y. J. E.; SLOTTE, J. P.; RAMSTEDT, B. Differences in the domain forming properties of N-palmitoylated neutral glycosphingolipids in bilayer membranes. BIOCHIM BIOPHYS ACTA 2007, 1768 (2), 336-345.

17. Grabowski, G. A. Phenotype, diagnosis, and treatment of Gaucher's disease. Lancet 2008, 372 (9645), 1263-1271.

18. Fuller, M.; Rozaklis, T.; Lovejoy, M.; Zarrinkalam, K.; Hopwood, J. J.; Meikle, P. J. Glucosylceramide accumulation is not confined to the lysosome in fibroblasts from patients with Gaucher disease. Mol Gen Metab 2008, 93 (4), 437-443.

19. Matsuzaki, K.; Murase, O.; Sugishita, K. I.; Yoneyama, S.; Akada, K. Y.; Ueha, M.; Nakamura, A.; Kobayashi, S. Optical characterization of liposomes by right angle light scattering and turbidity measurement. Biochim Biophys Acta 2000, 1467 (1), 219-226.

20. Hope, M. J.; Bally, M. B.; Webb, G.; Cullis, P. R. Production of large unilamellar vesicles by a rapid extrusion procedure. Characterization of size distribution, trapped volume and ability to maintain a membrane potential. Biochim Biophys Acta 1985, 812 (1), 55-65.

21. Pinto, S. N.; Silva, L. C.; de Almeida, R. F. M.; Prieto, M. Membrane Domain Formation, Interdigitation, and Morphological Alterations Induced by the Very Long Chain Asymmetric C24:1 Ceramide. Biophys J 2008, 95 (6), 2867-2879.

22. Sarmento, M. J.; Prieto, M.; Fernandes, F. Reorganization of lipid domain distribution in giant unilamellar vesicles upon immobilization with different membrane tethers. Biochim Biophys Acta 2012, 1818 (11), 2605-2615.

23. Lakowicz, J. R. 3rd ed.; Springer: New York, 2006.

24. Birch, D. S.; Imhof, R. Time-Domain Fluorescence Spectroscopy Using Time-Correlated Single-Photon Counting. In Topics in Fluorescence Spectroscopy, Lakowicz, J., Ed.; Springer US, 2002; Vol. 1, pp 1-95.

25. de Almeida, R. F. M.; Fedorov, A.; Prieto, M. Sphingomyelin/Phosphatidylcholine/Cholesterol Phase Diagram: Boundaries and Composition of Lipid Rafts. Biophys J 2003, 85, 2406-2416.

26. Fidorra, M.; Duelund, L.; Leidy, C.; Simonsen, A. C.; Bagatolli, L. A. Absence of Fluid-Ordered/Fluid-Disordered Phase Coexistence in Ceramide/POPC Mixtures Containing Cholesterol. Biophys J 2006, 90 (12), 4437-4451.

27. Castro, B. M.; de Almeida, R. F. M.; Silva, L. C.; Fedorov, A.; Prieto, M. Formation of Ceramide/Sphingomyelin Gel Domains in the Presence of an Unsaturated Phospholipid: A Quantitative Multiprobe Approach. Biophys J 2007, 93, 1639-1650.

28. de Almeida, R. F. M.; Loura, L. M. S.; Fedorov, A.; Prieto, M. Lipid Rafts have Different Sizes Depending on Membrane Composition: A Time-resolved Fluorescence Resonance Energy Transfer Study. J Mol Biol 2005, 346, 1109-1120.

29. Castro, B. M.; de Almeida, R. F. M.; Fedorov, A.; Prieto, M. The photophysics of a Rhodamine head labeled phospholipid in the identification and characterization of membrane lipid phases. Chem Phys Lipids 2012, 165 (3), 311-319.

30. Bagatolli, L. A.; Gratton, E. Two Photon Fluorescence Microscopy of Coexisting Lipid Domains in Giant Unilamellar Vesicles of Binary Phospholipid Mixtures. Biophys J 2000, 78, 290-305.

31. Heberle, F. A.; Feigenson, G. W. Phase Separation in Lipid Membranes. Cold Spring Harb Perpect Biol 2011, 3 (4), a004630.

32. Brown, D. A.; London, E. Structure and Origin of Ordered Lipid Domains in Biological Membranes. J Membr Biol 1998, 164 (2), 103-114.

33. Bakht, O.; Delgado, J.; Amat-Guerri, F.; Acuña, A. U.; London, E. The phenyltetraene lysophospholipid analog PTE-ET-18-OMe as a fluorescent anisotropy probe of liquid ordered membrane domains (lipid rafts) and ceramide-rich membrane domains. Biochim Biophys Acta 2007, 1768 (9), 2213-2221.

34.   Sot, J.; Ibarguren, M.; Busto, J. V.; Montes, L. R.; Goñi, F. M.; Alonso, A. Cholesterol displacement by ceramide in sphingomyelin-containing liquid-ordered domains, and generation of gel regions in giant lipidic vesicles. FEBS Lett 2008, 582 (21-22), 3230-3236.

35.   Massey, J. B. Interaction of ceramides with phosphatidylcholine, sphingomyelin and sphingomyelin/cholesterol bilayers. Biochim Biophys Acta 2001, 1510 (1–2), 167-184.

36.   Krause, M. R.; Regen, S. L. The Structural Role of Cholesterol in Cell Membranes: From Condensed Bilayers to Lipid Rafts. Acc Chem Res 2014, 47 (12), 3512-3521.

37.   Ruocco, M. J.; Shipley, G. G. Interaction of cholesterol with galactocerebroside and galactocerebroside-phosphatidylcholine bilayer membranes. Biophys J 1984, 46 (6), 695-707.

38.   Björkqvist, Y. J. E.; Nyholm, T. K. M.; Slotte, J. P.; Ramstedt, B. Domain Formation and Stability in Complex Lipid Bilayers as Reported by Cholestatrienol. Biophys J 2005, 88 (6), 4054-4063.

39.   Chiantia, S.; Kahya, N.; Ries, J.; Schwille, P. Effects of Ceramide on Liquid-Ordered Domains Investigated by Simultaneous AFM and FCS. Biophys J 2006, 90 (12), 4500-4508.

40.   Westerlund, B.; Slotte, J. P. How the molecular features of glycosphingolipids affect domain formation in fluid membranes. Biochim Biophys Acta 2009, 1788 (1), 194-201.

41.   Nyholm, P.-G.; Pascher, I. Orientation of the Saccharide Chains of Glycolipids at the membrane Surface: Conformational Analysis of the Glucose-Ceramide and the Glucose-Glyceride Linkages Using Molecular Mechanics (MM3). Biochemistry 1993, 32, 1225-1234.

42.   Dewick, P. M. Acids and Bases. In Essentials of Organic Chemistry: For Students of Pharmacy, Medicinal Chemistry and Biological Chemistry, Dewick, P. M., Ed.; John Wiley & Sons, Inc.: Hoboken, 2006, pp 120-164.

43.   Petelska, A. D.; Naumowicz, M.; Figaszewski, Z. A. Influence of pH on Sphingomyelin Monolayer at Air/Aqueous Solution Interface. Langmuir 2012, 28 (37), 13331-13335.

44.   Bernchou, U.; Midtiby, H.; Ipsen, J. H.; Simonsen, A. C. Correlation between the ripple phase and stripe domains in membranes. Biochim Biophys Acta 2011, 1808 (12), 2849-2858.

45.   Doux, Jacques P. F.; Hall, Benjamin A.; Killian, J. A. How Lipid Headgroups Sense the Membrane Environment: An Application of 14N NMR. Biophys J 2012, 103 (6), 1245-1253.

46.   Sillence, D. J. Glucosylceramide modulates membrane traffic along the endocytic pathway. J Lipid Res 2002, 43 (11), 1837-1845.

47.   Oku, H.; Wongtangtintharn, S.; Iwasaki, H.; Inafuku, M.; Shimatani, M.; Toda, T. Tumor specific cytotoxicity of glucosylceramide. Cancer Chemother Pharmacol 2007, 60 (6), 767-775.

48.   Jmoudiak, M.; Futerman, A. H. Gaucher disease: pathological mechanisms and modern management. Br J Haematol 2005, 129 (2), 178-188.

49.   Zigmond, E.; Preston, S.; Pappo, O.; Lalazar, G.; Margalit, M.; Shalev, Z.; Zolotarov, L.; Friedman, D.; Alper, R.; Ilan, Y. b-Glucosylceramide: a novel method for enhancement of natural killer T lymphoycte plasticity in murine models of immune-mediated disorders. Gut 2007, 56 (1), 82-89.

50.   Svetlovics, James A.; Wheaten, Sterling A.; Almeida, Paulo F. Phase Separation and Fluctuations in Mixtures of a Saturated and an Unsaturated Phospholipid. Biophys J 2012, 102 (11), 2526-2535.

51.   Surma, M. A.; Klose, C.; Simons, K. Lipid-dependent protein sorting at the trans-Golgi network. Biochim Biophys Acta 2012, 1821 (8), 1059-1067.

52.   Sillence, D.; Platt, F. Glycosphingolipids in endocytic membrane transport. Semin Cell Dev Biol 2004, 15 (4), 409-416.

53.   Sillence, D. J. Glucosylceramide modulates endolysosomal pH in Gaucher disease. Mol Gen Metab 2013.

9 Supporting Material for: Glucosylceramide-induced biophysical changes in artificial and cell membranes
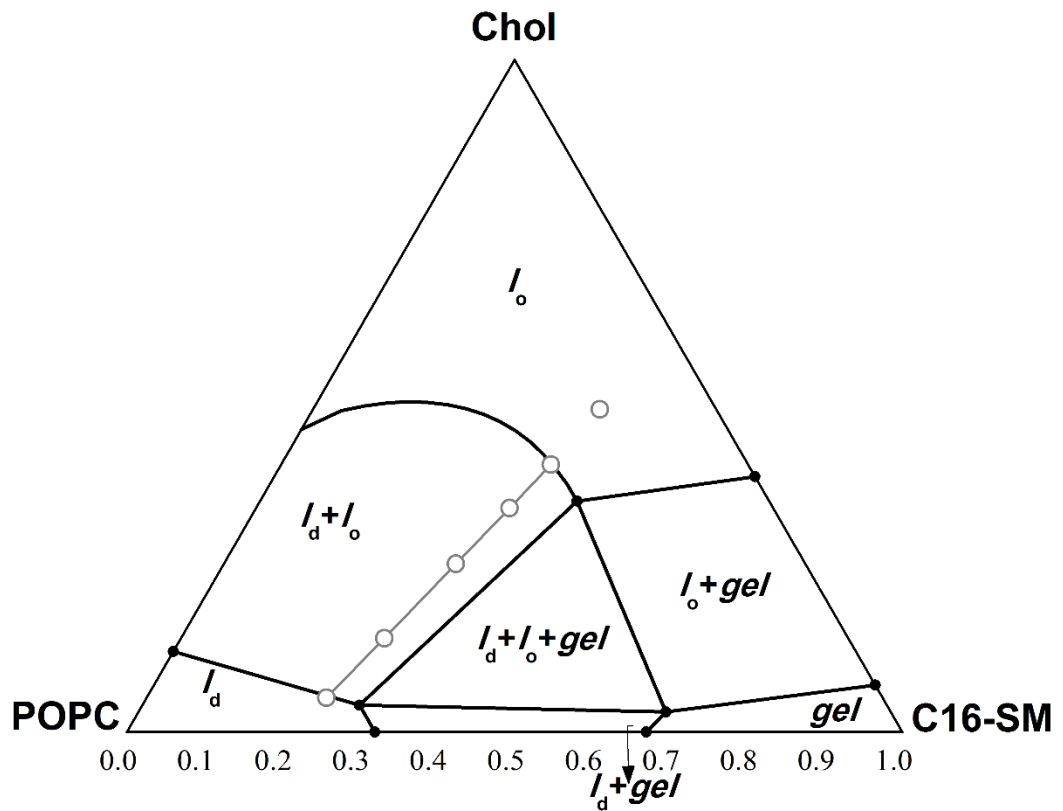
Figure S1 - POPC/C16-SM/Chol ternary phase diagram

The grey line is a tie-line that contains a 1:1:1 POPC/C16-SM/Chol mixture. The grey dots correspond to the mixtures used in this study. **(adapted from de Almeida et al.[25]).**
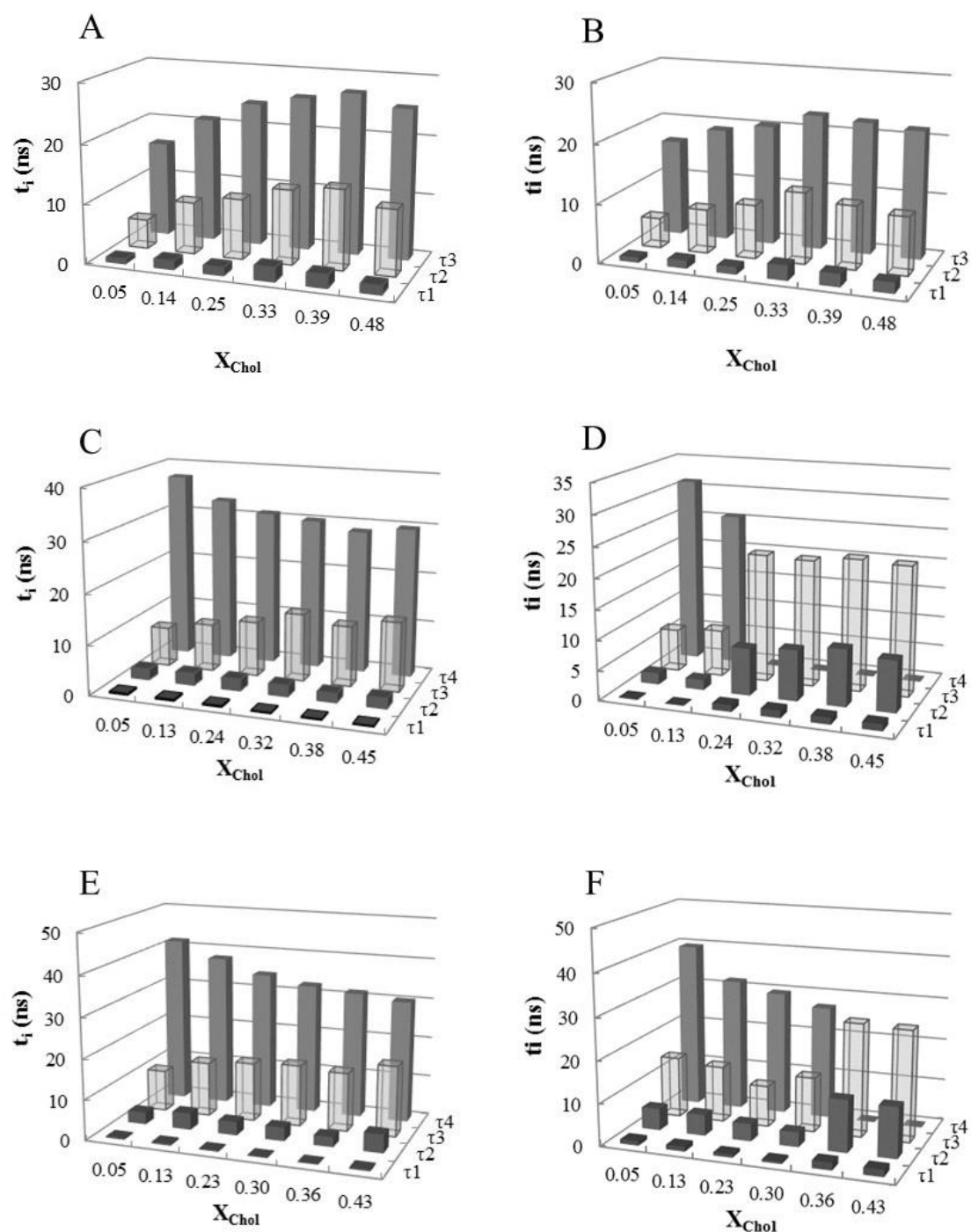
Figure S2 - Analysis of t-PnA fluorescence intensity decay components in POPC/C16-SM/Chol and POPC/C16-SM/Chol/C16-GlcCer mixtures.

Variation of the lifetime components of t-PnA intensity decay, in POPC/C16-SM/ Chol mixtures containing (A, B) 0, (C, D) 5 and (E, F) 10 mol% of C16-GlcCer. Measurements were performed at pH 7.4 (A, C, E) or at pH 5.5 (B, D, F). Values are means ± SD of at least 3 independent experiments.
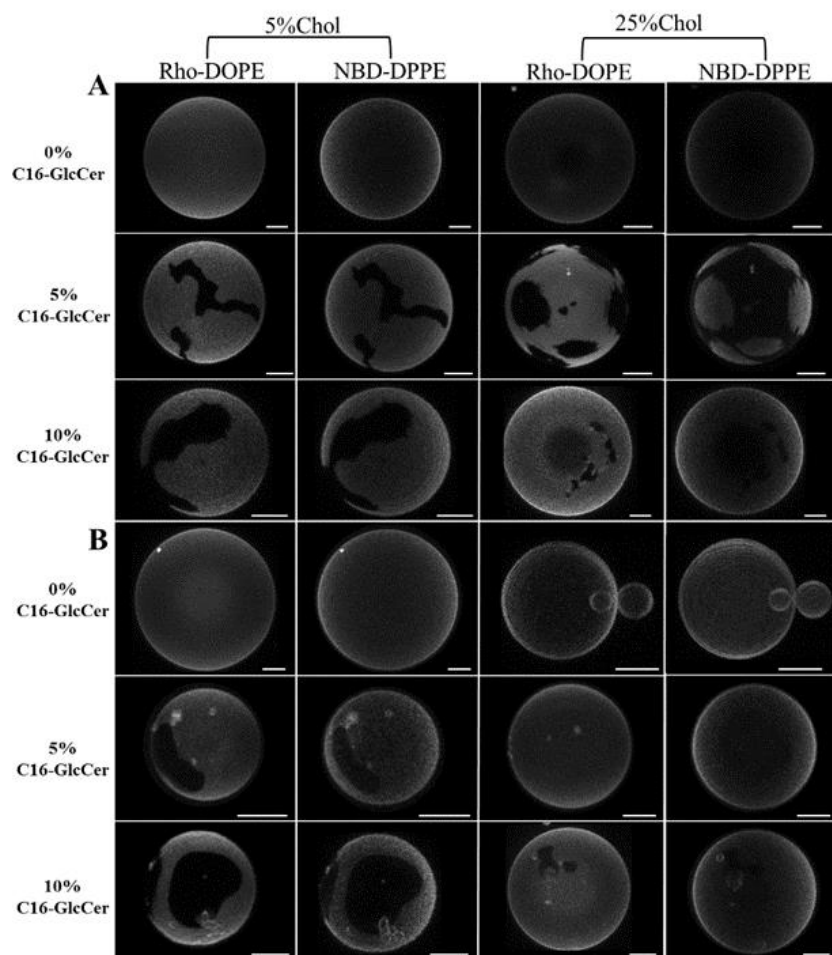
Figure S3 - Confocal fluorescence microscopy of POPC/C16-SM/Chol mixtures with and without C16-GlcCer.

3D projection images from 0.4 µm confocal slices of POPC/C16-SM/Chol GUVs containing increasing amounts of C16-GlcCer. Mixtures were, labelled with NBD-DPPE and Rho-DOPE, and images were taken at (A) neutral (7.4) and (B) acidic pH (5.5). Scale bar, 5 µm.

Chapter VI

Conclusions

Chapter VI

Conclusions

The biophysical properties of GlcCer had already been explored by other authors [1, 2, 3, 4, 5], however none of them made a systematic characterization of GlcCer biophysical impact in model and cell membranes.

Therefore, the aims of this work were to perform an exhaustive characterization of GlcCer properties, which was done by studying the effect of GlcCer in simple fluid model membranes (Chapter II); the impact of pH on the modulation of GlcCer biophysical properties (Chapter III); the influence of GlcCer in the biophysical behavior of model membranes containing Chol, without (chapter IV) and with SM (Chapter V), since Chol is a central element in the formation of l_o phase, associated with the formation of specialized membrane domains, and SM a lipid commonly associated to membrane compartmentalization. In addition, the impact of GlcCer in the biophysical properties of cell membranes (Chapter V), was also studied.

This work was designed aiming to obtain a detailed analysis of GlcCer biophysical properties. In order to do so, a multi-probe and multi-parameter approach was applied and complementary techniques such as fluorescence spectroscopy and microscopy were used. Moreover the use of fluorescence methodologies allowed using very low total lipid concentrations, which might reduce the possibility of GlcCer aggregation, due to its high hydrophobicity. Furthermore, the use of probes with different phase partition properties in confocal microscopy and fluorescence spectroscopy enabled the identification of coexistent lipid phases, as well as of morphological alterations promoted by the lipids used in this study. Further biophysical characterization of the membranes was possible through the use of other techniques such as the Langmuir trough, DLS, and electrophoretic light scattering. The monolayer studies enabled to clarify the effect of the subphase pH in the lipid-lipid interactions. The determination of vesicles size and charge, complemented and confirmed the evidence firstly obtained by the spectroscopy and microscopy techniques.

In Chapter II the biophysical properties of POPC and C16-GlcCer were characterized. In this study it was possible to conclude that C16-GlcCer, in resemblance to C16-Cer[6], influences membrane biophysical properties segregating into very compact gel domains that exclude probes that normally would be incorporated into them[6]. It is worthy to stress that the only probe that incorporates into these highly packed gel domains is t-PnA, which

in addition evidences a high sensitivity towards these domains. Nevertheless, even this probe is excluded when the concentration of GlcCer reaches more than 80 mol % of the lipid mixture[6, 7]. Furthermore, more molecules of GlcCer are needed to promote gel-fluid phase separation (≈10mol %)[8] in comparison to Cer (4 mol %)[6]. A partial binary phase diagram was determined, based in the thermotropic studies with mixtures of POPC/GlcCer. This phase diagram provides important information about the phase behavior of membranes that contain fluid lipids and GlcCer. For example, an extrapolation of the biophysical state of membranes containing-GlcCer could be made for physiological temperature. In addition, it was possible to identify that GlcCer promotes morphological changes in the membranes, through the formation of tubule-like structures. This type of structures were also found in very long asymmetrical ceramides such as C24:1 Cer and C24:0 Cer[9]. GlcCer induced-tubules could be involved in different cell events, such as cell to cell communication[10] or in the stabilization of protein fibrils[11].

In Chapter III, the effect of pH on the biophysical properties of membranes containing GlcCer and other SLs was studied. It was concluded that pH affects the properties of binary GlcCer-rich membranes, mainly by disturbing the packing of the gel domains. This property was specific of C16-GlcCer, since other non-charged SLs were insensitive (C16-Cer) or only showed any effect when very high concentrations (C24:1-Cer and C16-SM) were used, which are out of the biological scope. Acidic pH disturbs the hydrogen interactions between glucose headgroups in the GlcCer molecules, which form looser gel domains, in comparison to neutral conditions. In addition, the tubule-like structures induced by GlcCer are also affected by the environment pH, showing a stiffer nature at acidic pH. These alterations suggest that pH fluctuations, as in the endo-lysosomal pathway, might function as a fine tuning of the properties of GlcCer containing membranes, for example, by affecting protein sorting and conformation [12, 13].

Moreover, the study on Chapter IV highlights the interaction between GlcCer and one of the key lipids in the formation of membrane domains, Cholesterol. The spectroscopic study of POPC/Chol/C16-GlcCer mixtures, mainly by the analysis of the photophysical properties of *t*-PnA, together with the confocal images of GUVs composed by different mixtures of POPC/Chol with and without GlcCer enabled to determine a partial ternary phase diagram for such mixtures. This phase diagram is a valuable tool in the study of

(G)SLs phase behavior, in defined conditions. By comparing the POPC/Chol/GlcCer ternary phase diagram with diagrams where the GSL was replaced by other bioactive SLs, it is evident that there is a different interplay between GlcCer and Chol in comparison to the other bioactive SLs namely C16-Cer[14] and C16-SM[15] with the same sterol.

GlcCer is able to significantly increase the packing of membranes with low Chol content, promoting l_d-*gel* phase separation. However, increasing the molar fraction of Chol reduced the packing of the membranes and led to the formation of l_o domains, which can coexist with the l_d and *gel* domains. In opposition, ceramide displays a very low solubility into domains enriched in cholesterol, which precludes the formation of l_o phases. On other hand, mixtures containing C16-SM and Chol display a very large l_d-l_o phase coexistence in comparison to the mixtures containing C16-GlcCer. These differences in the interactions between different (G)SLs and Chol show that they have different effects on membrane organization. In addition, different fractions of each of these lipids in the membrane have a completely different effect in their biophysical properties, suggesting that alterations in SLs profile might impact on cell function through changes in membrane properties.

In Chapter V, the impact of GlcCer in model membranes mimicking the so-called raft domains shows that GlcCer is able to modulate the properties of those domains, especially in the presence of low Chol levels. In resemblance to the observations made in the simpler mixtures explored in the framework of Chapter IV, the increase in Chol levels reduced the ability of GlcCer to form gel domains and increase membrane packing properties. Nonetheless, the overall results obtained in the different model membranes studied show that GlcCer has a strong impact on membrane organization and packing properties, which suggests that increased levels of this lipid might promote strong alterations in the biophysical properties of biological membranes. Indeed, when the effect of GlcCer levels in membrane properties was directly studied in living cells, using wild type fibroblast versus GD type I fibroblasts, which have an abnormal higher level of GlcCer, it was concluded that GlcCer accumulation significantly affects the overall membrane fluidity, leading to an increase in their packing properties. These observations suggest that membrane biophysical properties might have a role in the molecular mechanisms underlying GD pathology. The increased rigidity of the membranes from GD

fibroblasts could alter protein conformation and consequently its activity, and also lipid and protein sorting, disturbing several signaling events [12,14,15].

In summary, in this work it was possible to conclude that:

I) C16-GlcCer increases the packing of fluid membranes

II) The increase of the environment pH affects the properties of GlcCer in a specific manner. The increase in the pH acidity disturbs the packing properties of the GlcCer-containing membranes, driving a lower packing at acidic in comparison to neutral environments.

III) C16-GlcCer promotes the formation of tubule-like structures which are pH sensitive.

IV) GlcCer interacts with Cholesterol forming l_o domains, suggesting that GlcCer has an active role in the formation of such domains

V) GlcCer modulates the properties of raft-like membranes, supporting the hypothesis that this lipid has an active participation in the formation of membrane domains thought to be involved in signaling modulation.

VI) Pathological elevation of GlcCer in cells leads to a global increase in membrane packing.

Altogether the evidence obtained from this work provide biophysical support to the known biological effects of GlcCer[16]. Regarding the particular case of Gaucher Disease, this work provides new insights into the interaction of GlcCer within membranes with different compositions. The alterations in membrane fluidity observed in cells derived from patients with Gaucher Disease, could affect the normal activity of different proteins and alter the trafficking of lipids and proteins. In addition, the impact that GlcCer exhibited in the modulation of lipid domains suggests that increase in GlcCer levels might also directly affect cell signaling events. Moreover, the formation of tubule like structures could also have deleterious effects in the cell, by affecting its adherence or communication with other cells. Therefore, this work provided new insights regarding the membrane biophysical alterations that might be triggered by GlcCer accumulation in the cells. Whether such alterations underlie GlcCer induced-deleterious effects in cell function that ultimately lead to the development of Gaucher Disease is still not known. Further studies aiming at addressing the link between membrane biophysical properties and GD are required to obtain further insight into this subject.

References

1.   Saxena, K.; Duclos, R. I.; Zimmermann, P.; Schmidt, R. R.; Shipley, G. G. Structure and properties of totally synthetic galacto- and gluco-cerebrosides. J Lipid Res 1999, 40, 839-849.

2.   Slotte, J. P.; Oestman, A. L.; Kumar, E. R.; Bittman, R. Cholesterol interacts with lactosyl and maltosyl cerebrosides but not with glucosyl or galactosyl cerebrosides in mixed monolayers. Biochemistry 1993, 32 (31), 7886-7892.

3.   Maunula, S.; Björkqvist, Y. J. E.; Slotte, J. P.; Ramstedt, B. Differences in the domain forming properties of N-palmitoylated neutral glycosphingolipids in bilayer membranes. Biochim Biophys Acta 2007, 1768 (2), 336-345.

4.   Dicko, A. Interactions between glucosylceramide and galactosylceramide I3 sulfate and microstructures formed. Biochim Biophys Acta 2003, 1613 (1-2), 87-100.

5.   Maggio, B. Favorable and unfavorable lateral interactions of ceramide, neutral glycosphingolipids and gangliosides in mixed monolayers. Chem Phys Lipids 2004, 132 (2), 209-224.

6.   Silva, L.; De Almeida, R. F. M.; Fedorov, A.; Matos, A. P. A.; Prieto, M. Ceramide-platform formation and -induced biophysical changes in a fluid phospholipid membrane. Mol Membr Biol 2006, 23 (2), 137-148.

7.   Castro, B. M.; de Almeida, R. F. M.; Silva, L. C.; Fedorov, A.; Prieto, M. Formation of Ceramide/Sphingomyelin Gel Domains in the Presence of an Unsaturated Phospholipid: A Quantitative Multiprobe Approach. Biophys J 2007, 93, 1639-1650.

8.   Varela, A. R. P.; Gonçalves da Silva, A. M. P. S.; Fedorov, A.; Futerman, A. H.; Prieto, M.; Silva, L. C. Effect of glucosylceramide on the biophysical properties of fluid membranes. Biochim Biophys Acta 2013, 1828 (3), 1122-1130.

9.   Pinto, S. N.; Silva, L. C.; de Almeida, R. F. M.; Prieto, M. Membrane Domain Formation, Interdigitation, and Morphological Alterations Induced by the Very Long Chain Asymmetric C24:1 Ceramide. Biophys J 2008, 95 (6), 2867-2879.

10.   D'Angelo, G.; Capasso, S.; Sticco, L.; Russo, D. Glycosphingolipids: synthesis and functions. FEBS J 2013, 280 (24), 6338-6353.

11.   Mazzulli, Joseph R.; Xu, Y.-H.; Sun, Y.; Knight, Adam L.; McLean, Pamela J.; Caldwell, Guy A.; Sidransky, E.; Grabowski, Gregory A.; Krainc, D. Gaucher Disease Glucocerebrosidase and a-Synuclein Form a Bidirectional Pathogenic Loop in Synucleinopathies. Cell 2011, 146 (1), 37-52.

12.   van Meer, G.; Wolthoorn, J.; Degroote, S. The fate and function of glycosphingolipid glucosylceramide. Phil Trans R Soc B 2003, 358 (1433), 869-873.

13.   Sillence, D. J. Glucosylceramide modulates endolysosomal pH in Gaucher disease. Mol Gen Metab 2013.

14.   Castro, B. M.; Silva, L. C.; Fedorov, A.; de Almeida, R. F. M.; Prieto, M. Cholesterol-rich Fluid Membranes Solubilize Ceramide Domains: Implcations for the Structure and Dynamics of Mammmalian Intracellular and Plasma Membranes. J Biol Chem 2009, 284 (34), 22978-22987.

15.   de Almeida, R. F. M.; Fedorov, A.; Prieto, M. SPhingomyelin/Phosphatidylcholine/Cholesterol Phase Diagram: Boundaries and Composition of Lipid Rafts. Biophys J 2003, 85, 2406-2416.

16.   Messner, M. C.; Cabot, M. C. Glucosylceramide in humans. Adv Exp Med Biol 2010, 688, 154-64.

Chapter VI

Chapter VII

Future Perspectives

Chapter VII

Future Perspectives

GlcCer has already been implicated in several cell processes and in the development of diseases, namely Gaucher Disease. Assuming that the main mechanism by which GlcCer is involved in the modulation of cell signaling is due to the GlcCer-induced alterations in the membranes biophysical properties[1, 2, 3], and that the direct effects of the abnormal high levels of GlcCer in the GD patients are still unknown, might be hindering significant information that could be valuable for the development of new treatments for GD[4]. The main purpose of this PhD project was to study the effect of increasing values of GlcCer in the biophysical properties of membranes.

In this dissertation, GlcCer biophysical impact was characterized using a bottom-up approach that encompasses studies in simpler model membranes up to the cell level. As it was showed throughout this thesis, the effect of GlcCer was characterized in model membranes containing 2 to 4 lipids and in the membranes of healthy and GD patient´s fibroblasts. It was concluded that GlcCer increases the global membrane packing, and the involvement of GlcCer in the formation of lipid domains was supported. In resemblance to the studies performed in this dissertation, a multiparameter and multiprobe approach could also be applied to characterize other model systems, which might provide relevant information regarding how GlcCer interacts with other bioactive lipids and affects membrane properties. Namely, the characterization of the interaction between GlcCer and Cer or SM, might provide additional insight on how these bioactive lipids regulate cell signaling events. It should also be interesting to study if the biophysical behavior of D-glucosyl-ß-1,1'-N-stearoyl-D-erythro-sphingosine (C18-GlcCer) is similar to the one of C16-GlcCer, since differences were reported between C18- and C16-Cer, mainly regarding thermal stability[5]. The last studies have a high biological relevance since C18-GlcCer is one of the most abundant GlcCers in the central nervous system[6, 7], which is one of the main systems affected in GD, leading to severe damages in the patient quality of life[8].

Moreover, the experimental strategy employed in the present work is also a valuable tool to further characterize the biophysical properties of cell membranes and lipid extracts from specific subcellular fractions. Of particular interest is the determination of the membrane biophysical properties in cells with different type of GD mutations, in

homozygote and heterozygotes, in order to understand if those are correlated to the different types of GD, particularly to the severity of the disease. Additionally, it might be important to investigate if the alterations in membrane properties of cells derived from patients with the same type of GD but carrying different types of mutations, are comparable, in order to understand whether a specific mutation leads to similar or different biophysical features. Besides from fibroblasts, studies should also be performed in those cells that are mainly affected in the pathophysiology of GD - the macrophages that digest enormous amounts of GlcCer and transform into storage cells, known as Gaucher Cells[8]. It is reported that these cells are highly enriched in GlcCer, compared to other cells in a GD patient, and therefore it is expected that the effect of GlcCer accumulation on their membrane properties is more notorious.

In addition, to determine if GlcCer effect on the biophysical properties of cell membranes is dependent on the cell site, organelle purification and/or lipid extraction could be performed in several membranous fractions, and membrane properties could be evaluated in the purified organelles or through the use of lipid vesicles prepared with the different lipid extracts.

The results in this dissertation, and the future ones to be obtained on the above suggested studies may provide fundamental information regarding how GlcCer affects membrane organization in different cells and in different cell sites, allowing to understand the direct effects of GlcCer increased concentration in the cells of the patients with GD. In addition, such results could trigger the identification of new therapeutic targets and development of new therapies that can improve the quality of life of the patients with Gaucher Disease, and possibly of the patients with pathologies that have abnormal levels of this glycosphingolipid, e.g. Parkinson Disease[9], cancer[10] and polycystic kidney disease[11].

References

1.   Varela, A. R. P.; Gonçalves da Silva, A. M. P. S.; Fedorov, A.; Futerman, A. H.; Prieto, M.; Silva, L. C. Effect of glucosylceramide on the biophysical properties of fluid membranes. Biochim Biophys Acta 2013, 1828 (3), 1122-1130.

2.   Maunula, S.; Björkqvist, Y. J. E.; Slotte, J. P.; Ramstedt, B. Differences in the domain forming properties of N-palmitoylated neutral glycosphingolipids in bilayer membranes. Biochim Biophys Acta 2007, 1768 (2), 336-345.

3.   Messner, M. C.; Cabot, M. C. Glucosylceramide in humans. Adv Exp Med Biol 2010, 688, 154-64.

4.   Bennett, L. L.; Mohan, D. Gaucher Disease and Its Treatment Options. Annals of Pharmacotherapy 2013, 47 (9), 1182-1193.

5.   Pinto, S. N.; Silva, L. C.; Futerman, A. H.; Prieto, M. Effect of ceramide structure on membrane biophysical properties: The role of acyl chain length and unsaturation. Biochim Biophys Acta 2011, 1808 (11), 2753-2760.

6.   Zhang, W.; Quinn, B.; Barnes, S.; Grabowski, G.; Sun, Y. Metabolic Profiling and Quantification of Sphingolipids by Liquid Chromatography-Tandem Mass Spectrometry. J Glycomics Lipidomics 2013, 3 (107), 2153-0637.1000107.

7.   Farfel-Becker, T.; Vitner, E. B.; Kelly, S. L.; Bame, J. R.; Duan, J.; Shinder, V.; Merrill, A. H.; Dobrenis, K.; Futerman, A. H. Neuronal accumulation of glucosylceramide in a mouse model of neuronopathic Gaucher disease leads to neurodegeneration. Hum Mol Gen 2014, 23 (4), 843-854.

8.   Jmoudiak, M.; Futerman, A. H. Gaucher disease: pathological mechanisms and modern management. Br J Haematol 2005, 129 (2), 178-188.

9.   Mazzulli, Joseph R.; Xu, Y.-H.; Sun, Y.; Knight, Adam L.; McLean, Pamela J.; Caldwell, Guy A.; Sidransky, E.; Grabowski, Gregory A.; Krainc, D. Gaucher Disease Glucocerebrosidase and a-Synuclein Form a Bidirectional Pathogenic Loop in Synucleinopathies. Cell 2011, 146 (1), 37-52.

10.   Liu, Y.-Y.; Gupta, V.; Patwardhan, G. A.; Bhinge, K.; Zhao, Y.; Bao, J.; Mehendale, H.; Cabot, M. C.; Li, Y.-T.; Jazwinski, S. M. Glucosylceramide synthase upregulates MDR1 expression in the regulation of cancer drug resistance through cSrc and b-catenin signaling. Mol Cancer 2010, 9 (1), 145.

11.   Natoli, T. A.; Smith, L. A.; Rogers, K. A.; Wang, B.; Komarnitsky, S.; Budman, Y.; Belenky, A.; Bukanov, N. O.; Dackowski, W. R.; Husson, H.; Russo, R. J.; Shayman, J. A.; Ledbetter, S. R.; Leonard, J. P.; Ibraghimov-Beskrovnaya, O. Inhibition of glucosylceramide accumulation results in effective blockade of polycystic kidney disease in mouse models. Nat Med 2010, 16 (7), 788-792.